The role of surface albedo changes in tropical forest loss and its climate impact

Jamie Martin Wilson

University of Leeds

School of Earth and Environment

Submitted in accordance with the requirements for a degree of:

Doctor of Philosophy

April 2020

Declaration of Authorship

The candidate confirms that the work submitted is his own and that the appropriate credit has been given where reference has been made to the work of others.

Acknowledgements

Firstly, I would like to thank my academic supervisory team, Dominic Spracklen, Steve Arnold and Piers Forster. Their help, advice and patience through the execution of this work have been instrumental in its completion. Dom has been key in helping steer my ideas, ready to discuss results at every stage, Steve helped provide strategic input and Piers always contributed enthusiasm and helped me to believe this was possible. I am extremely grateful for the opportunities provided to me by them.

Secondly, I would like to thank the Leeds-York SPHERES NERC Doctoral Training Partnership, who provided me with the opportunity (and the funding) to undertake this research and the United Bank of Carbon who provided the CASE award for this project.

For her contribution in teaching me how to undertake SOCRATES simulations, as well as providing me with output from the Community Land Model used in Chapter 5, I wish to thank Catherine Scott. Many thanks also to Richard Rigby in IT support, who helped save many hours of fighting technology.

Through the course of my PhD, I have been part of the Biosphere-Atmosphere Group, who have helped support and supplement everyone's research (and provided great coffee mugs). Thanks too to the Physical Climate Change group and the Aerosol Modelling group, who also made me feel very welcome throughout my time with them.

Through my time in Leeds, I've been supported by a lot of different people, but special thanks go to Chetan, Arjan, Dan (and everyone at the docks), Josh, Sam, Naomi, and Sam for providing support and keeping me sane. My parents, Lorraine and Martin, and my wider family have been key, not only through this period, but throughout my life, and deserve a huge thanks.

Finally, a special mention to my wife, Magdalene, without whom, reaching this stage would not have happened.

Abstract

Surface albedo plays a significant role in the Earth's climate system, dictating the amount of incoming solar radiation that is reflected by the surface. Historic land use change has been estimated to change this by 0.2 W m^{-2}. Deforestation in the tropics now exceeds that at other latitudes and surface albedo changes associated with forest loss provide the second largest radiative impact, after CO_2.

This study evaluates the surface albedo changes associated with tropical deforestation across the Amazon and South East Asia using a range of observation methods. Satellite observations from the Moderate Resolution Imaging Spectroradiometer (MODIS) is combined with data from aircraft campaigns and *in-situ* observations to investigate the albedo of forest and non-forested regions.

A consistent overestimation of surface albedo changes associated with tropical deforestation is observed as a result of comparing such observations with modelling simulations within the literature, which is reflected both across the Amazon and South East Asia regions.

Differences between the behaviour of surface albedo within oil palm concessions is highlighted, as is a dependency of surface albedo on the time since forest loss occurred across South East Asia.

The influence the various surface albedo observations has on the global climate is assessed by radiative forcing calculations using the Suite of Community Radiative Codes based on Edwards and Slingo (SOCRATES), where the impacts of the overestimation of albedo changes in models is shown.

Contents

List of Figures

List of Tables

Abbreviations

ABRACOS	**A**nglo-**Bra**zilian **C**limate **O**bservational **S**tudy
ANOVA	**An**alysis **o**f **Va**riance
AR5	IPCC Fifth **A**ssessment **R**eport
ARME	**A**mazon **R**egion **M**icro-Meteorological **E**xperiment
BC	**B**lack **C**arbon
BRDF	**B**idirectional **R**eflectance **D**istribution **F**unction
BVOCs	**B**iogenic **V**olatile **O**rganic **C**ompounds
CCN	**C**loud **C**ondensation **N**uclei
DALYs	**D**isability-**A**djusted **L**ife **Y**ears
ECMWF	**E**uropean **C**entre **f**or **M**edium **R**ange **W**eather **F**orecasts
EOS	**E**arth **O**bserving **S**ystem
FAAM	UK **F**acility for **A**irborne **A**tmospheric **M**easurements
GEOS-Chem	**G**oddard **E**arth **O**bserving **S**ystem Atmospheric **Chem**istry model
GHG	**G**reen**h**ouse **G**as
GoAmazon	Observations and Modelling of the **G**reen **O**cean **Amazon** 2014-2015 experiment
GWP	**G**lobal **W**arming **P**otential
ICCP	**I**nternational **S**atellite **C**loud **C**limatology **P**roject
INPE	**I**nstituto **N**acional de **P**esquisas **E**spaciais (Brazilian National Institute for Space Research)
IPCC	**I**ntergovernmental **P**anel on **C**limate **C**hange
LBA-EUSTACH	**L**arge-Scale **B**iosphere-**A**tmosphere Experiment in Amazonia
LST	**L**and **S**urface **T**emperature
LUC	**L**and **U**se **C**hange
LW	**L**ong**w**ave
MISR	**M**ulti-angle **I**maging **S**pectro**r**adiometer
MODIS	**Mod**erate **R**esolution **I**maging **S**pectroradiometer
NASA	**N**ational **A**eronautics and **S**pace **A**dministration
NDVI	**N**ormalised **D**ifference **V**egetation **I**ndex
PCASP	**P**assive **C**avity **A**erosol **S**pectrometer **P**robe
PFT	**P**lant **F**unctional **T**ype
RCP	**R**epresentative **C**oncentration **P**athway
RF	**R**adiative **F**orcing
SAMBBA	**S**outh **A**merican **B**iomass **B**urning **A**nalysis
SEBAL	**S**urface **E**nergy **B**alance **A**lgorithm for **L**and
SLCP/F	**S**hort-**L**ived **C**limate **P**ollutant / **F**orcer
SOA	**S**econdary **O**rganic **A**erosol
SOCRATES	**S**uite **O**f **C**ommunity **Ra**diative **C**odes based on **E**dwards and **S**lingo
SW	**S**hort**w**ave
TOA	**T**op-**o**f-**A**tmosphere
VOC	**V**olatile **O**rganic **C**ompounds
$\Delta\alpha$	Albedo difference
$\Delta\alpha_s$	Spatial albedo difference (between forested and non-forested observations)
$\Delta\alpha_t$	Temporal albedo difference (between forest prior to and post forest loss)

Chapter 1: Introduction

1.1. Thesis Outline

The use of surface albedo as an influential climatic variable is well accepted and is used widely in climatic modelling. This thesis aims to improve the understanding of how surface albedo varies with forest coverage in the tropics and how land use change may lead to changes in the climate as a result.

This introductory chapter begins with an update on the global coverage of forests to date. It then lays out the important drivers of climate change, continuously touching on the role forests play. It explores a range of direct contributions, while discussing some of the smaller effects for completeness. Land-use change is then emphasised as a driving factor to alter the climate, with the individual processes stemming from deforestation being split into two broad areas: biogeochemical and biophysical. The overall impact from these is then discussed, before surface albedo (the focus of this work) is highlighted as a key, but largely unexplored, climate driver across the tropics.

Chapter 2 describes the datasets for forest coverage and surface albedo observations used through the results chapters, including an overview of the data processing used within those chapters.

In Chapter 3 the current usage of surface albedo in modelling studies is assessed and the values obtained through previous observational studies are also identified. The surface albedo over the Amazon is then explored using a range of observation types to identify the surface albedo of forested and non-forested land cover. Whether spatial analysis of forested and non-forested areas is able to be used to substitute for temporal changes in forest area (i.e. forest loss) is also explored. Finally, whether different observational techniques result in different albedo values and how closely observations match the current model usage is discussed.

Chapter 4 explores the surface albedo over South East Asian landmasses across forested and non-forested regions. The influence of oil palm concessions and whether surface albedo differs within them is then examined. The dependency of surface albedo of previously deforested areas on the year of forest loss is also explored.

In chapter 5, the radiative impact of albedo changes as a result of forest loss across the regions is quantified and compared to other radiative impacts. The magnitude of the

radiative effect due to surface albedo is estimated and the influence different observation techniques and different deforestation pathways has on the net climatic impact of deforestation is discussed.

1.2. The changing dynamics of forests

Forests account for approximately 30 % of the world's total land area (Food and Agriculture Organsiation of the United Nations, 2015), providing range of essential ecosystem services (Brandon, 2015; Foley et al., 2005; Myers, 1997). The majority (1.7 Gha / 39 %), is found in the tropics, with the boreal (31 %), temperate (15 %) and subtropical (7 %) making up the total of 4 Gha (Food and Agriculture Organsiation of the United Nations, 2015).

Historically, the amount of forests has varied based on climatic factors, with Europe's forested area peaking during the mid-Holocene (Zanon et al., 2018), however humans have undertaken significant forest clearance since the establishment of farming practices. Much of the early land use change was centred on Europe, followed by the North American temperate regions, since 1,000 AD (Williams, 2000).

Increasing populations required expansion of agricultural land into forested areas, combined with use of forests for raw materials, a strong increase in deforested area followed population growth through the 19th and 20th century (Figure 1.1).

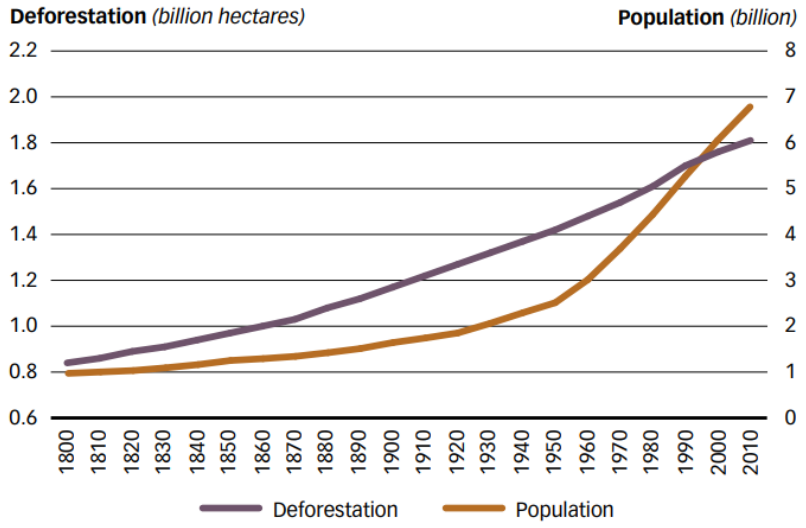

Figure 1.1: Cumulative deforestation and population growth since 1800. Source: (Food and Agriculture Organization, 2016).

Much of this forest loss has been coupled with an increase in cropland and pasture, with estimates from Goldewijk, (2001) and Goldewijk et al., (2007), highlighting increases in cropland from 265 to 1,471 Mha and pasture from 524 to 3,451 Mha between 1700 and 1990.

The last century has seen a shift from forest loss in the temperate regions to the tropics, which now accounts for the largest loss of forest area of the climatic regions. Between 1990 to 1997, 34 Mha of tropical forest were reportedly lost, with greatest area occurring in South America, whilst South East Asia displayed the greatest percentage loss (Achard et al., 2002). South East Asia reflected past forest loss in being driven by a push for greater agricultural land (H. K. Gibbs et al., 2010; Holly K. Gibbs et al., 2008; Meijide et al., 2018; Miettinen et al., 2011), and although these drivers are seen in South America, a push for land conversion to cattle ranches is a major factor (Fearnside, 2005; Rudel et al., 2009; Sakai et al., 2004).

As tropical deforestation has been increasingly targeted by policy (e.g. Federative Republic of Brazil, 2015), the rate of deforestation in the tropics slowed in the first decade of the 21st century, driven by a reduction in Amazonian deforestation (Food and Agriculture Organization of the United Nations, 2015; M. C. Hansen et al., 2013; Moutinho et al., 2016; Reddington et al., 2015). However, large areas of forest continued to be cleared and rates increased in Indonesia, surpassing Brazil as undergoing the greatest forest loss (M. C. Hansen et al., 2013; Margono et al., 2014; Miettinen et al., 2011; Richards & Friess, 2016).

However, measures in place, such as a moratorium on new concessions for oil palm, timber and logging in Indonesia, which accounts for approximately 60 % of South East Asia's forest loss, has led to a reduction in deforestation in recent years (Busch et al., 2018; Estoque et al., 2019). Conversely, Figure 1.2**Error! Reference source not found.** shows deforestation in the Amazon has begun to increase again over the last decade since 2012's low (Stabile et al., 2020). A result of economic drivers coupled with policy choices from the new government, it is not clear whether these rates will continue to rise in the near future (Ferrante & Fearnside, 2019; Freitas et al., 2018).

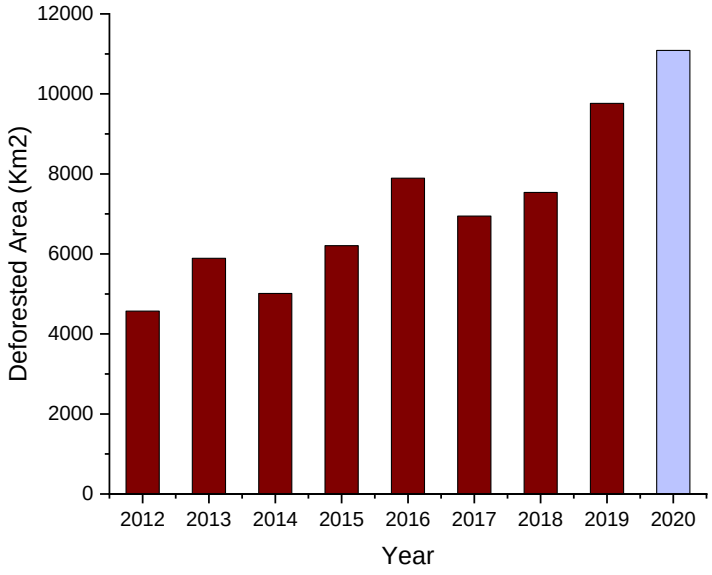

Figure 1.2: Deforestation rate in the Amazon since 2012. Value for 2020 is estimated from 45% of the monitored area and is not yet final (Silva Junior et al., 2020). Data from PRODES.

1.3. **Well-mixed Greenhouse Gases**

Anthropogenic activities have a strong impact on the climate, with global changes that influence all parts of the climate system. Direct emissions of CO_2 from burning fossil fuels, cement production and flaring, forestry and land use changes have all increased heavily since preindustrial times (Forster et al., 2007; Pachauri et al., 2014). Such activities have driven an increase in global temperature of approximately 1 K since preindustrial (Allen et al., 2018).

Carbon dioxide acts as a greenhouse gas (GHG), effectively trapping radiation reflected from the Earth's surface in the atmosphere. The behaviour of GHGs, such as CO_2, are important in the energy balance of the Earth system. Shortwave (SW) radiation from the Sun reaching the atmosphere and the Earth's surface is both absorbed and reflected at different quantities, dependant on the properties of the surfaces that it interacts with.

Seventy percent of the incoming solar radiation is absorbed by the atmosphere and the surface (Figure 1.4). As the Earth's surface is colder than the Sun, its behaviour as a black body means that it emits radiation at a longer wavelength compared to that which it absorbs. This emitted radiation does not directly leave the Earth system, instead it gets reabsorbed by the atmosphere. This in turn requires the system to adjust and raise its temperature to keep the system balanced.

Perturbations to this energy balance, such as the result of CO_2 emissions, can be calculated as a radiative forcing (RF); how much energy is required to restore equilibrium over a time period. A RF is defined as the change in net (down minus up) irradiance (solar plus long-wave; in Wm^{-2}) at the tropopause after allowing for stratospheric temperatures to readjust to radiative equilibrium (Figure 1.3), but with surface and tropospheric temperatures and state held fixed at the unperturbed values (Ramaswamy et al., 2001).

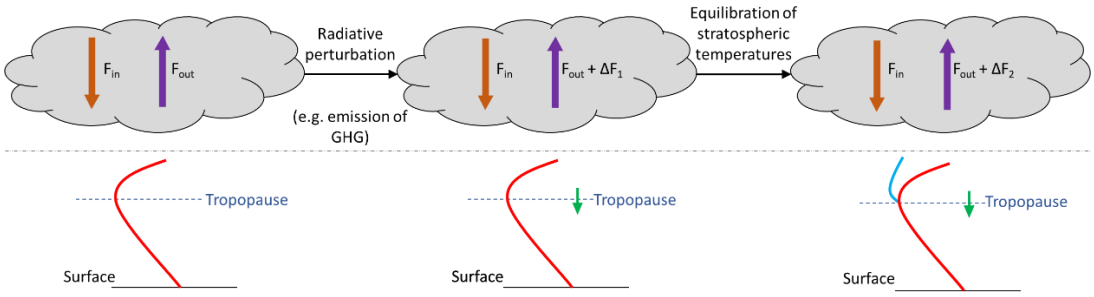

Figure 1.3: Energy balance (top) and atmospheric temperature profile (below) prior to a radiative energy perturbation (left), immediately after (centre) and once stratospheric temperatures have been allowed to equilibrate (right). The perturbation results in an instantaneous radiative forcing (ΔF_1) and an adjusted radiative forcing (ΔF_2).

Through the global mean climate sensitivity parameter (λ), there exists a relationship between the global mean radiative forcing and the global mean equilibrium temperature response (ΔT_S):

$$\lambda\, RF = \Delta T_S \qquad \text{Equation 1.1}$$

The coupling of the troposphere and the surface through convective heat transfer, and the fast equilibration of the stratosphere (months as opposed to decades in the surface-tropospheric system) mean the tropopause can be taken as the top of atmosphere for the RF definition, and Equation 1.1 holds.

Due to the relative inertness of atmospheric CO_2, it possesses a long atmospheric lifetime despite dynamic exchange between the atmosphere, ocean and terrestrial sources/sinks. As a result, increases of CO_2 lead to long-term changes in the global temperature. Due to the long atmospheric lifetime, complete mixing across the atmosphere can be assumed and so changes in CO_2 concentrations lead to a radiative forcing that is consistent across the Earth system. Driven by anthropogenic emissions, the annual mean concentration of CO_2, as measured at the long-running observatory at Mauna Loa, surpassed 400 ppm for the first time in 2015 and continued to rise to 411 ppm in 2019, 45 % above the 1850 pre-industrial

concentration (280 ppm). However, where forcing agents are localised to a specific area or are relatively short-lived in the atmosphere, these exert a forcing that is spatially inhomogeneous, and so the climatic impact of these will also vary spatially.

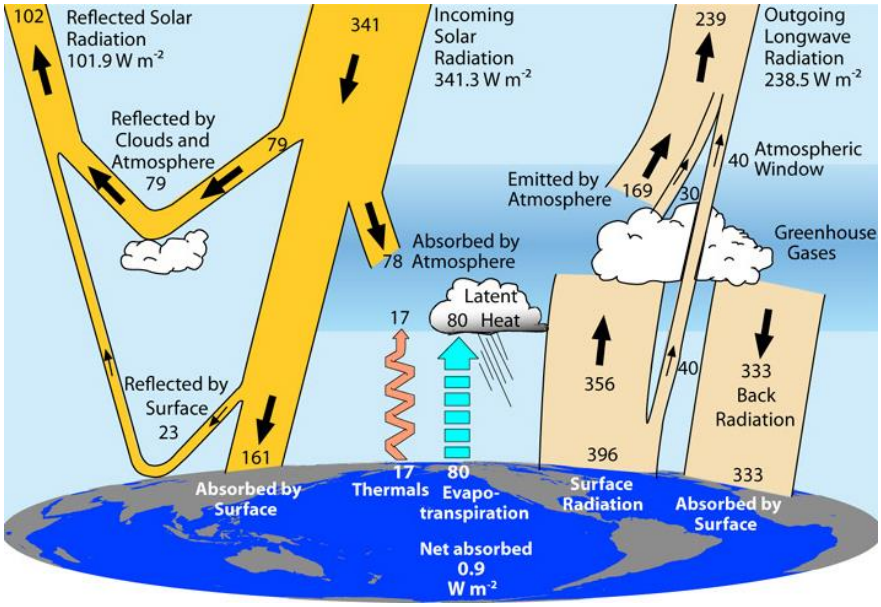

Figure 1.4: Global annual mean Earth's energy budget (W m^{-2}) between March 2000 – May 2004. Source: Trenberth et al., (2009).

Other well mixed GHGs, such as methane (CH_4), nitrous oxide (N_2O) and other hydrocarbons are described as such due to their relatively long atmospheric lifetime, allowing an assumption of horizontal homogeneity across the atmosphere. These behave similarly to CO_2, absorbing radiation and warming the atmosphere, but many of these other GHGs have a global warming potential (GWP) many times that of CO_2. GWPs provide a simplified estimate of the climatic impact of emissions of different gases relative to CO_2. It is defined in Equation 1.2 as the ratio of the radiative forcing resulting from the instantaneous release of 1 kg of a trace substance relative to 1 kg of CO_2, integrated over time:

$$GWP(x) = \frac{\int_0^{TH} a_x \times [x(t)]\, dt}{\int_0^{TH} a_{CO_2} \times [CO_2(t)]\, dt} \qquad \text{Equation 1.2}$$

Where TH is the time horizon over which the GWP is calculated, a_x is the radiative efficiency due to a unit increase in atmospheric abundance of the respective gas, [x(t)] is the time-dependent decay in abundance of the instantaneous release of the respective gas, and where x is replaced with CO_2, the quantities describe the same whilst using the values for CO_2, as the reference gas. In general, concentrations of these have also been increasing as a result of anthropogenic activity, resulting in a warming effect (Figure 1.5).

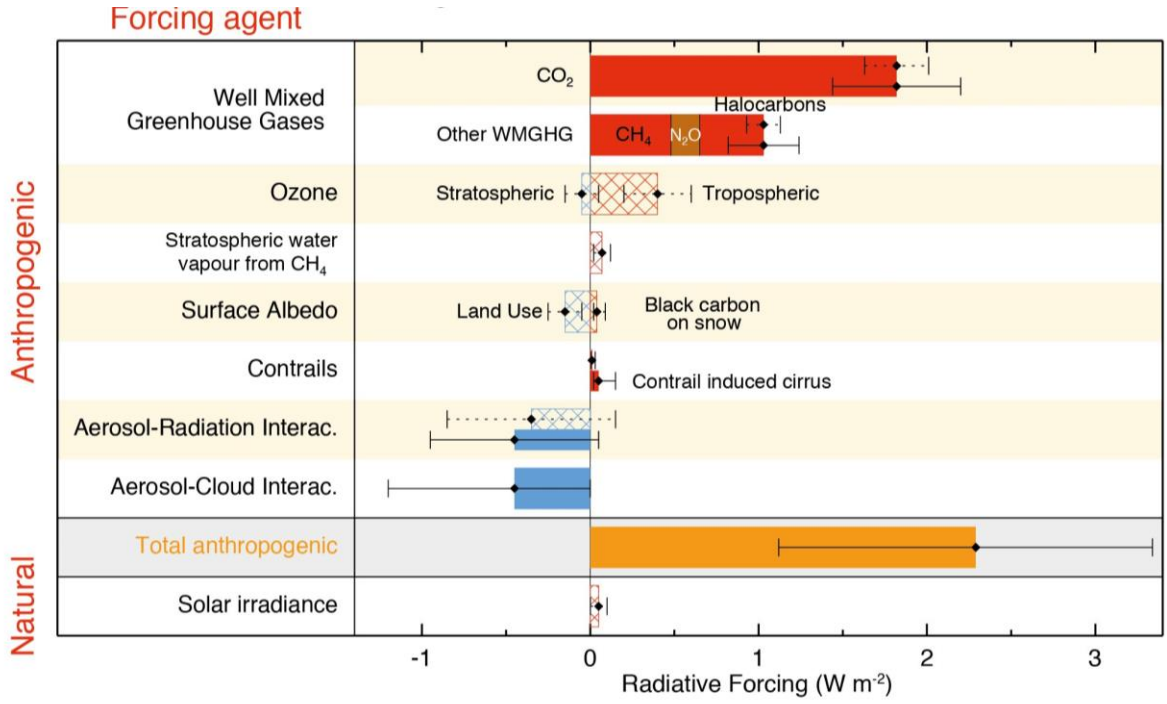

Figure 1.5: Radiative forcing for the period 1750-2011. Source: Myhre et al., (2013)

As forests cover a large proportion of the earth's surface, they play an important role in the climate system. Through photosynthesis, forests take in atmospheric carbon in the form of carbon dioxide (CO_2) and convert it to biomass. Tropical and boreal forests are able to store similar amounts of carbon (~2.4 Gt C ha^{-1}), whilst temperate forests are reported to store approximately 1.5 Gt C ha^{-1} (Pan et al., 2011).

Alongside behaving as carbon pools, storing ~45 % of terrestrial carbon, globally forests are important in regulating the global climate by acting as carbon sinks; absorbing approximately 30 % of carbon emissions from fossil fuels and land use change (Bonan, 2008b). However, it is through land use change that forests can become a source of CO_2 – removal and burning of forests release the stored carbon back into the atmosphere, as well as reducing the size of the carbon sink.

1.4. Short-lived climate pollutants

Short-lived climate pollutants (SLCPs) are components of the atmosphere which primarily impact the climate system within the first decade after they're emitted (Stocker et al., 2013). They have a shorter lifetime than well-mixed GHGs and therefore do not accumulate as an

atmospheric species on timescales beyond decadal or centennial, therefore their climate response is felt mainly in the near term.

SLCPs: Aerosols

Atmospheric particles interact with the climate in a variety of ways, comprising broadly of the direct effect, two indirect effects and the semi-indirect effect. Aerosols reflect, absorb and scatter solar radiation directly depending on their physical and chemical properties. Although certain particles, such as black carbon (BC), may be exceptionally strong absorbers of radiation (R. Wang et al., 2016), the global direct radiative forcing has resulted in a cooling overall (Figure 1.5).

The non-direct effects of aerosols relate to aerosol-cloud interactions. In order to condense, atmospheric water vapour requires a surface provided by cloud condensation nuclei (CCN) upon which to condense and form cloud droplets. Once formed, these droplets are able to grow by further condensation of water vapour and collision-coalescence. Fewer particles in the atmosphere result in less opportunity for condensation to take place, resulting in larger cloud droplet particles. Conversely, more CCN results in more but smaller cloud droplets, which result in a more reflective cloud overall: the cloud albedo effect (Kreidenweis et al., 2018; Twomey, 1977). The reduced cloud droplet size increases the time taken to coalesce into raindrops, reducing precipitation. This leads to longer lifetimes of the affected clouds, increasing the overall cloud coverage and thus the reflectivity of the atmosphere – resulting in a further cooling mechanism: the lifetime effect (Albrecht, 1989). A semi-direct effect also occurs as a result of specifically high-absorption particles (such as BC). As these particles absorb radiation, they increase the temperature and in turn reduce the amount of cloud cover. Although this effect was first proposed to result in a positive RF (e.g. J. Hansen et al., 1997; Lohmann & Feichter, 2001), recent work has highlighted potential negative rapid adjustments in temperature as a result of greater longwave (LW) radiation emitted to space, creating greater uncertainty in the role of BC (Bellouin et al., 2019; Johnson et al., 2019; Stjern et al., 2017; Yang et al., 2019).

Forests are an important source of natural biogenic volatile organic compounds (BVOCs), with approximately 70 % sourced from tropical forests (Karl et al., 2007). BVOCs are small, carbon-based molecules which are emitted by vegetation as a by-product of biological processes. Broadly speaking, monoterpenes and isoprene dominate the reaction profiles of these species due to their abundances, although different BVOCs are released by certain flora at different rates and their reaction profiles depend on the local atmospheric

composition (Guenther et al., 1995). The emitted species react quickly with oxidising agents in the atmosphere (Figure 1.6), the products of which can then go on to react further with other oxidising agents or oligomerise with each other, increasing the size and complexity of the compound (Camredon et al., 2007). These then undergo gas-particle phase transfer via nucleation, condensation and multiphase reactions, forming secondary organic aerosol (SOA) (Hallquist et al., 2009).

This SOA formation plays a key role in the radiative balance of the Earth system, through both the direct radiative effects and the aerosol-cloud interactions described above. Although an important cooling mechanism, aerosol formation from sources other than BVOC emissions, such as sulfate, may play a more influential role on the climate (O'Donnell et al., 2011; Rap et al., 2013).

SLCPs: Ozone and methane

The climate can also be perturbed through other means by reactions involving BVOCs. Firstly, the SLCP tropospheric ozone (O_3) can be produced through a complex cycle involving NO_x and hydroxyl radicals (Figure 1.6). However, the behaviour of the reaction depends on the conditions and the concentrations of NO_x and volatile organic compounds (VOCs) relative to each other. The response of O_3 to increased BVOC emissions can therefore vary in both location and magnitude (Situ et al., 2013).

The majority of BVOC emissions in forested regions occur in areas of low pollution (i.e. NO_x limited regimes). Studies have generally observed an increase in tropospheric O_3 due to the effects of climate change, attributing a large role in biogenic emission increases due to increased temperature (Hogrefe et al., 2004; Knowlton et al., 2004).

The effect of temperature alone is considered the biggest climatic factor influencing ozone concentrations, however there is a large discrepancy between the changes in the above studies and when emissions are fixed (Dawson et al., 2007). Using CHIMERE, a regional air quality model, Meleux et al., (2007) observe an increase in temperature results in increased BVOC emissions and ultimately higher O_3 concentrations. Fu et al., (2007) also estimates higher O_3 concentrations in South and East Asia as a result of higher observed BVOC emissions.

While exposure to O_3 has been shown to damage plants, there are also suggestions of a positive feedback with increased exposure resulting in enhanced VOC emissions in a number

of species (Kivimäenpää et al., 2016; Llusià et al., 2002; Peñuelas et al., 1999; Rinnan et al., 2005).

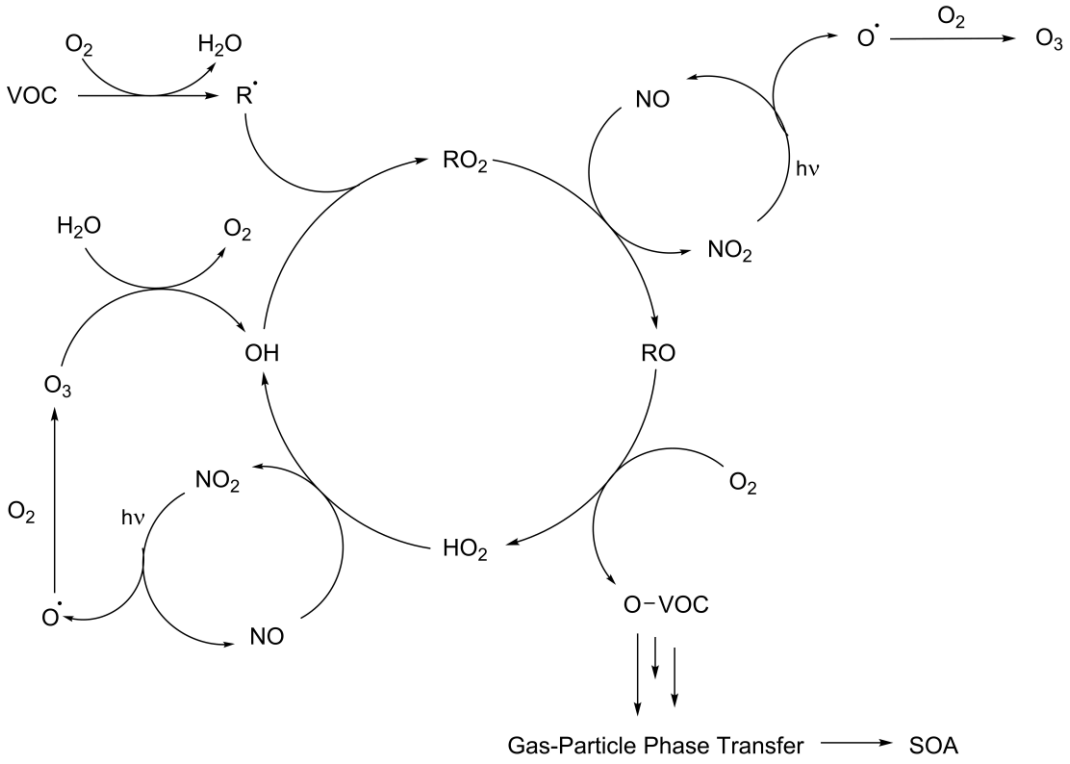

Figure 1.6: Simplified reaction scheme of the formation of ozone from VOCs.

Atmospheric BVOC reactions are not limited to the production of O_3; O_3 is also destroyed as it oxidises VOCs and thus NO_x concentrations control the fate of O_3. However, by being oxidised in fast rate reactions, BVOCs effectively reduce the oxidising potential of the atmosphere and may impact the ability for isoprene to recycle hydroxyl radicals in low NO_x regimes (Fuchs et al., 2013; Lelieveld et al., 2008; Peeters et al., 2014; Taraborrelli et al., 2012).

Atmospheric methane's primary sink is through reactions with the hydroxyl radical and anthropogenic emissions of VOCs has already been suggested to increase methane lifetime in this way, therefore higher BVOC emissions may do likewise (Naik et al., 2013; Stevenson et al., 2013). Additionally, increased CO_2 may reduce isoprene emissions, thus increasing hydroxyl radical concentrations and having the reverse effect on methane (Young et al., 2009). The effects of deforestation may also counteract the increased BVOC emissions as a result of climate change in some locations, so the impact on their concentrations and thus the impacts on the lifetimes of methane, the hydroxyl radical and ozone are uncertain (Young et al., 2013; G. Zeng et al., 2007).

SLCPs: Air quality

Impacts of atmospheric changes are not limited to the climate; both SOA and tropospheric O_3 are extremely important in air quality. Not only is this a large economic issue, but it has profound implications for health, resulting in respiratory diseases, increased disability-adjusted life years (DALYs) and even direct premature deaths (Stedman, 2004; Strong et al., 2013; Turnock et al., 2016). Deforestation particularly has a significant impact on air quality in specific regions. Indonesian peat fires have been discussed already for their CO_2 emissions, but such fires in the dry season often leads to large air quality issues across Indonesia, Malaysia and Singapore due to fires in Sumatra and Indonesian Borneo, particularly from the palm oil and timber industries (Marlier et al., 2015; Tosca et al., 2011). Peat fires are especially significant for air quality due to their two-stage burning; with a second hypoxic burning phase featuring a smokier burn, producing higher ratios of incomplete combustion products (CO, CH_4, and multiple VOCs) (Elvidge et al., 2015; Rein et al., 2009). Such emissions can have a large role in both atmospheric chemistry and air quality. The formation of SOA is coupled alongside the primary aerosol and BC produced from the combustion process, all of which can have large impacts on human health and the climate (Heald & Spracklen, 2015; Karl et al., 2007; Reddington et al., 2015). However, similar arguments can be used for deforestation fires in regions such as the Amazon basin, boreal forests and across Africa, and are also mirrored in natural wildfires (M. C. Hansen et al., 2013; Lawrence & Vandecar, 2015; Reddington et al., 2015).

1.5. Land use change

As a result of the conversion of forest to agricultural land, there has historically been a large warming due to the release of CO_2. When forested land is cleared, it often results in decay of biomass or burning of forest as a means of removal. This results in the emission of CO_2 and contributes to the positive CO_2 RF in Figure 1.5 potentially providing a warming effect of 0.16 – 0.18 K (Pongratz et al., 2010). However, deforestation also leads to other climatic effects, the largest contributing a RF being the surface albedo effect. As forests are generally better absorbers than the replacement land surface afterwards (e.g. cropland, pasture), deforestation results in more radiation being reflected at the surface and a negative RF of approximately -0.4 W m^{-2} (Figure 1.5**Error! Reference source not found.**, Andrews et al., 2017).

1.6. **Biogeochemical mechanisms**

In general, forests influence the climate in two major ways: through mechanisms associated with chemical changes, biogeochemical mechanisms, and the direct, physical impacts, biogeophysical mechanisms (Figure 1.7).

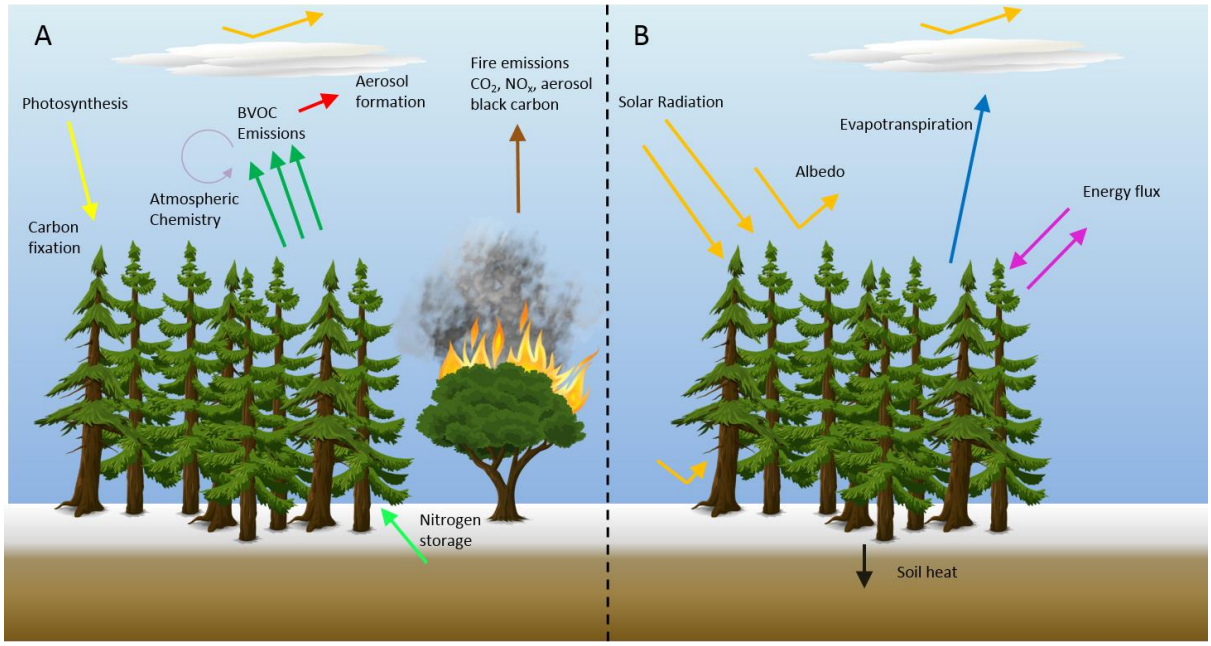

Figure 1.7: Representation of some of the (A) biogeochemical and (B) biophysical mechanisms of forests' climate interactions.

The primary biogeochemical influence of forests is their role in the carbon cycle, storing approximately 2.4 GtC annum^{-1} (Pan et al., 2011). Deforestation removes the capacity of this sink process to occur and further releases CO_2 as the removed vegetation decomposes or is burned, with such carbon losses in the Amazon forests potentially turning the region into a net source by 2040 (Hubau et al., 2020). Globally, this resulted in an increase in atmospheric CO_2 of 0.9 GtC annum^{-1} between 2002-2011 (Stocker et al., 2013), approximately 10 % of the 8.7 GtC annum^{-1} released by fossil fuel combustion, cement production and gas flaring in 2008 (Le Quéré et al., 2009).

Between 1750 and 1850, emissions from land use change substantially contributed to the rise in atmospheric CO_2 concentrations (Reick et al., 2010). The relative contribution to anthropogenic CO_2 emissions has reduced with time, due to a marked increase in emissions from fossil fuel burning. However its contribution is still significant, contributing 180 GtC (approximately 50 % of CO_2 emissions from fossil fuel burning: 375 GtC) between 1750 and 2011 (Stocker et al., 2013).

Although removal of trees both releases CO_2 and reduces the potential for carbon uptake, different types of forests vary in their behaviour. Annual carbon emissions from tropical deforestation averaged 2.3 GtC between 2001-2013 (Zarin et al., 2016), resulting in greater losses in storage than in boreal or temperate forests (Y. Y. Liu et al., 2015). Indonesia's mangrove forests have a high stored carbon content relative to other forests, making them one of the most carbon rich in the tropics (Donato et al., 2011; Richards & Friess, 2016; Siikamäki et al., 2012). As a result, deforestation of mangroves account for up to 31 % of the estimated emissions form Indonesia's land use sector; accounting for 2-8 % of the emissions from global deforestation (Pendleton et al., 2012), despite contributing only 6 % of the overall deforestation within the country. Additionally, much of Indonesia's forest clearance occurs on peatland, where the peat is drained and dried out, thus making it extremely flammable. When set aflame, they become a considerable contributor to the CO_2 emissions of the region and the global land use change (LUC) sector (Van Der Werf et al., 2009, 2010).

1.7. Biophysical mechanisms

While forest growth leads to a net CO_2 uptake, forests also exert important biophysical factors, as observed in Figure 1.7. The effects forests have on the climate are dependent on location, partly because of the type of forest differs (i.e. the species of tree and the size of the forests) but also because of the nature of the location, the ground type, the radiation budget and the atmospheric dynamics (A. Wang & Price, 2007). It is in these biophysical effects that a large latitudinal dependence is observed. At high latitudes especially, these can lead to the biogeochemical cooling effects being masked, thus leading to an overall warming effect of forests.

Surface Albedo

One of the key parameters is the reflectance, or the albedo of the surface (Davin & de Noblet-Ducoudre, 2010). Albedo is a dimensionless quantity, as it is defined as the ratio of radiant energy scattered by a surface to that received, described as a spectral albedo if restricted to a specific wavelength, or narrowband, wideband and broadband albedo if more wavelengths are measured over. Albedo is climatically important across as a broadband albedo (across the whole SW domain, 0.3 – 4 μm) in particular, as it dictates the amount of insolation that is absorbed or reflected. Table 1.1 lists typical surface albedo values for various natural surfaces.

Table 1.1: Typical albedo values of various natural surfaces. Data from *(Coakley, 2002)*.

Surface type	Typical albedo value
Mixed farming	0.16 – 0.18
Grassland	0.20 – 0.21
Evergreen forest	0.12 – 0.16
Deciduous forest	0.17 – 0.18
Tropical broadleaf forest	0.12 – 0.15
Desert	0.36
Tundra	0.17
Snow/sea ice	0.62 – 0.66
Ocean	0.07

The scattering behaviour of a surface is anisotropic and can be described using the bidirectional reflectance distribution function (BRDF). BRDF measures the deviation from a pure Lambertian behaviour, where scattering occurs evenly in all directions. On many natural surfaces (e.g. vegetation, snow and bare soil), the anisotropic behaviour means that an increasing solar zenith angle results in an increased albedo (Bourgeois et al., 2006; Henderson-Sellers & Wilson, 1983; Zheng et al., 2017). The interaction can be split into two parts – a diffuse component, where the surface generally behaves with a Lambertian albedo, and a direct component, where the albedo is dependent on the solar zenith angle. As such, the blue-sky albedo (ρ) is made up of the diffuse bihemispherical reflectance, or white-sky albedo (ρ_d), and the direct directional hemispherical reflectance, or black-sky albedo (ρ_b), via a weighting of the diffuse component (K) of radiation and the solar zenith angle (Z):

$$\rho = \rho_d K + \rho_b(Z)\,(1 - K) \qquad \text{Equation 1.3}$$

Equation 1.3 leads to an increasing surface albedo as the solar zenith angle increases, with lower values around noon at the maximum of Z (Gueymard, 2009), but is also dependent on the atmospheric conditions which define K, or the balance between the diffuse and direct radiation.

As forest canopies tend to be darker than surrounding agricultural or open land, an effect enhanced during high-latitudinal winters due to snowfall, more incoming radiation is absorbed by the surface, resulting in a local warming. (Bala et al., 2007; R. A. Betts, 2000; Richard A. Betts, 2001; Bonan, 2008a; He et al., 2015; Jackson et al., 2008; Lee et al., 2011; Y. Li et al., 2015). However, albedo varies even within the same land cover class, which suggests studies defining albedo simply by land cover could be a gross simplification and may lead to discrepancies between models and observations (J. Wickham et al., 2015). It has also been shown that the forest canopy can act as a buffer to temperature change, effectively trapping warm air in cooler regions, further exacerbating this warming effect (Rotenberg & Yakir, 2011). A coupling between surface albedo and the ocean is also shown to result in a further cooling, due to increased surface albedo. This results from the higher albedo producing both a cooler and drier troposphere, reducing the amount of LW radiation transferred to the oceans from the atmosphere, resulting in a decreased ocean temperature (Davin & de Noblet-Ducoudre, 2010).

Evapotranspiration and energy exchange

Forests also display a greater surface roughness than open land or agriculture, which plays a key role in both energy and moisture exchanges with the atmosphere, as there is a greater area over which this exchange can take place. The roughness therefore directly influences the ratio between latent and sensible heat fluxes, known as the Bowen ratio. For a forest, a low Bowen ratio suggests that it exerts a high evaporative cooling effect, resulting from a large evapotranspirative flux, enhanced by the larger surface roughness. In the tropics, there is a large incoming solar energy budget, which leads to a high rate of evapotranspiration and thus a large latent heat flux. This gives rise to a high Bowen ratio and a strong local evaporative cooling. This cooling effect dominates the biophysical mechanism and also leads to a radiative cooling effect, as the increased moisture content of the air leads to the production of clouds, which in turn reflect more radiation away from the surface (Bonan, 2008a; Jackson et al., 2008). At boreal latitudes, rates of evapotranspiration are comparatively low and so have a much lower latent heat flux and thus a lower Bowen ratio. Therefore this cooling effect is less influential, allowing the other effects, specifically albedo, to play enhanced roles (A. K. Betts et al., 2007). Where boreal and tropical forests sit at the extremes, temperate forests tend to lie in the middle; neither the warming nor the cooling effects dominate, thus making it difficult to determine the role of such forests in warming or cooling the climate (Bonan, 2008a; He et al., 2015). Such effects on warming and cooling the

local climate have the ability to influence the global climate through changes in circulation and precipitation (Swann et al., 2012).

Forest recovery and succession

Changes in boreal forests lead to large effects on the energy budget of the surface where such changes are amplified by snowfall. The effects of wildfire is a prime example – initially increasing winter albedo (increased snow coverage), while decreasing summer albedo (BC deposition) (B. M. Rogers et al., 2013). Lower surface roughness decreases energy transfer with the atmosphere, resulting in a greater surface temperature and an increase in outgoing LW radiation (H. Liu & Randerson, 2008). As succession progresses, the influence of BC in the summer diminishes in the early stages following a fire, as it is degraded and removed and as vegetation begins to recover, however the enhanced winter albedo continues (Jin et al., 2012). Due to the speed of growth, vegetation in the initial decades following the fire event are dominated by shrubs and saplings which maintain an increased albedo, reduced surface roughness and a strong influence from snowfall compared to mature forests.

The effects on the climate of these biophysical factors changes based on forest structure and composition. North American boreal forests contribute a greater negative forcing than Eurasian boreal forests, where such forests are dominated by species more resistant to crown fires and thus such fires are of lower intensities (B. M. Rogers et al., 2015). The biogeochemical effects of succession after wildfires are yet to be explored in the same context; while initial emissions from the fire itself are considered, the long-term changes in VOC emissions and aerosol production are less explored (B. M. Rogers et al., 2013). Additionally, the effects of succession climatically is less understood in lower-latitudes, where succession can be much more rapid, and as a result of anthropogenic LUC, where the effect on VOC fluxes, aerosol formation and energy fluxes after conversion to cropland is largely unexplored (Bazzaz & Pickett, 1980; Finegan, 1996; Saldarriaga & Luxmoore, 1991).

1.8. Balancing the impacts

The impact of forests on the climate relies on a consideration of each of these factors and any feedbacks between them. Deforestation perturbs each of these processes individually (Table 1.2), altering the balance at both regional and global scales (Figure 1.8). Despite this, many studies focusing on land use change only consider one or two of these influences, leaving many important changes unaccounted for.

The balance between the biophysical warming of forests and the evapotranspirative cooling effect at various latitudes is complex and, especially in the mid-latitudes, possess a lot of uncertainty. Remote sensing and field observations have attempted to assess the local temperature differences between forested and adjacent open areas, taking direct measurements from both locations and attributing the differences to the type of land surface (He et al., 2015; Lee et al., 2011; Y. Li et al., 2015). Despite this, the results from such studies still display considerable variation, from a difference of a few degrees, to less than 1 K across all latitudes (Lee et al., 2011; Y. Li et al., 2015; Montenegro et al., 2009; Peng et al., 2014; Rotenberg & Yakir, 2011).

Table 1.2: Description of some of the effects of deforestation and whether they contribute to an overall warming or cooling effect. These changes vary in magnitude depending on the type of forest and location, so the overall cooling/warming effect can vary accordingly.

Effect of deforestation	Biophysical or Biogeochemical	Warming/Cooling
CO_2 release	Biogeochemical	Warming
Reduced CO_2 uptake	Biogeochemical	Warming
Increase in surface albedo	Biophysical	Cooling
Reduced evapotranspiration	Biophysical	Warming
Reduced surface roughness	Biophysical	Warming
Reduced biogenic VOC emissions	Biogeochemical	Slight warming (warming from reduced aerosol precursors, cooling from reduced ozone and methane formation) (Scott et al., 2018)

While this spatial difference approach has been used extensively in ecological studies, it can have limitations (Blois et al., 2013). It may fail to account for differences in altitude, solar exposure or other localised effects which may influence both plant growth and temperature. However, model-based simulations of deforestation also display a large variation in the regional climate effect of forests, with some studies suggesting a cooling in the temperate region (Bala et al., 2007; Claussen et al., 2001; Devaraju et al., 2015), despite observations suggesting otherwise (He et al., 2015; Montenegro et al., 2009; J. D. Wickham et al., 2013).

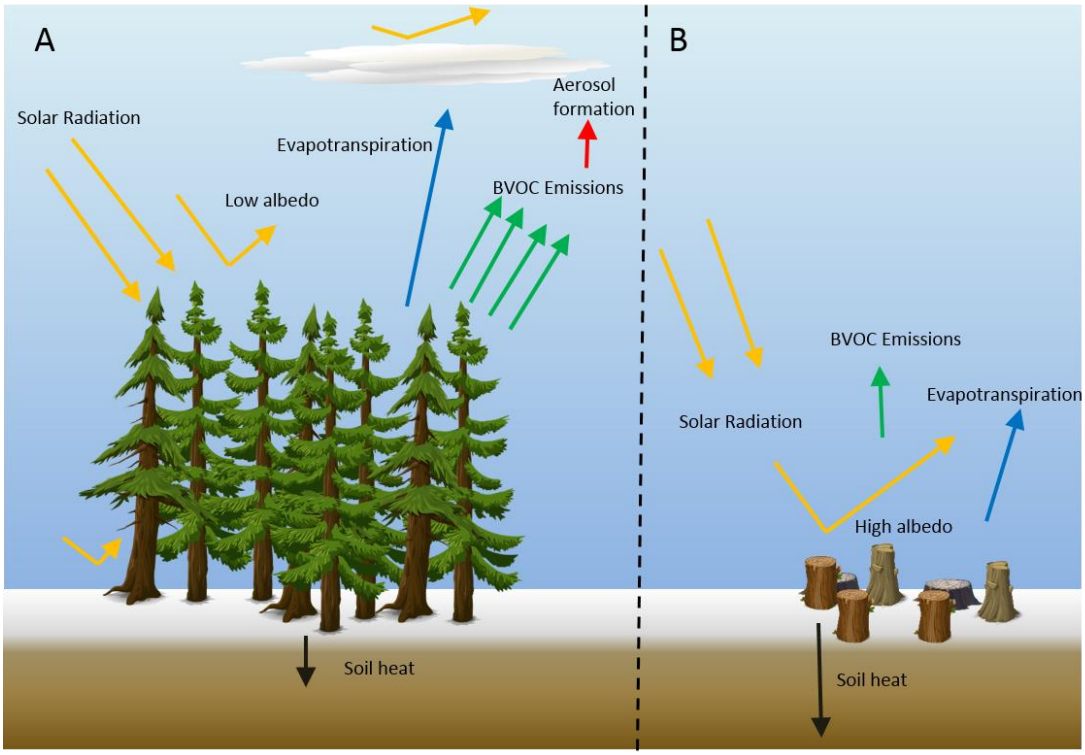

Figure 1.8: Difference in biophysical and biogeochemical factors (A) before and (B) after deforestation occurs. The size of the arrows indicates the direction of the resultant changes. The albedo change is greatest during snowfall at high latitudes.

The magnitude of the warming/cooling effects have also varied between studies, with some suggesting tropical deforestation leads to a larger warming effect than boreal cooling (Bala et al., 2007; Devaraju et al., 2015), while others suggest caution when drawing such a conclusion (Bathiany et al., 2010; Lee et al., 2011; Montenegro et al., 2009). Additionally, differences between modelling studies and observations may be due to the lack of realistic forest cover change portrayed by model simulations (Arora & Montenegro, 2011). Remote sensing, in-situ and modelling studies all suggest a large difference between forests at high latitudes and in the tropics, with boreal deforestation resulting in a local cooling due to the biophysical contribution (Bala et al., 2007).

Using direct satellite observations, Alkama & Cescatti, (2016) assessed the change in land and air surface temperatures from known locations of forest cover change between 2003 and 2012. They observed that areas with 100 % forest loss displayed an increase in annual mean air surface temperature in all regions, except for high latitudinal Eurasia and local regions in high latitudinal North America. They conclude that deforestation in all regions contributes to a specific local warming. The lack of cooling from deforestation in boreal

regions is justified by the fine-scale variations in forest cover, which are measured, therefore large-scale interactions (e.g. ocean-albedo coupling) which may override local temperature variations are not captured.

However, the actual biophysical changes arising from deforestation are yet to be quantified. The multiple roles that global forests have on the local and global climate mean that it is important for any strategy that changes the ecosystem in a dramatic way, to fully appreciate and understand the complexity and then target policy appropriately. However, often the direct CO_2 benefit has been the only consideration when it comes to mitigation policy (Jackson et al., 2008).

1.9. The importance of surface albedo

While the difference in the albedo of forested and non-forested surfaces is widely accepted, there has been discrepancy in the scale of the changes between observations and models. Satellite observations from the Moderate Resolution Imaging Spectroradiometer (MODIS) and in-situ observations through flux towers have been shown to be in good agreement, for various vegetation types across a range of latitudes, and during snowfall (Román et al., 2009; Zhuosen Wang et al., 2014). Availability of data from MODIS has improved the estimates of surface albedo (Rechid et al., 2009).

However, marked differences have been noted between satellite observations and albedos prescribed within climate models from lookup tables, with a number of studies suggesting that the albedos derived from such models are often higher than the observations and overlook key characteristics (Gao et al., 2014; Matsui et al., 2007; Tian et al., 2004; Zhuo Wang et al., 2004). It has been argued that the difference between surface albedo of forest and cropland is simulated as too large, therefore the land use change RF is artificially strengthened in these simulations (Kvalevåg et al., 2010; Gunnar Myhre et al., 2005). During the summer months, these differences are significant, yet remain relatively small, however Oleson et al., (2003) reported that winter values derived from the Community Land Model overestimate albedo by up to 20 %. Additionally, Loranty et al., (2014) concluded that declines in albedo due to tree cover are poorly represented by coupled climate models and tree cover fails to correlate with model albedo.

The importance of surface albedo, and in turn improving the agreement between observations and modelling, has been highlighted by recent quantifications of the relative contributions to radiative forcing from deforestation experiments by Scott et al., (2018). Not

only does albedo change contribute a large negative RF in the high latitudes, resulting in an overall negative RF, the experiments also indicate surface a RF second in magnitude only to CO_2 release on the global scale, mid-latitudes and in the tropics. Thus, better constraining an important radiative climate variable is important at all latitudes.

Chapter 2: Methodology and datasets

This chapter introduces some of the core methodology and datasets used through this thesis, as relevant to chapters 3 and 4. Further data and tools used will be introduced in each respective chapter, alongside any additional information relating to the methods described here where relevant.

2.1. MODIS Data – MCD43A3

Remote sensing of the Earth's surface using instruments onboard satellites has cemented itself as a key tool in understanding the Earth's climate system since initial observations of cloud reflectance and irradiance from Vanguard 2's radiometers in 1959. This has allowed for atmospheric, terrestrial and oceanic observations to be made at temporal and spatial scales that were unachievable before.

Since then, there have been large improvements in spatial resolution of the instruments' viewing area and greater temporal range, as satellite and sensors have increased their durability (and in some cases, outlived their projected lifetime).

From geostationary satellites, such as the Meteosat or the Geostationary Operational Environment Satellite (GOES) series, which provide regular data over specific locations of the Earth, to polar-orbiting satellites (including sun-synchronous orbits; designed to pass over the surface at the same local mean solar time, thus making temporal changes to the Earth system easier to assess) such as the A-train constellation, providing global coverage from their sensors, the number of satellites providing observational data has continued to grow.

Earth observation of surface albedo was acquired from the MODerate resolution Imaging Spectroradiometer (MODIS), aboard the NASA Terra EOS AM-1 and the NASA Aqua EOS PM-1 satellites. Both satellites travel with circular, near-polar, sun-synchronous orbits. Terra crosses the equator in an ascending node at 10:30 and Aqua in a descending node at 13:30. Terra was launched in 1999 as part of the Earth Observing System (EOS) program as the first NASA satellite to study Earth system science, with Aqua following as the earliest of the NASA A-Train satellites, launched in 2002. MODIS supplies data across 36 spectral bands, between 0.4 μm and 1.4 μm, at multiple spatial resolution. In tandem, the instruments provide global coverage every 1 to 2 days with a nadir-viewed 2,300 km by 10 km footprint. Surface albedo from MODIS has undergone multiple verification and intercomparison studies to ensure

good agreement with its observations over a range of surface types (Cescatti et al., 2012; Jin et al., 2003; Oliveira & Moraes, 2013; Zhuosen Wang et al., 2014).

The way a surface scatters incident light is described by the Bidirectional Reflectance Distribution Function (BRDF), which the MODIS algorithm calculates by combining measurements from both MODIS and the Multi-angle Imaging Spectroradiometer (MISR) instruments (Strahler et al., 1996). The spectral albedo of a surface as measured is dependent on both the BRDF of that surface and the scattering profile of the atmosphere that the radiation travels through between source, surface and instrument.

The MODIS product, MCD43A3 version 5, provided surface albedo data at 500 m every 8 days, with each file generated using 16 days of data, centred on the labelled day of the file (Schaaf et al., 2002). Each file provides both black-sky and white-sky albedo for each MODIS surface reflectance band (band 1 to band 7), and 3 broad spectral bands (visible, near infrared, and shortwave). For the MODIS observations presented in this thesis, black-sky, shortwave albedo was used.

Issues with aerosol quantity measurements in MODIS C6 MYD09 and MOD09 surface reflectance products have been highlighted as potentially affecting downstream products, particularly over arid, bright surfaces for version 6 of MCD43 products. It is not believed this issue was existent for version 5, nor should retrievals over the Amazon and South East Asia be particularly affected by this issue.

Previous studies have used both black-sky and white-sky albedo or have combined both with information on the atmosphere's optical thickness to produce blue-sky albedo. Black-sky albedo alone was selected to be used in this study for multiple reasons. Firstly, limitations in processing power limited the ability to utilise both white- and black-sky albedo to calculate blue-sky albedo at the temporal presented scale in this thesis, and as Strahler et al., (1996) explains, as the albedo products are dependent only on the surface and not the atmospheric state, either black- or white-sky albedo products are able to be used to provide true surface albedo. As most ground-based retrievals occur close to solar-noon and under cloud-free conditions, a calculated blue-sky retrieval would be dominated by the directional-hemispheric reflectance, or black-sky albedo, supported by the closer relationship between all-sky albedo to direct retrievals rather than diffuse in Giambelluca et al., (1997). Additionally, at low latitudes, Zhang et al., (2010) found black-sky albedo retrievals from MODIS to show less seasonal variation than white sky, meaning smaller changes are less likely to be masked by the seasonal pattern.

The MODIS observations were gridded on a 0.05° and 0.01° global grid for analysis. The MODIS MCD43 products contain up to 37 % data gaps as a result of cloud coverage, seasonal snow cover and sensor malfunction (N. F. Liu et al., 2013). For each pixel, the mean monthly value was calculated over 3 years at the start (2000-2002 for March to November, 2001-2003 for January, February and December) and the end (2013-2015 for all months) of the study period to improve data coverage. A MODIS water cover mask at 250m was then used to determine the percentage of water cover featured in each gridded analysis pixel. Due to the optical properties of water leading to high surface reflectivity, only pixels featuring less than 10 % surface water were considered for analysis.

2.2. Global Forest Change

Data on forest cover, loss and gain were sourced from the Global Forest Change dataset, first published by Hansen et al., (2013). Using Google Earth Engine, Landsat 7 imagery was analysed using a machine-learning image interpretation method to map areas of tree cover across multiyear periods. Alternative data was used to improve the training of the interpretation. These provide a global map of forest cover for the year 2000, forest loss between 2000 – 2014 and forest gain over the same period at a spatial resolution of 30 m. The forest loss pixels also have a loss year associated, indicating the year the pixel transitioned from forest to non-forest, as defined by Hansen as either “a stand-replacement disturbance or the complete removal of tree cover canopy at the Landsat pixel scale”. Gain pixels were defined as the reverse, the emergence of forest canopy. For each product, trees were defined as vegetation with a minimum height of 5 m. Other definitions and information pertaining to these datasets can be found within the supplementary information of Hansen et al., (2013). Each of these datasets were also gridded to the same 0.05° and 0.01° global grids as the MODIS surface albedo data. As the loss and gain products are produced to supply a binary flag (either loss/gain or no loss/no gain), the percentage loss / gain was calculated over the grid cell and used in all analysis. For the Amazon analysis, the forest cover grid was clipped to the boundary of the Amazon basin using a shapefile from the Center for Geographic Analysis at Harvard University.

2.3. Flight data from field campaigns

Although satellite data now provides unprecedented global coverage on a wide range of remote sensed products, *in situ* data obtained via permanent measurement stations, or field campaigns remain incredibly valuable. Although the spatial (and often temporal) coverage is

not as large as for satellites, with some campaigns only lasting weeks or months, *in situ* data provides fundamental observations with complete understanding of the location and conditions, while allowing for observations that are unable to be measured via remote sensing. Satellite retrievals are also validated against *in situ* observations, laying the groundwork to ensure satellite retrievals provide accurate measurements.

2.3.1. SAMBBA

The 2012 South American Biomass Burning Analysis (SAMBBA) campaign investigated the properties of pollution from biomass burning using a mix of satellite, ground and aircraft measurements, centred on Porto Velho, the capital of the state of Rondônia (Allan et al., 2014; Brito et al., 2014; Marenco et al., 2016). The project was led by the UK Met Office and the National Institute for Space Research (INPE) Brazil, in partnership with seven UK universities (the University of Leeds, the University of York, the University of Manchester, the University of Exeter, the University of Reading, the University of East Anglia and King's College London) and the University of São Paulo. During the campaign, the UK Facility for Airborne Atmospheric Measurements (FAAM) conducted 20 flights while carrying a range of scientific instrumentation to measure various atmospheric properties. The aircraft featured two pyranometers, one upward and one downward facing, which recorded the downwelling and reflected radiation throughout the flights at a rate of 1 Hz. Surface albedo is able to be calculated using the ratio of these measurements. However, as the primary aim of SAMBBA was to investigate biomass burning, a number of the flights that were conducted were over or through areas of fire or smoke from burning biomass, rather than open vegetation. Additionally, issues with airborne pyranometers maintaining thermal equilibrium during flights have been reported previously, due to slow equilibration of the instruments' domes during altitude changes (Foot, 1982; Haeffelin et al., 2001). To account for this, and to minimise the effects of the aircraft's movement on the pyranometer measurements, data featuring regular fluctuations of pitch and roll were chosen to be discarded. This was done by removing data points featuring a pitch greater than ± 10° and a roll greater than ± 15°. Data above an altitude of 1,000 m was also discarded to reduce the data acquisition during plume exposure.

The aircraft feature an optical particle counter, namely a Passive Cavity Aerosol Spectrometer Probe (PCASP) instrument to measure the number concentration of aerosol particles as a function of particle size. Using a helium-neon laser, the scattering properties of

particles that enter the instrument's focused inlet are measured and the size of the measured particle is determined based on the scattering intensity and Mie scattering theory.

Using measurements from the PCASP instrument, data points acquired under high aerosol load were also determined and removed. Combining the number concentration across all 30 bins to provide a total number concentration for each data point, measurements above 6,000 cm^{-3} were discarded, consistent with the third quartile of measurements from the Large-Scale Biosphere-Atmosphere Experiment in Amazonia (LBA-EUSTACH) during the burning season (Guyon et al., 2003).

Measurements from the SAMBBA campaign carried a data flag indicating good data, minor issues, major issues or bad quality data. For the analysis presented here, only data points featuring the highest quality data for irradiance and from the GPS/Inertial Navigation equipment were used.

Measurements from each flight were compiled and averaged onto the 0.01° global analysis grid to allow comparison with the MODIS measurements.

2.3.2. GoAmazon

The Observations and Modelling of the Green Ocean Amazon 2014-2015 (GoAmazon2014/5) experiment was another scientific campaign designed to investigate the impacts of human activities, specifically pollution, on a tropical environment (Martin et al., 2016). The campaign was centred on Manaus, the capital of the state of Amazonas, on the bank of the Amazon river. Multiple ground and aircraft measurements were taken in a mix of clean and polluted air across the 2-year study period. The aircraft used during the campaign were equipped similarly to the FAAM aircraft during SAMBBA, with two pyranometers measuring the irradiance throughout the flights. Similar data quality filtering was undertaken, with equivalent data removal based on tilt, roll, high aerosol load and altitude. Additionally, measurements with tilt up to 10 ° were corrected for as described in Long et al., (2010). An additional removal of data featuring clouds was able to take place, to ensure clear sky measurements were taken. Similarly, the measurements were compiled and averaged onto the same 0.01° global analysis grid as MODIS and SAMBBA.

2.4. Determination of forest cover and forest loss

Through much of the MODIS analysis, pixels were defined as either forest or non-forest, and forest loss or no loss, depending on data from the Global Forest Change dataset. Initial

analysis conducted over the Amazon region consisted of analysing the MODIS albedo response with respect to percentage forest cover. By analysing the entire Amazon basin, a steeper decline in surface albedo with increasing forest cover was observed for forest cover greater than 70-75 % for all months (Figure 2.1). In order to determine areas of high forest cover, this change in response at 70 %, cover was used as a lower bound (70 – 100 %) with the upper bound for no forest determined by creating an equally sized bin from 0 % forest cover to 30 %. As the response to percentage forest loss remained linear, the same threshold was applied for the temporal analysis: areas of forest over 30 % which had seen forest loss of 70 % or more were assigned as loss, whereas pixels containing 30 % or greater forest and lower than 30 % forest loss were defined as no loss.

Two main analysis approaches were used to compare the albedo changes. Firstly, a spatial analysis compared forested pixels with non-forested pixels, combining data within the two time periods (2000 – 2003 and 2013 – 2015), except for direct intercomparisons between them. Forested pixels and non-forested pixels were grouped together and the differences in their surface albedo were compared in Section 3.3. The temporal analysis compared each pixel in the 2000 – 2003 period directly with the same pixel in the 2013 – 2015 period to provide a change over time. These were grouped into forest loss pixels and no loss pixels and the behaviour between these two groups were also analysed.

The analysis was undertaken across multiple spatial domains, selected for areas of transitioning forest area to enable the data to be collected and analysed at multiple scales. For each domain analysed, the forest (loss) and non-forest (no loss) pixels were selected for the spatial (temporal) analysis and analysed independently as both an annual average and monthly datasets. Across both analysis type (spatial and temporal) the term Δ albedo (Δα) is used to refer to both the difference between forested pixels and non-forested pixels during the spatial analysis ($\Delta\alpha_s$) and the change in albedo of pixels following forest loss ($\Delta\alpha_t$) during the temporal analysis. As the spatial analysis is conducted to investigate the viability of a so-called spatial-for-temporal approach, whereby spatial differences are interpreted as the result of hypothetical land use change, the use of a general term for both analyses was selected.

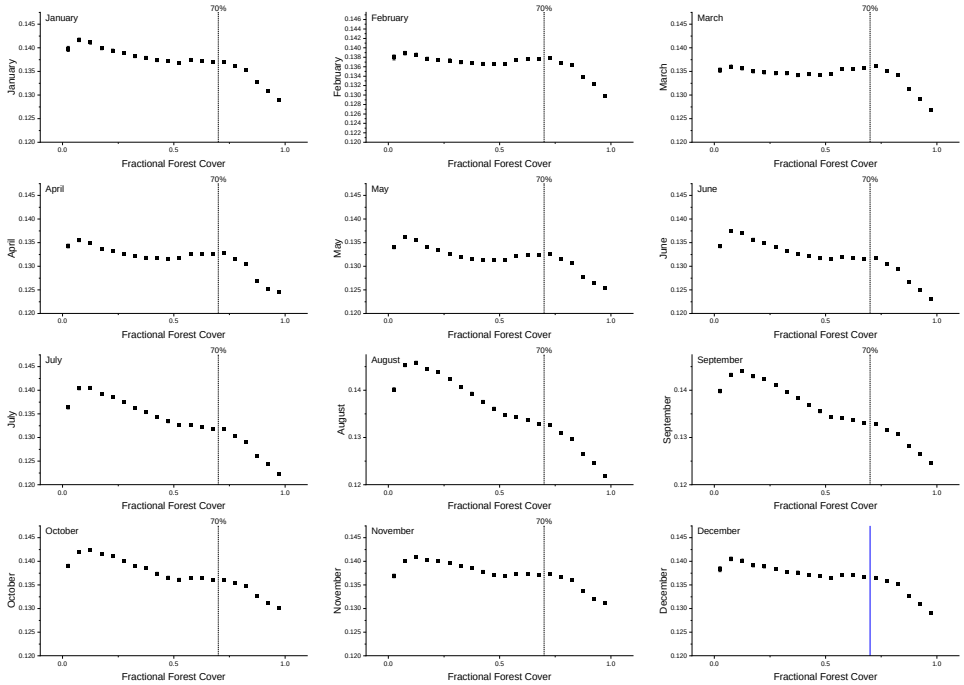

Figure 2.1: Response of surface albedo from MODIS to fractional forest cover for each month. The reference line at 70 % forest cover was decided to be the cut-off for the forest category. Error bars show standard error for each data point.

2.5. Intercomparison between flight, MODIS and in-situ data

To support the observations taken over the Amazon with MODIS, data from SAMBBA, GoAmazon and in-situ measurements from Culf et al., (1995) were used. As the flight and the MODIS data were gridded onto the same 0.01° global analysis grid, spatially overlapping pixels were selected and were categorised into either forest or non-forest based on the selection process described above. To match the data temporally as best as possible, the MODIS grid from September 2013 – 2015 was used for this comparison. Initially, the forested and non-forested categories were directly analysed as for the MODIS spatial analysis. However the pixels from the flight tracks designated as forest outnumbered the non-forest pixels by a factor of 13 from SAMBBA and 15 for GoAmazon, and the number of observations made by Culf et al., (1995) were substantially fewer than those from both flight campaigns. Additionally, non-normality within the flight data strongly reduces the robustness of results from ANOVA, which assumes normality (although the large number of data points means that such tests are still able to provide reasonable information when conducted on the raw data). To adjust for this, the data was bootstrapped with replacement to provide evenly sized, normally distributed datasets. Using these bootstrapped datasets, analysis of the forest and non-forest categories was undertaken to compare the measurement techniques.

Chapter 3: Albedo changes from deforestation in the Amazon

3.1. Introduction

3.1.1. Chapter Outline

This chapter seeks to understand the size of the albedo changes that have previously been reported across the tropics through an initial literature search. Using MODIS satellite observations, the albedo was determined for forested and non-forested areas at a number of sites in the Amazon, and across the Amazon basin at large. These measurements were then used to compare albedo change spatially across the Amazon, spatially as a proxy for time and temporally across the two time periods. Measurements from MODIS were compared to observations from aircraft campaigns, in-situ observations and values from modelling studies.

3.1.2. Amazonian deforestation

Globally, the tropical regions feature the greatest areas of deforestation, with the Amazon contributing the highest of any individual region. Land use change (LUC) in the Amazon has resulted in nearly 20 million ha of forest cleared between 2000 – 2015 due to pressure from logging, agriculture and ranching (Godar et al., 2015; Moutinho et al., 2016; Sena et al., 2013). Such changes have a variety of local and global impacts on the climate, by altering carbon stocks, emissions of biogenic volatile organic compounds (bVOCs), and the surface energy flux through evapotranspiration, surface roughness, and albedo (Heald & Spracklen, 2015; Y. Li, Zhao, et al., 2016; Pan et al., 2011; Le Quéré et al., 2009; Scott et al., 2017; Spracklen et al., 2008; Stocker et al., 2013). Forested areas also have a lower surface albedo than crop and grassland, therefore deforestation results in greater reflection of incoming radiation, producing a local cooling effect (Bala et al., 2007; Bathiany et al., 2010; Richard A. Betts, 2001; A. Wang & Price, 2007). Through altering the energy balance in the atmosphere, and a coupling with the ocean, a wider cooling effect is also modelled (Davin & de Noblet-Ducoudre, 2010).

The magnitude of the local effect is heavily latitudinally dependent, due to the influence of snowfall in the high and mid-latitudes, which exacerbates the difference in albedo between forested and non-forested land during the winter months (R. A. Betts, 2000; Lee et al., 2011; G. Myhre & Myhre, 2003). As such, it is suggested deforestation may cause a biophysical cooling in the high latitudes, while still producing a warming in the tropics due to the strength of evapotranspirative cooling (Y. Li et al., 2015). Comparisons between different levels of tree

cover have demonstrated cooler temperatures over forested areas when compared to non-forested land in the tropics (Lawrence & Vandecar, 2015; Y. Li et al., 2015).

Many previous studies have investigated how surface albedo varies between forest and non-forest at mid to high latitudes, where the differences are at their greatest magnitude (See section 3.2.2 and Appendix A), but there have been few studies investigating the impact of albedo in the tropics; the world's most heavily deforested regions. This work seeks to address that by bringing together previous observations with data from MODIS and two flight campaigns for analysis.

The albedo effect from land use change at high latitudes has been regarded as an important climate driver both locally and radiatively, but recent work has highlighted its relative importance in the tropics too. Scott et al., (2018) model idealised deforestation scenarios globally and across the boreal, temperate and tropical regions, calculating the radiative forcing (RF) from changes in CO_2 concentrations, short-lived climate forcings (SLFCs) concentrations, and surface albedo (Figure 3.1). The albedo changes were shown to contribute the largest RF in the boreal regions and was the next-largest after CO_2 globally and for the other regions.

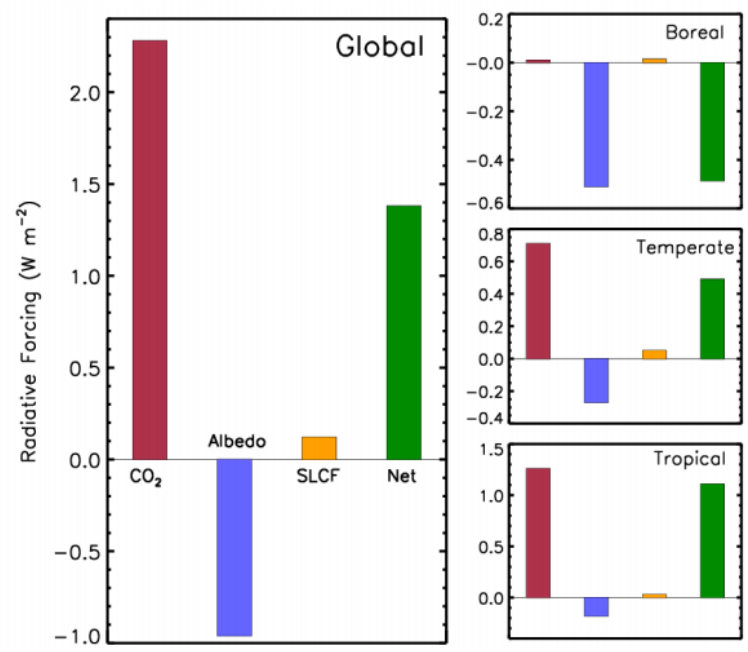

Figure 3.1: Global annual mean radiative forcings (RF) due to changes in concentrations of CO_2 (red), SLCFs (orange) and surface albedo (blue) under global and regional deforestation scenarios. Source: *(Scott et al., 2018)*

3.1.3. Previous albedo measurements

While the decrease in albedo post deforestation is widely accepted, there has been some discrepancy between observations and modelling studies on the scale of the change. Observations of surface albedo from flux towers and the Moderate Resolution Imaging Spectroradiometer (MODIS) instruments have been shown to be in good agreement across a range of vegetation types and latitudes (Román et al., 2009; Zhuosen Wang et al., 2014). However, observational values have been shown to be lower than prescribed values for specific plant functional types (PFTs) in land surface models (Loranty et al., 2014; Matsui et al., 2007). Additionally, models lose much of the complexity of the vegetation surface by employing a certain homogeneity within PFT classes, whilst behaving differently between different models (Matsui et al., 2007; Tian et al., 2004).

Observations of albedo have previously been limited to spatial-for-temporal analysis, where spatial differences are assumed to act as a proxy for temporal changes. However contrasting spatially-comparable regions of high and low forest cover may introduce biases by potentially overlooking certain geographical climatic influences (Alkama & Cescatti, 2016a; Culf et al., 1995; Y. Li et al., 2015; de Oliveira et al., 2016; Oliveira & Moraes, 2013). This study aims to overcome this, by directly tracking albedo changes during periods of active deforestation using satellite observations.

3.2. Literature search

Using the scientific library Web of Knowledge, supplemented by searches on Google Scholar, a literature search for both modelling and observational studies featuring albedo changes was conducted. Two search strings were used:

"Amazon*" & "Deforest*" & "Albedo"

"Amazon*" "Albedo" "Observ*" OR "Amazon*" "Albedo" "Satellite" OR "Amazon*" "Albedo" "Tower*"

The first search string was designed to highlight studies containing albedo changes due to deforestation, while the second was used to specifically investigate observational studies of albedo over the Amazon region as opposed to modelling experiments.

The requirement for selected documentation was that it was published in a scientific peer-reviewed journal, the literature included values of albedo (or albedo change between categories) for tropical, evergreen broadleaf forest and grassland or crops and must include

analysis of the Amazon, at least in part. From the initially highlighted papers, a number were rejected due to non-specific attribution of values across the scenarios and shared model setup between studies. Whilst many of the papers identified reported multiple simulations, generally one set of values was used, unless there were specific differences between the simulations (e.g. different replacement vegetation). This filtering resulted in albedo values of the difference between forested and non-forested (Δ albedo) being obtained for 55 modelling studies and 13 observational studies (Figure 3.2). The studies and values obtained are presented in Appendix A.

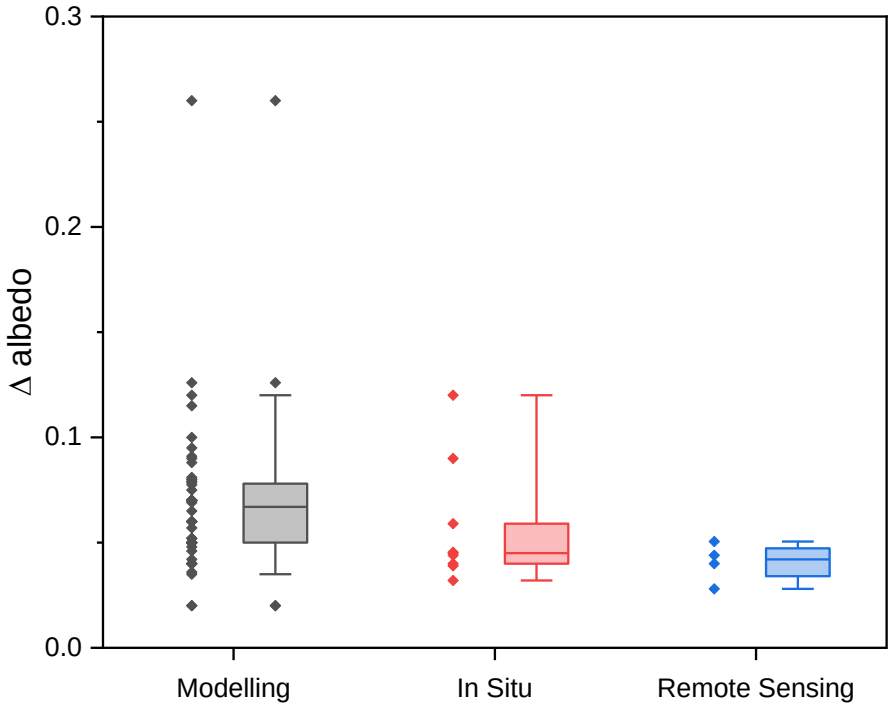

Figure 3.2: Surface albedo differences (Δ albedo) between tropical forest and an equivalent deforested land cover from a systematic search of the literature using the Scientific library, Web of Knowledge highlighting modelling studies (n = 55), *in situ* (n = 9) and remote sensing (n = 4) studies.

3.2.1. Modelling values

A total of 55 simulations using a range of global circulation models (GCMs), land surface models (LSMs) or earth system models (ESMs) were identified containing albedo values from forest and an alternative vegetation surface in the Amazon region. Most (92 %) of the simulations were designed to analyse deforestation scenarios, converting evergreen broadleaf forest across the region into different vegetation (Figure 3.3). Simulations

compared evergreen broadleaf forest to a mix of grassland (57.1 %), pasture (23.1 %), bare soil (10.7 %), soybean (5.4 %) or using a forced albedo increase (3.6 %).

Whilst albedo differences from forest for both grass and pasture yielded similar averages (Table 3.1), the grass simulations displayed a larger diversity, with a range from 0.02 to 0.10, as opposed to 0.046 to 0.081 with pasture. Soybean simulations averaged slightly higher (0.073), however only a small number of simulations modelled this change. Both Costa et al., (2007) and Sampaio et al., (2007) highlight how variable soybean albedo is in relation to its growing season, with high peaks at certain points through the year (Andre & Viswanadham, 1983; Blad & Baker, 1971; Fontana et al., 1991). It is also suggested that the practice of double cropping may increase the albedo for longer periods throughout the year, were it to be employed, creating a greater albedo difference than for grassland and pasture.

Table 3.1: Mean albedo change for different replacement vegetation from modelling studies following deforestation.

Replacement vegetation	Number of studies	Mean albedo change	Coefficient of Variation
Grass	32	0.0601	0.5368
Pasture	13	0.0612	0.1667
Bare Soil	6	0.1248	0.3259
Soybean	3	0.0733	0.1849
Forced albedo increase	2	0.0600	0.2318

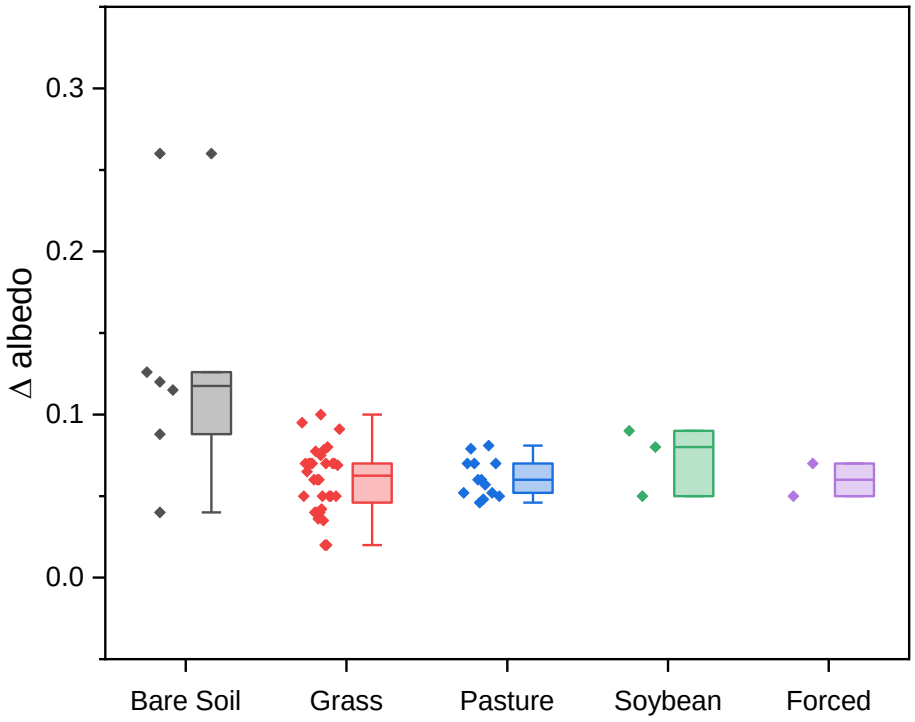

Figure 3.3: Published values of albedo differences within model simulations between Evergreen Broadleaf Forest and alternative vegetation types, generally used as a replacement in deforestation scenarios.

The simulations that forced albedo values without specifying a resultant vegetation type are most likely to have mirrored the replacement of forest with grass or pasture, given the average of 0.060. Simulations resulting in bare soil display the greatest values of the simulations, with an average albedo difference of 0.125.

3.2.2. Observational values

Observations of the surface albedo of tropical forest taken in-situ are provided by use of an albedometer, which consists of an upward and a downward-facing pyranometer. The upward-facing pyranometer measures the global solar radiation, whilst reflected solar radiation is measured via the downward-facing pyranometer. The surface albedo is then given as the ratio between the reflected and the incoming radiation.

Attaching an albedometer to a mast allows for the instrument to be raised above the forest canopy, and thus measurements of the albedo of the forest's surface. Many initial studies in

albedo measurements were taken at high latitudes, often over snow-covered surfaces with a lack of tropical vegetation measurements undertaken. Values used in GCM simulations across the tropics were initially taken from measurements conducted at higher latitudes (Oguntoyinbo, 1970). Those that did feature vegetation in the tropics were limited to cultivated crops, overlooking the albedo of natural vegetation and forest.

In 1995, Culf, Fisch and Hodnett analysed albedo measurements from the Anglo-Brazilian Climate Observational Study (ABRACOS). This featured multiple sites in the Brazilian Amazon to compare pasture on ranch land and forest over a three-year period, building on previous observations in the region from Bastable et al., (1993) during the Amazon Region Micro-meteorological Experiment (ARME), and Bastable et al., (1993). Prior to Culf et al., (1995), albedo values for deforested areas used in deforestation experiments were taken from measurements over the vegetation type assumed to replace the forest.

This experiment was the first to measure albedo from deforested land in the Amazon region and directly compared three forest-reserve sites to three post-deforestation cattle ranch sites. The long-term nature of this study allowed for observations of the seasonality of the absolute forest albedo, while the pasture sites remained stable throughout the year.

Culf et al., (1995) presents higher forest albedo values, and lower pasture value (by 0.134 and 0.180 respectively) than those used in GCM experiments; highlighting albedo changes may be too high in many of the highlighted experiments.

Wright et al., (1996) built on the ABRACOS experiment results, with the seasonal variation of the forest albedo shown to correlate with soil moisture and suggestions of variation in the pasture sites' albedo being explained by the amount of dead leaf material, whilst being independent of the height of the pasture grass. The ARME data was also furthered by Eltahir & Humphries, (1998), with an albedo difference between forest and pasture of 0.04 - 0.05.

Progressive recovery of vegetation after deforestation was analysed by Giambelluca et al., (1997) at a single site within the Amazon. The albedo of secondary vegetation decreased with time since abandonment from 0.175 for unused pasture, to 0.163 as secondary vegetation recovered over 2 years. Advanced secondary vegetation (10 years growth) is shown to be in line with values of primary forest (0.132). All of the land cover types post-deforestation were shown to have lower Δ albedo values from primary forest than those simulated in GCM experiments.

More recently, Oliveira & Moraes, (2013), and Souza et al., (2013) analysed tower measurements of forest, soybean and pasture within the Amazon. Both studies presented greater albedo differences between forest and post deforestation vegetation cover than previous in-situ measurements. Whilst Souza et al., (2013) reported soybean albedo values similar to other resultant cover types (0.15 – 0.22), they also presented forest albedo values lower than the other studies (0.09 – 0.11). The forest site used is a section of *terra firme* rainforest, approximately 180 km east of the Marajó Bay. These forest albedo measurements were similar to albedo measurements found by Carswell et al., (2002) in *terra firme* forest in the Caxiuanã National Forest. In the case of Oliveira & Moraes, (2013), daily mean albedo for forests was reported as 0.12, but measurements over pasture were high (0.24). The paper also used the Surface Energy Balance Algorithm for Land (SEBAL) model to calculate surface albedo from MODIS data, which resulted in forest albedo values in line with previous values (0.133) and pasture albedo values (0.173) similar to Culf et al., (1995). The authors published another set of values at different sites (de Oliveira et al., 2016), featuring albedo values for forest and pasture measured in-situ (0.110 and 0.169, respectively) and estimated using the SEBAL model (0.153 and 0.197 respectively).

Using Landsat, Querino et al., (2016) found an albedo change within areas deforested between 1991-2011 of 0.08, with no change found in areas with no deforestation. Similarly, Loarie et al., (2011) compared pixels from MODIS albedo data with the INPE's PRODES annual deforestation summaries for 2002, 2004 and 2006 and found pixels changes incurred an average albedo change of ~0.028.

Of the observational studies highlighted, 69 % presented in-situ measurements, with 31 % remote sensed. The remote sensing studies display an average albedo difference of 0.041, while the in-situ values are higher and closer to the modelling average for grass at 0.057. However, this is influenced by the high value from Oliveira & Moraes, (2013), which if removed brings the average (0.049) in closer agreement to the remote sensing measurements.

The observational studies display an average albedo difference lower than all the modelled land cover differences, only with the inclusion of the Oliveira & Moraes, (2013) value, does this value fall in a similar range to the lowest vegetation transition (forest to grass).

3.3. Results/Discussion

Forest cover and forest loss between 2000-2014 within the southern Amazon basin were extracted from the Global Forest Change dataset, compiled by Hansen et al., (2013), clipped to the Amazon basin using a shapefile from the Center for Geographic Analysis at Harvard University. Areas that had undergone forest loss between the periods 2000 – 2003 and 2013 – 2015 were highlighted as in Figure 3.4. Surface albedo data from the MODIS albedo product MCD43A3 was overlaid on 0.01° and 0.05° analysis grids, with the tree cover data and both the change in albedo after forest loss, and the differences in albedo between forested pixels and non-forested pixels were evaluated.

3.3.1. Domain selection and resolution

Analysis was initially undertaken across approximately 1.5 million km^2 of the southern Amazon at a resolution of 0.05° (Figure 3.4), with a number of areas with high deforestation rates then analysed at higher resolution (0.01°). These selected locations ranged from 4.3 % to 7.4 % of the forested area being lost between 2000 – 2015 (Table 3.2).

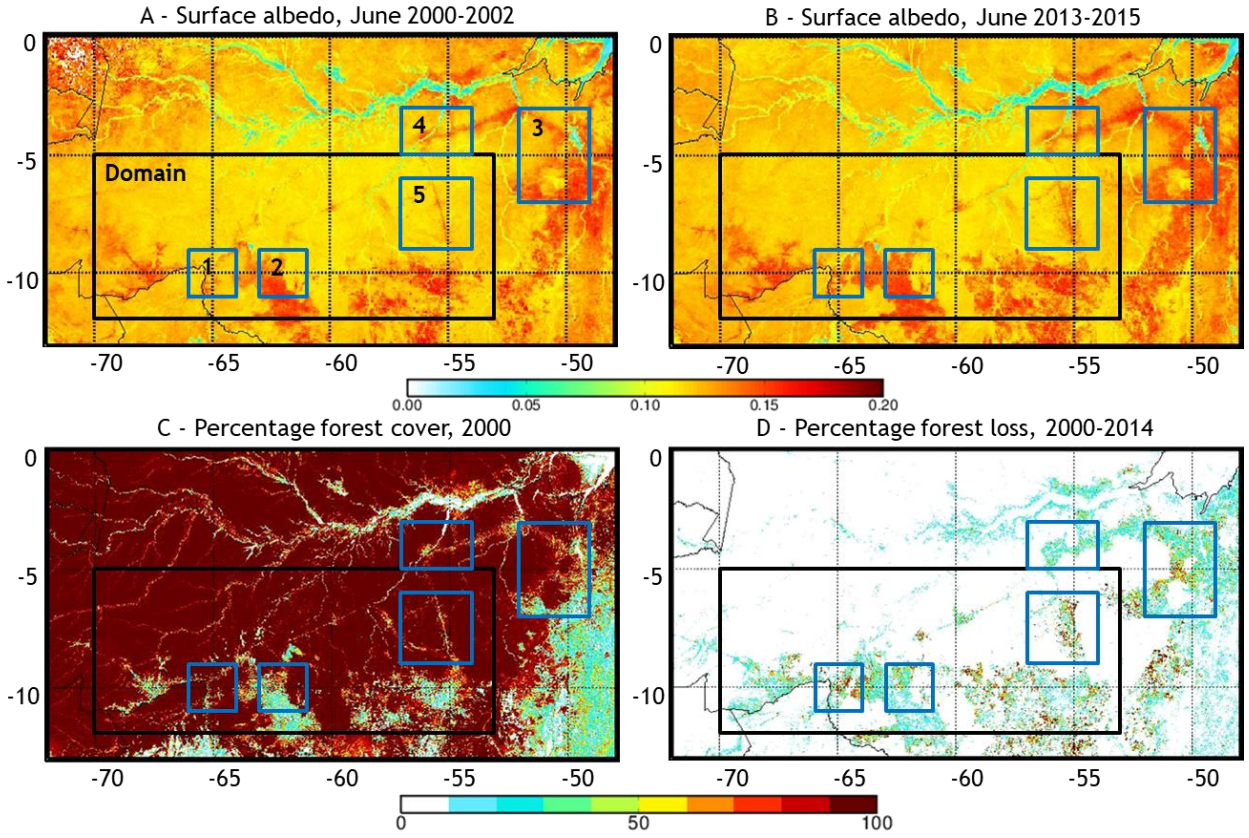

Figure 3.4: Boundary of the 0.05° analysis domain, and the five (1 – 5) 0.01° analysis domains, as labelled in Panel A. Panels A and B display surface 3-year averaged albedo data from the MODIS product MCD43A3 for June. The lower panels (C and D) display percentage forest cover and loss as calculated using the Global Forest Watch dataset.

Table 3.2: Analysed domain and subdomain properties. Values give number of pixels that fall within each category, unless otherwise stated.

Domain name	Top right (latitude, longitude)	Bottom left (latitude, longitude)	Total pixel number	Area / km^2	Forest in 2000	Non-forest in 2000	Forest loss	No loss	Water
Domain	**(-5, -53)**	**(-12, -70)**	**47600**	**1,439,900**	**42,830 (90.0 %)**	**1146 (2.4 %)**	**150 (0.3 %)**	**44671 (93.8 %)**	**0 (0.0 %)**
Subdomain 1	**(-9, -64)**	**(-11, -66)**	**40000**	**48,400**	**36,465 (91.2 %)**	**947 (2.4 %)**	**2951 (7.4 %)**	**30658 (76.6 %)**	**835 (2.1 %)**
Subdomain 2	**(-9, -61)**	**(-11, -63)**	**40000**	**48,400**	**25,720 (64.3 %)**	**7511 (18.8 %)**	**1788 (4.5 %)**	**29914 (74.8 %)**	**239 (0.6 %)**
Subdomain 3	**(-3, -49)**	**(-7, -52)**	**120000**	**145,200**	**83,077 (69.2 %)**	**14673 (12.2 %)**	**5156 (4.3 %)**	**84294 (70.2 %)**	**4346 (3.6 %)**
Subdomain 4	**(-3, -54)**	**(-5, -57)**	**60000**	**74,000**	**56,029 (93.4 %)**	**1,520 (2.5 %)**	**14,962 (24.9 %)**	**42,534 (70.9 %)**	**2051 (3.4 %)**
Subdomain 5	**(-6, -54)**	**(-9, -57)**	**90000**	**108,900**	**87,043 (96.7 %)**	**811 (0.9 %)**	**3577 (4.0 %)**	**80769 (89.7 %)**	**427 (0.5 %)**

3.3.2. Albedo values

Absolute values

Spatial differences

Forested pixels were defined as containing >70 % forest cover according to the Forest Cover Change dataset. These forested pixels exhibited a median surface albedo value of 0.136, similar to tropical rainforest albedos previously reported (Culf et al., 1995). Pixels featuring low forest cover (those below 30 % forest cover) were defined as non-forested, and at both 0.05° and 0.01° resolution showed higher surface albedo values than forested pixels by 0.018 and 0.017 respectively (Figure 3.5). Overall, the albedo difference between forested and non-forested pixels ($\Delta\alpha_s$) displayed a mean annual average of 0.017.

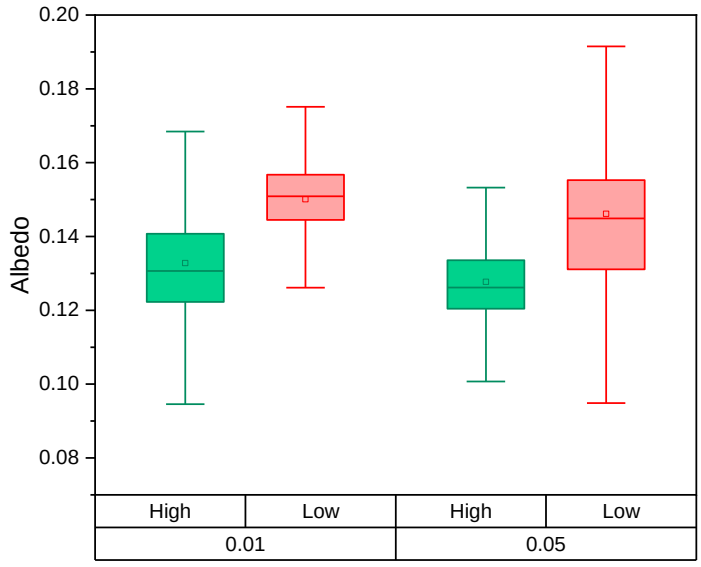

Figure 3.5: Annual mean albedo values for each tree cover category across the large analysis domain (0.05°), and the smaller subdomains (0.01°). Low tree cover categories feature a higher albedo than high tree cover categories. Boxes show interquartile range (IQR), with whiskers extending to minimum/maximum values excluding outliers (exceeding 3 times IQR from Q1 or Q3 respectively).

A clear decline in surface albedo with increasing forest cover was observed across both time periods (Figure 3.6) and within each analysis area (Figure 3.7). The response of the albedo change to forest

cover is broadly linear, however the gradient tended to change close to 100 % forest cover. A similar response is seen between both time periods.

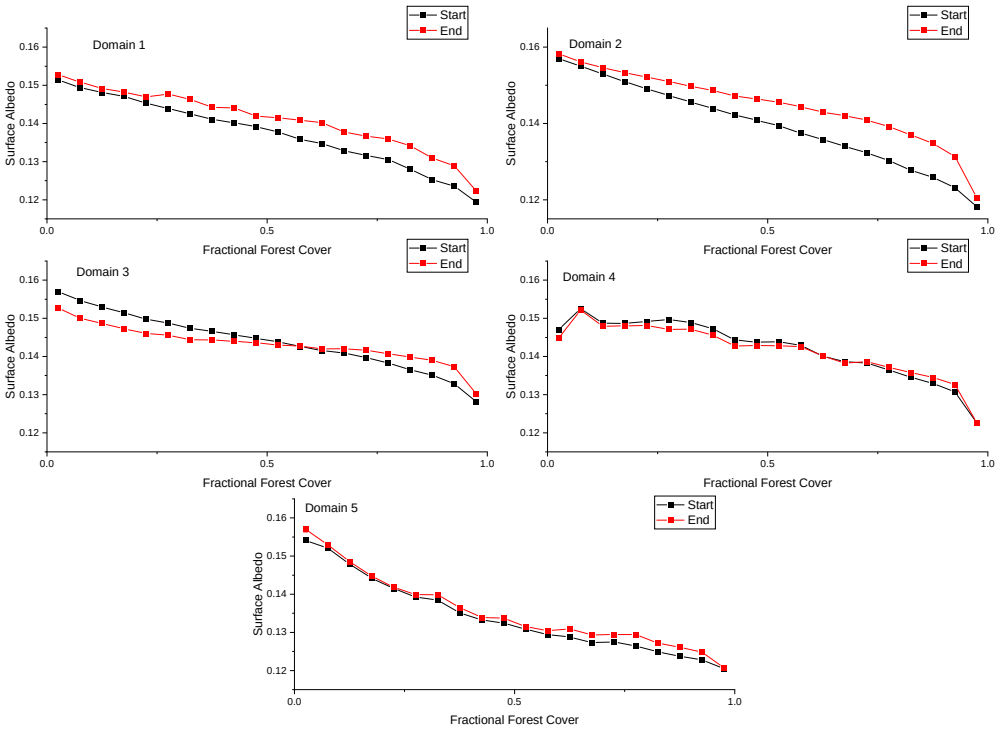

Figure 3.6: Albedo response to increasing forest cover percentage for each of the 5 small analysis domains for the month of July. Start and end refer to the periods 2000-2003 (black) and 2013 – 2015 (red).

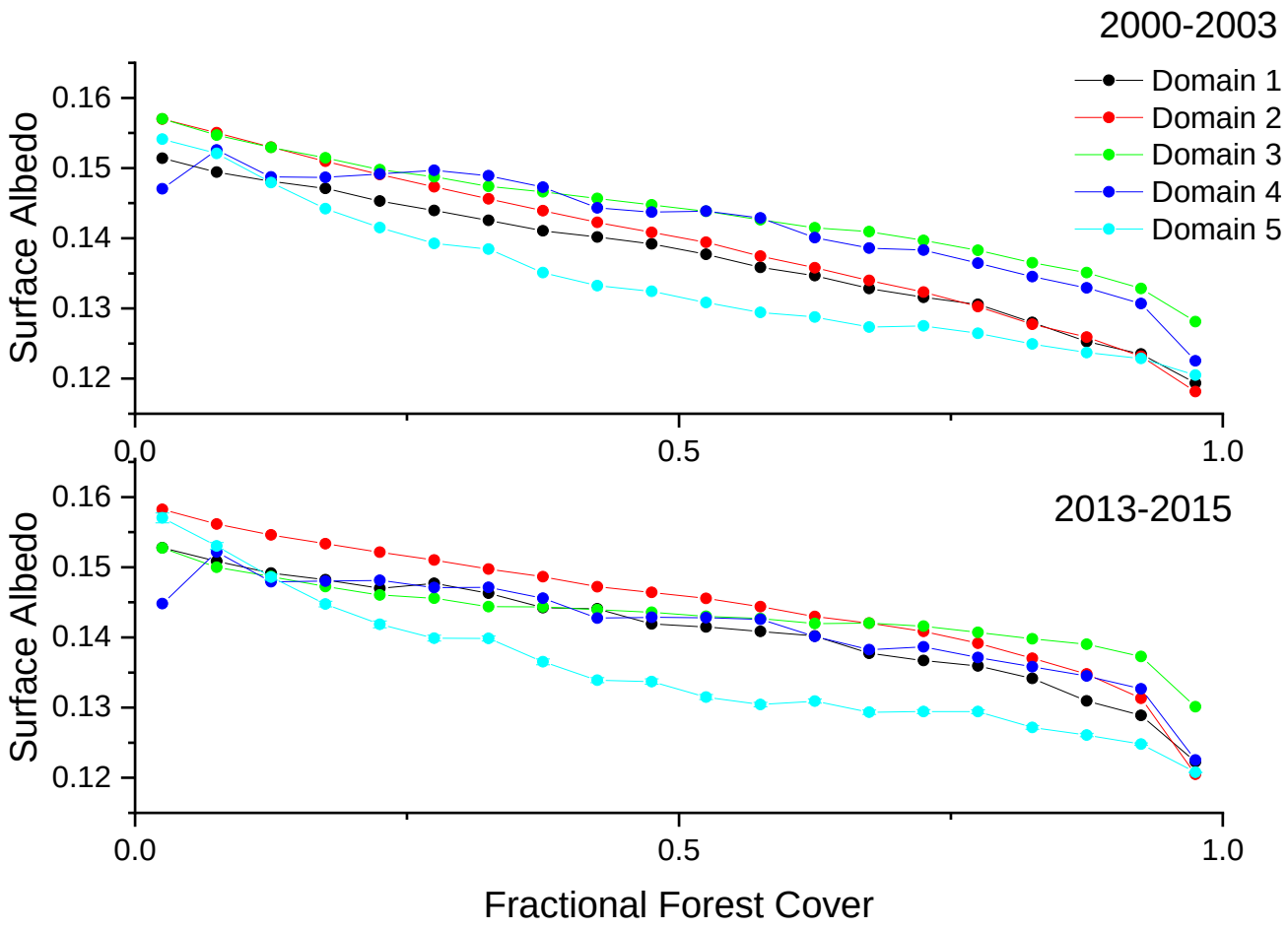

Figure 3.7: Albedo response to increasing forest cover percentage in July for the 2000 – 2003 period (top) and 2013 – 2015 period (bottom). Each small analysis domain is separated out. All other months are shown in Appendix B.

Across the high-resolution subdomains, the annual average albedo of forests was consistent, with the median values averaging at 0.133, the same as measured in Culf et al., (1995). The average surface albedo for non-forest pixels across these analysis domains (0.150) was in line with the lower end of previous observations.

Forested pixels displayed greater variability through the year than non-forest pixels (Figure 3.8), which remained consistently higher than non-forest pixels (Figure 3.9). Forest pixels displayed an increase in albedo through the dry season, leading to a peak in November, while displaying lowest measurements in June.

Figure 3.8 and Figure 3.9 also show little difference was observed between the two time periods, for forest and non-forest respectively. The intra-annual variability is supported by observations from both time periods, with the minimum in forested corresponding to the closest agreement between the periods.

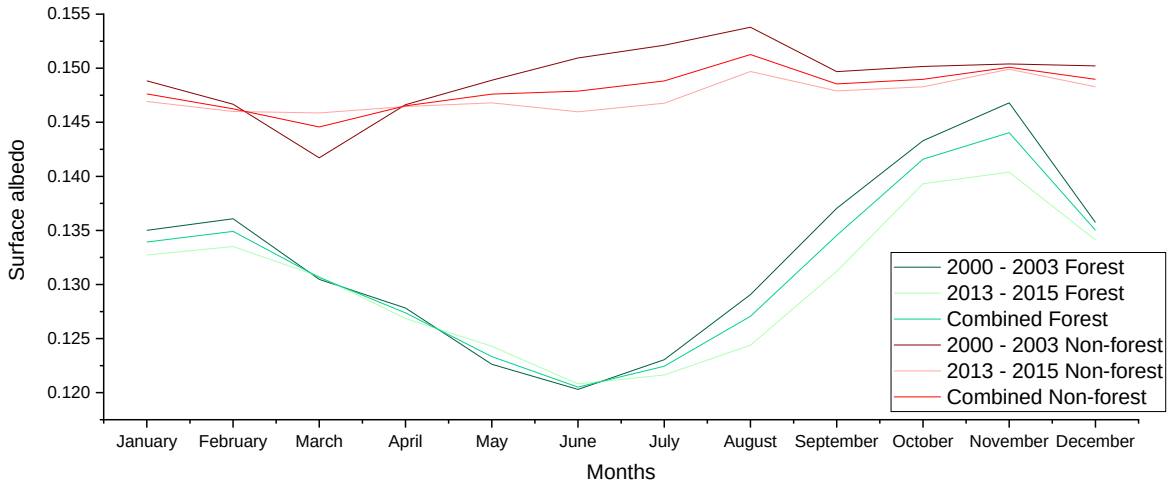

Figure 3.8: Seasonality of albedo observations over forest (green) and non-forest (red) pixels. Data is separated into 2000 – 2003 (dark), 2013 – 2015 (light) and combined (middle).

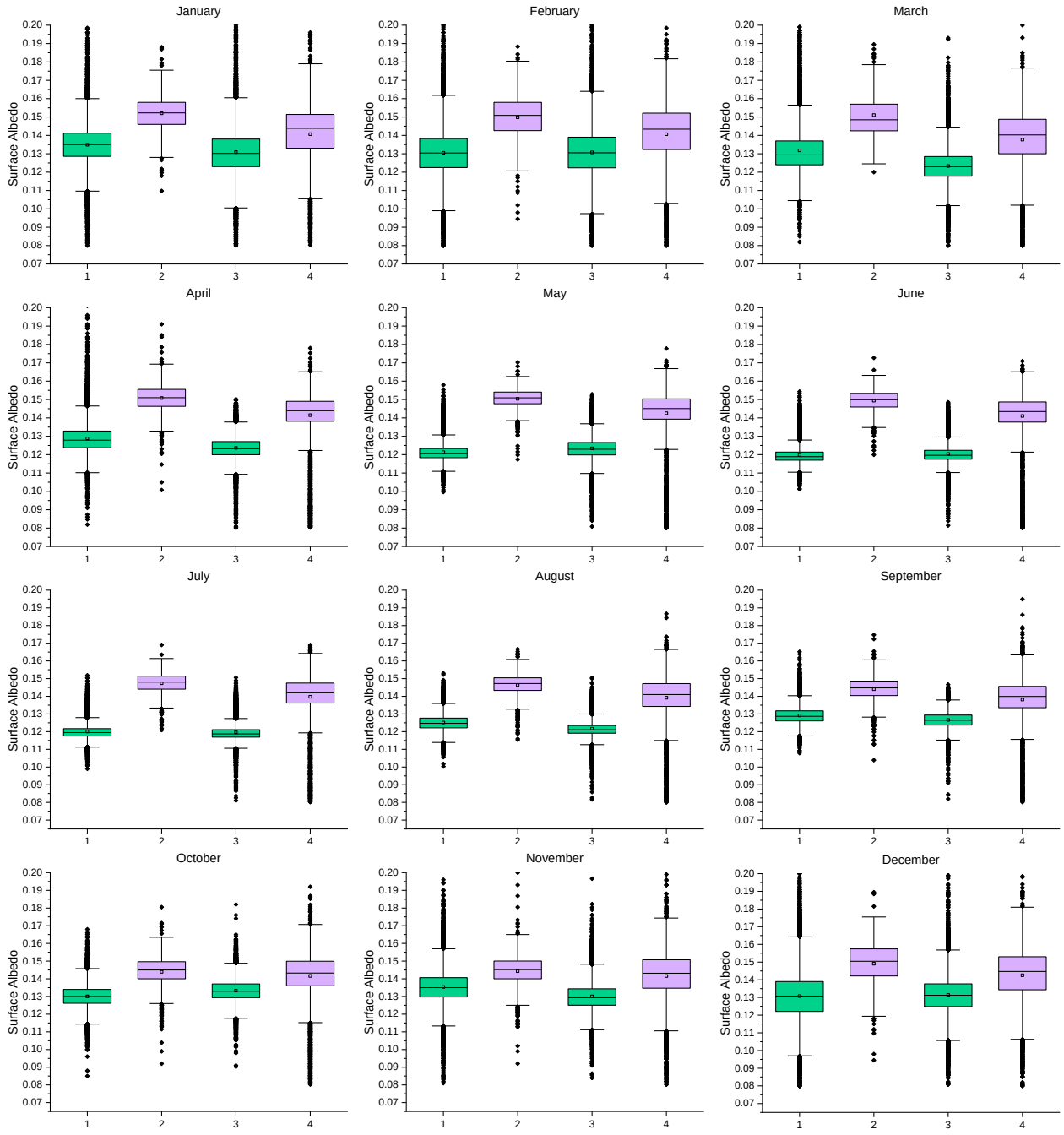

Figure 3.9: Box plots for surface albedo for monthly forested (green) and non-forested (purple) pixels for subdomain 1, separated into the 2000 – 2003 period (labels 1 and 2) and 2013 – 2015 (labels 3 and 4). The boxes display the interquartile ranges with the median line and mean values displayed as a square. Outliers are considered any value more than 3 standard deviations from the mean.

Spatial analysis

Initially, spatial analysis was carried out on the surface albedo observations. This directly compared individual pixels featuring forest with non-forest within the same time periods: 2000 – 2003 and 2013 – 2015 (Figure 3.10).

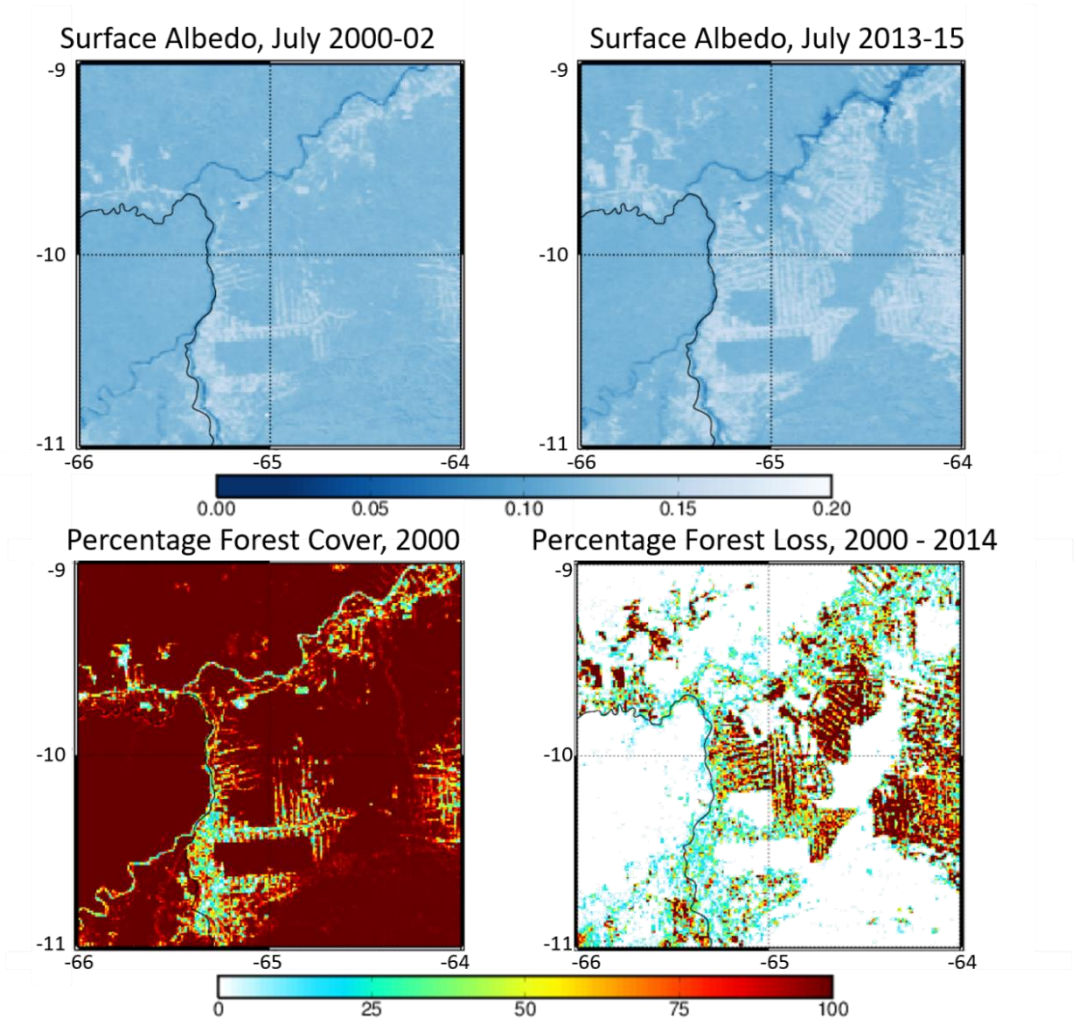

Figure 3.10: Analysis of Subdomain 1, with MODIS surface albedo in the top two panels, with percentage forest cover and loss in the lower two panels. Spatial analysis compared pixels featuring different forest cover (designated by the bottom left panel) within the same time periods (either top left or top right panels individually). Temporal analysis used the forest loss (bottom right panel) to assess changes between the start time period (top left) and the 2013-2015 period (top right).

Subdomains 1 and 2 displayed similar albedo values for the high forest pixels, however subdomains 3, 4 and 5 showed slightly higher values (Table 3.3, Figure 3.11). The albedo of the low forest pixels was higher in subdomains 2 and 3 compared to the other locations analysed.

Within each subdomain, higher albedo values were observed for non-forested pixels consistently (Figure 3.11). The difference between the forested and non-forested pixel albedo values ($\Delta\alpha_S$) in Subdomain 2 was considerably higher than in the other locations. Subdomain 2 contained both the smallest area of forested pixels, and the greatest area of non-forested pixels in the year 2000 (Table 3.2), therefore although being geographically close to Subdomain 1, the inclusion of multiple settlements (such as Ji-Paraná) may lead to the increased non-forested albedo.

Table 3.3: Mean MODIS albedo values from spatial analysis of each domain and subdomain across both the 2000-2003 and the 2013-2015 periods.

	Domain	Subdomain 1	Subdomain 2	Subdomain 3	Subdomain 4	Subdomain 5	Average
Forested albedo	0.12773	0.12689	0.12719	0.13947	0.13493	0.13034	0.13125
Non-forested albedo	0.14614	0.14141	0.15104	0.15256	0.14351	0.14425	0.14819
$\Delta\alpha_S$	0.01841	0.01452	0.02385	0.01309	0.00858	0.01391	0.01694

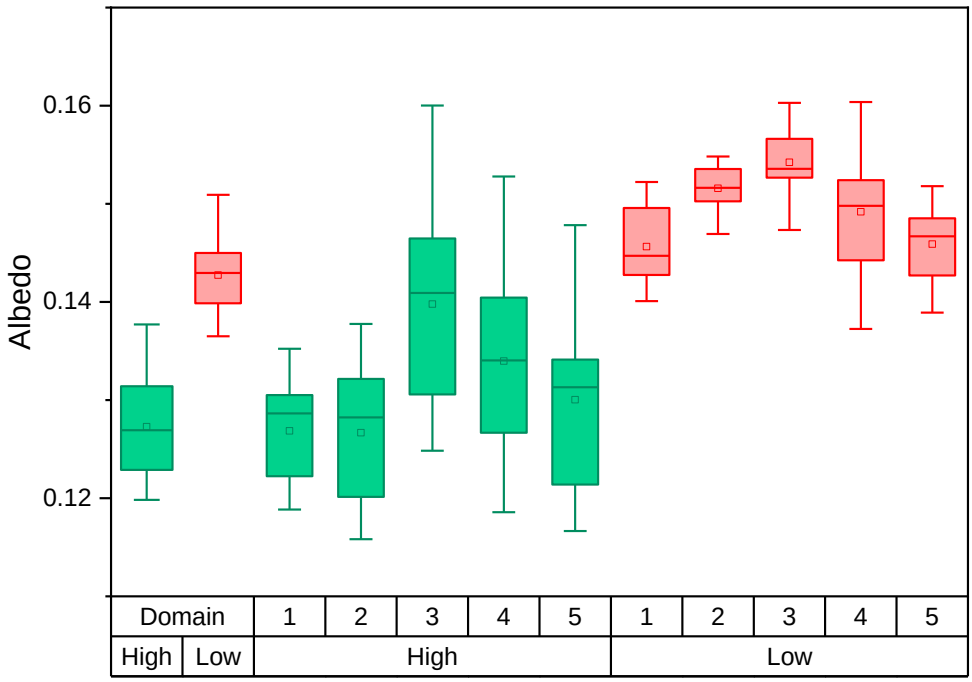

Figure 3.11: Albedo values for high (green) and low (red) forest cover pixels within each subdomain. For each, the high forest pixels display a lower albedo than the low forest pixels. The box limits show the interquartile range, with the whiskers displaying the 5th and 95th percentiles.

Differences between the forested and non-forested albedo of each subdomain were subjected to ANOVA analysis to ascertain whether the differences observed between the subdomains were significantly different from each other. It was found for all pairings that there was no significant difference in the means at the 0.05 level, except for subdomain 2, which presented the highest $\Delta\alpha_S$ values (Figure 3.12) and was shown to differ significantly from subdomains 3, 4 and 5. No significant differences were also observed between the 0.05° resolution domain and the 0.01° resolution subdomains, except for subdomain 2. This suggests that the behaviour in surface albedo between forested and non-forested regions across the Amazon is generally consistent.

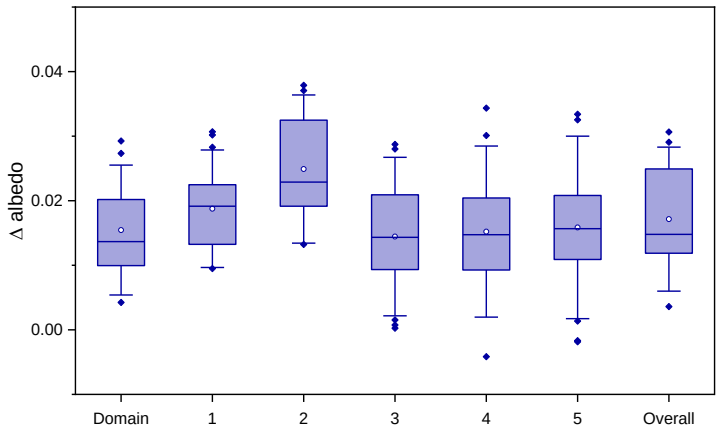

Figure 3.12: Difference in albedo values between forested and non-forested forest pixels for the large analysis domain and each subdomain.

The $\Delta\alpha_s$ values observed across each subdomain peak in May-July, coinciding with the lowest observed albedo values over high forest areas. This declines during the dry season, culminating in a minimum in November; rising as the wet season begins (Figure 3.13).

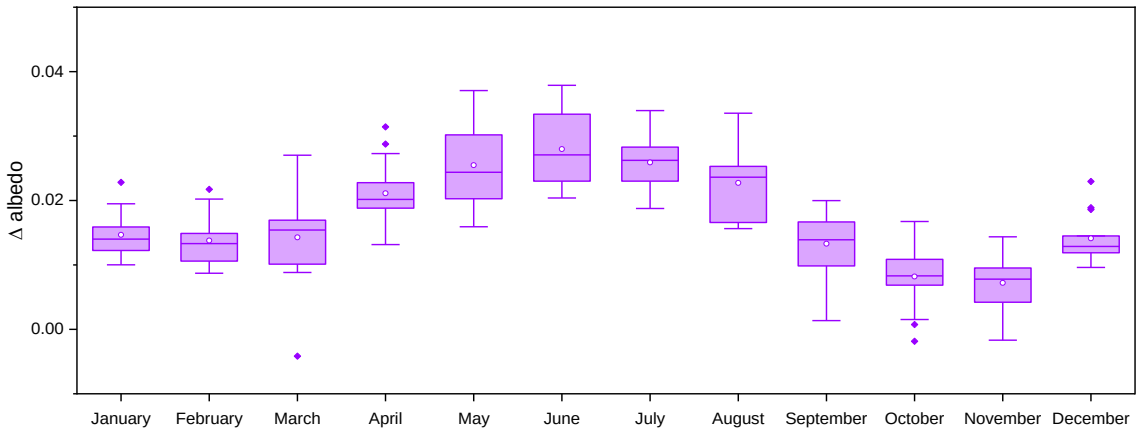

Figure 3.13: Difference in surface albedo values for each subdomain between forested and non-forested pixels.

Temporal analysis

Temporal analysis

Direct impacts of deforestation on individual pixels was then analysed, using a temporal approach. Here, pixels featuring deforestation (forest loss ≥ 70 %) during the analysis period were selected using

the Global Forest Watch forest loss data. The changes between the start and the end (prior and post the forest loss) were analysed against those of unchanged pixels.

Figure 3.8 indicated the similarity between high and low forest cover across the two time periods, but to assess whether any changes in either the surface albedo or the measurements from MODIS have occurred, pixels that have remained consistent with respect to forest cover (≤ 30 % forest loss) were initially analysed within the domains. These differences are presented in Figure 3.14. Subdomain 2 showed a small increase, with the other domains displaying a decrease. Each of the domains only showed a percentage change of 2.8 % (subdomain 4), 1.8 % (subdomain 5) and less than 1 % (large analysis domain and subdomains 1-3).

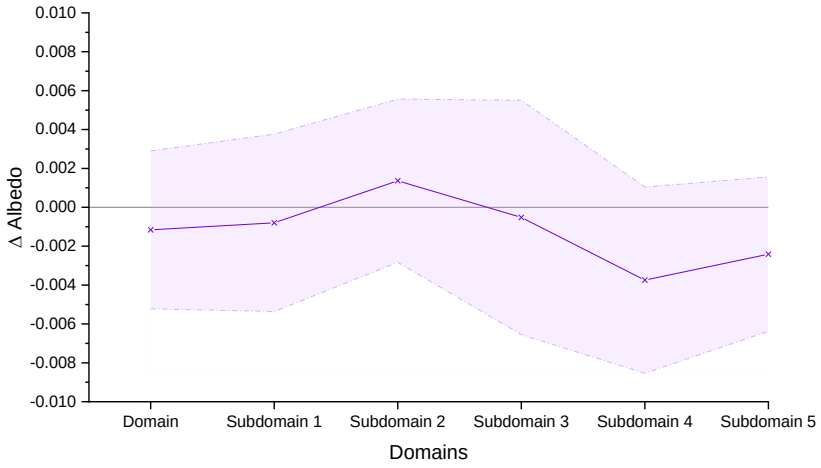

Figure 3.14: Annual mean change in surface albedo for pixels featuring no change in forest cover between the periods 2000 – 2003 and 2013 – 2015. The shaded area represents 3 standard deviations.

Table 3.4 displays the average change in surface albedo after forest loss occurred ($\Delta\alpha_T$). Each subdomain experienced an increase in surface albedo for pixels containing forest loss, with the large analysis domain showing the largest change. Similarly to the spatial analysis, the response of the surface albedo to forest loss was almost linear (Figure 3.15). Following ANOVA analysis, no significant differences were found between any of the subdomain locations, however analysis at 0.05° resolution was shown to differ significantly to subdomains 3, 4 and 5 (all at 0.01°) at the 0.05 confidence interval.

Table 3.4: Albedo change values post forest loss for each subdomain

	Domain	Subdomain 1	Subdomain 2	Subdomain 3	Subdomain 4	Subdomain 5	Average
Temporal Δ albedo ($\Delta\alpha_T$)	0.02096	0.0157	0.0169	0.0113	0.0128	0.0141	0.0153

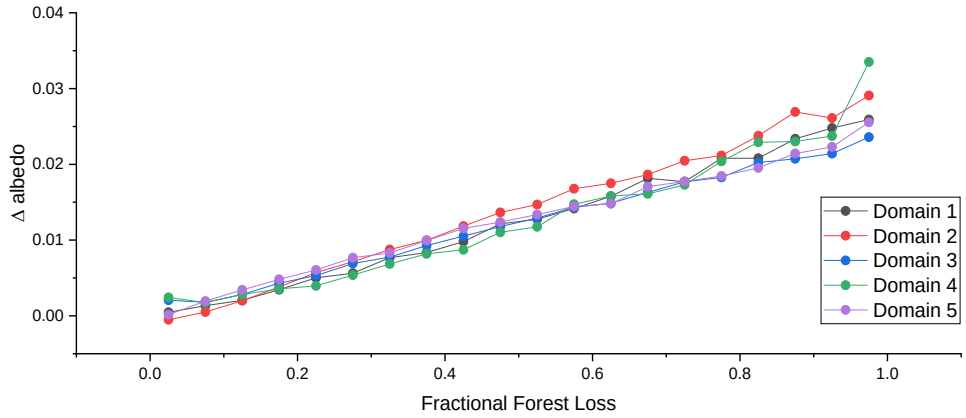

Figure 3.15: Response of surface albedo to the fraction of forest loss within each pixel for every subdomain in July. All other months are shown in Appendix B.

For each subdomain, the temporal analysis shows similar $\Delta\alpha_T$ to the $\Delta\alpha_S$ from the spatial analysis, with subdomain 2 showing the largest difference (Figure 3.16). The two analysis approaches also display similar Δ albedo values for much of the year, with the difference being less than 0.002 for 8 months (Figure 3.17). The seasonal pattern is largely the same for the temporal analysis as for the spatial; the greatest Δα occurring in May to July, with a minimum occurring during the October to November period.

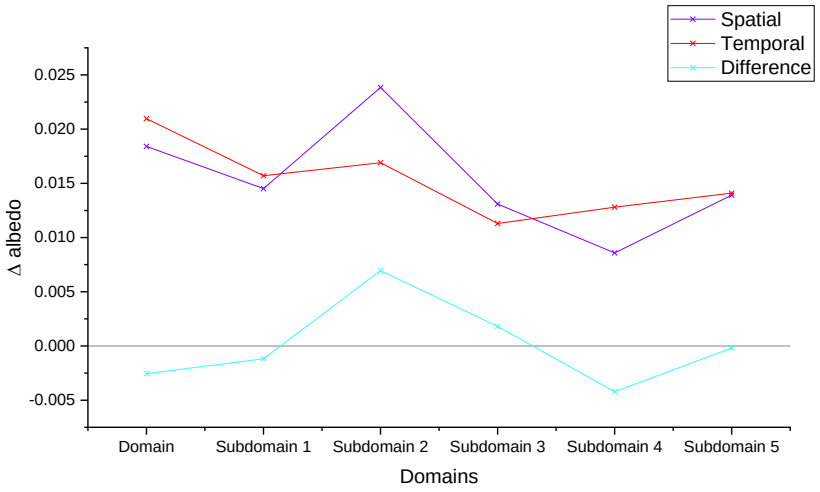

Figure 3.16: Spatial (purple) and Temporal (red) Δ albedo values for each domain, with the difference between both shown in cyan.

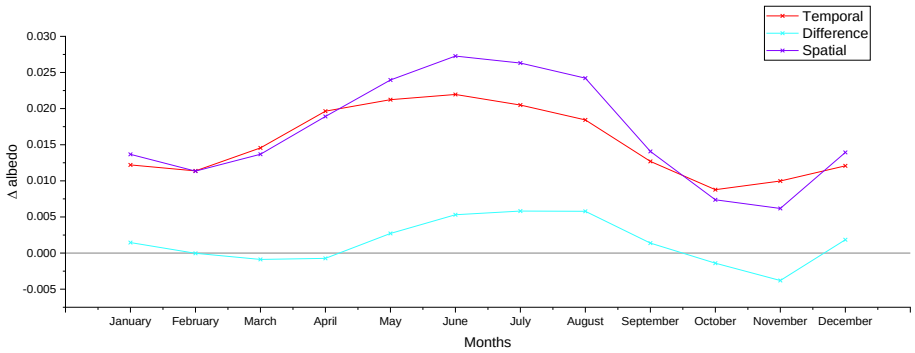

Figure 3.17: Spatial (purple) and Temporal (red) Δ albedo values for each month, with the difference between both shown in cyan.

Flights

Data from aircraft irradiance measurements over the Amazon, during the South American Biomass Burning Assessment (SAMBBA, September/October 2012) and The Green Ocean Amazon Experiment (GoAmazon, 2014/15) campaigns were used to analyse remotely sensed surface albedo measurements within the atmosphere. Flights during SAMBBA took place from Porto Velho, the capital of the state of Rondônia, whilst GoAmazon was centred on the capital of the state of Amazonas, Manaus (Figure 3.18).

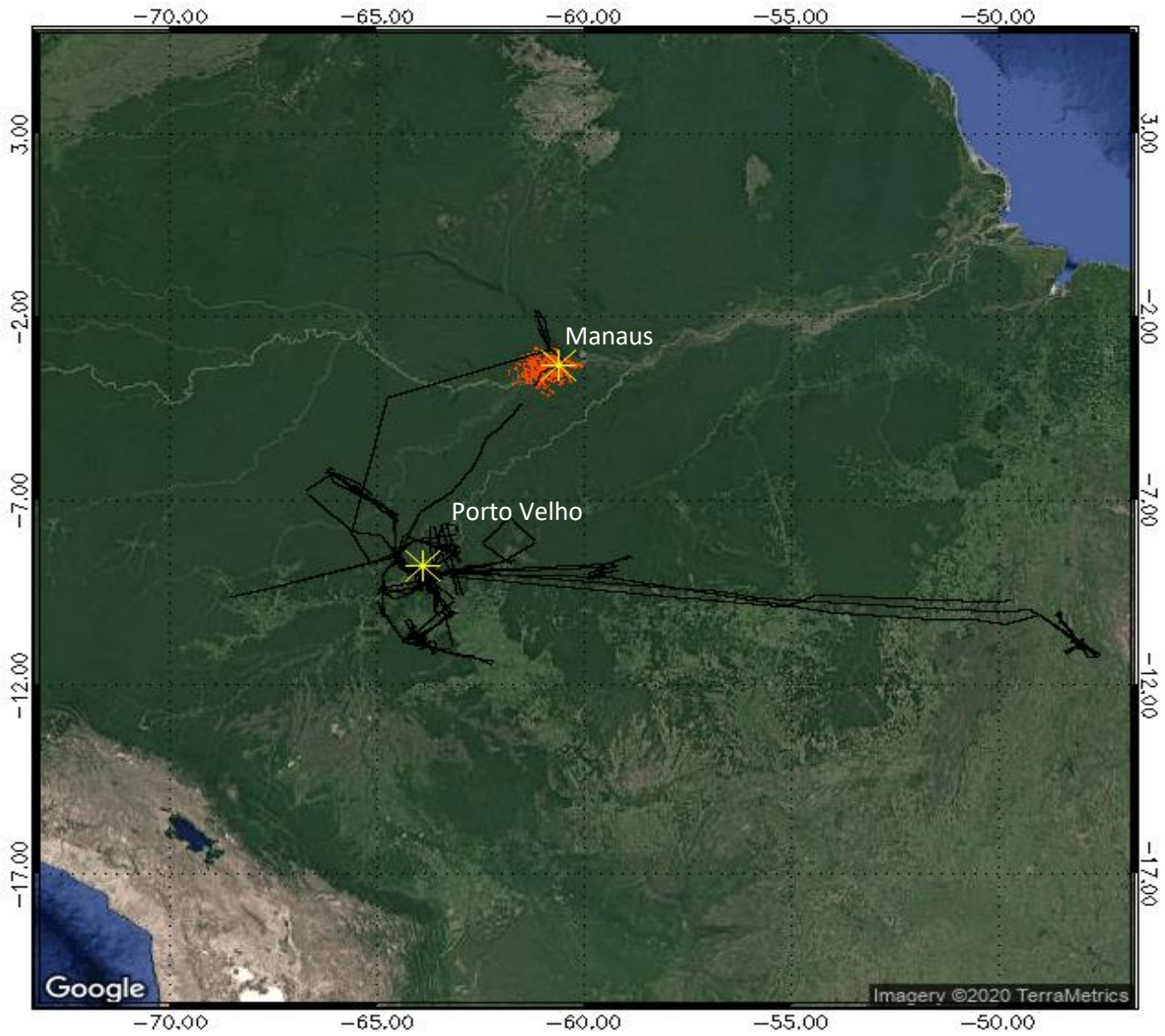

Figure 3.18: Flight tracks from GoAmazon (red) and SAMBBA (black). Manaus and Porto Velho are highlighted as the campaigns' base locations.

Albedo data from the flights was filtered based on quality assurance flags, atmospheric conditions and aircraft navigation data, as described in section 2.3, then placed on the same 0.01° resolution grid as the data from MODIS, with data in overlapping pixels averaged within each campaign. Forested and non-forested pixels were highlighted using the Global Forest Watch dataset (M. C. Hansen et al., 2013).

Measurements from GoAmazon resulted in similar albedo values to SAMBBA (averaging 0.005 higher for high forest and 0.005 lower for the low forest category). Across both flight campaigns, the forested

pixels displayed an average surface albedo (0.157) lower than the non-forested pixels (0.161). However greater variance was displayed in the non-forested pixels (Figure 3.19).

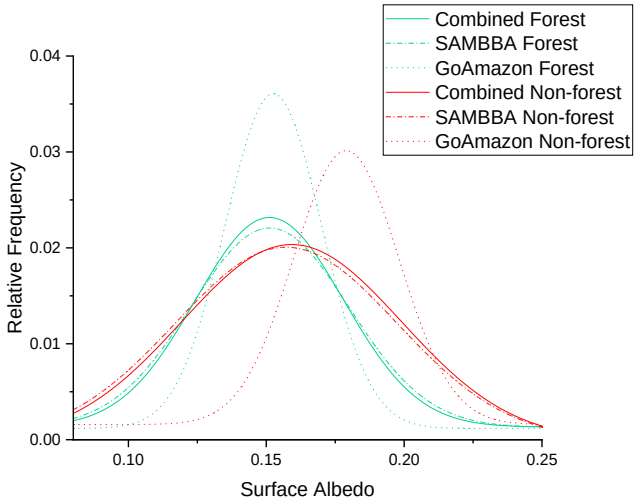

Figure 3.19: Results from the bootstrap of surface albedo for forested pixels (green) and non-forested pixels (red) for SAMBBA (dot-dash), GoAmazon (dot) and both campaigns combined (solid lines)

The flight campaigns provided a much larger range of albedo measurements than obtained from MODIS, and whilst the GoAmazon flights displayed an increase in albedo between high forest cover and low forest cover, the SAMBBA flights appeared to show very little difference (Figure 3.20).

The MODIS pixels across the flight tracks were compared directly to the flight pixels. Figure 3.20 shows that both the forested and non-forested MODIS values are at the lower end of the distributions of the observations made during the flight campaigns. The MODIS values over the flight tracks display similar albedo values for forested and non-forested pixels as the subdomains in the above analysis, however higher variance results from fewer pixels being analysed. This suggests the difference between the flight observations and MODIS results from the observation techniques.

To test this further, in-situ measurements from Culf et al., (1995) for natural forest and cleared land were also compared. The study provided a full set of 3 years' worth of monthly measurements across multiple sites, to which the results from this study could be compared.

Forested pixels from the in-situ measurements were similar to those from MODIS, displaying an average albedo value approximately 0.025 lower than for the flights. However, the non-forested pixels

were shown to have higher values, being only 0.005 higher than the non-forested albedo measured by the GoAmazon campaign.

An ANOVA analysis was performed across each set of measurements. Results from this suggested the mean albedos are significantly different at the 0.05 confidence interval, but individual pairings of the forested in-situ with the forested MODIS (over both flight tracks), the forested SAMBBA and GoAmazon, the non-forested GoAmazon and non-forested in-situ were indicated as not having significant differences at the 0.05 confidence level. This was also true for comparable MODIS categories over each set of flight tracks, and for both forested and non-forested categories measured during SAMBBA – suggesting that there's no significant differences between the means of these measurements.

Both flights produced datasets that were non-normally distributed (Figure 3.22), although normality for the low flight data for both SAMBBA and the combined flights was unable to be rejected based on the D'Agostino's K-squared test for skewness, kurtosis and the omnibus K^2 statistic. However, normality was rejected by both the Lilliefors-corrected Kolmogorov-Smirnov test and the Shapiro Wilk tests.

Since there proved to be a large discrepancy between the size of the datasets, with forested pixels from both flight campaigns numbering fifteen and thirteen times as many non-forested pixels for SAMBBA and GoAmazon, and to address the non-normality of the data, the data was bootstrapped with replacement to provide evenly-sized datasets with normal distributions. For the resulting data, normality could not be rejected using the D'Agostino's K^2, Lilliefors or Shapiro Wilk tests on all but the low tree cover GoAmazon data at the 95 % confidence level.

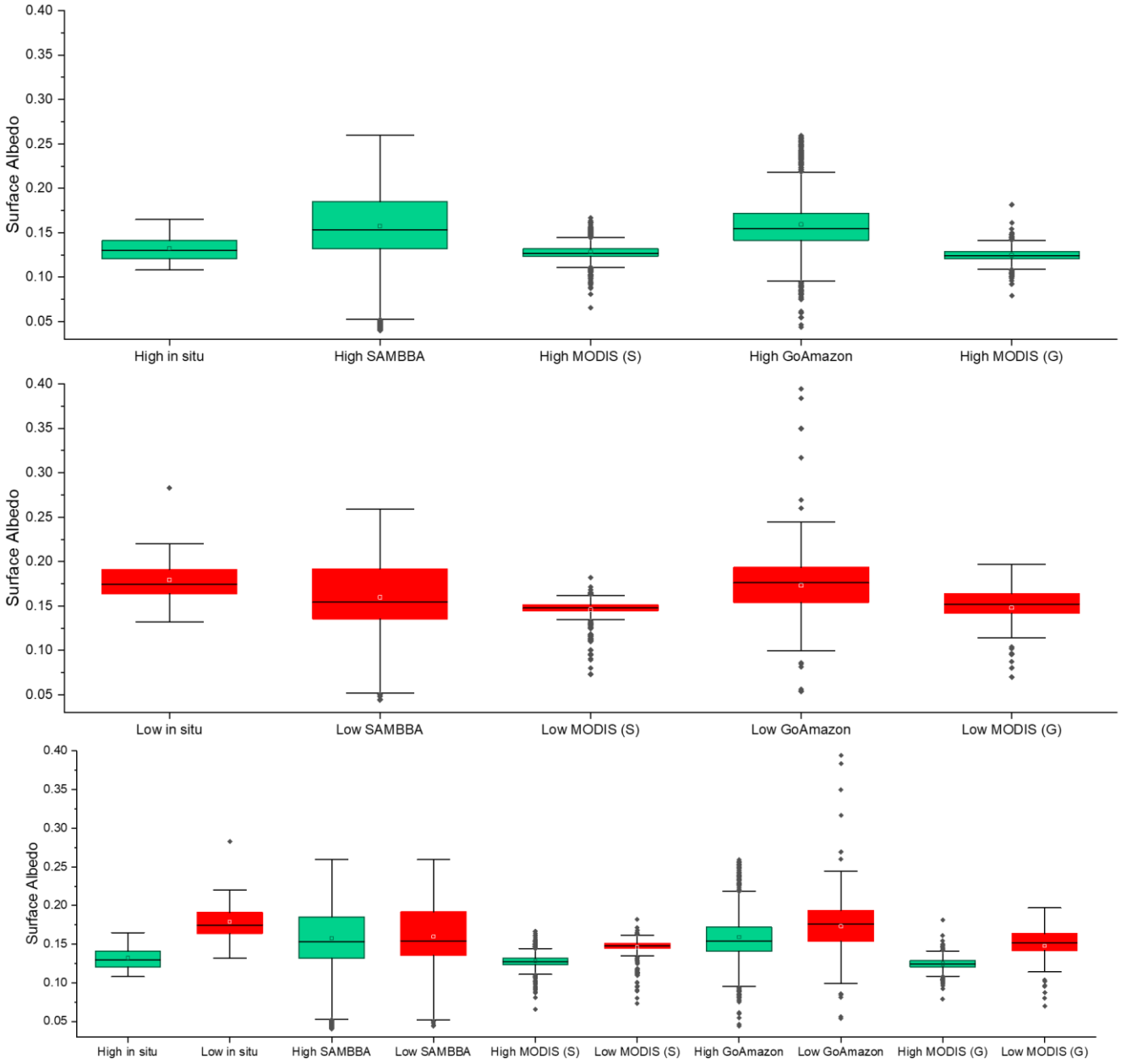

Figure 3.20: Distributions of the measurements used in this section. In-situ data came from *Culf et al., (1995)*, with MODIS data being separated into that recovered over the flight track of SAMBBA (S) and GoAmazon (G). The top panel shows the forested pixels (green), middle the non-forested pixels (red) and the bottom panel combines them both.

Bootstrapping the data reduced the spread across the datasets, reducing the number of outliers and the ranges. However, the means for the flights remained the same, with forested pixels displaying a lower surface albedo than the non-forested pixels (Figure 3.21). This can be reasoned to help reduce

spread from other factors that might influence albedo between measurements, such as atmospheric conditions, differences between surface cover and altitude, that were only partly adjusted for in the processing of the data, as described in section 2.5.

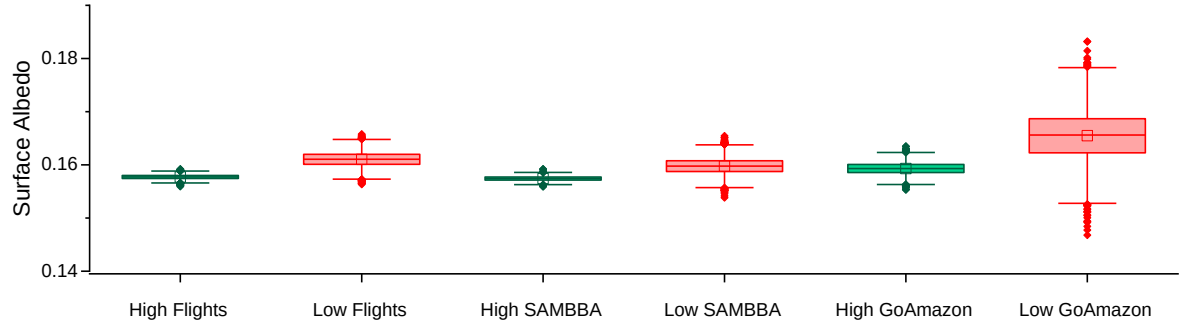

Figure 3.21: Box Plot for bootstrapped albedo measurements from the flight campaigns

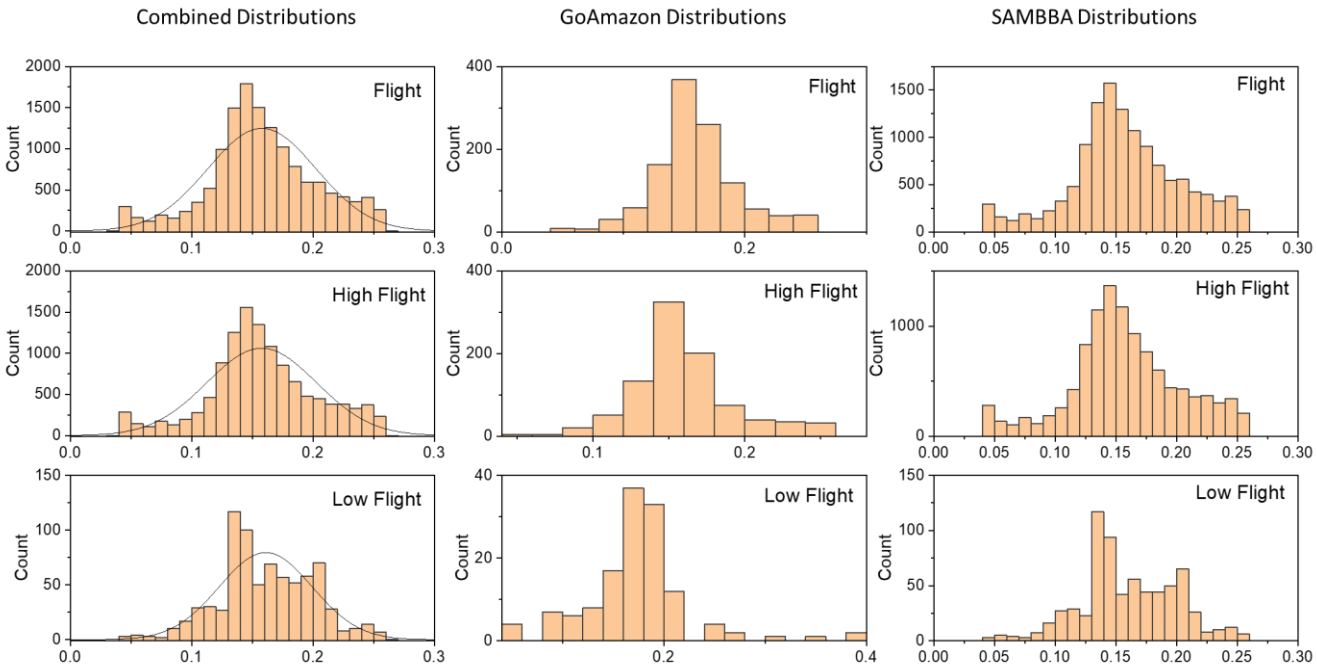

Figure 3.22: Distributions of the raw flight data, displaying the overall flight datapoints (top row), the forested regions (middle row) and the non-forested regions (bottom row).

The forested categories displayed similar means between the two flight campaigns, whilst the non-forested was shown to be higher during the GoAmazon measurements, although the wider range of observations mean that the SAMBBA observations lay within the lower quartile of GoAmazon (Figure 3.23). Due to similarities in observations from MODIS during March and September, this difference is

unlikely due to time of year, in spite of GoAmazon featuring flights during both months. Instead, it was reasoned to be due to differences in the measurement locations, with the SAMBBA flights covering a much greater area (Figure 3.18).

The MODIS pixels across the flight tracks and the in-situ data from Culf et al., (1995) were processed using the same bootstrapping method. Figure 3.23 shows that both the forested and non-forested MODIS values are lower than measured during the flight campaigns. The in-situ measurements are similar in the high tree category to MODIS, but now display the highest albedo in the low forest category. This results in a Δ albedo value of 0.0471 (Table 3.5). As the spread of the data has been reduced by bootstrapping and the differences still remain between the datasets, it suggests again that the measurement technique may give different albedo values over different forest cover levels.

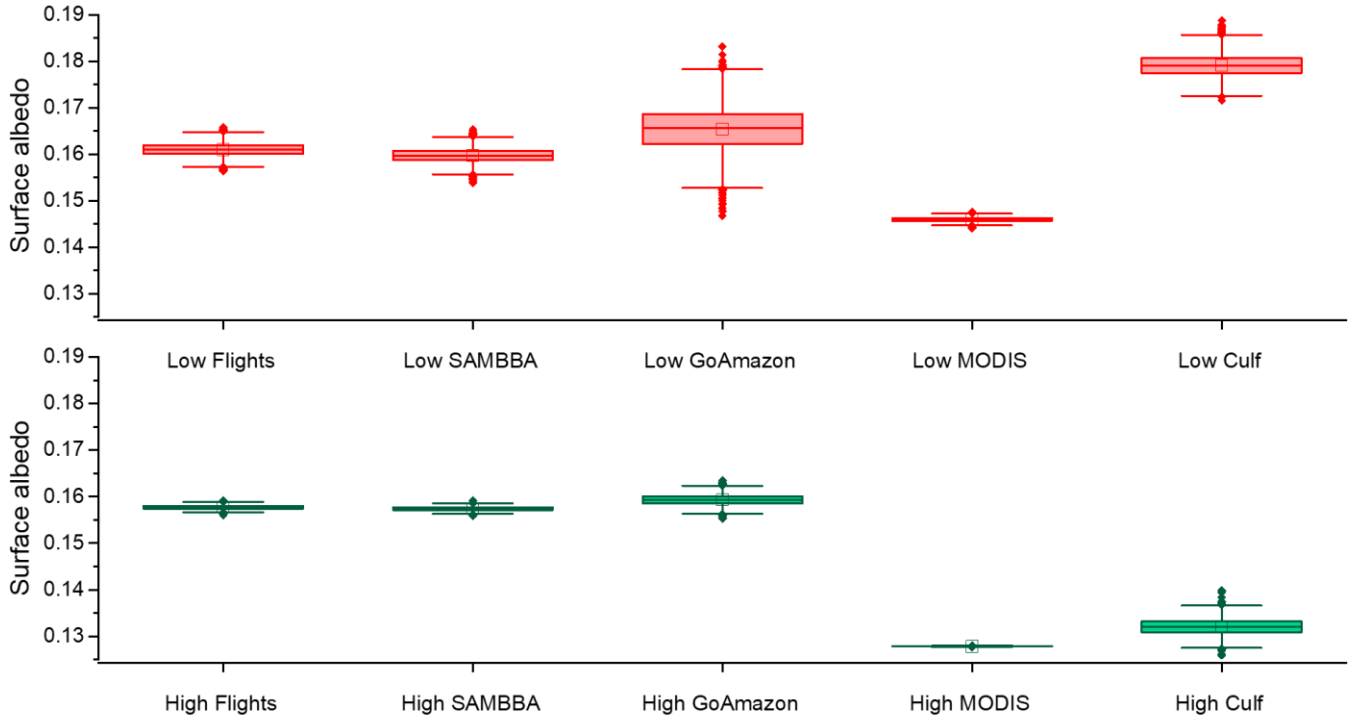

Figure 3.23: Box plot showing the bootstrapped data from non-forested pixels (red, top panel) and forested pixels (green, bottom panel) albedo values for the flight campaigns, for MODIS over the same flight tracks and for data from *(Culf et al., 1995)*.

Table 3.5: Albedo values for forested and non-forested measurements from each measurement technique.

	Forested albedo	Non-forested albedo	$\Delta\alpha_S$
MODIS	0.1279	0.1460	0.0181
SAMBBA	0.1574	0.1598	0.0023
GoAmazon	0.1593	0.1655	0.0062
Combined Flights	0.1577	0.1610	0.0043
In-situ	0.1321	0.1792	0.0471

The higher measuered albedo for low forest cover from Culf et al., (1995) compared to the measurements used within this study could be rationalised by looking at the albedo responses to forest cover (Figure 3.6 and Figure 3.15). The forested categories utilised in the MODIS and the flight measurements included forest cover greater than 70 %, with the non-forest categories having a range of lower than 30 %. Within these ranges, there is still significant albedo change as the forest cover increases or decreases. In-situ measurements were taken over areas of complete forest cover or pasture (Culf et al., 1995; Holdaway et al., 2010; Oliveira & Moraes, 2013), so present values at the extremes of the ranges used in this study. Figure 3.24 shows the effects of altering the high and low forest cover to include values closer to the extremes. Overall, were the forest cover categories reduced to encompass only 5 % from their extreme values (0 % and 100 %), the Δ albedo values observed increases to 0.0216 across the year. Even with this change, the in-situ measurements would still display a greater Δ albedo value.

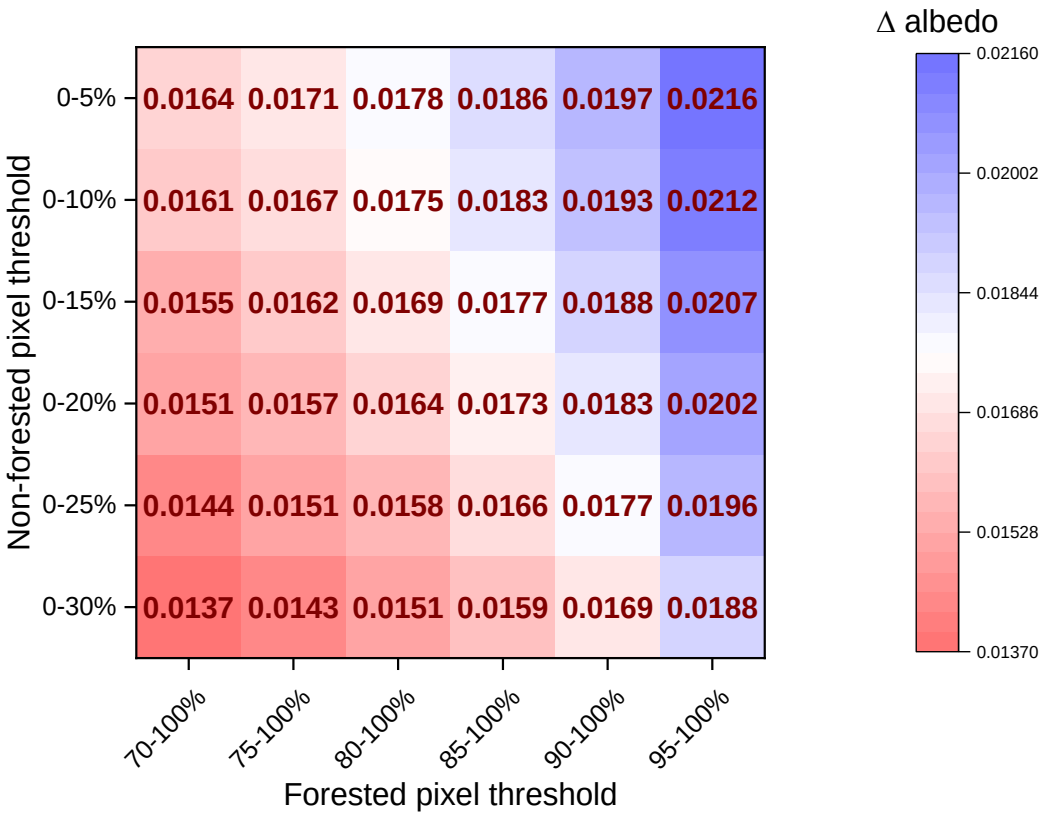

Figure 3.24: Effect of altering the forest and non-forest categories on the measured Δ albedo through the year using MODIS. Blue indicates lower Δ albedo values, with red a higher response.

Finally, the data from the modelling studies reviewed in section 3.2.1 are compared to the observations made on surface albedo in the Amazon. Measurements from the SAMBBA campaign displayed the lowest Δ albedo values, followed by GoAmazon – although the latter still retained a large spread. MODIS and in-situ measurements were both much higher than the flights, although there was some overlap between the highest GoAmazon values and those from MODIS. The values pulled from the modelling studies were shown to have the highest Δ albedo values, with a mean of 0.0649 (Figure 3.25).

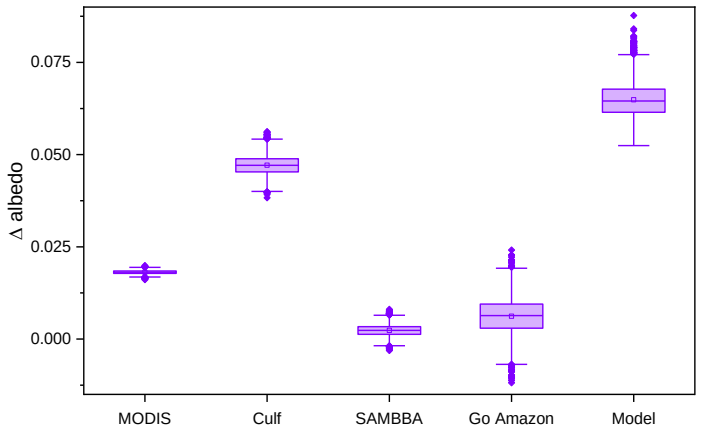

Figure 3.25: Δ albedo values for observations from MODIS, in-situ and flight campaigns and for values pulled from modelling studies featuring deforestation.

Even though the observations lack agreement, the modelling studies appear to strongly overestimate the Δ albedo values compared to any measurement technique. Values from MODIS suggest that this overestimation is on the scale of 3.5 times.

3.4. Conclusions

Surface albedo is shown to be lower for forested regions in the Amazon, both analysed spatially (by 0.017) and via deforestation (by 0.015) using MODIS. The agreement between the spatial and the temporal approaches support the previous use of spatial-for-temporal analysis of surface albedo in the region. Although there is some variation across the Amazon basin in the absolute albedo values, the low forest cover is still shown to be higher, both across the region at 0.05° resolution and at multiple locations at 0.01° resolution. There is also a larger variation in surface albedo through the year for high levels of forest, which results in albedo differences as large as 0.025 being observed during May-August – although this difference was greater when the data was analysed spatially.

The difference between high and low forest cover was also observed when considering flight observations made during the GoAmazon and SAMBBA campaigns and taking in-situ measurements from a previous study. Where MODIS observations led to a difference of 0.017, the flight campaigns displayed a difference of only 0.004, both of which were lower than the in-situ measurements presented (0.05). However, in spite of these differences, it was shown that each of these measurement types have still displayed lower albedo differences than what is commonly used in

modelling studies for deforestation in the Amazon (0.06), resulting in potential underestimation of the warming impact of such forest loss.

Chapter 4: South East Asia and the role of oil palm

4.1. Introduction

4.1.1. Chapter Outline

Using satellite data from MODIS, the surface albedo of forested and non-forested areas of South East Asia were investigated. Specific analysis of Borneo, Java, Sumatra, Sulawesi and the Malay Peninsula were carried out to understand the albedo differences across the region. The change in albedo with time, between the 2000 – 2003 and 2013 – 2015 periods, was also explored by investigating areas of forest that had undergone forest loss. Areas conceded to oil palm plantations were analysed separately to investigate the role of oil palm conversion on surface albedo in the region. Finally, the dependency of surface albedo changes due to forest loss occurring on the year of forest loss is examined.

4.1.2. Land use change in South East Asia

South East Asia is home to 5 % of the world's forests and 12 % of tropical forests, featuring one of the world's most biodiverse regions (Sodhi et al., 2004, 2010; Uryu et al., 2008; Wilcove et al., 2013). However, a range of anthropogenic pressures in the region has led to extensive deforestation (Abood et al., 2015; Estoque, et al., 2019). Habitat loss is the amongst the highest globally, with the region hosting some of the highest densities of threatened species across globe (Sodhi et al., 2004; Wilcove et al., 2013).

Deforestation in the region is second by area only to that found in the Amazon basin, with 1.6 million ha of forest lost annually between 1990 and 2015 (Estoque et al., 2019; MacDicken, 2015). As a percentage loss, this deforestation rate is greater than Latin America and Africa (0.4 to 0.5 %), increasing from 0.83 % during 1990 – 2000, to approximately 1 % for the period 2000-2010 (FAO, 2006; Miettinen et al., 2011). Much of the region's deforestation has occurred in Malaysia and Indonesia, which dominate Insular South East Asia's deforestation (Achard et al., 2002; FAO, 2015; Wicke et al., 2011).

Much of the deforestation in the region is driven by industrial activities, including logging, agricultural concessions and mining (Abood et al., 2015). In the thirty years between 1975 to 2005, mature oil palm increased in area from 0.5 to 7.5 Mha across Malaysia and Indonesia, with a further increase of 2 Mha of immature oil palm (Wicke et al., 2011). Malaysia and Indonesia are the greatest producers

of palm oil, however the expansion of oil palm in the region has mostly come at the expense of forest (Austin et al., 2015; Curtis et al., 2018; Koh & Wilcove, 2008).

In conjunction with the different drivers of LUC, Caiazzo et al., (2014) highlight large differences in albedo between tropical rainforest in Amazonia (0.120) and South East Asia (0.066 – 0.091), as well as differences between other vegetation types in the region, although only a handful of sites are used for each classification. This chapter seeks to verify the surface albedo at scale and explore the size of surface albedo changes driven by land use change across South East Asia.

4.1.3. South East Asia's oil palm

Chong et al., (2017) report that, as of 2015, 17 Mha of oil palm exists across Malaysia and Indonesia. The oil palm crop grows as a perennial tree crop, which despite being distinguishable due to its eight-pointed star shape from above, resembles a forest tree more than other agricultural crops grown in the region (McMorrow, 2001). In spite of this, oil palm is able to be differentiated via remote sensing using high-resolution imagery (Shafri et al., 2011), microwave (Miettinen et al., 2015), and RADAR (L. Li et al., 2015) and a mix of moderate and high-resolution satellite measurements (Razali et al., 2014).

Measurements of the differences in ecological and climatic factors between forests and oil palm has also been reported previously. Meijide et al., (2017) analysed the energy and water fluxes of young and mature plantations *in-situ*, finding lower evapotranspiration and sensible heat flux, and a higher Bowen ratio in the young plantation. Transpiration and evapotranspiration rates were also calculated. Meijide et al., (2018) explored the replacement of forests with monoculture rubber and oil palm plantations and highlight the impacts the 2015 El Niño Southern Oscillation (ENSO) had on each microclimate. They build on the idea that conversion from forest reduces biodiversity, but also leads to less stable, more open microclimates. Sabajo et al., (2017) used Landsat data to present increased Land Surface Temperature (LST) in plantations of oil palm and rubber compared to forest in Indonesia's Jambi province.

There have also been a few reported measurements of surface albedo over palm oil plantations. Sabajo et al., (2017) used Landsat measurements to calculate albedo using the equation presented by Liang, (2000). Although only a single July retrieval was used in the calculation, they presented an albedo 0.015 and 0.030 higher than forest from mature and young oil palm, respectively. This chapter seeks to explore the transition of surface albedo in oil palm concessions after forest has been cleared.

4.2. Spatial variations of surface albedo in South East Asia

Measurements of surface albedo were taken from the MODIS product MCD43A3 across the region, before being separated into five major landmasses within South East Asia: Borneo, Sumatra, Java, Sulawesi and the Malay Peninsula (Figure 4.1). Albedo measurements from MODIS were combined with the tree cover data from Hansen et al., (2013) to analyse the changes associated with tree loss. The area analysed covered approximately 2.6 million km^2 of land, featuring 76 % tree coverage (Table 4.1). Levels of forest loss between 2000-2015 were observed at this scale to be 4.6 % of the recorded forested area (Figure 4.2), however higher rates were found across Borneo, the Malay Peninsula and Sumatra (6.8 %, 9.5 %, and 12.6 % respectively).

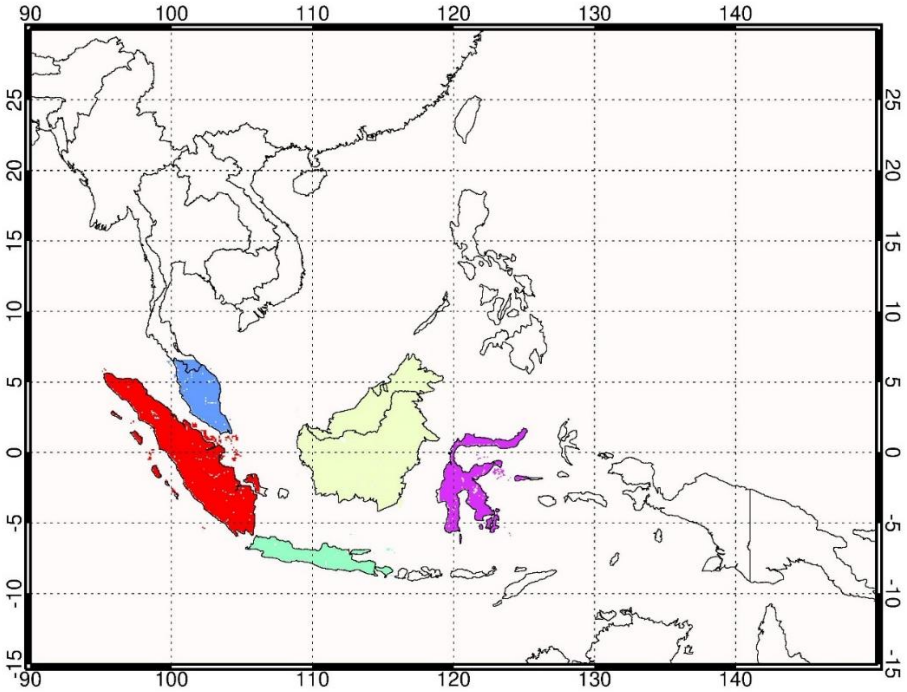

Figure 4.1: Areas analysed as individual landmasses in this chapter. Borneo (yellow), Java (green), Sulawesi (purple), Sumatra (red) and the Malay Peninsula (blue).

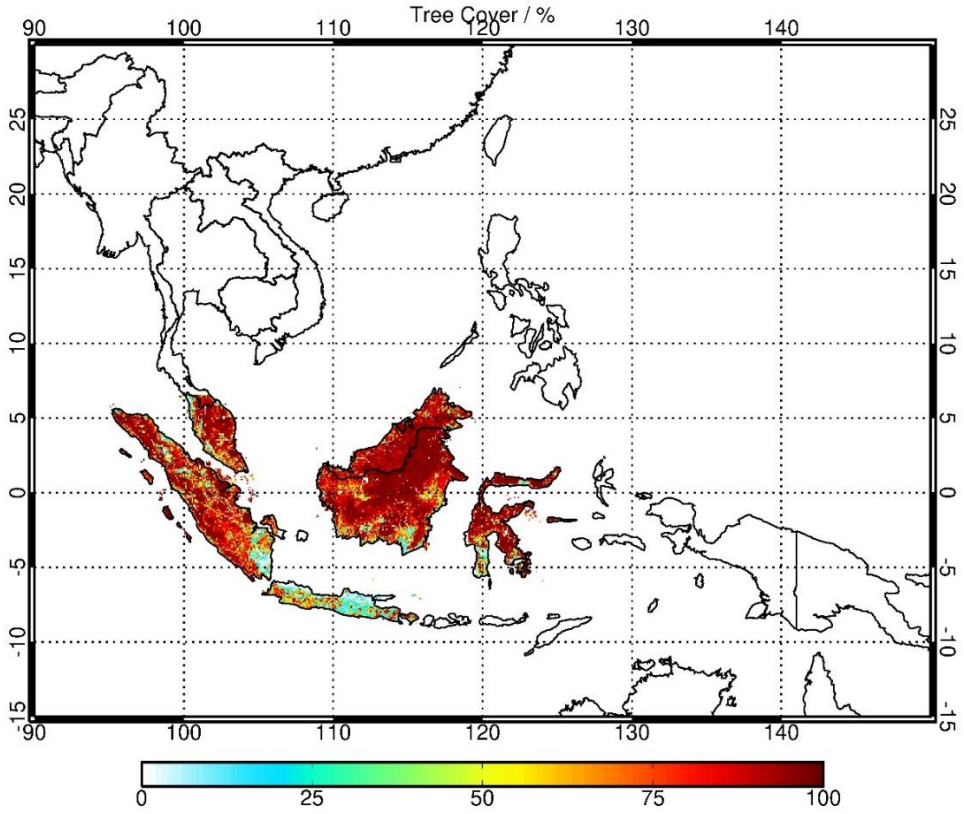

Figure 4.2: Percentage forest cover across the main landmasses analysed in this chapter.

At the regional scale, forested pixels displayed an annual surface albedo mean of 0.119, with a higher albedo value of 0.127 observed for the non-forest pixels. A similar increase was observed across observation for each island (Figure 4.3).

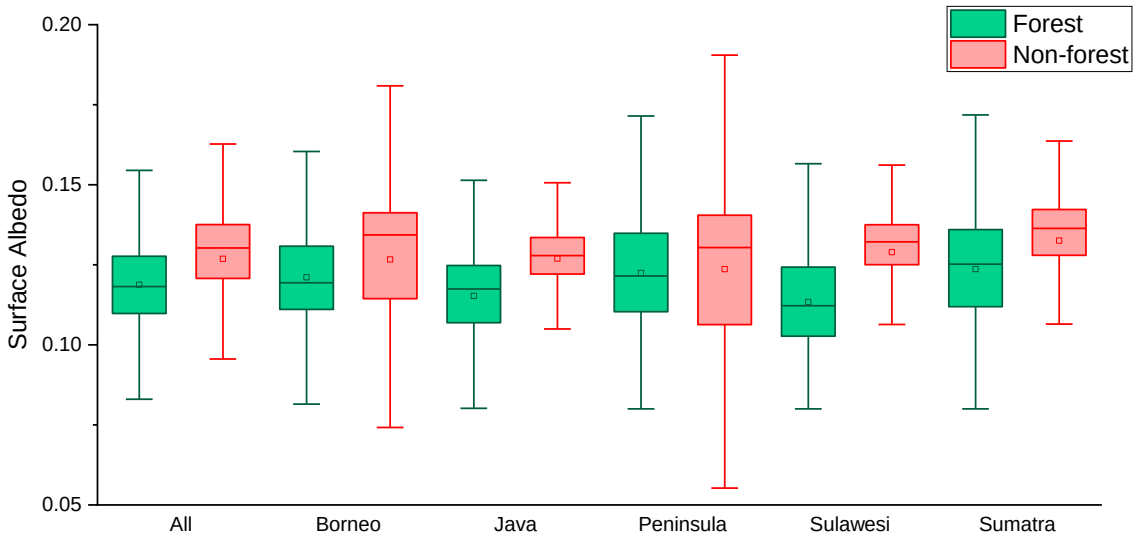

Figure 4.3: Annual average albedo values for observed MODIS albedo values for each major landmass for forested (green) and non-forested (red) pixels.

Annual average albedo values of forested pixels were highest over Sumatra, averaging 0.124, with Sulawesi displaying the lowest (0.113). Non-forest pixels were found to be between 0.124 (Malay Peninsula) to 0.133 (Sumatra) across the islands.

Forested pixels gave consistent albedo values from MODIS across the year, with little variation between months (Figure 4.4). Non-forested pixels displayed greater variability, with a peak albedo value observed in June (0.134) and a minimum in October (0.118).

Table 4.1: Properties of analysed domains. Values give number of pixels that fall within each category, other than the albedo (α) values, which were retrieved from the MODIS analysis. Percentages are calculated with respect to the total dry pixel number.

Domain name	Dry pixels[a]	Area / km^2	High forest cover in 2000	Low forest cover in 2000	Forest loss	No loss	High tree α mean	Low tree α mean
South East Asia	2,142,238	2,592,108	1,640,660 (77.0 %)	191,508 (1.6 %)	75,818 (0.6 %)	1,838,149 (15 %)	0.11875	0.12688
Borneo	583,520	706,059	499,276 (85.6 %)	17,603 (3.0 %)	33,908 (5.8 %)	483,558 (82.9 %)	0.12108	0.12664
Java	108,418	131,186	22,342 (20.6 %)	52,022 48.0 %)	26 (0.02 %)	80,602 (74.3 %)	0.11527	0.12697
Peninsula	117,606	142,303	83,382 (70.9 %)	9,893 (8.4 %)	7,900 (6.7 %)	90,795 (77.2 %)	0.12244	0.12364
Sumatra	363,789	440,185	250,845 (69.0 %)	35,475 (9.8 %)	31,585 (8.7 %)	267,484 (73.5 %)	0.12363	0.13257
Sulawesi	142,198	172,060	104,981 (73.8 %)	13,355 (9.4 %)	919 (0.7 %)	129,199 (90.9 %)	0.11336	0.12895

[a] Dry pixels refer to pixels featuring less than 10 % water, as determined by the MODIS water mask at 0.01° resolution

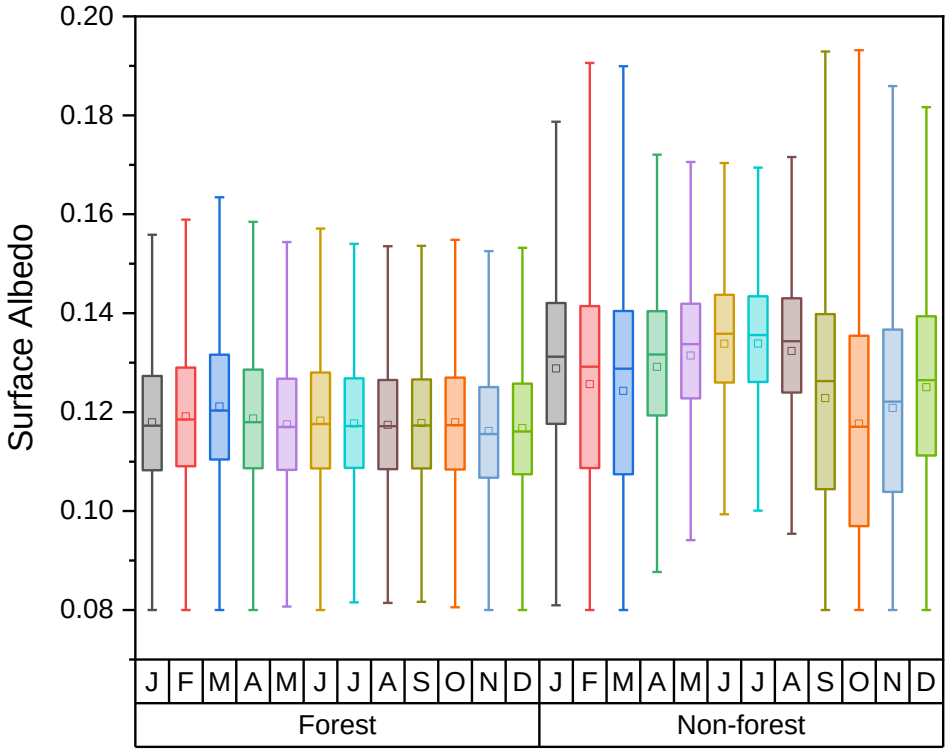

Figure 4.4: Absolute surface albedo measurements from MODIS for each month across the two time periods (2000 – 2003 and 2013 – 2015)

Each of the selected islands exhibit similar maxima/minima around June/July and October for non-tree pixels and remained consistent through the year for the forested pixels (Figure 4.5). Forested pixels for both Java and Sulawesi were shown to be lower throughout the year than the rest of the islands, displaying a reduction in albedo from July through to November not observed across the other islands.

The profile of forest across Java is shown to be made up of smaller, less expansive forested area than the other landmasses (Figure 4.2 and Arjasakusuma et al., 2018; Guan et al., 2015) and the island typically receives less rainfall than the other islands (As-syakur et al., 2013). From June through to October, Java experiences a more pronounced dry season than the slightly more northern equatorial landmasses. Although not quite as distinct, As-syakur et al., (2013) also show a larger rainfall fluctuation across parts of Sulawesi during the same period. The reduction in albedo for these two

islands therefore aligns with the dry season (Y. Zhang et al., 2016), as the peak in forested albedo did over the Amazon (Chapter 3).

Analysis from Zhang et al., (2016) support the low-magnitude seasonality of forests, where they found consistent normalised difference vegetation index (NDVI) anomalies through the year across the regions analysed in this study. The minima observed in non-forested pixels (Figure 4.4) coincide with slight maxima in incoming SW radiation in the region (Y. Zhang et al., 2016).

The peak in non-forested albedo begins with the onset of the dry season over northern Indonesia in May through to October (Hendon, 2003).

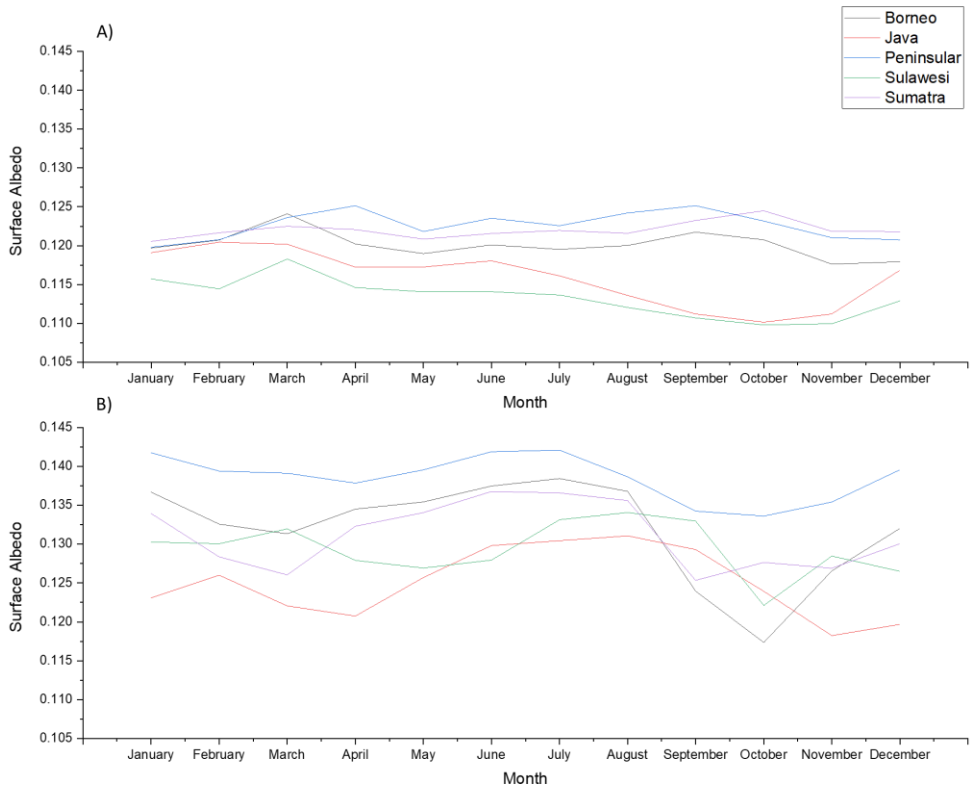

Figure 4.5: Absolute surface albedo measurements from MODIS across each major analysed landmass. Forested pixels are described in panel A (top) and non-forest pixels in B (bottom).

Across Sulawesi and Java, high tree pixels maintained similar surface albedo between observations during 2000 – 2003 and 2013 – 2015, however small decreases in measured albedo were shown across Borneo, the Malay Peninsula and Sumatra. Non-forested pixels displayed similar magnitude differences between the two periods, although there was less consistency regarding the intraannual

pattern between them, with a low observed in October across Borneo, Sulawesi and the Malay Peninsula in the 2013-2015 period that was not observable during the 2000-2003 period.

Spatial analyses comparing forested and non-forested areas within the same 2000-2003 and 2013-2015 time periods were carried out and the difference in albedo values ($\Delta\alpha_s$) were compared across each location.

Within each island and the larger regional domain, higher albedo values were consistently observed for non-forest pixels compared to forested pixels (Figure 4.7). These annual average $\Delta\alpha_s$ values range between 0.009 for Sumatra to 0.016 for Sulawesi. Noticeably, the absolute albedo values for forest and non-forest for the region were lower than those reported within the Amazon basin in Chapter 3 (Table 4.2 and Table 3.3). The $\Delta\alpha_s$ across the Malay Peninsula was comparable to the Amazon basin, however the broad region displayed smaller values than much of the Amazon.

Through the year, the $\Delta\alpha_s$ values peaked in July, corresponding to the maxima observed for the low forest pixels. The minimum in October also matches the behaviour of the low forest pixels, coinciding with the lowest observed albedo for low tree pixels. However, a second $\Delta\alpha_s$ minimum is also shown to occur during March, where a decrease in the albedo of low tree pixels was also observed across Borneo and Sumatra.

Table 4.2: Annual mean MODIS albedo values from spatial analysis of the domain and each individually analysed region.

	Regional domain	Borneo	Java	Peninsula	Sulawesi	Sumatra
Forested albedo	0.11875	0.1201	0.11588	0.12267	0.1133	0.12202
Non-forest albedo	0.12688	0.1303	0.12475	0.13849	0.12904	0.13069
$\Delta\alpha_s$	0.00813	0.0102	0.00887	0.01582	0.0159	0.00867

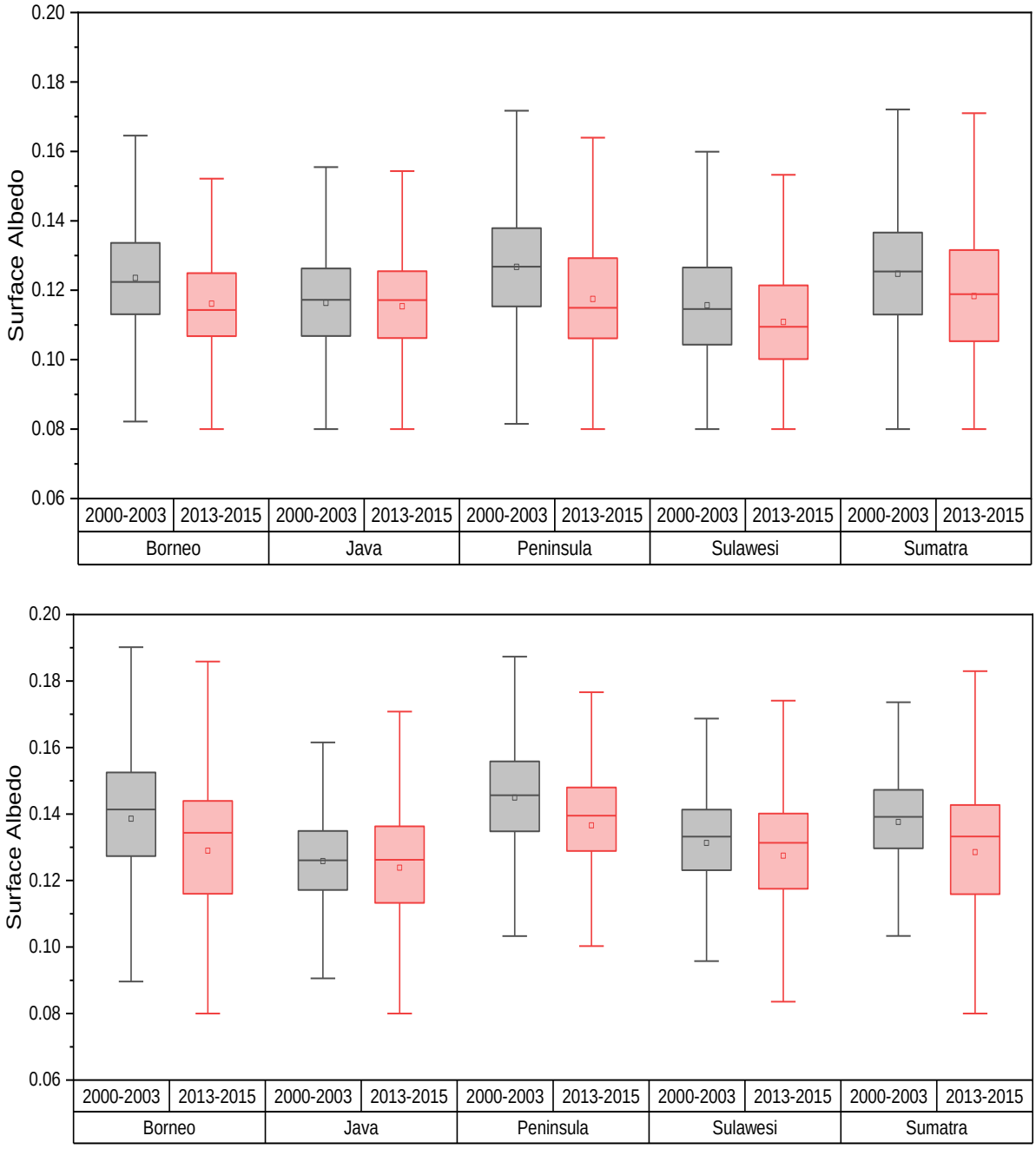

Figure 4.6: Absolute surface albedo values from MODIS across each major landmass for 2000 – 2003 (grey) and 2013 – 2015 (red) for forest (top panel) and non-forest (bottom panel).

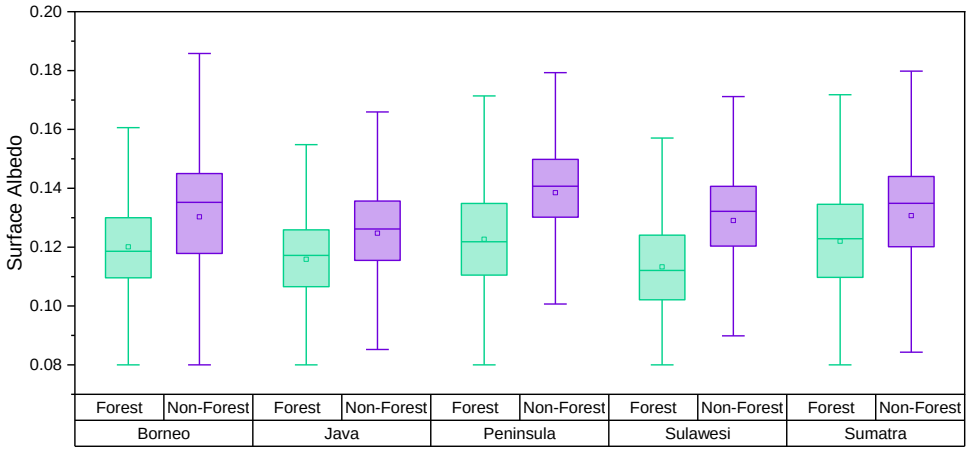

Figure 4.7: Absolute albedo values from MODIS across each major landmass for forest (green) and non-forest (purple) pixels.

The $\Delta\alpha_s$ were in similar ranges for each time period (Figure 4.8), although taken across the large regional domain, the observations corresponding to 2000 – 2003 were at the lower end of the 2013 – 2015 observations. The 2000 – 2003 period also gave much smaller ranges of $\Delta\alpha_s$ across the regional domain, Sumatra and Borneo in comparison to 2013 – 2015.

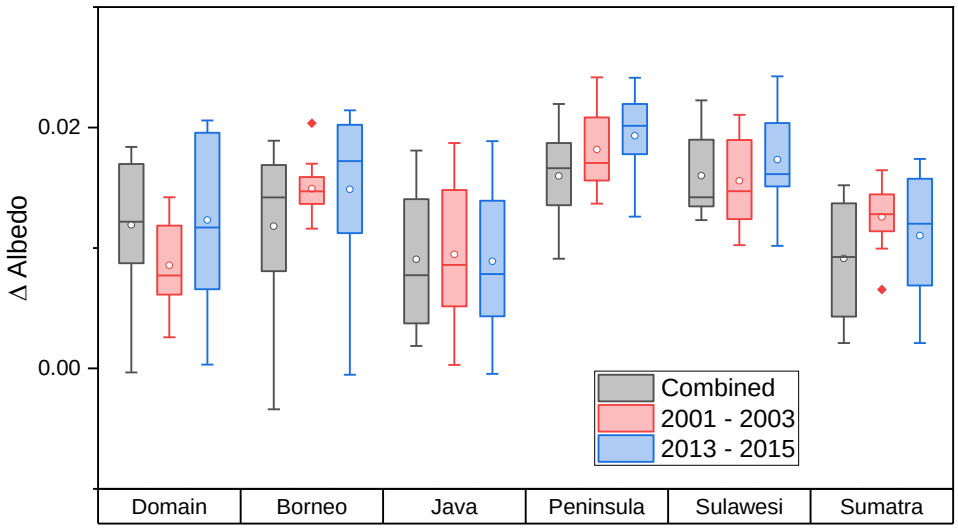

Figure 4.8: Δ albedo values across each major landmass for both time periods combined (grey), the 2001-2003 period (red) and the 2013-2015 period (blue).

4.3. Temporal analysis

A temporal analysis approach was then employed to analyse the albedo changes associated with direct forest loss ($\Delta\alpha_t$). Pixels denoted as undergoing forest loss using the Global Forest Change dataset were analysed alongside those that were unchanged.

Across the unchanged pixels, small changes were observed across the regional domain and across each of the individual islands between the 2000 – 2003 period and 2013 – 2015. These observed changes were shown to be slightly larger than those observed across the Amazon Basin (Section 3.3.2), with the whole region displaying a decrease of approximately 4.0 %. The Malay Peninsula showed the largest change, with a decrease of 5.2 %, whereas Java was the only selected location that showed an increase (+1.4 %) for the non-deforested pixels.

By correcting for this, pixels which underwent tree loss underwent an average albedo increase of 0.0172 across the regional domain. Table 4.3 displays the observed changes for each analysed location; Sulawesi displayed the greatest changes (0.0185), with Java having the lowest (0.0142). This lower value is observed strongly when the monthly $\Delta\alpha_t$ is analysed (Figure 4.9), where Java behaves similarly to the other locations from December through to April, but then experiences a steady decline, with a sharp decrease in October to a value less than half of that observed in the other locations. Zhang et al., (2016) discusses strong differences between the incoming SW radiation observed in Java and the other landmasses in the region, with the decline in Δ albedo here coinciding with a sharp increase in incoming radiation at the end of the dry season. Other than this behaviour, there was no clear pattern observable through the year.

Table 4.3: Average Δ albedo values of pixels undergoing tree loss across each analysis location.

	Regional domain	Borneo	Java	Peninsula	Sulawesi	Sumatra	Average
Temporal Δ albedo	0.0172	0.0190	0.0142	0.0170	0.0185	0.0162	0.0170

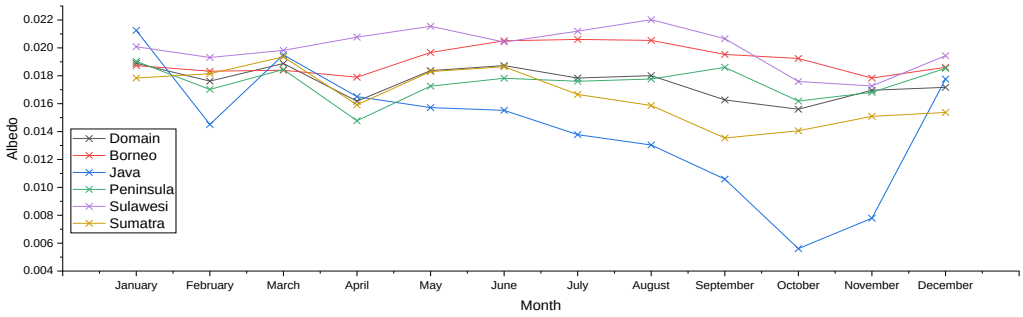

Figure 4.9: Monthly variation of $\Delta\alpha_T$ for each analysis location.

Other than for Sulawesi, the temporal analysis displayed a greater $\Delta\alpha_T$ than during the spatial analysis ($\Delta\alpha_S$). The largest difference occurred over Borneo, averaging 0.008 larger.

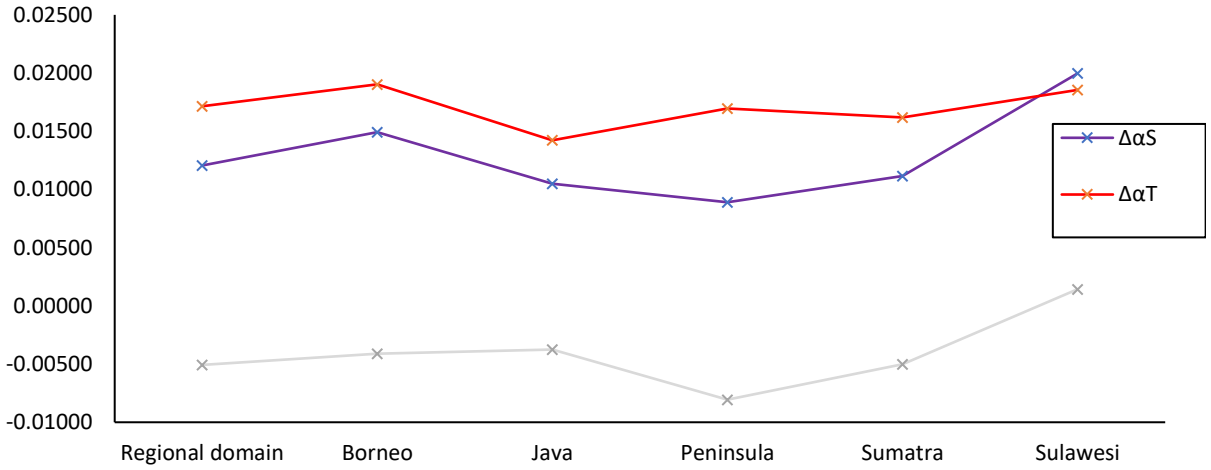

Figure 4.10: $\Delta\alpha_s$ and $\Delta\alpha_t$ across each analysis location.

4.4. Oil palm concessions

This section focuses on the behaviour of oil palm concessions in comparison to non-conceded land in the region. Due to the assignment of trees as vegetation over 5 metres in height with the Global Forest Change dataset, there is no direct differentiation between intact forest, degraded forest or managed oil palm. Therefore, maps of oil palm concessions from the Global Forest Watch were projected onto the analysis grid, allowing pixels to be marked as either part of concessions for oil palm, or not, alongside designations of forest cover and loss.

Both a spatial and a temporal approach were used to understand whether the albedo of forests within oil palm concessions behaved differently to that of forests not conceded. Although concession maps do not necessarily designate forests within them as oil palm, albedo differences could be a way to improve characterisation of oil palm plantations across forested areas in South East Asia.

Across the regional domain, pixels within oil palm concession areas consistently displayed a higher surface albedo than outside across both areas of high forest and low forest. Across forested areas, these differences average 0.017 through the year. Comparing the values obtained across the two time periods for July, the average higher albedo of oil palm concessions of 0.019 matches well with the calculations from Sabajo et al., (2017). The notable difference between concession and non-concession areas being around the measured range suggests these differences are attributable to oil palm.

These higher albedo values were observed across each of the analysed islands (Table 4.4), with the largest difference in forested areas occurring on the Malay Peninsula (0.020), while Borneo displayed the largest difference between non-forested areas (0.021).

Table 4.4: Annual average albedo values measured between pixels granted oil palm concessions and those not granted.

	Forest		Non-forest		$\Delta\alpha_T$	
	Concession	No Concession	Concession	No Concession	Concession	No Concession
SE Asia	0.134	0.117	0.139	0.123	0.0179	0.0169
Borneo	0.134	0.119	0.141	0.120	0.0205	0.0161
Java	0.120	0.115	0.129	0.125	0.0199	0.0156
Peninsula	0.137	0.118	0.145	0.134	0.0177	0.0189
Sulawesi	0.131	0.112	0.137	0.128	0.0208	0.0164
Sumatra	0.134	0.119	0.137	0.126	0.0157	0.0185

Through the year, high forest pixels remained relatively consistent (Figure 4.11 and Figure 4.12), displaying a small maximum in March both within and without granted concessions for most locations. The low forest pixels displayed larger variation in observed albedo, but this was much greater for pixels not marked as conceded land (Figure 4.14). As with the previous analysis in this chapter, the maxima

in July and the minima in October were observed away from concessions. However, these were not shared by pixels within concession areas (Figure 4.13).

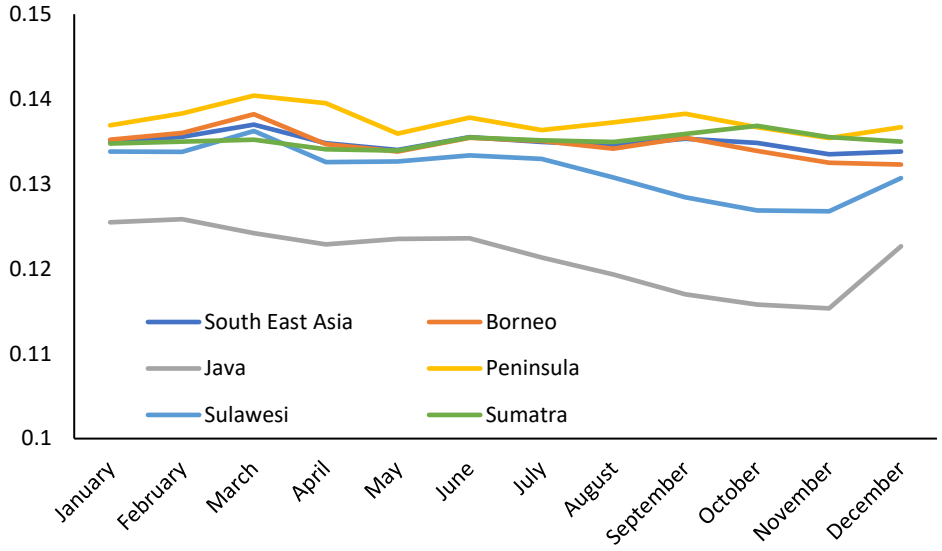

Figure 4.11: Annual variation of forested albedo within palm oil concession areas.

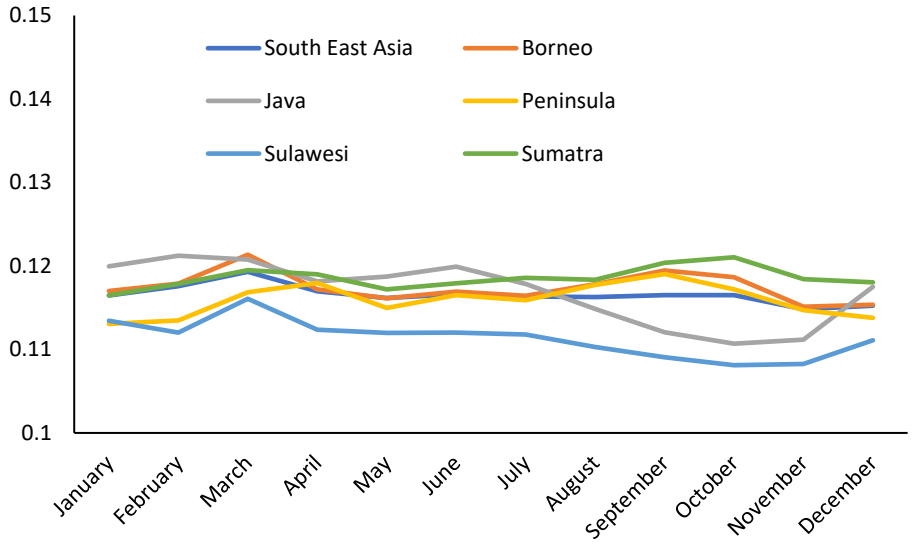

Figure 4.12: Annual variation of forested albedo outside palm oil concession areas.

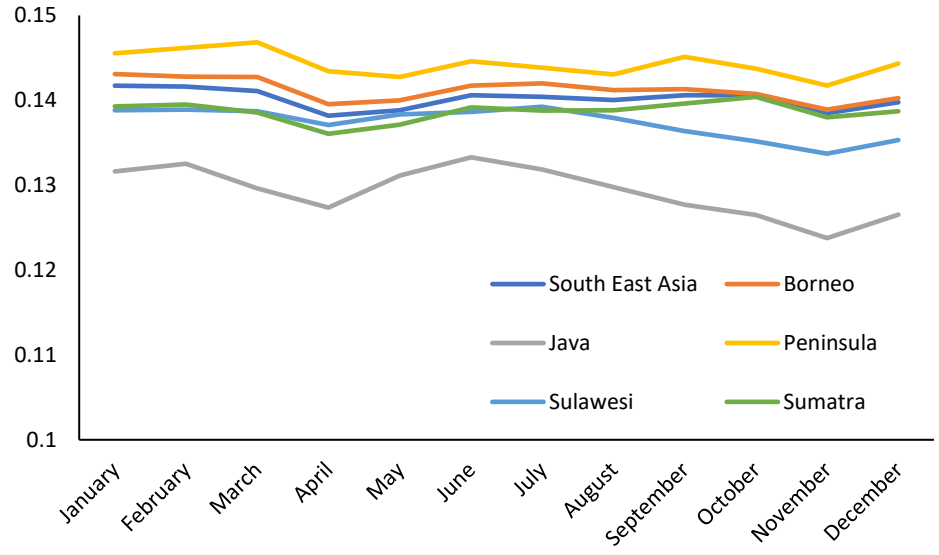

Figure 4.13: Annual variation of non-forested albedo within palm oil concession areas.

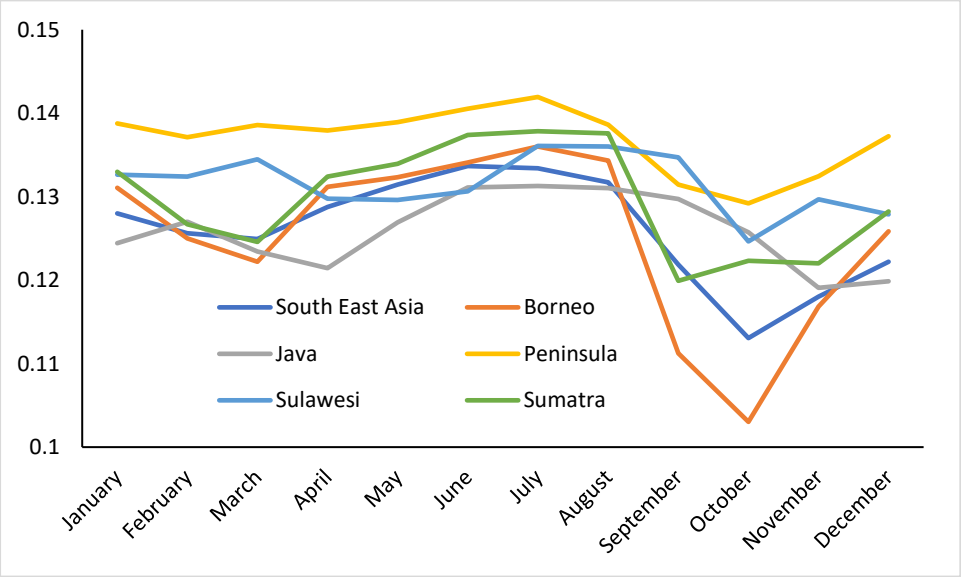

Figure 4.14: Annual variation of non-forested albedo outside palm oil concession areas

Table 4.4 also shows the average annual temporal albedo changes ($\Delta\alpha_t$) occurring with forest loss between the 2000-2003 and 2013-2015 periods. Across the region, this was slightly higher within concession areas, but this differed between the islands, with Sumatra and the Malay Peninsula giving higher values outside concession pixels.

Within concessions, a consistent pattern was observed between the locations (Figure 4.15), displaying peaks in June and December/January, although the magnitude of the changes varied between the

islands. Outside concessions, two patterns were observed: one across the Malay Peninsula and Sumatra, with the other islands displaying different behaviour. Sumatra and the peninsula display similar levels of forest and forest loss, while also sharing a similar density of concession land.

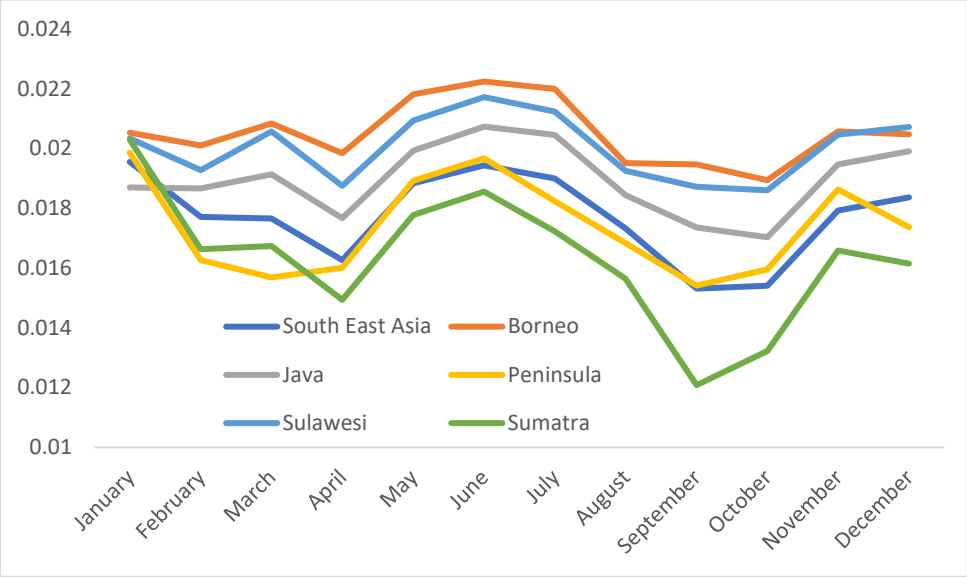

Figure 4.15: Average annual temporal albedo changes (Δαt) for concession pixels.

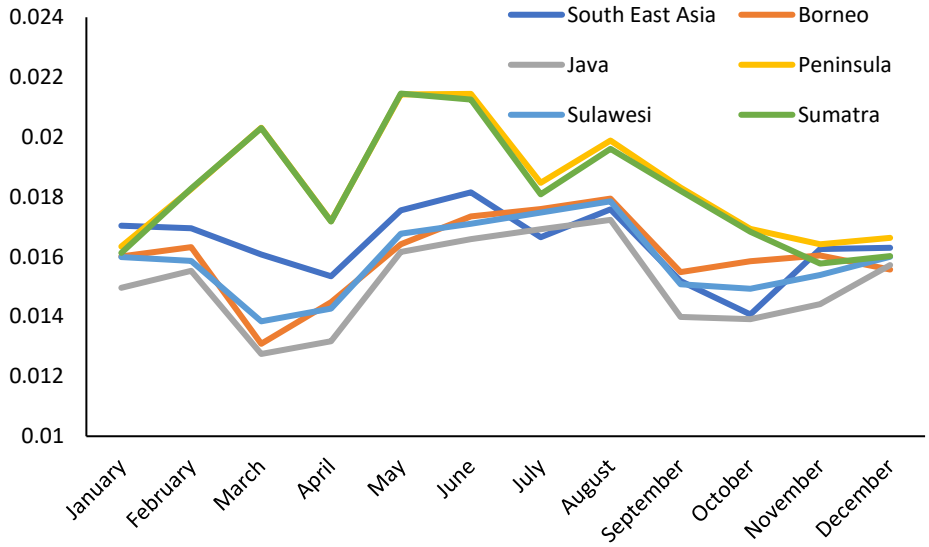

Figure 4.16: Average annual temporal albedo changes (Δαt) for non-concession pixels.

Both within and outside of oil palm concessions, ΔαT was shown to be greater than ΔαS in all locations, suggesting that undertaking a spatial analysis to assess the impact of deforestation leads to underestimating the associated albedo change.

4.5. Year of forest loss

The final section of this chapter explores the impact of tree loss year on the observed albedo changes. Here, the lossyear product from the Global Forest Watch is used to assign an average loss year of each pixel that had been marked as deforested and the gain product used to target pixels that had seen regrowth of forest. In order to test whether the age of oil palm, or other forest, affected the albedo, pixels featuring forest gain between 2000 – 2015 were analysed.

As Sabajo et al., (2017) found higher albedo for young oil palm, it was reasoned that newly deforested pixels featuring forest gain, as indicated by the Global Forest Watch dataset, would also display higher albedo values within palm oil concessions compared to pixels deforested earlier.

Firstly, pixels that featured forest gain of greater than 70 % within oil palm concessions were analysed. Between 2001 to 2012, a small decline in measured surface albedo was found – indicating that newer planted trees in the areas observed displayed a lower surface albedo (Figure 4.17). However, no pixels containing above 70 % forest gain and a forest loss year of later than 2012 were observed across the domain. In order to increase the number of observations of newer-growth trees, the forest gain percentage was relaxed to a 30 % threshold.

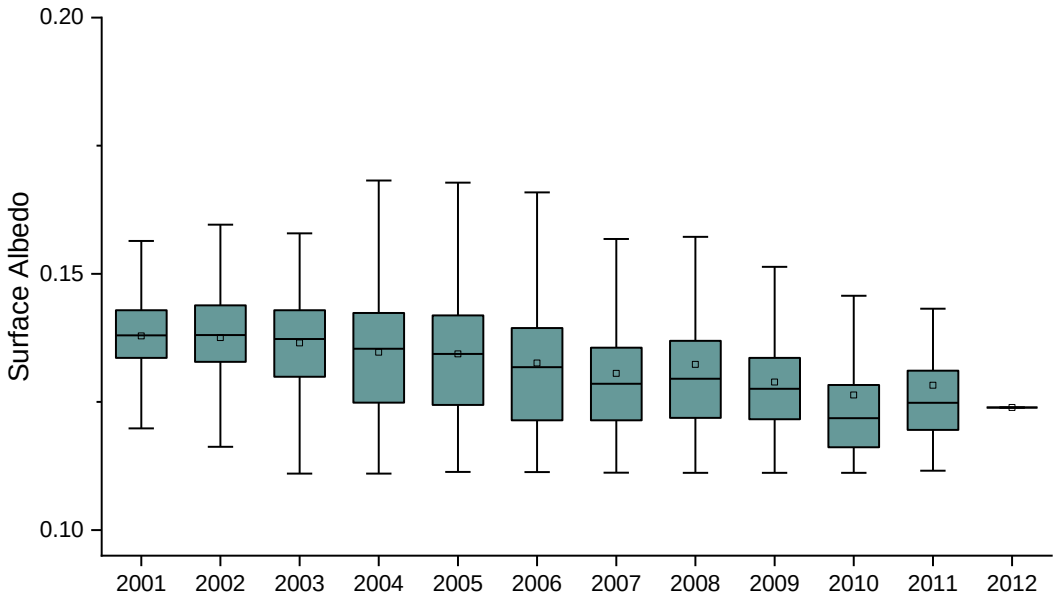

Figure 4.17: Average July absolute albedo values for 2013 – 2015 based on loss year across the South East Asia domain within oil palm concessions for pixels featuring at least 70 % forest gain since 2001.

Using this new dataset, observations across the domain were collected and a similar decline in surface albedo was still observed between 2001 – 2012. The updated observations allowed for surface albedo for pixels featuring gain between 2012 – 2014 to be observed, and these pixels showed a marked increase in surface albedo (Figure 4.18).

This falls in line with observations from Sabajo et al., (2017), where young oil palm showed an albedo approximately 0.013 higher than mature oil palm, in line with the increase between trees planted before and after 2011 in these observations. Additionally, as the Global Forest Watch dataset only indicates forest gain once a tree height of 5 metres has been established, measurements of oil palm using this method would highlight more mature trees rather than youthful vegetation – as such the albedo difference is unlikely to persist for as long in our datasets.

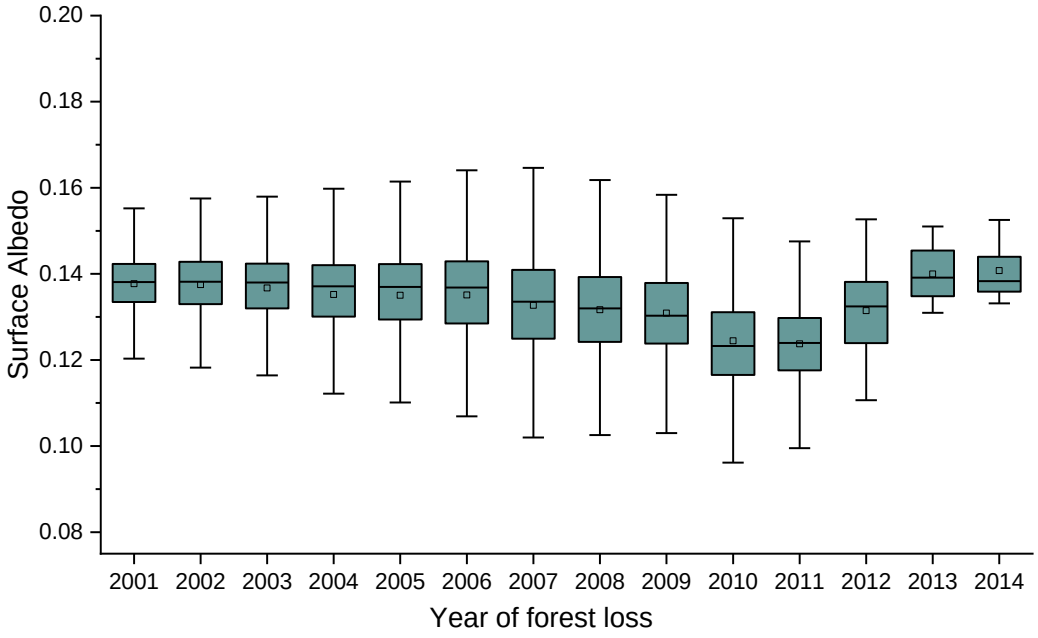

Figure 4.18: Average July absolute albedo values for 2013 – 2015 based on loss year across the South East Asia domain within oil palm concessions for pixels featuring at least 70 % forest gain since 2001.

At smaller geographic levels, a similar pattern is observed. Although no observations of pixels featuring forest gain above either threshold were found over Java and few observations were found over Sulawesi, analysis took place over Borneo, Sumatra and the Malay Peninsula.

Both Borneo and Sumatra displayed a similar decline in surface albedo as the time since forest loss reduced, although the observations for a loss year of 2013 were the highest of all years across Sumatra

and 2013/2014 also rose across Borneo. However, surface albedo across the Peninsula was consistent and no surface albedo dependence on year of forest loss was observed for any month, although observations were only available up to a loss year of 2010 (Figure 4.19).

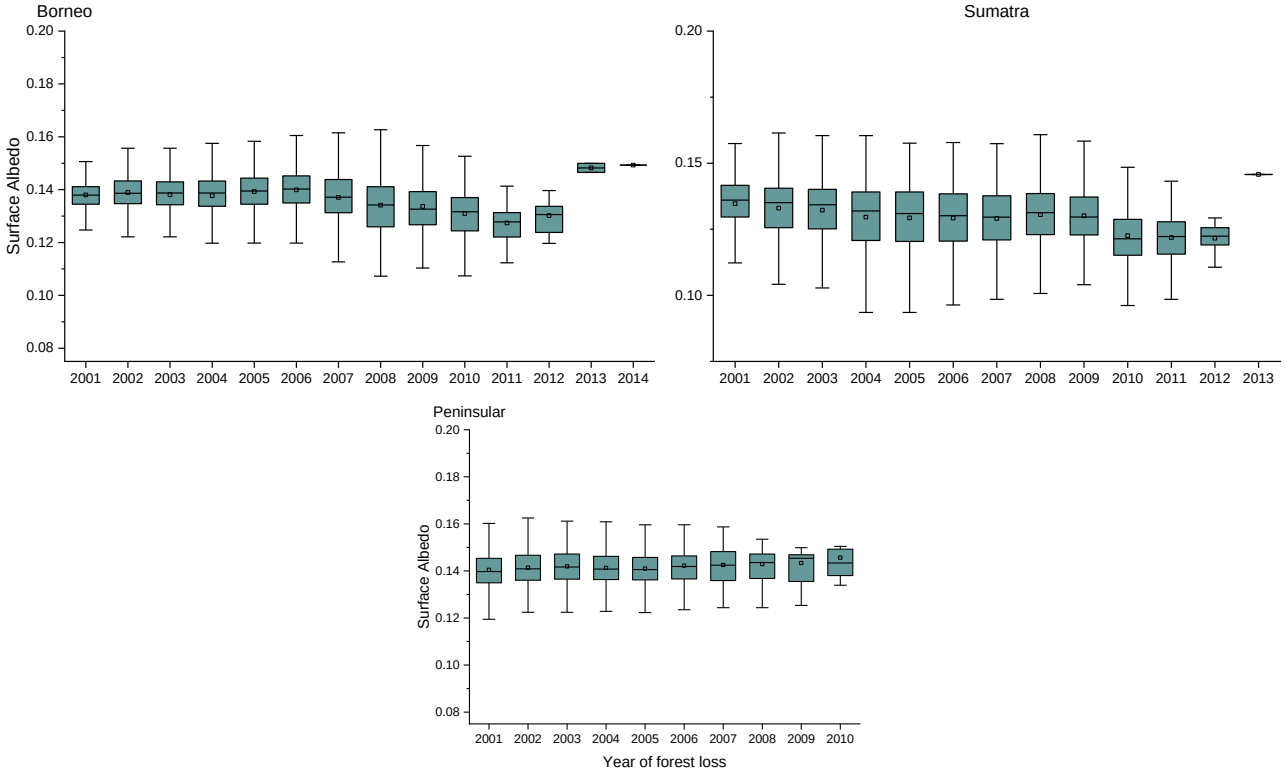

Figure 4.19: Average July absolute albedo for 2013 – 2015 of forested pixels in oil palm concessions, featuring a percentage gain of at least 30 %, by year of forest loss.

4.6. **Conclusions**

Across South East Asia, analysis of MODIS observations show surface albedo for areas of non-forest is approximately 0.008 higher than forest, smaller than the difference in the Amazon. Although there are differences between the major land masses, the albedo change from tree loss between 2000 – 2003 to 2013 – 2015 is shown to increase the albedo by a greater extent (approximately 0.017). Generally, this temporal change is seen to be larger than the spatial differences in the region.

Analysing land within oil palm concessions displays distinct behaviour both for forested and non-forest albedo, with high forest showing a surface albedo 0.017 higher than forest outside of the concession areas, while non-forest areas display reduced variability through the year, alongside a higher albedo. The difference between forest and non-forested albedo in and outside of concession areas are

comparable, with similar magnitudes of differences. As with outside of concession areas, temporal changes following forest loss give a larger albedo change than the spatial differences observed within one time period.

Finally, a slight decline in forested albedo for areas where forest loss has occurred is shown with increasing year of loss, except for forest established in the last three years of observations, which showed a surface albedo approximately 0.019 higher than the years immediately preceding them. Similar observations were shown across Sumatra and Borneo, although the other major landmasses lacked enough data to observe this phenomenon elsewhere.

Chapter 5: Climatic impact of Tropical Forest Loss

5.1. Introduction

5.1.1. Chapter outline

This chapter evaluates the albedo changes across the tropics as a result of deforestation using the Suite Of Community RAdiative Transfer codes based on Edwards and Slingo (SOCRATES) with respect to their radiative impact. A range of idealised deforestation experiments are conducted across the Amazon, South East Asia and the combined locations to assess the role different measurements techniques of surface albedo may have. Finally, experiments featuring deforestation consistent with the Intergovernmental Panel on Climate Change's (IPCC) Representative Concentration Pathway 8.5 (RCP8.5) from 2000 to 2050 and 2100 are conducted to analyse the impact of realistic deforestation across the same regions.

5.1.2. Radiative forcing of albedo

The global energy budget is strongly dependent on the albedo of the Earth's surface, which dictates the fraction of incoming radiation that is either absorbed or reflected. As land use change occurs, the albedo of the surface changes with it – deforestation results in an increase as darker forest is replaced with vegetation of a higher surface albedo (Bonan, 2008a; Foley et al., 2005). Radiative forcing is able to compare different climate forcing mechanisms over time, driven by both natural and anthropogenic means (Houghton et al., 2001).

Much of the radiative forcing of surface albedo changes as a result of land use change is associated with deforestation, driven by increased agricultural activity. Overall, this radiative forcing is estimated at approximately -0.2 W m^{-2} since pre-industrial times (Houghton et al., 2001; Pongratz et al., 2011).

This forcing calculation has contained a large range of uncertainty, with this being attributed in part to uncertainty relating to the snow-albedo feedback mechanisms (R. A. Betts, 2000; Richard A. Betts, 2001; Y. Li et al., 2015). However, further uncertainty also comes from the surface albedo of cropland, where using different albedo observations result in large differences in the radiative forcing (G. Myhre & Myhre, 2003).

5.2. Model description

The Suite Of Community RAdiative Transfer codes based on Edwards and Slingo (SOCRATES), was developed from the set of radiative codes derived by Edwards & Slingo, (1996) by the Met Office. As a suite of radiative transfer codes, SOCRATES is used to calculate radiative fluxes and heating rates based on input parameters describing the atmosphere and the surface. The radiative code takes the two-stream approach to calculate fluxes (where only radiative propagation in two discrete direction is considered) and uses spherical harmonics to calculate radiances (allowing the scattered radiation field to be defined by directly integrating along rays). Six shortwave (SW) bands and nine longwave (LW) bands are used to model the atmospheric absorption, each of which are modelled as a pair of fluxes (downward and upward).

SOCRATES was built as the sophisticated radiative transfer scheme of the Unified Model (UM), but was used in an offline, standalone mode for this analysis. The model runs at 2.5 ° × 2.5 ° resolution, with 23 homogeneous vertical layers from the surface. The code utilises cloud fields taken from the International Satellite Cloud Climatology Project archive (ISCCP-D2) for the year 2000 (Rossow & Schiffer, 1999) and accounts for the radiative effects of cloud liquid, cloud ice and snow, with reanalysis data from the European Centre for Medium-Range Weather Forecasts (ECMWF) used to calculate monthly mean water vapour concentrations and temperatures.

The top-of-atmosphere (TOA) all-sky radiative flux was calculated for control and deforestation experiments, with the difference between the two giving the radiative effect of the albedo change. Running the codes in this offline configuration allowed the clear isolation of the surface albedo effect, with the only changes in output stemming directly from changes in the magnitude of Δ albedo. Although exploring these changes using a full-scale climate model would allow for multiple feedbacks to be included, such work was out of the scope of this project due to the computational expensive and the need for an initial contribution of these values.

5.3. Radiative forcing contributions

As mentioned in previous chapters, although deforestation results in increased CO_2 concentrations in the atmosphere, contributing a positive (warming) radiative effect, the change in surface albedo due to LUC leads to a negative (cooling) radiative effect. As the net radiative effect is determined by the contributions from combining the CO_2 and albedo (amongst other smaller contributions) effects, establishing an accurate albedo change post deforestation is important (Figure 5.1, Scott et al., 2018).

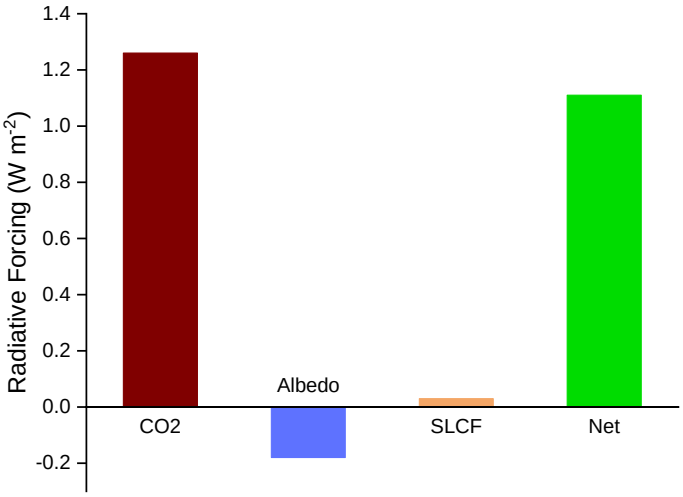

Figure 5.1: Global annual mean radiative forcings due to changes in the concentrations of CO_2 (red), changes to surface albedo (purple) and changes to concentrations of short-lived climate forcings (SLCFs - orange) under an idealised tropical deforestation scenario. Figure adapted from Scott et al., (2018**)**.

Using the results obtained from previous chapters, this chapter seeks to analyse the influence of the albedo changes from tropical deforestation on the climate. In order to do this, the radiative impact of deforestation-induced albedo changes across the Amazon basin and South East Asia was calculated using the Suite Of Community Radiative Transfer codes based on Edwards and Slingo (SOCRATES).

SOCRATES was then used to calculate the radiative effect of various deforestation experiments detailed below by calculating the difference in net top-of-atmosphere all-sky radiative flux with control runs. For each of the deforestation experiments, the forest cover was calculated, and areas of high forest had their albedo values altered to that of low forest cover.

It has been calculated previously (Scott et al., 2018) that global deforestation results in an albedo RF of approximately 40 % of the RF due to changes in CO_2. However, this weighting is reduced in the tropics to approximately 15 % of the CO_2 change as there is no enhanced surface albedo change due to snow cover, as there is in the boreal regions.

The first set of experiments were designed to investigate the contributions of albedo change from deforestation within the Amazon and South East Asia to global and tropical deforestation experiments. The control experiment utilises the distribution of forests within the Community Land Model (CLMv4.0), which are based on recorded plant functional types (PFTs) from MODIS data, to produce

global forest coverage maps. Idealised deforestation scenarios were then implemented, with forested regions of the land surface removed globally, within the Tropics (between 20° N – 20° S), across the Amazon (80° W – 35° W, 20° S – 13° N), and across South East Asia (90° E – 150° E, 15° S – 30° N, excluding China).

The albedo changes from deforestation within these experiments were all calculated to give an annual mean negative radiative forcing. The albedo change from global deforestation led to an RF of -0.96 W m^{-2} (Table 5.1). Tropical deforestation accounted for 19 % (-0.18 W m^{-2}) of this total.

Table 5.1: Global annual mean radiative forcings due to idealised deforestation experiments

Experiment number	Experiment name	RF due to Δ albedo (W m^{-2})
1.1	Global deforestation	-0.960
1.2	Tropical deforestation	-0.182
1.3	Amazonian deforestation	-0.072
1.4	South East Asian deforestation	-0.047

Albedo changes from regional deforestation across the Amazon and South East Asia were calculated to contribute RFs 39 % and 26 % respectively, of the tropical deforestation scenario.

5.4. Amazon deforestation experiments

In order to investigate how the observations of surface albedo across the Amazon from chapter 1, influence the radiative forcings, a second set of deforestation experiments were conducted. Each experiment resulted in deforestation of an area of high forest cover (≥70 %), as measured by the Global Forest Watch dataset (M. C. Hansen et al., 2013). The forested and non-forested pixels were assigned the average monthly albedo measurement from each measurement method (MODIS, flights, in-situ and modelling average) for the control runs of each experiment. The deforestation runs were then performed by replacing the forested pixels with non-forested pixels.

Table 5.2 describes the annual mean RF of each experiment featuring Amazon deforestation. Experiments 2.1 – 2.5 utilised a control run, with forest and non-forest albedo values taken from MODIS spatial measurements. Replacement 'deforested' albedos were then selected from MODIS spatial, MODIS temporal, and modelling Δ albedo values for experiments 2.1 – 2.3 respectively.

Experiments 2.4 – 2.7 used individual control runs, where the high and low forest albedo were assigned based on the measurement technique prior to deforestation; i.e. non-forested regions were assigned the non-forest albedo measured during the aircraft campaigns or the in-situ campaigns, as were the forested regions. The deforestation runs for these experiments then updated the forested albedo accordingly to align with low forest, simulating widespread deforestation across forested pixels.

Table 5.2: Global annual mean radiative forcings due to Amazon deforestation experiments.

Experiment number	Experiment name	Δ albedo[a]	RF due to Δ albedo (W m^{-2})
2.1	MODIS spatial deforestation	0.017	-0.027
2.2	MODIS temporal deforestation	0.015	-0.022
2.3	Modelling deforestation	0.060	-0.097
2.4	Flight forest deforestation	0.003	-0.006
2.5	Flight change deforestation	0.003	-0.005
2.6	In-situ forest deforestation	0.047	-0.075
2.7	In-situ change deforestation	0.048	-0.075

[a]The albedo change displayed here is the annual average for each experiment; the radiative code used monthly albedo values.

The magnitude of the calculated RF increased with the magnitude of the Δ albedo within the deforestation experiments linearly (Figure 5.2). With a Δ albedo of 0.06, the modelling experiment resulted in the largest negative RF, whereas using values from each of the measurement techniques provide smaller RFs, reflecting their smaller Δα post deforestation.

5.5. South East Asia deforestation experiments

The third set of experiments performed similar runs to the second but focus on measurements over South East Asia. Forested and non-forested pixels were determined using the Global Forest Watch dataset (M. C. Hansen et al., 2013) and the monthly albedo values changed for each experiment.

Each experiment in this section used control runs displaying surface albedo values as calculated from the MODIS spatial analysis. The high forest pixels were then replaced with values of low forest pixels

from the MODIS spatial analysis (exp. 3.1), MODIS temporal analysis (exp. 3.2), oil palm albedo values (exp. 3.3), and increasing the low forest cover by Δα from modelling studies (exp. 3.4).

The deforestation experiments based on MODIS observations of high and low forest cover display the smallest RF (Table 5.3). This again corresponds to the size of the Δ albedo measured across the domains, with a linear relationship shown (Figure 5.2). Simulating deforestation using values obtained from modelling studies resulted in the largest negative radiative forcing from the experiments. This is due to the modelling studies providing a greater Δα than those measured in the region using MODIS.

Table 5.3: Global annual mean radiative forcings due to South East Asia deforestation experiments

Experiment number	Experiment name	Δ albedo[a]	RF due to Δ albedo (W m^{-2})
3.1	MODIS spatial deforestation	0.009	-0.002
3.2	MODIS temporal deforestation	0.017	-0.004
3.3	Oil palm conversion	0.016	-0.003
3.4	Modelling deforestation	0.060	-0.012

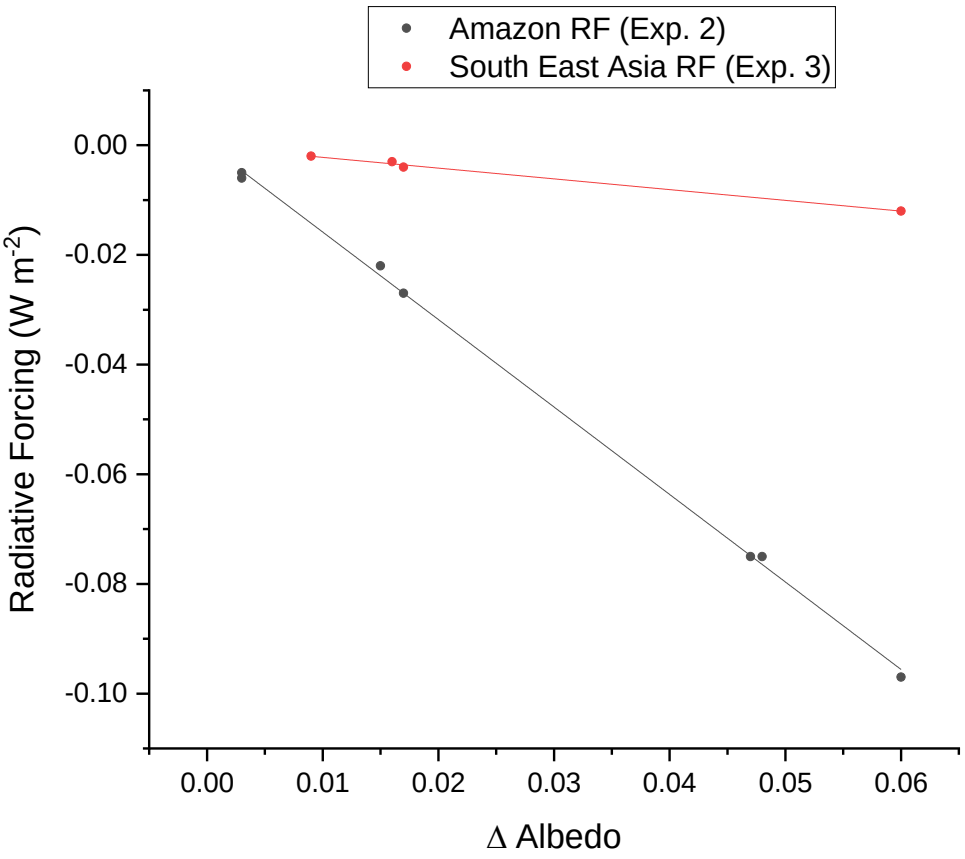

Figure 5.2: The response on Radiative forcing by changing Δ albedo across the different experiment sets. The calculated RF from the deforestation experiments in both the Amazon and South East Asia shows a linear relationship with the magnitude of the albedo changes featured in the experiments (R^2 = 0.99). The response in South East Asia (Exp. 3, red line) is much weaker than across the Amazon (Exp. 2, black line); this is discussed further in Section 5.8.

5.6. Tropical deforestation experiments

As has been shown, deforestation in the Amazon and South East Asia combined is calculated to contribute approximately 65 % of the RF form surface albedo changes due to tropical deforestation. As a result, deforestation across the two regions were combined to assess the potential deforestation across both regions on a global scale.

Four different experiments were performed: three involving MODIS measurements directly and the fourth utilising the changes calculated from models (Table 5.4). Experiment 4.1 uses high and low forest cover observations, 4.2 used Δ albedo values calculated across time from the temporal analysis over each region. Experiment 4.3 utilises the same observations from the spatial analysis as 4.1 over

the Amazon but updates the low forest cover to observations over oil palm concessions over South East Asia to simulate oil palm conversion.

As with the regional sets of experiments, the difference between the measured contributions to surface albedo change from MODIS and the changes contributed by modelling studies is large, with a much greater global annual mean radiative forcing calculated when using the modelling values.

Table 5.4: Global annual mean radiative forcings due to deforestation experiments across the combined tropical regions of the Amazon and South East Asia

Experiment number	Experiment name	RF due to Δ albedo (W m^{-2})
4.1	MODIS spatial deforestation	-0.028
4.2	MODIS temporal deforestation	-0.026
4.3	Oil palm conversion	-0.030
4.4	Modelling deforestation	-0.140

5.7. RCP8.5 scenario experiments

To further understand the impact of deforestation-driven surface albedo changes, experiments utilising representative deforestation rather than idealised deforestation scenarios were conducted. For the IPCC's fifth assessment report (AR5), a number of RCPs were developed to describe a representative pathway to reach a given greenhouse gas concentration trajectory by the year 2100 (Moss et al., 2010). Four of these pathways were carried forward into AR5 (RCP2.6, RCP4.5, RCP6 and RCP8.5) to describe potential trajectories to reach a range of radiative forcing values (2.6, 4.5, 6 and 8.5 W m^{-2} respectively) in 2100 (G. Myhre et al., 2013).

RCP8.5 was often described as the 'business as usual' scenario, describing a trajectory where no policy-driven mitigation of climate change was included, however it is better described as a "very high baseline" scenario, creating a forcing near the 90th percentile for baseline scenarios (van Vuuren et al., 2011). The scenario was developed by the International Institute for Applied Systems Analysis (IIASA) Internal Assessment (IA) Modelling Framework; a set of models describing GHG-related industries (Riahi et al., 2007) and used the MESSAGE energy system model to link the forest management model

DIMA (Dynamic Integrated Model of Forestry and Alternative Land Use) with the world food system model AEZ-WFS (Agro-Ecological Zoning – World Food System).

The scenario led to an increase in cultivated land by over 300 Mha between 2000 – 2100, coupled with a decrease in forested area by 300 Mha between 2000 – 2050, then a further 150 Mha from 2050 – 2100 (Hurtt et al., 2011). Using the datasets created by the Land Use Harmonization project for World Climate Research Program Coupled Model Intercomparison Project phase 5 (CMIP5), forest cover projections consistent with the RCP 8.5 scenario were created for the years 2005, 2050 and 2100 to simulate deforestation consistent with such a scenario over these timescales (Hurtt et al., 2011). Using these projections, two experiments were executed to simulate the changes in forest between 2005 and 2050/2100 respectively (Table 5.5). Forested pixels across the Amazon and South East Asia were assigned albedo values consistent with MODIS forest measurements and changes consistent with MODIS measurements and previous modelling studies were applied to simulate deforestation for non-forested pixels.

Table 5.5: Global annual mean radiative forcings due to deforestation across Amazon and South East Asia consistent with RCP8.5 from a base year of 2005

Experiment number	Experiment name	RF due to Δ albedo (W m^{-2})
5.1	2050 MODIS deforestation	-0.002
5.2	2100 MODIS deforestation	-0.003
5.3	2050 Modelling deforestation	-0.011
5.4	2100 Modelling deforestation	-0.016

As the rates of deforestation in these scenarios are lower compared to the idealised scenarios, where all areas of high forest cover are removed in the same regions, the annual mean radiative forcings for this set of experiments are also lower

5.8. Discussion

The results from this chapter further show the importance of understanding albedo changes in the tropics. Using current model values for surface albedo changes from deforestation in the Amazon, the radiative forcing potentially offsets the carbon dioxide induced radiative forcing of tropical deforestation by 8 % (Figure 5.1). However, using measurements taken during this study, it is suggested this negative radiative forcing contribution is more likely to be approximately 2 %. Using in-

situ measurements from Culf et al., (1995), this value could be raised to 6 %, again much lower than what is currently modelled.

Similar conclusions are drawn from the South East Asia experiments; with the radiative forcing from modelling-assigned albedo changes being calculated almost an order of magnitude larger than those from MODIS observations. This additionally holds true for the modelled conversion to oil palm, which results in a similar radiative response to more general drivers of deforestation.

Combining observations made across South East Asia and the Amazon results in a large range of calculated radiative forcings (Table 5.4). Using these values, the variation of Δ albedo measurements is carried forward into the RF calculations. Contributing a global annual mean radiative forcing between -0.14 W m^{-2} for modelling Δ albedo values, to -0.028 W m^{-2} for MODIS observations, we can assess the impact this has on the net radiative forcing from tropical deforestation by using values from Scott et al., (2018).

Firstly, the assumption is made that the relationship between radiative forcing contributions from each region and the area of forest loss is linear; that is each region gives the same contribution towards albedo change induced RF as it does to CO_2 and SLCF RFs as a result of deforestation. By making this assumption, the contribution to CO_2 and SLCF from South East Asia and the Amazon can be estimated.

Using the contribution ratios calculated within the first set of experiments, the RF is attributed and the impact of changing the surface albedo is seen in Figure 5.3. The MODIS observations result in a reduced impact of surface albedo within the tropics, but updating the surface albedo changes to typical model values leads to large reductions in the potential net RF.

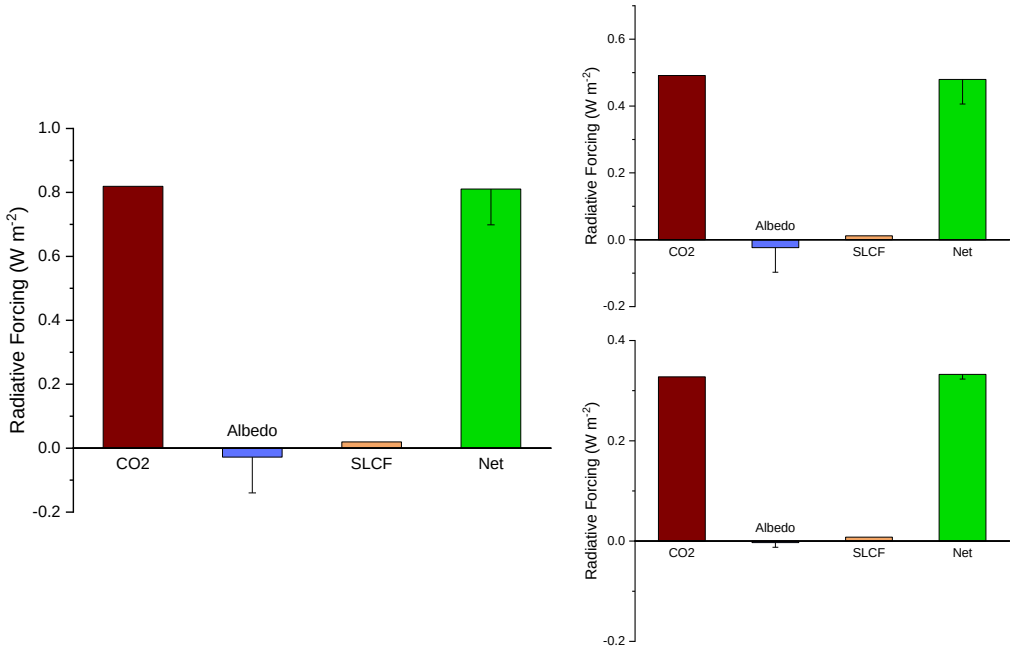

Figure 5.3: Global annual mean radiative forcings (RF) due to changes in the concentrations of CO2 (red), changes to surface albedo derived from MODIS observations (purple) and changes to concentrations of short-lived climate forcings (SLCFs - orange) for deforestation across the combined regions of South East Asia and the Amazon (left panel), with individual regions of the Amazon (top right) and South East Asia (bottom right). Error bar on albedo and net RF show the potential RF when albedo changes are taken from modelling studies. Values for CO_2 and SLCF RFs are calculated in Scott et al., 2018.

Values of Δ albedo derived from MODIS measurements give a negative RF 5 % of the CO_2 RF in the Amazon, 1 % in South East Asia and 3.5 % when combined over the two regions. Altering these Δ albedo to typical model values give a negative contribution to the net RF 20 %, 4 % and 17 % of the CO_2 RF across the Amazon, South East Asia and the combined region respectively. This implies that estimating the impact of albedo changes from deforestation in the tropics can lead to an overestimation using current models by a factor of between 4 and 5.

In the experiment set 1, South East Asia contributes 65 % of the Amazonian contribution for radiative forcing, however this relative contribution drops greatly for experiment set 3. As the model, and thus the selection of forest cover, are performed on a 2.5° grid, the nature of the islands across South East Asia mean many pixels in the region are unable to meet the requirement of 70 % forest cover, or overlap strongly with water and are thus excluded from the analysis. This resulted in only 75 Mha of

forest, compared to almost 260 Mha used in the RCP experiments (set 5), being deforested in the experiments. Two approaches were taken to overcome this issue and to investigate whether doing so increased the low contributions to deforestation induced radiative forcing from South East Asia.

Firstly, the restriction on water cover was removed, allowing pixels with greater than 10 % water cover to be selected. Then two approaches were taken, firstly the threshold for forest cover was reduced from 70 % to 50 % of the pixel. This tripled the number of pixels that were selected for deforestation in the model scenarios, and the experiment set 3 were rerun (set 3a). The greater number of pixels resulted in larger radiative forcing (Table 5.6) and a stronger response to Δ albedo, although still not as strong as observed in the Amazon experiments (Figure 5.4).

Table 5.6: Global annual mean radiative forcings due to South East Asia deforestation experiments using a 50 % forest cover threshold for selecting pixels to be deforested.

Experiment number	Experiment name	Δ albedo	RF due to Δ albedo (W m^{-2})
3.1a	MODIS spatial deforestation	0.009	-0.006
3.2a	MODIS temporal deforestation	0.017	-0.012
3.3a	Oil palm conversion	0.016	-0.011
3.4a	Modelling deforestation	0.060	-0.042

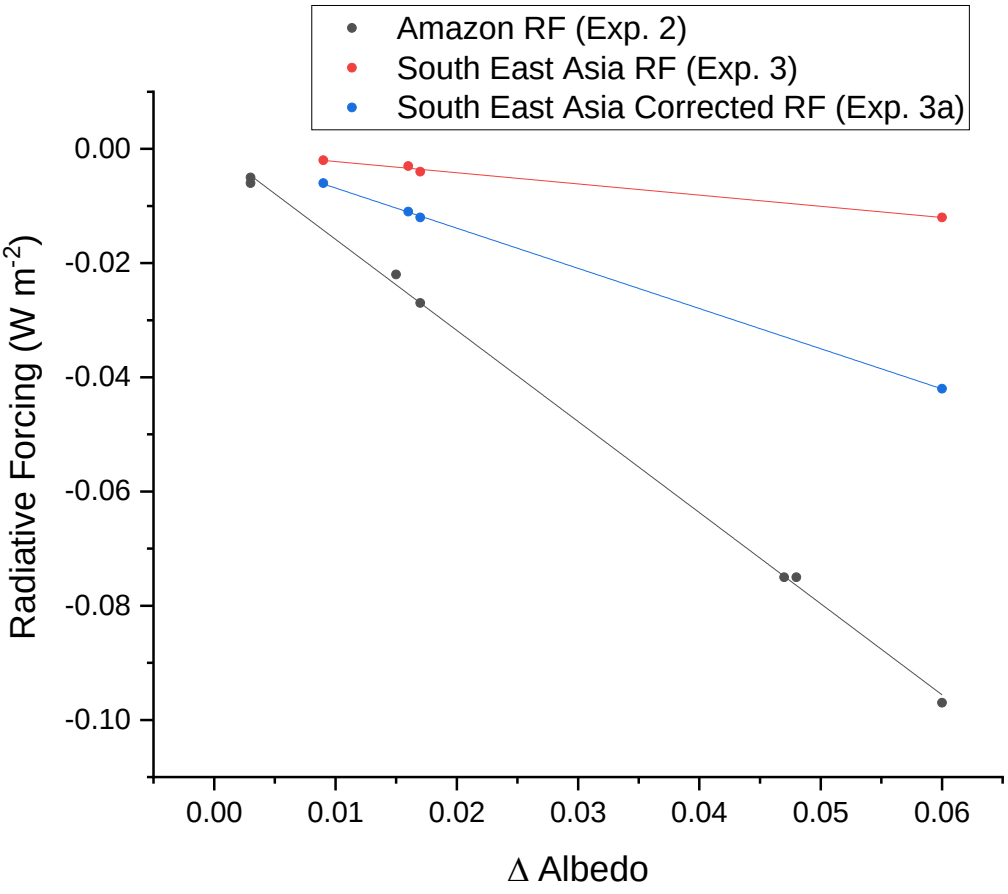

Figure 5.4: The response on Radiative forcing by changing Δ albedo across the different experiment sets. Decreasing the threshold to detect high forest cover to 50% of the pixel's area (Exp. 3a, blue line) results in a greater response than the original South East Asia experiments (Exp. 3, red line), although the Amazon's response is still stronger (Exp. 2, black line).

Pixels covering approximately 250 Mha were identified as forest using this method, the equivalent area of total forest in the region. However, the calculated RFs for South East Asia are between approximately 25 – 50 % those of the Amazon.

The second method normalised the RF to the area deforested in experiment set 3, then calculated the expected RF given as a result of complete deforestation in the region. Using the 258 Mha calculated with the methodology from Hurtt et al., (2011) for experiment set 5, the RF associated with complete deforestation in the region was calculated (Table 5.7).

Table 5.7: Global annual mean radiative forcings due to South East Asia deforestation experiments, calculated by expanding the RF response to area deforested from experiment set 3 to 258 Mha, in line with the area of forest calculated for experiment set 5.

Experiment number	Experiment name	Δ albedo	RF due to Δ albedo (W m^{-2})
3.1b	MODIS spatial deforestation	0.009	-0.006
3.2b	MODIS temporal deforestation	0.017	-0.012
3.3b	Oil palm conversion	0.016	-0.011
3.4b	Modelling deforestation	0.060	-0.042

Both methods result in a similar deforestation area in the region, and result in similar RFs, suggesting the model has a linear response to the deforestation area in the region, as well as to the magnitude of the surface albedo change.

Changing the forest threshold over South East Asia allows a combined simulation using SOCRATES with the increased South East Asia contribution. Rerunning experiment set 4 results in a similar RF across each of the MODIS experiments of approximately -0.035, with the oil palm conversion slightly higher than the spatial and temporal Δα experiments (Table 5.8). As with the previous experiment sets in this chapter, the simulation using modelling Δα results in a greater radiative forcing.

Table 5.8: Global annual mean radiative forcings due to deforestation experiments across the combined tropical regions of the Amazon and South East Asia, increasing the forest area deforested in South East Asia.

Experiment number	Experiment name	RF due to Δ albedo (W m^{-2})
4.1a	MODIS spatial deforestation	-0.033
4.2a	MODIS temporal deforestation	-0.034
4.3a	Oil palm conversion	-0.037
4.4a	Modelling deforestation	-0.169

Figure 5.5 shows the impact of increasing the deforested area across South East Asia; the RF contributed by the albedo changes is larger than the positive RF from SLCFs for the combined deforestation case and is approximately equal in South East Asia when the MODIS albedo changes are

used. Using model assigned Δα values, the combined regional deforestation now offsets approximately 20 % of the positive CO_2 RF, and 12.5 % across South East Asia.

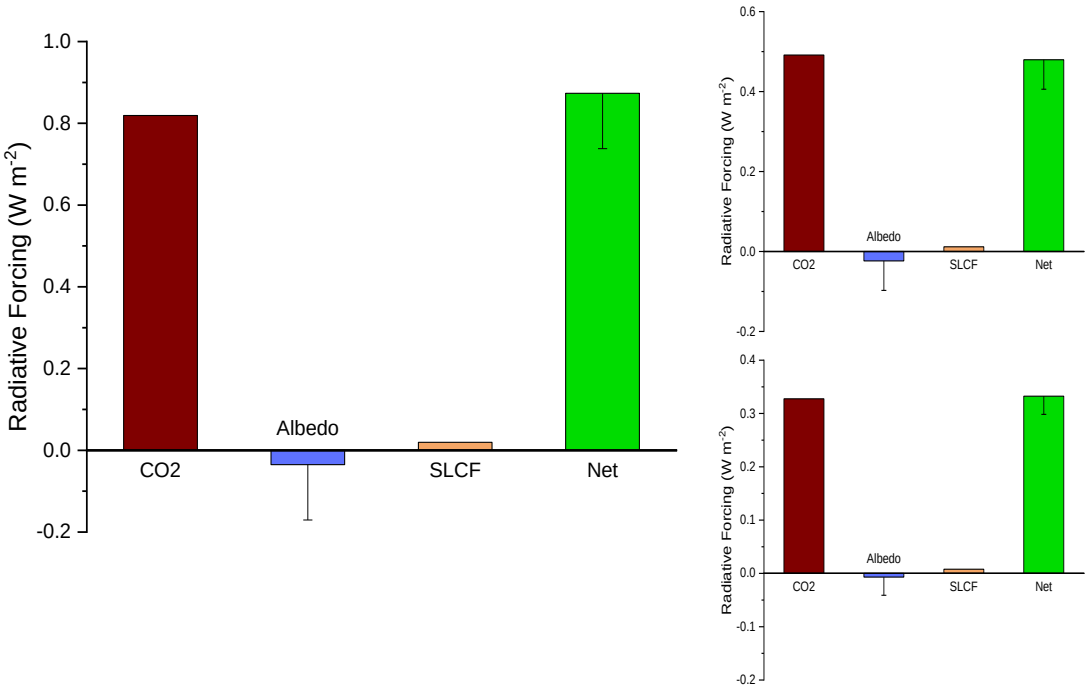

Figure 5.5: As for Figure 5.3, with updated forest cover over South East Asia to align with a greater area of forest cover aligning with a lower (50 %) threshold as defined by the Global Forest Watch dataset.

This strongly suggests using surface albedo values from models may be underestimating the net RF, and thus the warming impact of deforestation in these regions.

5.9. Conclusions

The analysis presented here further enhance the argument that albedo changes within the tropics should be carefully considered when simulating deforestation in the region. As different measurement techniques appear to provide different surface albedo measurements, and thus variable surface albedo changes post deforestation, there is no consistency in global annual mean radiative forcing from such land use change.

Combined, the Amazon and South East Asia deforestation contribute 65 % of the RF due to albedo changes across the tropics, which in turn contributes 19 % of the albedo change RF for global deforestation. However, as albedo measurements differ in both regions, the albedo induced RFs are shown to be poorly constrained, with large variation observed dependent on measurement technique.

The values obtained from the idealised deforestation scenarios are shown to be large, but differences between albedo measurements from MODIS and typical modelling study values are shown to give stark differences, even in non-extreme deforestation scenarios, following RCP8.5.

Overall, a need for better constrained surface albedo measurements across the tropics is presented here. Without such improvements, models featuring deforestation in the tropics may be strongly overestimating the surface albedo cooling effect. As a result, the warming impact of deforestation may be strongly underestimated, potentially by 43 % of the warming effect that CO_2 contributes.

Chapter 6: Conclusions and Further Work

6.1. Conclusions

This project aimed to assess the changes in albedo after tropical deforestation and the role it plays in affecting the climate. Chapter 3 analysed previous measurements of albedo and its use in modelling scenarios, whilst using a range of observation techniques to lead a discussion on the albedo change of deforestation across the Amazon. Chapter 4 used MODIS satellite observations to compare deforestation-related albedo changes in South East Asia across its major land masses, whilst assessing the impact that oil palm conversion has had on the surface albedo in the region. Chapter 4 also explored the relationship of time since the occurrence of forest loss on the surface albedo. Chapter 5 focused on the climatic implications of deforestation-driven albedo changes across the regions.

In Chapter 3, evaluation of the literature resulted in 56 modelling studies and 13 observational studies highlighting albedo changes between forested areas and non-forested areas in the tropics. Surface albedo of forests is lower than that of replacement vegetation (e.g. grass for pasture, or crops), but values used in the modelling studies have previously prescribed changes 25 % higher than were presented in observations.

MODIS observations of surface albedo, whilst providing good spatial and temporal data, presents challenges in data collection over the tropics due to cloud coverage. Aggregating the data over three years into monthly files presented near-complete coverage of the Amazon region. Areas of forest in the Amazon exhibit lower surface albedo than areas of non-forest across the entire region, displaying a near-linear response to percentage forest cover.

Observations of surface albedo were similar between the periods 2000-2003 and 2013-2015, with the same monthly variation displayed across each domain analysed. Although areas of non-forest were consistent through the year, the forested pixels displayed a strong seasonal cycle through the year – with a peak albedo in October / November and a minimum in June / July.

Both temporal and spatial approaches were used to improve validation of spatial-for-temporal analysis that has previously been undertaken. Across the Amazon, both approaches resulted in similar albedo differences between forest and non-forested pixels, with similar intra-annual variation also observed.

Observations from the SAMBBA and GoAmazon flight campaigns presented their own difficulties in their usage, as the campaigns were focused on air pollution monitoring, much of the data acquisition was unsuitable for surface albedo measurements due to poor atmospheric conditions. The usable data was scaled up with a bootstrapping method and observations from each campaign displayed similar surface albedo measurements to each other, although the absolute albedos of both forest and non-forested areas were higher than MODIS observations. The flight campaigns also exhibited lower albedo differences between forested and non-forested pixels than those from MODIS over the same areas.

Using a full dataset from an in-situ study, measured albedo values for forested areas were similar to MODIS observations (approximately 0.13), but non-forested measurements displayed a surface albedo 0.03 and 0.02 greater than MODIS and the flight data, respectively. Hence, differences between forest and non-forested land were shown to be higher using the in-situ data.

Although the observations displayed varying albedo differences, the magnitude of each were significantly lower than those used in modelling studies in the literature. As a result, the observations over the Amazon suggest that modelling studies may be underestimating the warming impact of deforestation.

Chapter 4 further analyses the relationship between surface albedo changes and deforestation. Across South East Asia, deforestation has been higher at times across the last decade than within the Amazon, with a major driver being conversion of forest to palm oil. Similar to the Amazonian region, the surface albedo differences between forest and non-forest ($\Delta\alpha_S$) generally across the region is much lower than reported in modelling studies in the literature. However, the behaviour between albedo of non-forested areas across the landmasses of Borneo, Java, the Malay Peninsula, Sulawesi and Sumatra showed considerable variability; with Sumatra and Borneo displaying a similar seasonal relationship.

The change in albedo following forest loss also showed lower changes than are observed in modelling studies, with each landmass showing slightly higher albedo changes post-deforestation than $\Delta\alpha_S$, although the size of difference between the two techniques was small. Similarly to the Amazonian analysis, a spatial-for-temporal analysis technique across the region appears to be a reasonable proxy for a direct temporal comparison.

The conversion of forest to oil palm is an important driver of deforestation in the region and large areas of land are conceded to oil palm plantations. The albedo of both forest and non-forested land

within these concessions show significantly higher albedo observations than areas outside of concessions. Java, potentially as a result of its state-owned plantation companies focusing their plantations on tea, sugar, coffee and tobacco rather than oil palm, displayed consistently lower surface albedo within concession areas than the other islands' concession areas (Potter, 2015). The higher albedo of non-forested land in concessions may point to less mature oil palm having been planted, but not reaching the size to be considered a tree using the Global Forest Watch dataset.

Regarding the $\Delta\alpha_s$ and $\Delta\alpha_T$ values observed between concession and non-concession areas, no discernible differences were observed. So, whilst analysis of the absolute albedo measurements appears to be a good indicator for locations of palm oil across South East Asia, this would be difficult to distinguish by assessing the change alone, provided no new concessions are granted.

The albedo of forested areas that had undergone forest loss within concession areas showed a slight decrease with time since loss occurring, except for the most recent years of forest loss (2013 onwards), which display a surface albedo 0.19 higher than the immediately preceding years. This higher albedo could be an indicator of young oil palm in the region.

Chapter 5 explores the radiative forcing that results from surface albedo changes from a range of idealised deforestation scenarios using the Suite Of Community RAdiative Transfer codes based on Edwards and Slingo (SOCRATES). Even in the tropics, the surface albedo change is the second largest radiative effect following deforestation, so modelling incorrect changes could lead to significant impacts in the overall radiative forcing. As forest loss results in an increase in surface albedo, a negative radiative forcing contribution from this change results.

Crucially, these results indicate albedo values within South East Asia and the Amazon are both unique to each region and to the values commonly used in models. Therefore, modelling studies of deforestation in the tropics should carefully consider the magnitude of the smaller biophysical changes associated with deforestation to ensure that they are capturing accurate changes and further observational studies aimed to collect such data may be required.

The magnitudes of the radiative forcing changes were explored across the Amazon and South East Asia based on the observations made in Chapters 3 and 4. Approximately 40 % of the RF contribution from albedo change due to tropical deforestation is due to changes across the Amazon, with 26 % from South East Asia. The magnitude of the radiative forcing depended on the magnitude of the albedo changes observed, thus modelling the change across the Amazon using the flight albedo

observations results in a smaller albedo RF contribution than using values from MODIS. In turn, in-situ observations were shown produce a larger RF than MODIS, although each based on observations were smaller than the changes based on model-prescribed changes.

Similarly, simulations based on MODIS observations across South East Asia result in smaller RFs than simulations using model-prescribed changes as a result of the smaller Δ albedo. The RF in the region is strongly dependent on the replacement vegetation, however. Conversion from forest to oil palm, rather than to grass/crops, results in a much larger albedo change and thus an RF on a similar magnitude of the model-prescribed simulation.

Combining the deforestation across the two regions results in more dramatic variation of the RFs. Increasing the surface albedo in line with the modelling studies highlighted in Chapter 3 results in a large RF (~-0.14 W m^{-2}), approximately 8 times that derived from forest loss as measured by MODIS. Combining oil palm conversion in South East Asia with conversion to grass/crops in the Amazon also results in a larger change. Finally, the combined simulations allow for the separation of a spatial-for-temporal approach with a purely temporal analysis. The former, where observations are made between land cover classes within the same time period, results in a lower RF than comparing direct change over time. Much of this difference is driven by the higher $\Delta\alpha_T$ across most of South East Asia, as seen in Chapter 3. This difference suggests that, whilst a spatial-for-temporal approach may lead to a reasonable estimation, measuring direct changes from forest loss is important.

Realistic deforestation scenarios were also explored, with forest levels consistent with RCP8.5 for the years 2000, 2050 and 2100 simulated. Assigning the albedo changes to be consistent with the MODIS observations result in a small RF (-0.002 and -0.003) for both years, however model-derived values increase these approximately fivefold (-0.011 and -0.016).

The results presented within this work suggest that the warming from tropical deforestation thus far has been underestimated. The reduction in the cooling influence of surface albedo in the tropics results in a larger net warming effect for deforestation. Previously, historic land use change between 800 – 1992 has been estimated to result in an RF from surface albedo change of -0.2 W m^{-2}, with strongly negative values in the tropical region, due to the combination of a large albedo change and high insolation (Houghton et al., 2001; Pongratz et al., 2011). These results suggest that this cooling is likely too large, and thus the net RF of +0.15 W m^{-2} that was calculated is likely larger.

As these results suggest tropical deforestation is contributing a larger positive radiative forcing than previously thought, putting a pause to the increasing rates and pushing to reduce the amount of deforestation in the tropics is more important to mitigate climate change than before.

6.2. Further Work

Analysing the surface albedo across two of the continental tropical forests has shown their uniqueness in terms of albedo values and changes and grouping their values has been shown to lead to inconsistencies versus observations. As such, this work highlights the need for the albedo across the tropical forests of the African continent to also be analysed to ensure the correct changes are being captured in modelling studies. However, the discrepancies between observations are also important to highlight here: although MODIS has been evaluated multiple times previously over a range of vegetation surfaces, the inconsistency between previous in-situ observations and modelling studies is concerning. Therefore, further work on scaling up observations to the satellite pixel level would also be needed. Although the Amazon displayed relative consistency across the region, the behaviour of the surface albedo across the land masses of South East Asia contained significant variability. It would therefore be important to understand the type of land use and the types of forest between the islands, so that this variability can be attributed. Further observational studies in this area would allow for this. Integrating the use of high-resolution satellite imagery to improve identification of oil palm in the region (e.g. Descals et al., 2020) would also provide better awareness as to the climatic differences between plantations and forest classifications.

Understanding the impact of historic land use on the current climate is important, and so there is scope for reevaluating the historic RF, as well as predicting the change based on other futuristic deforestation scenarios with updated surface albedo changes. Further to this, using a more complex model, such as an Earth system model (e.g. UKESM1), which both dynamically updates vegetation and the atmosphere as changes occur, would allow more accurate estimations of the RFs from surface albedo changes and would put it in context with RFs from changes in CO_2 and SLCFs, as well as other the climate influences forests have, as discussed in Chapter 1.

Whilst the design of further experiments to explore the research space surrounding albedo changes would provide valuable insight to the research community on the overall impact of LUC, the implementation of the findings reported here should be used in the continuous improvement of climate models. That models' albedo values appear not to match observations across the tropics is

concerning and further verification should take place, potentially with a recommendation that more complexity should be focused on how albedo values of vegetated surfaces within models are derived. As computational expense of models becomes less of an issue with time and the complexity of models is able to grow, traditional land cover classifications should also be broken down to add further granularity regarding vegetation types and their climatic influence. Implementing both of these will enable our understanding of how changing forests in various regions will impact the climate to grow further.

References

Abood, S. A., Lee, J. S. H., Burivalova, Z., Garcia-Ulloa, J., & Koh, L. P. (2015). Relative Contributions of the Logging, Fiber, Oil Palm, and Mining Industries to Forest Loss in Indonesia. *Conservation Letters*, *8*(1), 58–67. https://doi.org/10.1111/conl.12103

Achard, F., Eva, H. D., Stibig, H. J., Mayaux, P., Gallego, J., Richards, T., & Malingreau, J. P. (2002). Determination of deforestation rates of the world's humid tropical forests. *Science*, *297*(5583), 999–1002. https://doi.org/10.1126/science.1070656

Albrecht, B. A. (1989). Aerosols, Cloud Microphysics, and Fractional Cloudiness. *Science*, *245*, 1227–1230. https://doi.org/10.1126/science.245.4923.1227

Alkama, R., & Cescatti, A. (2016a). Biophysical climate impacts of recent changes in global forest cover. *Science*, *351*(6273), 600–604.

Alkama, R., & Cescatti, A. (2016b). Supplementary: Biophysical climate impacts of recent changes in global forest cover. *Science*, *351*(6273), 600–604. https://doi.org/10.1126/science.aac8083

Allan, J. D., Morgan, W. T., Darbyshire, E., Flynn, M. J., Williams, P. I., Oram, D. E., et al. (2014). Airborne observations of IEPOX-derived isoprene SOA in the Amazon during SAMBBA. *Atmospheric Chemistry and Physics*, *14*(20), 11393–11407. https://doi.org/10.5194/acp-14-11393-2014

Allen, M. R., Dube, O. P., Solecki, W., Aragón-Durand, F., Cramer, W., Humphreys, S., et al. (2018). Framing and Context. In *Global Warming of 1.5°C. An IPCC Special Report on the impacts of global warming of 1.5°C above pre-industrial levels and related global greenhouse gas emission pathways, in the context of strengthening the global response to the threat of climate change,*.

Andre, R. G. B., & Viswanadham, Y. (1983). Radiation balance of soybeans grown in Brazil. *Agricultural Meteorology*, *30*(3), 157–173. https://doi.org/10.1016/0002-1571(83)90049-3

Andrews, T., Betts, R. A., Booth, B. B. B., Jones, C. D., & Jones, G. S. (2017). Effective radiative forcing from historical land use change. *Climate Dynamics*, *48*(11–12), 3489–3505. https://doi.org/10.1007/s00382-016-3280-7

Arjasakusuma, S., Yamaguchi, Y., Hirano, Y., & Zhou, X. (2018). ENSO-and rainfall-sensitive vegetation regions in Indonesia as identified from multi-sensor remote sensing data. *ISPRS International*

Journal of Geo-Information, *7*(3). https://doi.org/10.3390/ijgi7030103

Arora, V. K., & Montenegro, A. (2011). Small temperature benefits provided by realistic afforestation efforts. *Nature Geoscience*, *4*(8), 514–518. https://doi.org/10.1038/ngeo1182

As-syakur, A. R., Tanaka, T., Osawa, T., & Mahendra, M. S. (2013). Indonesian rainfall variability observation using TRMM multi-satellite data. *International Journal of Remote Sensing*, *34*(21), 7723–7738. https://doi.org/10.1080/01431161.2013.826837

Austin, K. G., Kasibhatla, P. S., Urban, D. L., Stolle, F., & Vincent, J. (2015). Reconciling oil palm expansion and climate change mitigation in Kalimantan, Indonesia. *PLoS ONE*, *10*(5), 1–17. https://doi.org/10.1371/journal.pone.0127963

Bala, G., Caldeira, K., Wickett, M., Phillips, T. J., Lobell, D. B., Delire, C., & Mirin, a. (2007). Combined climate and carbon-cycle effects of large-scale deforestation. *Proceedings of the National Academy of Sciences of the United States of America*, *104*(16), 6550–5. https://doi.org/10.1073/pnas.0608998104

Bastable, H. G., Shuttleworth, W. J., Dallarosa, R. L. G., Fisch, G., & Nobre, C. A. (1993). Observations of climate, albedo, and surface radiation over cleared and undisturbed amazonian forest. *International Journal of Climatology*, *13*(7), 783–796. https://doi.org/10.1002/joc.3370130706

Bathiany, S., Claussen, M., Brovkin, V., Raddatz, T., & Gayler, V. (2010). Combined biogeophysical and biogeochemical effects of large-scale forest cover changes in the MPI earth system model. *Biogeosciences*, *7*(5), 1383–1399. https://doi.org/10.5194/bg-7-1383-2010

Bazzaz, E. A., & Pickett, S. T. A. (1980). TROPICAL SUCCESSION: A Comparative Review. *Ann Rev. Ecol. Syst.*, *11*(20), 287–310.

Bellouin, N., Quaas, J., Gryspeerdt, E., Kinne, S., Stier, P., Watson-Parris, D., et al. (2019). Bounding global aerosol radiative forcing of climate change. *Reviews of Geophysics*, 1–45. https://doi.org/10.1029/2019rg000660

Berbet, M. L. C., & Costa, M. H. (2003). Climate change after tropical deforestation: Seasonal variability of surface albedo and its effects on precipitation change. *Journal of Climate*, *16*(12), 2099–2104. https://doi.org/10.1175/1520-0442(2003)016<2099:CCATDS>2.0.CO;2

Betts, A. K., Desjardins, R. L., & Worth, D. (2007). Impact of agriculture, forest and cloud feedback on

the surface energy budget in BOREAS. *Agricultural and Forest Meteorology*, *142*(2–4), 156–169. https://doi.org/10.1016/j.agrformet.2006.08.020

Betts, R. A. (2000). Offset of the potential carbon sink from boreal forestation by decreases in surface albedo. *Nature*, *408*(6809), 187–190. https://doi.org/10.1038/35041545

Betts, Richard A. (2001). Biogeophysical impacts of land use on present-day climate: Near-surface temperature change and radiative forcing. *Atmospheric Science Letters*, *2*(1–4), 39–51. https://doi.org/10.1006/asle.2001.0023

Blad, B. L., & Baker, D. G. (1971). Reflected Radiation from a Soybean Crop. *Agronomy Journal*, *64*(3), 277–280.

Blois, J. L., Williams, J. W., Fitzpatrick, M. C., Jackson, S. T., & Ferrier, S. (2013). Financial Contraints of Ethnic Entreprenurs. *Proceedings of the National Academy of Sciences*, *110*(23), 9374–9379. https://doi.org/10.5061/dryad.d5f1r.1

Bonan, G. B. (2008a). Forests and climate change: forcings, feedbacks, and the climate benefits of forests. *Science*, *320*, 1444–1449. https://doi.org/10.1126/science.1155121

Bonan, G. B. (2008b). Forests in Flux Forests and Climate of Forests Climate Benefits Change, and the Climate benefit of Forests. *Science*, *320*(5882), 1444–1449.

Bourgeois, C. S., Calanca, P., & Ohmura, A. (2006). A field study of the hemispherical directional reflectance factor and spectral albedo of dry snow. *Journal of Geophysical Research Atmospheres*, *111*(20), 1–13. https://doi.org/10.1029/2006JD007296

Brandon, K. (2015). *Ecosystem Services from Tropical Forests: Review of Current Science*. *CGD Climate and Forest Paper Series #7*. https://doi.org/10.2139/ssrn.2622749

Branković, Č., Molteni, F., & Viterbo, P. (2006). GCM sensitivity experiments with locally modified land surface properties over tropical South America. *Climate Dynamics*, *26*(7–8), 729–749. https://doi.org/10.1007/s00382-006-0112-1

Brito, J., Rizzo, L. V., Morgan, W. T., Coe, H., Johnson, B., Haywood, J., et al. (2014). Ground-based aerosol characterization during the South American Biomass Burning Analysis (SAMBBA) field experiment. *Atmospheric Chemistry and Physics*, *14*(22), 12069–12083. https://doi.org/10.5194/acp-14-12069-2014

Busch, J., Ferretti-gallon, K., Engelmann, J., Wright, M., Kemen, G., Stolle, F., et al. (2018). Reductions in emissions from deforestation from Indonesia's moratorium on new oil palm, timber, and logging concessions, *112*(5), 1–6. https://doi.org/10.7910/DVN/28615

Caiazzo, F., Malina, R., Staples, M. D., Wolfe, P. J., Yim, S. H. L., & Barrett, S. R. H. (2014). Quantifying the climate impacts of albedo changes due to biofuel production: A comparison with biogeochemical effects. *Environmental Research Letters*, *9*(2). https://doi.org/10.1088/1748-9326/9/2/024015

Camredon, M., Aumont, B., Lee-Taylor, J., & Madronich, S. (2007). The SOA/VOC/NOx system: An explicit model of secondary organic aerosol formation. *Atmospheric Chemistry and Physics*, *7*(21), 5599–5610. https://doi.org/10.5194/acp-7-5599-2007

Carswell, F. E., Costa, A. L., Palheta, M., Malhi, Y., Meir, P., Costa, J. D. P. R., et al. (2002). Seasonality in CO2 and H2O flux at an eastern Amazonian rain forest. *Journal of Geophysical Research D: Atmospheres*, *107*(20). https://doi.org/10.1029/2000JD000284

Cescatti, A., Marcolla, B., Santhana Vannan, S. K., Pan, J. Y., Román, M. O., Yang, X., et al. (2012). Intercomparison of MODIS albedo retrievals and in situ measurements across the global FLUXNET network. *Remote Sensing of Environment*, *121*, 323–334. https://doi.org/10.1016/j.rse.2012.02.019

Chong, K. L., Kanniah, K. D., Pohl, C., & Tan, K. P. (2017). A review of remote sensing applications for oil palm studies. *Geo-Spatial Information Science*, *20*(2), 184–200. https://doi.org/10.1080/10095020.2017.1337317

Claussen, M., Brovkin, V., & Ganopolski, A. (2001). Biophysical versus biogeochemical feedbacks of large-scale land cover change. *Geophysical Research Letters*, *28*(6), 1011–1014. https://doi.org/10.1029/2000GL012471

Coakley, J. A. (2002). Reflectance and Albedo, Surface. In J. A. Curry & J. A. Pyle (Eds.), *Encyclopedia of Atmospheric Sciences* (1st ed., pp. 1914–1923). https://doi.org/10.1016/B0-12-227090-8/00069-5

Correia, F. W. S., Alvalá, R. C. S., & Manzi, A. O. (2008). Modeling the impacts of land cover change in Amazonia: A regional climate model (RCM) simulation study. *Theoretical and Applied Climatology*, *93*(3–4), 225–244. https://doi.org/10.1007/s00704-007-0335-z

Costa, M. H., Yanagi, S. N. M., Souza, P. J. O. P., Ribeiro, A., & Rocha, E. J. P. (2007). Climate change in Amazonia caused by soybean cropland expansion, as compared to caused by pastureland expansion. *Geophysical Research Letters*, *34*(7), 2–5. https://doi.org/10.1029/2007GL029271

Culf, A. D., Fisch, G., & Hodnett, M. G. (1995). The Albedo of Amazonian Forest and Ranch Land. *Journal of Climate*, *8*, 1544–1554.

Curtis, P. G., Slay, C. M., Harris, N. L., Tyukavina, A., & Hansen, M. C. (2018). Classifying drivers of global forest loss. *Science*, *361*(6407), 1108–1111. https://doi.org/10.1126/science.aau3445

Davin, E. L., & de Noblet-Ducoudre, N. (2010). Climatic impact of global-scale Deforestation: Radiative versus nonradiative processes. *Journal of Climate*, *23*(1), 97–112. https://doi.org/10.1175/2009JCLI3102.1

Dawson, J. P., Adams, P. J., & Pandis, S. N. (2007). Sensitivity of ozone to summertime climate in the eastern USA: A modeling case study. *Atmospheric Environment*, *41*(7), 1494–1511. https://doi.org/10.1016/j.atmosenv.2006.10.033

Descals, A., Wich, S., Meijaard, E., Gaveau, D., Peedell, S., & Szantoi, Z. (2020). High-resolution global map of smallholder and industrial closed-canopy oil palm plantations. *Earth System Science Data Discussions*, *Preprint*(August), 1–22. https://doi.org/10.5194/essd-2020-159

Devaraju, N., Bala, G., & Nemani, R. (2015). Modelling the influence of land-use changes on biophysical and biochemical interactions at regional and global scales. *Plant, Cell and Environment*, *38*(9), 1931–1946. https://doi.org/10.1111/pce.12488

Dickinson, R. E., & Henderson-Sellers, A. (1988). Modelling tropical deforestation: A study of GCM land-surface parametrizations. *Quarterly Journal of the Royal Meteorological Society*, *114*(480), 439–462. https://doi.org/10.1256/smsqj.48008

Dickinson, R. E., & Kennedy, P. (1992). Impacts on regional climate of Amazon deforestation. *Geophysical Research Letters*, *19*(19), 1947–1950. https://doi.org/10.1029/92GL01905

Donato, D. C., Kauffman, J. B., Murdiyarso, D., Kurnianto, S., Stidham, M., & Kanninen, M. (2011). Mangroves among the most carbon-rich forests in the tropics. *Nature Geoscience*, *4*(5), 293–297. https://doi.org/10.1038/ngeo1123

Eck, T. F., Holben, B. N., Slutsker, I., & Setzer, A. (1998). Measurements of irradiance attenuation and

estimation of aerosol single scattering albedo for biomass burning aerosols in Amazonia. *Journal of Geophysical Research Atmospheres*, *103*(D24), 31865–31878. https://doi.org/10.1029/98JD00399

Edwards, J. M., & Slingo, A. (1996). Studies with a flexible new radiation code. I: Choosing a configuration for a large-scale model. *Quarterly Journal of the Royal Meteorological Society*, *122*(531), 689–719. https://doi.org/10.1256/smsqj.53106

Eltahir, E. A. B., & Humphries, E. J. (1998). The role of clouds in the surface energy balance over the Amazon forest. *International Journal of Climatology*, *18*(14), 1575–1591. https://doi.org/10.1002/(SICI)1097-0088(19981130)18:14<1575::AID-JOC316>3.0.CO;2-U

Elvidge, C. D., Zhizhin, M., Hsu, F. C., Baugh, K., Khomarudin, M. R., Vetrita, Y., et al. (2015). Long-wave infrared identification of smoldering peat fires in Indonesia with nighttime Landsat data. *Environmental Research Letters*, *10*(6). https://doi.org/10.1088/1748-9326/10/6/065002

Estoque, R. C., Ooba, M., Avitabile, V., Hijioka, Y., DasGupta, R., Togawa, T., & Murayama, Y. (2019). The future of Southeast Asia's forests. *Nature Communications*, *10*(1), 1–12. https://doi.org/10.1038/s41467-019-09646-4

Estoque, R. C., Ooba, M., Avitabile, V., Hijioka, Y., Dasgupta, R., Togawa, T., & Murayama, Y. (2019). The future of Southeast Asia's forests. *Nature Communications*, *10*, 1–12. https://doi.org/10.1038/s41467-019-09646-4

FAO. (2006). *Global Forest Resources Assessment 2005: Progress towards sustainable forest management*.

Fearnside, P. M. (2005). Deforestación en la Amazonía Brasileña: Historia, Tasas y Consecuencias. *Conservation Biology*, *19*(3), 680–688. https://doi.org/10.1111/j.1523-1739.2005.00697.x

Federative Republic of Brazil. (2015). *Brazil Intended Nationally Determined Contribution*. Retrieved from http://www.loc.gov/law/help/guide/nations/brazil.php

Ferrante, L., & Fearnside, P. M. (2019). Brazil's new president and "ruralists" threaten Amazonia's environment, traditional peoples and the global climate. *Environmental Conservation*, 11–13. https://doi.org/10.1017/S0376892919000213

Finegan, B. (1996). Pattern and process in neotropical secondary rain forests: The first 100 years of

succession. *Trends in Ecology and Evolution*, *11*(3), 119–124. https://doi.org/10.1016/0169-5347(96)81090-1

Foley, J. A., DeFries, R., Asner, G. P., Barford, C., Bonan, G., Carpenter, S. R., et al. (2005). Global consequences of land use. *Science*, *309*(5734), 570–574. https://doi.org/10.1126/science.1111772

Fontana, D. C., Berlato, M. A., & Bergamaschi, H. (1991). Balanço de radiação da soja em região subtropical do Brasil. *Pesquisa Agropecuária Brasileira*.

Food and Agricultural Organization of the United Nations. (2015). *Global Forest Resources Assessment 2015*. Rome.

Food and Agriculture Organization. (2016). *State of the World's Forests*. *Food and Agriculture Organization of the United Nations* (2012th ed.). Rome: Food and Agriculture Organization.

Food and Agriculture Organsiation of the United Nations. (2015). *Global Forest Resources Assessment 2015*. *Desk Reference*. https://doi.org/10.1002/2014GB005021

Foot, J. S. (1982). Meterological Research Flight Technical Note 13: Thermal Lag of Hercules' Pyranometers.

Forster, P., Ramaswamy, V., Artaxo, P., Berntsen, T., Betts, R., Fahey, D. W., et al. (2007). 2007: Changes in Atmospheric Constituents and in Radiative Forcing. In M. T. and H. L. M. Solomon, S., D. Qin, M. Manning, Z. Chen, M. Marquis, K.B. Averyt (Ed.), *Climate Change 2007: The Physical Science Basis. Contribution of Working Group I to the Fourth Assessment Report of the Intergovernmental Panel on Climate Change*. Cambridge, United Kingdom and New York, NY, USA: Cambridge University Press.

Franchito, S. H., & Rao, V. B. (1992). Climatic change due to land surface alterations. *Climatic Change*, *22*(1), 1–34. https://doi.org/10.1007/BF00143341

Freitas, F. L. M., Sparovek, G., Berndes, G., Persson, U. M., Englund, O., Barretto, A., & Mörtberg, U. (2018). Potential increase of legal deforestation in Brazilian Amazon after Forest Act revision. *Nature Sustainability*, *1*(11), 665–670. https://doi.org/10.1038/s41893-018-0171-4

Fu, T. M., Jacob, D. J., Palmer, P. I., Chance, K., Wang, Y. X., Barletta, B., et al. (2007). Space-based formaldehyde measurements as constrains on volatile organic compound emissions in east and

south Asia and implications for ozone. *Journal of Geophysical Research Atmospheres*, *112*(6), 1–15. https://doi.org/10.1029/2006JD007853

Fuchs, H., Hofzumahaus, A., Rohrer, F., Bohn, B., Brauers, T., Dorn, H. P., et al. (2013). Experimental evidence for efficient hydroxyl radical regeneration in isoprene oxidation. *Nature Geoscience*, *6*(12), 1023–1026. https://doi.org/10.1038/ngeo1964

Gandu, A. W., Cohen, J. C. P., & de Souza, J. R. S. (2004). Simulation of deforestation in eastern Amazonia using a high-resolution model. *Theoretical and Applied Climatology*, *78*(1–3), 123–135. https://doi.org/10.1007/s00704-004-0048-5

Gao, F., He, T., Wang, Z., Ghimire, B., Shuai, Y., Masek, J., et al. (2014). Multiscale climatological albedo look-up maps derived from moderate resolution imaging spectroradiometer BRDF/albedo products. *Journal of Applied Remote Sensing*, *8*(1), 083532. https://doi.org/10.1117/1.jrs.8.083532

Giambelluca, T. W., Nullet, M. A., Ziegler, A. D., & Tran, L. (2000). Latent and sensible energy flux over deforested land surfaces in the eastern Amazon and northern Thailand. *Singapore Journal of Tropical Geography*, *21*(2), 107–130. https://doi.org/10.1111/1467-9493.00070

Giambelluca, Thomas W., Hölscher, D., Bastos, T. X., Frazão, R. R., Nullet, M. A., & Ziegler, A. D. (1997). Observations of albedo and radiation balance over postforest land surfaces in the eastern Amazon Basin. *Journal of Climate*, *10*(5), 919–928. https://doi.org/10.1175/1520-0442(1997)010<0919:OOAARB>2.0.CO;2

Gibbs, H. K., Ruesch, A. S., Achard, F., Clayton, M. K., Holmgren, P., Ramankutty, N., & Foley, J. A. (2010). Tropical forests were the primary sources of new agricultural land in the 1980s and 1990s. *Proceedings of the National Academy of Sciences of the United States of America*, *107*(38), 16732–16737. https://doi.org/10.1073/pnas.0910275107

Gibbs, Holly K., Johnston, M., Foley, J. A., Holloway, T., Monfreda, C., Ramankutty, N., & Zaks, D. (2008). Carbon payback times for crop-based biofuel expansion in the tropics: The effects of changing yield and technology. *Environmental Research Letters*, *3*(3). https://doi.org/10.1088/1748-9326/3/3/034001

Godar, J., Gardner, T. A., Tizado, E. J., & Pacheco, P. (2015). Correction: Sustainability science, environmental sciences (Proc Natl Acad Sci USA 111:15591-15596(2014)). *Proceedings of the*

National Academy of Sciences of the United States of America, *112*(23), E3089. https://doi.org/10.1073/pnas.1508418112

Goldewijk, K. K. (2001). Estimating global land use change over the past 300 years: The HYDE database. *Global Biogeochemical Cycles*, *15*(2), 417–433. https://doi.org/10.1029/1999GB001232

Goldewijk, K. K., Hall, F. G., Collatz, G. J., Meeson, B. W., Los, S. O., Brown De Colstoun, E., & Landis, D. R. (2007). ISLSCP II Historical Land Cover and Land Use, 1700-1990. *ORNL DAAC*. Oak Ridge,k Tennesee, USA. https://doi.org/10.3334/ORNLDAAC/967

Gruber, N., & Galloway, J. N. (2008). An Earth-system perspective of the global nitrogen cycle. *Nature*, *451*(7176), 293–296. https://doi.org/10.1038/nature06592

Guan, K., Pan, M., Li, H., Wolf, A., Wu, J., Medvigy, D., et al. (2015). Photosynthetic seasonality of global tropical forests constrained by hydroclimate. *Nature Geoscience*, *8*(4), 284–289. https://doi.org/10.1038/ngeo2382

Guenther, A., Nicholas, C., Fall, R., Klinger, L., Mckay, W. A., & Scholes, B. (1995). A global model of natural volatile organic compound emissions s Raja the balance Triangle changes in the atmospheric accumulation rates of greenhouse Triangle Several inventories of natural and Exposure Assessment global scales have been two classes Fores. *J. Geophys. Res.*, *100*(94), 8873–8892.

Gueymard, C. A. (2009). Direct and indirect uncertainties in the prediction of tilted irradiance for solar engineering applications. *Solar Energy*, *83*(3), 432–444. https://doi.org/10.1016/j.solener.2008.11.004

Guyon, P., Graham, B., Beck, J., Boucher, O., Gerasopoulos, E., Mayol-Bracero, O. L., et al. (2003). Physical properties and concentration of aerosol particles over the Amazon tropical forest during background and biomass burning conditions. *Atmospheric Chemistry and Physics*, *3*(4), 951–967. https://doi.org/10.5194/acp-3-951-2003

Haeffelin, M., Kato, S., Smith, A. M., Rutledge, C. K., Charlock, T. P., & Mahan, J. R. (2001). Determination of the thermal offset of the Eppley precision spectral pyranometer. *Applied Optics*, *40*(4), 472. https://doi.org/10.1364/ao.40.000472

Hahmann, A. N., & Dickinson, R. E. (1997). RCCM2-BATS model over tropical South America: Applications to tropical deforestation. *Journal of Climate*, *10*(8), 1944–1964.

https://doi.org/10.1175/1520-0442(1997)010<1944:RBMOTS>2.0.CO;2

Hallquist, M., Wenger, J. C., Baltensperger, U., Rudich, Y., Simpson, D., Claeys, M., et al. (2009). The formation, properties and impact of secondary organic aerosol: Current and emerging issues. *Atmospheric Chemistry and Physics*, *9*(14), 5155–5236. https://doi.org/10.5194/acp-9-5155-2009

Hamilton, R. L., Trimmer, M., Bradley, C., & Pinay, G. (2016). Deforestation for oil palm alters the fundamental balance of the soil N cycle. *Soil Biology and Biochemistry*, *95*, 223–232. https://doi.org/10.1016/j.soilbio.2016.01.001

Hansen, J., Sato, M., & Ruedy, R. (1997). Radiative forcing and climate response Abstract . We examine the sensitivity of a climate model to a wide range of radiative including changes of solar forcing introduced times the climate response , specifically the global mean temperature change , is se, *102*, 6831–6864.

Hansen, M. C., Potapov, P. V, Moore, R., Hancher, M., Turubanova, S. a, & Tyukavina, A. (2013). High-Resolution Global Maps of 21st-Century Forest Cover Change. *Science*, *342*(6160), 850–853. https://doi.org/10.1126/science.1244693

He, T., Shao, Q., Cao, W., Huang, L., & Liu, L. (2015). Satellite-observed energy budget change of deforestation in northeastern china and its climate implications. *Remote Sensing*, *7*(9), 11586–11601. https://doi.org/10.3390/rs70911586

Heald, C. L., & Spracklen, D. V. (2015). Land Use Change Impacts on Air Quality and Climate. *Chemical Reviews*, *115*, 4476–4496. https://doi.org/10.1021/cr500446g

Henderson-Sellers, A., Dickinson, R. E., Durbidge, T. B., Kennedy, P. J., McGuffie, K., & Pitman, A. J. (1993). Tropical deforestation: modeling local- to regional-scale climate change. *Journal of Geophysical Research*, *98*(D4), 7289–7315. https://doi.org/10.1029/92JD02830

Henderson-Sellers, A., & Wilson, M. F. (1983). Surface Albedo Data for Climatic Modeling. *Reviews of Geophysics and Space Physics*, *21*(8), 1743–1778.

Hendon, H. H. (2003). Indonesian rainfall variability: Impacts of ENSO and local air-sea interaction. *Journal of Climate*, *16*(11), 1775–1790. https://doi.org/10.1175/1520-0442(2003)016<1775:IRVIOE>2.0.CO;2

Hogrefe, C., Lynn, B., Civerolo, K., Ku, J. Y., Rosenthal, J., Rosenzweig, C., et al. (2004). Simulating changes in regional air pollution over the eastern United States due to changes in global and regional climate and emissions. *Journal of Geophysical Research D: Atmospheres*, *109*(22), 1–13. https://doi.org/10.1029/2004JD004690

Holdaway, R. J., Sparrow, A. D., & Coomes, D. A. (2010). Trends in entropy production during ecosystem development in the Amazon Basin. *Philosophical Transactions of the Royal Society B: Biological Sciences*, *365*(1545), 1437–1447. https://doi.org/10.1098/rstb.2009.0298

Houghton, J. T., Ding, Y., Griggs, D. J., Noguer, M., van der Linden, P. J., Dai, X., et al. (Eds.). (2001). *IPCC, 2001: Climate Change 2001: The Scientific Basis. Contribution of Working Group I to the Third Assessment Report of the Intergovernmental Panel on Climate Change*. Cambridge, United Kingdom and New York, NY, USA: Cambridge University Press.

Hubau, W., Lewis, S. L., Phillips, O. L., Affum-Baffoe, K., Beeckman, H., Cuní-Sanchez, A., et al. (2020). Asynchronous carbon sink saturation in African and Amazonian tropical forests. *Nature*, *579*(7797), 80–87. https://doi.org/10.1038/s41586-020-2035-0

Hurtt, G. C., Chini, L. P., Frolking, S., Betts, R. A., Feddema, J., Fischer, G., et al. (2011). Harmonization of land-use scenarios for the period 1500-2100: 600 years of global gridded annual land-use transitions, wood harvest, and resulting secondary lands. *Climatic Change*, *109*(1), 117–161. https://doi.org/10.1007/s10584-011-0153-2

Jackson, R. B., Randerson, J. T., Canadell, J. G., Anderson, R. G., Avissar, R., Baldocchi, D. D., et al. (2008). Protecting climate with forests. *Environmental Research Letters*, *3*(4). https://doi.org/10.1088/1748-9326/3/4/044006

Jin, Y., Schaaf, C. B., Woodcock, C. E., Gao, F., Li, X., Strahler, A. H., et al. (2003). Consistency of MODIS surface bidirectional reflectance distribution function and albedo retrievals: 1. Validation. *Journal of Geophysical Research D: Atmospheres*, *108*(5), 1–15. https://doi.org/10.1029/2002jd002804

Jin, Y., Randerson, J. T., Goetz, S. J., Beck, P. S. A., Loranty, M. M., & Goulden, M. L. (2012). The influence of burn severity on postfire vegetation recovery and albedo change during early succession in North American boreal forests. *Journal of Geophysical Research: Biogeosciences*, *117*(1), 1–15. https://doi.org/10.1029/2011JG001886

Johnson, B. T., Haywood, J. M., & Hawcroft, M. K. (2019). Are Changes in Atmospheric Circulation Important for Black Carbon Aerosol Impacts on Clouds, Precipitation, and Radiation? *Journal of Geophysical Research: Atmospheres*, *124*(14), 7930–7950. https://doi.org/10.1029/2019JD030568

Karl, T., Guenther, A., Yokelson, R. J., Greenberg, J., Potosnak, M., Blake, D. R., & Artaxo, P. (2007). The tropical forest and fire emissions experiment: Emission, chemistry, and transport of biogenic volatile organic compounds in the lower atmosphere over Amazonia. *Journal of Geophysical Research*, *112*(D18), 1–17. https://doi.org/10.1029/2007jd008539

Kivimäenpää, M., Ghimire, R. P., Sutinen, S., Häikiö, E., Kasurinen, A., Holopainen, T., & Holopainen, J. K. (2016). Increases in volatile organic compound emissions of Scots pine in response to elevated ozone and warming are modified by herbivory and soil nitrogen availability. *European Journal of Forest Research*, *135*(2), 343–360. https://doi.org/10.1007/s10342-016-0939-x

Kleidon, A., & Heimann, M. (1999). Deep-rooted vegetation, Amazonian deforestation, and climate: Results from a modelling study. *Global Ecology and Biogeography*, *8*(5), 397–405. https://doi.org/10.1046/j.1365-2699.1999.00150.x

Knowlton, K., Rosenthal, J. E., Hogrefe, C., Lynn, B., Gaffin, S., Goldberg, R., et al. (2004). Assessing ozone-related health impacts under a changing climate. *Environmental Health Perspectives*, *112*(15), 1557–1563. https://doi.org/10.1289/ehp.7163

Koh, L. P., & Wilcove, D. S. (2008). Is oil palm agriculture really destroying tropical biodiversity? *Conservation Letters*, *1*(2), 60–64. https://doi.org/10.1111/j.1755-263x.2008.00011.x

Kreidenweis, S. M., Petters, M., & Lohmann, U. (2018). 100 Years of Progress in Cloud Physics, Aerosols, and Aerosol Chemistry Research. *Meteorological Monographs*, *59*, 11.1-11.72. https://doi.org/10.1175/amsmonographs-d-18-0024.1

Kvalevåg, M. M., Myhre, G., Bonan, G., & Levis, S. (2010). Anthropogenic land cover changes in a GCM with surface albedo changes based on MODIS data. *International Journal of Climatology*, *30*(13), 2105–2117. https://doi.org/10.1002/joc.2012

Lawrence, D., & Vandecar, K. (2015). Effects of tropical deforestation on climate and agriculture. *Nature Climate Change*, *5*(1), 27–36. https://doi.org/10.1038/nclimate2430

Lean, J., & Rowntree, P. R. (1997). Correction note on “Understanding the sensitivity of a GCM

simulation of Amazonian deforestation to the specification of vegetation and soil characteristics." *Journal of Climate*, *12*(5 PART 2), 1549–1551. https://doi.org/10.1175/1520-0442(1999)012<1549:cnouts>2.0.co;2

Lean, J., & Warrilow, D. A. (1989). Simulation of the regional climatic impact of Amazon deforestation. *Nature*, *342*(6248), 411–413. https://doi.org/10.1038/342411a0

Lee, X., Goulden, M. L., Hollinger, D. Y., Barr, A., Black, T. A., Bohrer, G., et al. (2011). Observed increase in local cooling effect of deforestation at higher latitudes. *Nature*, *479*(7373), 384–387. https://doi.org/10.1038/nature10588

Lelieveld, J., Butler, T. M., Crowley, J. N., Dillon, T. J., Fischer, H., Ganzeveld, L., et al. (2008). Atmospheric oxidation capacity sustained by a tropical forest. *Nature*, *452*(7188), 737–740. https://doi.org/10.1038/nature06870

Li, L., Dong, J., Tenku, S. N., & Xiao, X. (2015). Mapping oil palm plantations in cameroon using PALSAR 50-m orthorectified mosaic images. *Remote Sensing*, *7*(2), 1206–1224. https://doi.org/10.3390/rs70201206

Li, Y., Zhao, M., Motesharrei, S., Mu, Q., Kalnay, E., & Li, S. (2015). Local cooling and warming effects of forests based on satellite observations. *Nature Communications*, *6*. https://doi.org/10.1038/ncomms7603

Li, Y., Zhao, M., Mildrexler, D. J., Motesharrei, S., Mu, Q., Kalnay, E., et al. (2016). Potential and actual impacts of deforestation and afforestation on land surface temperature. *Journal of Geophysical Research*, *121*(24), 14372–14386. https://doi.org/10.1002/2016JD024969

Li, Y., De Noblet-Ducoudré, N., Davin, E. L., Motesharrei, S., Zeng, N., Li, S., & Kalnay, E. (2016). The role of spatial scale and background climate in the latitudinal temperature response to deforestation. *Earth System Dynamics*, *7*(1), 167–181. https://doi.org/10.5194/esd-7-167-2016

Liang, S. (2000). Narrowband to broadband conversions of land surface albedo I Algorithms. *Remote Sensing of Environment*, *76*, 213–238.

Liu, H., & Randerson, J. T. (2008). Interannual variability of surface energy exchange depends on stand age in a boreal forest fire chronosequence. *Journal of Geophysical Research: Biogeosciences*, *113*(1), 1–13. https://doi.org/10.1029/2007JG000483

Liu, N. F., Liu, Q., Wang, L. Z., Liang, S. L., Wen, J. G., Qu, Y., & Liu, S. H. (2013). A statistics-based temporal filter algorithm to map spatiotemporally continuous shortwave albedo from MODIS data. *Hydrology and Earth System Sciences*, *17*(6), 2121–2129. https://doi.org/10.5194/hess-17-2121-2013

Liu, Y. Y., Van Dijk, A. I. J. M., De Jeu, R. A. M., Canadell, J. G., McCabe, M. F., Evans, J. P., & Wang, G. (2015). Recent reversal in loss of global terrestrial biomass. *Nature Climate Change*, *5*(5), 470–474. https://doi.org/10.1038/nclimate2581

Llusià, J., Peñuelas, J., & Gimeno, B. S. (2002). Seasonal and species-specific response of VOC emissions by Mediterranean woody plant to elevated ozone concentrations. *Atmospheric Environment*, *36*(24), 3931–3938. https://doi.org/10.1016/S1352-2310(02)00321-7

Loarie, S. R., Lobell, D. B., Asner, G. P., & Field, C. B. (2011). Land-Cover and surface water change drive large albedo increases in south america. *Earth Interactions*, *15*(7), 1–16. https://doi.org/10.1175/2010EI342.1

Lohmann, U., & Feichter, J. (2001). Can the direct and semi-direct aerosol effect compete with the indirect effect on a global scale. *Geophysical Research Letters*, *28*(1), 159–161.

Long, C. N., Bucholtz, A., Jonsson, H., Schmid, B., Vogelmann, A., & Wood, J. (2010). A Method of Correcting for Tilt from Horizontal in Downwelling Shortwave Irradiance Measurements on Moving Platforms. *The Open Atmospheric Science Journal*, *4*(1), 78–87. https://doi.org/10.2174/1874282301004010078

Loranty, M. M., Berner, L. T., Goetz, S. J., Jin, Y., & Randerson, J. T. (2014). Vegetation controls on northern high latitude snow-albedo feedback: Observations and CMIP5 model simulations. *Global Change Biology*, *20*(2), 594–606. https://doi.org/10.1111/gcb.12391

MacDicken, K. G. (2015). Global Forest Resources Assessment 2015: What, why and how? *Forest Ecology and Management*, *352*, 3–8. https://doi.org/10.1016/j.foreco.2015.02.006

Manzi, A. O., & Planton, S. (1994). 58-Manzi_ISBA-parametrization-land-surface-in-GCM.pdf. *Journal of Hydrology*, *155*, 353–387.

Marenco, F., Johnson, B., Langridge, J. M., Mulcahy, J., Benedetti, A., Remy, S., et al. (2016). On the vertical distribution of smoke in the Amazonian atmosphere during the dry season. *Atmospheric Chemistry and Physics*, *16*(4), 2155–2174. https://doi.org/10.5194/acp-16-2155-2016

Margono, B. A., Potapov, P. V., Turubanova, S., Stolle, F., & Hansen, M. C. (2014). Primary forest cover loss in indonesia over 2000-2012. *Nature Climate Change*, *4*(8), 730–735. https://doi.org/10.1038/nclimate2277

Marlier, M. E., DeFries, R. S., Kim, P. S., Koplitz, S. N., Jacob, D. J., Mickley, L. J., & Myers, S. S. (2015). Fire emissions and regional air quality impacts from fires in oil palm, timber, and logging concessions in Indonesia. *Environmental Research Letters*, *10*(8). https://doi.org/10.1088/1748-9326/10/8/085005

Martin, S. T., Artaxo, P., MacHado, L. A. T., Manzi, A. O., Souza, R. A. F., Schumacher, C., et al. (2016). Introduction: Observations and Modeling of the Green Ocean Amazon (GoAmazon2014/5). *Atmospheric Chemistry and Physics*, *16*(8), 4785–4797. https://doi.org/10.5194/acp-16-4785-2016

Matsui, T., Beltrán-Przekurat, A., Pielke, R. A., Niyogi, D., & Coughenour, M. B. (2007). Continental-scale multiobservation calibration and assessment of Colorado State University Unified Land Model by application of Moderate Resolution Imaging Spectroradiometer (MODIS) surface albedo. *Journal of Geophysical Research: Biogeosciences*, *112*(2), 1–19. https://doi.org/10.1029/2006JG000229

McGuffie, K., Henderson-Sellers, A., Zhang, H., Durbidge, T. B., & Pitman, A. J. (1995). Global climate sensitivity to tropical deforestation. *Global and Planetary Change*, *10*(1–4), 97–128. https://doi.org/10.1016/0921-8181(94)00022-6

McMorrow, J. (2001). Linear regression modelling for the estimation of oil palm age from Landsat TM. *International Journal of Remote Sensing*, *22*(12), 2243–2264. https://doi.org/10.1080/01431160117188

Mei, R., & Wang, G. (2010). Rain follows logging in the Amazon? Results from CAM3-CLM3. *Climate Dynamics*, *34*(7), 983–996. https://doi.org/10.1007/s00382-009-0592-x

Meijide, A., Röll, A., Fan, Y., Herbst, M., Niu, F., Tiedemann, F., et al. (2017). Controls of water and energy fluxes in oil palm plantations: Environmental variables and oil palm age. *Agricultural and Forest Meteorology*, *239*, 71–85. https://doi.org/10.1016/j.agrformet.2017.02.034

Meijide, A., Badu, C. S., Moyano, F., Tiralla, N., Gunawan, D., & Knohl, A. (2018). Impact of forest conversion to oil palm and rubber plantations on microclimate and the role of the 2015 ENSO

event. *Agricultural and Forest Meteorology*, *252*(January), 208–219. https://doi.org/10.1016/j.agrformet.2018.01.013

Meleux, F., Solmon, F., & Giorgi, F. (2007). Increase in summer European ozone amounts due to climate change. *Atmospheric Environment*, *41*(35), 7577–7587. https://doi.org/10.1016/j.atmosenv.2007.05.048

Miettinen, J., Shi, C., & Liew, S. C. (2011). Deforestation rates in insular Southeast Asia between 2000 and 2010. *Global Change Biology*, *17*(7), 2261–2270. https://doi.org/10.1111/j.1365-2486.2011.02398.x

Miettinen, J., Liew, S. C., & Kwoh, L. K. (2015). Usability of sentinel-1 dual polarization C-band data for plantation detection in Insular Southeast Asia. *ACRS 2015 - 36th Asian Conference on Remote Sensing: Fostering Resilient Growth in Asia, Proceedings*.

Montenegro, A., Eby, M., Mu, Q., Mulligan, M., Weaver, A. J., Wiebe, E. C., & Zhao, M. (2009). The net carbon drawdown of small scale afforestation from satellite observations. *Global and Planetary Change*, *69*(4), 195–204. https://doi.org/10.1016/j.gloplacha.2009.08.005

Moss, R. H., Edmonds, J. A., Hibbard, K. A., Manning, M. R., Rose, S. K., Van Vuuren, D. P., et al. (2010). The next generation of scenarios for climate change research and assessment. *Nature*, *463*(7282), 747–756. https://doi.org/10.1038/nature08823

Moutinho, P., Guerra, R., & Azevedo-Ramos, C. (2016). Achieving zero deforestation in the Brazilian Amazon: What is missing? *Elementa*, *4*, 1–11. https://doi.org/10.12952/journal.elementa.000125

Myers, N. (1997). The world's forests and their ecosystem services. In G. C. Daily (Ed.), *Nature's Services: Societal Dependence On Natural Ecosystems* (pp. 215–236). Washington D.C.: Island Press.

Myhre, G., & Myhre, A. (2003). Uncertainties in Radiative Forcing due to Surface Albedo Changes Caused by Land-Use Changes. *Journal of Climate*, *16*(10), 1511–1524. https://doi.org/10.1175/1520-0442(2003)016<1511:uirfdt>2.0.co;2

Myhre, G., Shindell, D. T., Bréon, F.-M., Collins, W., Fuglestvedt, J., Huang, J., et al. (2013). Anthropogenic and natural radiative forcing. In T. F. Stocker, D. Qin, G.-K. Plattner, M. Tignor, S. K. Allen, J. Boschung, et al. (Eds.), *Climate Change 2013 the Physical Science Basis: Working Group*

I Contribution to the Fifth Assessment Report of the Intergovernmental Panel on Climate Change (pp. 659–740). Cambridge, United Kingdom and New York, NY, USA: Cambridge University Press. https://doi.org/10.1017/CBO9781107415324.018

Myhre, Gunnar, Kvalevåg, M. M., & Schaaf, C. B. (2005). Radiative forcing due to anthropogenic vegetation change based on MODIS surface albedo data. *Geophysical Research Letters*, *32*(21), 1–4. https://doi.org/10.1029/2005GL024004

Mylne, M. F., & Rowntree, P. R. (1992). Modelling the effects of albedo change associated with tropical deforestation. *Climatic Change*, *21*(3), 317–343. https://doi.org/10.1007/BF00139730

Naik, V., Voulgarakis, A., Fiore, A. M., Horowitz, L. W., Lamarque, J. F., Lin, M., et al. (2013). Preindustrial to present-day changes in tropospheric hydroxyl radical and methane lifetime from the Atmospheric Chemistry and Climate Model Intercomparison Project (ACCMIP). *Atmospheric Chemistry and Physics*, *13*(10), 5277–5298. https://doi.org/10.5194/acp-13-5277-2013

Nobre, C. A., Sellers, P. J., & Shukla, J. (1991). Amazonian Deforestation and Regional Climate Change. *Journal of Climate*. https://doi.org/10.1175/1520-0442(1991)004<0957:adarcc>2.0.co;2

O'Donnell, D., Tsigaridis, K., & Feichter, J. (2011). Estimating the direct and indirect effects of secondary organic aerosols using ECHAM5-HAM. *Atmospheric Chemistry and Physics*, *11*(16), 8635–8659. https://doi.org/10.5194/acp-11-8635-2011

Oguntoyinbo, J. S. (1970). Reflection coefficient of natural vegetation, crops and urban surfaces in Nigeria. *Quarterly Journal of the Royal Meteorological Society*, *96*(409), 430–441. https://doi.org/10.1002/qj.49709640907

Oleson, K. W., Bonan, G. B., Schaaf, C., Gao, F., Jin, Y., & Strahler, A. (2003). Assessment of global climate model land surface albedo using MODIS data. *Geophysical Research Letters*, *30*(8), 3–6. https://doi.org/10.1029/2002GL016749

Oliveira, G. de, & Moraes, E. C. (2013). Validação do balanço de radiação obtido a partir de dados MODIS/TERRA na Amazônia com medidas de superfície do LBA. *Acta Amazonica*, *43*(3), 353–363. https://doi.org/10.1590/S0044-59672013000300011

de Oliveira, G., Brunsell, N. A., Moraes, E. C., Bertani, G., dos Santos, T. V., Shimabukuro, Y. E., & Aragão, L. E. O. C. (2016). Use of MODIS sensor images combined with reanalysis products to retrieve net radiation in Amazonia. *Sensors (Switzerland)*, *16*(7). https://doi.org/10.3390/s16070956

Pachauri, R. K., Allen, M. R., Barros, V. R., Broome, J., Cramer, W., Christ, R., et al. (2014). *Climate Change 2014 Synthesis Report*.

Pan, Y., Birdsey, R. A., Fang, J., Houghton, R., Kauppi, P. E., Kurz, W. A., et al. (2011). A large and persistent carbon sink in the world's forests. *Science*, *333*(6045), 988–993. https://doi.org/10.1126/science.1201609

Peeters, J., Müller, J. F., Stavrakou, T., & Nguyen, V. S. (2014). Hydroxyl radical recycling in isoprene oxidation driven by hydrogen bonding and hydrogen tunneling: The upgraded LIM1 mechanism. *Journal of Physical Chemistry A*, *118*(38), 8625–8643. https://doi.org/10.1021/jp5033146

Pendleton, L., Donato, D. C., Murray, B. C., Crooks, S., Jenkins, W. A., Sifleet, S., et al. (2012). Estimating Global "Blue Carbon" Emissions from Conversion and Degradation of Vegetated Coastal Ecosystems. *PLoS ONE*, *7*(9). https://doi.org/10.1371/journal.pone.0043542

Peng, S. S., Piao, S., Zeng, Z., Ciais, P., Zhou, L., Li, L. Z. X., et al. (2014). Afforestation in China cools local land surface temperature. *Proceedings of the National Academy of Sciences of the United States of America*, *111*(8), 2915–2919. https://doi.org/10.1073/pnas.1315126111

Peñuelas, J., Llusià, J., & Gimeno, B. S. (1999). Effects of ozone concentrations on biogenic volatile organic compounds emission in the Mediterranean region. *Environmental Pollution*, *105*(1), 17–23. https://doi.org/10.1016/S0269-7491(98)00214-0

Pitman, A. J., Durbidge, T. B., Henderson-Sellers, A., & McGuffie, K. (1993). Assessing climate model sensitivity to prescribed deforested landscapes. *International Journal of Climatology*, *13*(8), 879–898. https://doi.org/10.1002/joc.3370130806

Polcher, J., & Laval, K. (1994). A statistical study of the regional impact of deforestation on climate in the LMD GCM. *Climate Dynamics*, *10*(4–5), 205–219. https://doi.org/10.1007/BF00208988

Pongratz, J., Reick, C. H., Raddatz, T., & Claussen, M. (2010). Biogeophysical versus biogeochemical climate response to historical anthropogenic land cover change. *Geophysical Research Letters*, *37*(8), 1–5. https://doi.org/10.1029/2010GL043010

Pongratz, J., Reick, C. H., Raddatz, T., Caldeira, K., & Claussen, M. (2011). Past land use decisions have increased mitigation potential of reforestation. *Geophysical Research Letters*, *38*(15), 1–5. https://doi.org/10.1029/2011GL047848

Potter, L. (2015). *Managing oil palm landscapes: A seven-country survey of the modern palm oil industry in Southeast Asia, Latin America and West Africa*. *Managing oil palm landscapes: A seven-country survey of the modern palm oil industry in Southeast Asia, Latin America and West Africa*. https://doi.org/10.17528/cifor/005612

Le Quéré, C., Raupach, M. R., Canadell, J. G., Marland, G., Bopp, L., Ciais, P., et al. (2009). Trends in the sources and sinks of carbon dioxide. *Nature Geoscience*, *2*(12), 831–836. https://doi.org/10.1038/ngeo689

Querino, A. C. S., Beneditti, C. A., Machado, N. G., Silva, M. J. G. da, Querino, J. K. A. da S., Neto, L. A. dos S., & Biudes, M. S. (2016). Spatiotemporal NDVI, LAI, albedo, and surface temperature dynamics in the southwest of the Brazilian Amazon forest. *Journal of Applied Remote Sensing*, *10*(2), 036012. https://doi.org/10.1117/1.JRS.10

Ramaswamy, V., Boucher, O., Haigh, J., Hauglustaine, D., Haywood, J., Myhre, G., et al. (2001). Radiative forcing of climate change. In *Climate Change 2001: The Scientific Basis, Contribution of Working Group I to the Third Assessment Report of the Intergovernmental Panel on Climate Change* (pp. 349–416). Cambridge: Cambridge University Press. https://doi.org/10.1023/A:1026752230256

Rap, A., Scott, C. E., Spracklen, D. V., Bellouin, N., Forster, P. M., Carslaw, K. S., et al. (2013). Natural aerosol direct and indirect radiative effects. *Geophysical Research Letters*, *40*(12), 3297–3301. https://doi.org/10.1002/grl.50441

Razali, S. M., Marin, A., Nuruddin, A. A., Shafri, H. Z. M., & Hamid, H. A. (2014). Capability of integrated MODIS imagery and ALOS for oil palm, rubber and forest areas mapping in tropical forest regions. *Sensors (Switzerland)*, *14*(5), 8259–8282. https://doi.org/10.3390/s140508259

Rechid, D., Hagemann, S., & Jacob, D. (2009). Sensitivity of climate models to seasonal variability of snow-free land surface albedo. *Theoretical and Applied Climatology*, *95*(1–2), 197–221. https://doi.org/10.1007/s00704-007-0371-8

Reddington, C. L., Butt, E. W., Ridley, D. A., Artaxo, P., Morgan, W. T., Coe, H., & Spracklen, D. V. (2015). Air quality and human health improvements from reductions in deforestation-related fire in Brazil. *Nature Geoscience*, *8*(10), 768–771. https://doi.org/10.1038/ngeo2535

Reick, C. H., Raddatz, T., Pongratz, J., & Claussen, M. (2010). Contribution of anthropogenic land cover

change emissions to pre-industrial atmospheric CO2. *Tellus, Series B: Chemical and Physical Meteorology*, *62*(5), 329–336. https://doi.org/10.1111/j.1600-0889.2010.00479.x

Rein, G., Cohen, S., & Simeoni, A. (2009). Carbon emissions from smouldering peat in shallow and strong fronts. *Proceedings of the Combustion Institute*, *32 II*, 2489–2496. https://doi.org/10.1016/j.proci.2008.07.008

Riahi, K., Grübler, A., & Nakicenovic, N. (2007). Scenarios of long-term socio-economic and environmental development under climate stabilization. *Technological Forecasting and Social Change*, *74*(7), 887–935. https://doi.org/10.1016/j.techfore.2006.05.026

Richards, D. R., & Friess, D. A. (2016). Rates and drivers of mangrove deforestation in Southeast Asia, 2000-2012. *Proceedings of the National Academy of Sciences of the United States of America*, *113*(2), 344–349. https://doi.org/10.1073/pnas.1510272113

Rinnan, R., Rinnan, Å., Holopainen, T., Holopainen, J. K., & Pasanen, P. (2005). Emission of non-methane volatile organic compounds (VOCs) from boreal peatland microcosms - Effects of ozone exposure. *Atmospheric Environment*, *39*(5), 921–930. https://doi.org/10.1016/j.atmosenv.2004.09.076

Rogers, B. M., Randerson, J. T., & Bonan, G. B. (2013). High-latitude cooling associated with landscape changes from North American boreal forest fires. *Biogeosciences*, *10*(2), 699–718. https://doi.org/10.5194/bg-10-699-2013

Rogers, Brendan M., Soja, A. J., Goulden, M. L., & Randerson, J. T. (2015). Influence of tree species on continental differences in boreal fires and climate feedbacks. *Nature Geoscience*, *8*(3), 228–234. https://doi.org/10.1038/ngeo2352

Román, M. O., Schaaf, C. B., Woodcock, C. E., Strahler, A. H., Yang, X., Braswell, R. H., et al. (2009). The MODIS (Collection V005) BRDF/albedo product: Assessment of spatial representativeness over forested landscapes. *Remote Sensing of Environment*, *113*(11), 2476–2498. https://doi.org/10.1016/j.rse.2009.07.009

Rossow, W. B., & Schiffer, R. A. (1999). Advances in Understanding Clouds from ISCCP. *Bulletin of the American Meteorological Society*, *80*(11), 2261–2287. https://doi.org/10.1175/1520-0477(1999)080<2261:AIUCFI>2.0.CO;2

Rotenberg, E., & Yakir, D. (2011). Distinct patterns of changes in surface energy budget associated with

forestation in the semiarid region. *Global Change Biology*, *17*(4), 1536–1548. https://doi.org/10.1111/j.1365-2486.2010.02320.x

Rudel, T. K., Defries, R., Asner, G. P., & Laurance, W. F. (2009). Changing drivers of deforestation and new opportunities for conservation. *Conservation Biology*, *23*(6), 1396–1405. https://doi.org/10.1111/j.1523-1739.2009.01332.x

Sabajo, C. R., Le Maire, G., June, T., Meijide, A., Roupsard, O., & Knohl, A. (2017). Expansion of oil palm and other cash crops causes an increase of the land surface temperature in the Jambi province in Indonesia. *Biogeosciences*, *14*(20), 4619–4635. https://doi.org/10.5194/bg-14-4619-2017

Sakai, R. K., Fitzjarrald, D. R., Moraes, O. L. L., Staebler, R. M., Acevedo, O. C., Czikowsky, M. J., et al. (2004). Land-use change effects on local energy, water, and carbon balances in an Amazonian agricultural field. *Global Change Biology*, *10*(5), 895–907. https://doi.org/10.1111/j.1529-8817.2003.00773.x

Salati, E., & Nobre, C. A. (1992). Possible climatic impacts of tropical deforestation. *Tropical Forests and Climate*, 177–196. https://doi.org/10.1007/978-94-017-3608-4_18

Saldarriaga, J. G., & Luxmoore, R. J. (1991). Solar energy conversion efficiencies during succession of a tropical rain forest in Amazonia. *Journal of Tropical Ecology*, *7*(2), 233–242. https://doi.org/10.1017/S0266467400005393

Sampaio, G., Nobre, C., Costa, M. H., Satyamurty, P., Soares-Filho, B. S., & Cardoso, M. (2007). Regional climate change over eastern Amazonia caused by pasture and soybean cropland expansion. *Geophysical Research Letters*, *34*(17), 1–7. https://doi.org/10.1029/2007GL030612

Schaaf, C. B., Gao, F., Strahler, A. H., Lucht, W., Li, X., Tsang, T., et al. (2002). First operational BRDF, albedo nadir reflectance products from MODIS. *Remote Sensing of Environment*, *83*, 135–148.

Scott, C. E., Monks, S. A., Spracklen, D. V., Arnold, S. R., Forster, P. M., Rap, A., et al. (2017). Impact on short-lived climate forcers (SLCFs) from a realistic land-use change scenario via changes in biogenic emissions. *Faraday Discussions*, *200*, 101–120. https://doi.org/10.1039/c7fd00028f

Scott, C. E., Monks, S. A., Spracklen, D. V., Arnold, S. R., Forster, P. M., Rap, A., et al. (2018). Impact on short-lived climate forcers increases projected warming due to deforestation. *Nature Communications*, *9*(1), 1–9. https://doi.org/10.1038/s41467-017-02412-4

Sena, E. T., Artaxo, P., & Correia, A. L. (2013). Spatial variability of the direct radiative forcing of biomass burning aerosols and the effects of land use change in Amazonia. *Atmospheric Chemistry and Physics*, *13*(3), 1261–1275. https://doi.org/10.5194/acp-13-1261-2013

Shafri, H. Z. M., Hamdan, N., & Saripan, M. I. (2011). Semi-automatic detection and counting of oil palm trees from high spatial resolution airborne imagery. *International Journal of Remote Sensing*, *32*(8), 2095–2115. https://doi.org/10.1080/01431161003662928

Siikamäki, J., Sanchirico, J. N., & Jardine, S. L. (2012). Global economic potential for reducing carbon dioxide emissions from mangrove loss. *Proceedings of the National Academy of Sciences of the United States of America*, *109*(36), 14369–14374. https://doi.org/10.1073/pnas.1200519109

Silva Junior, C. H. L., Pessôa, A. C. M., Carvalho, N. S., Reis, J. B. C., Anderson, L. O., & Aragão, L. E. O. C. (2020). The Brazilian Amazon deforestation rate in 2020 is the greatest of the decade. *Nature Ecology and Evolution*, 0–1. https://doi.org/10.1038/s41559-020-01368-x

Situ, S., Guenther, A., Wang, X., Jiang, X., Turnipseed, A., Wu, Z., et al. (2013). Impacts of seasonal and regional variability in biogenic VOC emissions on surface ozone in the Pearl river delta region, China. *Atmospheric Chemistry and Physics*, *13*(23), 11803–11817. https://doi.org/10.5194/acp-13-11803-2013

Snyder, P. K., Delire, C., & Foley, J. A. (2004). Evaluating the influence of different vegetation biomes on the global climate. *Climate Dynamics*, *23*(3–4), 279–302. https://doi.org/10.1007/s00382-004-0430-0

Sodhi, N. S., Koh, L. P., Brook, B. W., & Ng, P. K. L. (2004). Southeast Asian biodiversity: An impending disaster. *Trends in Ecology and Evolution*, *19*(12), 654–660. https://doi.org/10.1016/j.tree.2004.09.006

Sodhi, N. S., Posa, M. R. C., Lee, T. M., Bickford, D., Koh, L. P., & Brook, B. W. (2010). The state and conservation of Southeast Asian biodiversity. *Biodiversity and Conservation*, *19*(2), 317–328. https://doi.org/10.1007/s10531-009-9607-5

Souza, P. J. de O. P. de, Rocha, E. J. P. da, & Ribeiro, A. (2013). Impacts of soybean expansion on radiation balance in eastern Amazon. *Acta Amazonica*, *43*(2), 169–178. https://doi.org/10.1590/S0044-59672013000200006

Spracklen, D. V., Bonn, B., & Carslaw, K. S. (2008). Boreal forests, aerosols and the impacts on clouds

and climate. *Philosophical Transactions of the Royal Society A: Mathematical, Physical and Engineering Sciences*, *366*(1885), 4613–4626. https://doi.org/10.1098/rsta.2008.0201

Stabile, M. C. C., Guimarães, A. L., Silva, D. S., Ribeiro, V., Macedo, M. N., Coe, M. T., et al. (2020). Solving Brazil's land use puzzle: Increasing production and slowing Amazon deforestation. *Land Use Policy*, *91*(May 2019), 104362. https://doi.org/10.1016/j.landusepol.2019.104362

Stedman, J. R. (2004). The predicted number of air pollution related deaths in the UK during the August 2003 heatwave. *Atmospheric Environment*, *38*(8), 1087–1090. https://doi.org/10.1016/j.atmosenv.2003.11.011

Stevenson, D. S., Young, P. J., Naik, V., Lamarque, J. F., Shindell, D. T., Voulgarakis, A., et al. (2013). Tropospheric ozone changes, radiative forcing and attribution to emissions in the Atmospheric Chemistry and Climate Model Intercomparison Project (ACCMIP). *Atmospheric Chemistry and Physics*, *13*(6), 3063–3085. https://doi.org/10.5194/acp-13-3063-2013

Stjern, C. W., Samset, B. H., Myhre, G., Forster, P. M., Hodnebrog, Ø., Andrews, T., et al. (2017). Rapid Adjustments Cause Weak Surface Temperature Response to Increased Black Carbon Concentrations. *Journal of Geophysical Research: Atmospheres*, *122*(21), 11,462-11,481. https://doi.org/10.1002/2017JD027326

Stocker, T. F., Qin, D., Plattner, G.-K., Tignor, M., Allen, S. K., Boschung, J., et al. (Eds.). (2013). *IPCC, 2013: Climate Change 2013: The Physical Science Basis. Contribution of Working Group I to the Fifth Assessment Report of the Intergovernmental Panel on Climate Change*. Cambridge, United Kingdom and New York, NY, USA: Cambridge University Press. https://doi.org/10.1017/CBO9781107415324.Summary

Strahler, A. H., Wanner, W., Schaaf, C. B., Li, X., Hu, B., Muller, J. P., et al. (1996). MODIS BRDF/albedo product: Algorithm theoretical basis document version 4.0. *NASA EOS MODIS Technical Document, Greenbelt, MD, USA*, (November). Retrieved from papers3://publication/uuid/14BC3FA6-52A4-4B63-92E9-A7F3581D5C7B

Strong, J., Whyatt, J. D., Metcalfe, S. E., Derwent, R. G., & Hewitt, C. N. (2013). Investigating the impacts of anthropogenic and biogenic VOC emissions and elevated temperatures during the 2003 ozone episode in the UK. *Atmospheric Environment*, *74*(August 2003), 393–401. https://doi.org/10.1016/j.atmosenv.2013.04.006

Sud, Y. C., Lau, W. K.-M., Walker, G. K., Kim, J.-H., Liston, G. E., & Sellers, P. J. (1996). Biogeophysical Consequences of a Tropical Deforestation Scenario: A GCM Simulation Study. *Journal of Climate*. https://doi.org/10.1175/1520-0442(1996)009<3225:bcoatd>2.0.co;2

Swann, A. L. S., Fung, I. Y., & Chiang, J. C. H. (2012). Mid-latitude afforestation shifts general circulation and tropical precipitation. *Proceedings of the National Academy of Sciences of the United States of America*, *109*(3), 712–716. https://doi.org/10.1073/pnas.1116706108

Taraborrelli, D., Lawrence, M. G., Crowley, J. N., Dillon, T. J., Gromov, S., Groß, C. B. M., et al. (2012). Hydroxyl radical buffered by isoprene oxidation over tropical forests. *Nature Geoscience*, *5*(3), 190–193. https://doi.org/10.1038/ngeo1405

Thornton, P. E., Lamarque, J. F., Rosenbloom, N. A., & Mahowald, N. M. (2007). Influence of carbon-nitrogen cycle coupling on land model response to CO2 fertilization and climate variability. *Global Biogeochemical Cycles*, *21*(4). https://doi.org/10.1029/2006GB002868

Tian, Y., Dickinson, R. E., Zhou, L., Myneni, R. B., Friedl, M., Schaaf, C. B., et al. (2004). Land boundary conditions from MODIS data and consequences for the albedo of a climate model. *Geophysical Research Letters*, *31*(5), n/a-n/a. https://doi.org/10.1029/2003gl019104

Tosca, M. G., Randerson, J. T., Zender, C. S., Nelson, D. L., Diner, D. J., & Logan, J. A. (2011). Dynamics of fire plumes and smoke clouds associated with peat and deforestation fires in Indonesia. *Journal of Geophysical Research Atmospheres*, *116*(8), 1–14. https://doi.org/10.1029/2010JD015148

Trenberth, K. E., Fasullo, J. T., & Kiehl, J. (2009). Earth's global energy budget. *Bulletin of the American Meteorological Society*, *90*(3), 311–323. https://doi.org/10.1175/2008BAMS2634.1

Turnock, S. T., Butt, E. W., Richardson, T. B., Mann, G. W., Reddington, C. L., Forster, P. M., et al. (2016). The impact of European legislative and technology measures to reduce air pollutants on air quality, human health and climate. *Environmental Research Letters*, *11*(2), 0. https://doi.org/10.1088/1748-9326/11/2/024010

Twomey, S. (1977). The Influence of Pollution on the Shortwave Albedo of Clouds. *Journal of the Atmospheric Sciences*. https://doi.org/10.1175/1520-0469(1977)034<1149:tiopot>2.0.co;2

Uryu, Y., Mott, C., Foead, N., Yulianto, K., Budiman, A., Setiabudi, et al. (2008). Deforestation, Forest Degredation, Biodiversity Loss and CO2 Emissions in Riau, Sumatra, Indonesia. *WWF Indonesia*

Technical Report.

Varejao-Silva, M. A., Franchito, S. H., & Rao, V. B. (1998). A Coupled Biosphere-Atmosphere Climate Model Suitable for Studies of Climatic Change Due to Land Surface Alterations. *Journal of Climate*, *11*(7), 1749–1767. https://doi.org/10.1175/1520-0442(1998)011<1749:ACBACM>2.0.CO;2

Voldoire, A., & Royer, J. F. (2004). Tropical deforestation and climate variability. *Climate Dynamics*, *22*(8), 857–874. https://doi.org/10.1007/s00382-004-0423-z

van Vuuren, D. P., Edmonds, J., Kainuma, M., Riahi, K., Thomson, A., Hibbard, K., et al. (2011). The representative concentration pathways: An overview. *Climatic Change*, *109*(1), 5–31. https://doi.org/10.1007/s10584-011-0148-z

Wang, A., & Price, D. T. (2007). Estimating global distribution of boreal, temperate, and tropical tree plant functional types using clustering techniques. *Journal of Geophysical Research: Biogeosciences*, *112*(1), 1–15. https://doi.org/10.1029/2006JG000252

Wang, R., Balkanski, Y., Boucher, O., Ciais, P., Schuster, G. L., Chevallier, F., et al. (2016). Estimation of global black carbon direct radiative forcing and its uncertainty constrained by observations. *Journal of Geophysical Research*, *121*(10), 5948–5971. https://doi.org/10.1002/2015JD024326

Wang, Zhuo, Zeng, X., Barlage, M., Dickinson, R. E., Gao, F., & Schaaf, C. B. (2004). Using MODIS BRDF and albedo data to evaluate global model land surface albedo. *Journal of Hydrometeorology*, *5*(1), 3–14. https://doi.org/10.1175/1525-7541(2004)005<0003:UMBAAD>2.0.CO;2

Wang, Zhuosen, Schaaf, C. B., Strahler, A. H., Chopping, M. J., Román, M. O., Shuai, Y., et al. (2014). Evaluation of MODIS albedo product (MCD43A) over grassland, agriculture and forest surface types during dormant and snow-covered periods. *Remote Sensing of Environment*, *140*, 60–77. https://doi.org/10.1016/j.rse.2013.08.025

Wei, X., Hahmann, A. N., Dickinson, R. E., Yang, Z. L., Zeng, X., Schaudt, K. J., et al. (2001). Comparison of albedos computed by land surface models and evaluation against remotely sensed data. *Journal of Geophysical Research Atmospheres*, *106*(D18), 20687–20702. https://doi.org/10.1029/2001JD900218

Van Der Werf, G. R., Morton, D. C., Defries, R. S., Olivier, J. G. J., Kasibhatla, P. S., Jackson, R. B., et al. (2009). CO2 emissions from forest loss. *Nature Geoscience*, *2*(November), 9–11.

Van Der Werf, G. R., Randerson, J. T., Giglio, L., Collatz, G. J., Mu, M., Kasibhatla, P. S., et al. (2010). Global fire emissions and the contribution of deforestation, savanna, forest, agricultural, and peat fires (1997-2009). *Atmospheric Chemistry and Physics*, *10*(23), 11707–11735. https://doi.org/10.5194/acp-10-11707-2010

Wicke, B., Sikkema, R., Dornburg, V., & Faaij, A. (2011). Exploring land use changes and the role of palm oil production in Indonesia and Malaysia. *Land Use Policy*, *28*(1), 193–206. https://doi.org/10.1016/j.landusepol.2010.06.001

Wickham, J., Barnes, C. A., Nash, M. S., & Wade, T. G. (2015). Combining NLCD and MODIS to create a land cover-albedo database for the continental United States. *Remote Sensing of Environment*, *170*, 143–152. https://doi.org/10.1016/j.rse.2015.09.012

Wickham, J. D., Wade, T. G., & Riitters, K. H. (2013). Empirical analysis of the influence of forest extent on annual and seasonal surface temperatures for the continental United States. *Global Ecology and Biogeography*, *22*(5), 620–629. https://doi.org/10.1111/geb.12013

Wilcove, D. S., Giam, X., Edwards, D. P., Fisher, B., & Koh, L. P. (2013). Navjot's nightmare revisited: Logging, agriculture, and biodiversity in Southeast Asia. *Trends in Ecology and Evolution*, *28*(9), 531–540. https://doi.org/10.1016/j.tree.2013.04.005

Williams, M. (2000). Dark ages and dark areas: Global deforestation in the deep past. *Journal of Historical Geography*, *26*(1), 28–46. https://doi.org/10.1006/jhge.1999.0189

Wright, I. R., Nobre, C. A., Tomasella, J., Rocha, H. R. da, Roberts, J. M., Vertamatti, E., et al. (1996). Towards a GCM surface parameterisation for Amazonia. *Amazonian Deforestation and Climate*, (September 2015).

Yang, Y., Smith, S. J., Wang, H., Mills, C. M., & Rasch, P. J. (2019). Variability, timescales, and nonlinearity in climate responses to black carbon emissions. *Atmospheric Chemistry and Physics*, *19*(4), 2405–2420. https://doi.org/10.5194/acp-19-2405-2019

Young, P. J., Arneth, A., Schurgers, G., Zeng, G., & Pyle, J. a. (2009). The CO2 inhibition of isoprene significantly affects future ozone projection. *Atmos. Chem. Phys.*, *9*, 2793–2803. https://doi.org/10.5194/acp-9-2793-2009

Young, P. J., Archibald, a. T., Bowman, K. W., Lamarque, J.-F., Naik, V., Stevenson, D. S., et al. (2013). Pre-industrial to end 21st century projections of tropospheric ozone from the Atmospheric

Chemistry and Climate Model Intercomparison Project (ACCMIP). *Atmospheric Chemistry and Physics*, *13*(4), 2063–2090. https://doi.org/10.5194/acp-13-2063-2013

Zanon, M., Davis, B. A. S., Marquer, L., Brewer, S., & Kaplan, J. O. (2018). European forest cover during the past 12,000 years: A palynological reconstruction based on modern analogs and remote sensing. *Frontiers in Plant Science*, *9*(March), 1–25. https://doi.org/10.3389/fpls.2018.00253

Zarin, D. J., Harris, N. L., Baccini, A., Aksenov, D., Hansen, M. C., Azevedo-Ramos, C., et al. (2016). Can carbon emissions from tropical deforestation drop by 50% in 5 years? *Global Change Biology*, *22*(4), 1336–1347. https://doi.org/10.1111/gcb.13153

Zeng, G., Pyle, J. a., & Young, P. J. (2007). Impact of climate change on tropospheric ozone and its global budgets. *Atmospheric Chemistry and Physics Discussions*, *7*(4), 11141–11189. https://doi.org/10.5194/acpd-7-11141-2007

Zeng, N., & Neelin, J. D. (1999). A land-atmosphere interaction theory for the tropical deforestation problem. *Journal of Climate*, *12*(2–3), 857–872. https://doi.org/10.1175/1520-0442(1999)012<0857:alaitf>2.0.co;2

Zeng, N., Dickinson, R. E., & Zeng, X. (1996). Climatic Impact of Amazon Deforestation - A Mechanistic Model Study. *Journal of Climate*, *9*, 859–883.

Zhang, H., Henderson-Sellers, A., & McGuffie, K. (1996). Impacts of tropical deforestation. Part I: Process analysis of local climatic change. *Journal of Climate*. https://doi.org/10.1175/1520-0442(1996)009<1497:IOTDPI>2.0.CO;2

Zhang, H., Henderson-Sellers, A., & Mcguffie, K. (2001). The compounding effects of tropical deforestation and greenhouse warming on climate. *Climatic Change*, *49*(3), 309–338. https://doi.org/10.1023/A:1010662425950

Zhang, X., Gui, S., Li, L., Zhang, X., Gui, S., Liang, S., & Wang, K. (2010). Analysis of Global Land Surface Shortwave Broadband Albedo From Multiple Data Sources. *IEEE Journal of Selected Topics in Applied Earth Observations and Remote Sensing*, *3*(3), 296–305. https://doi.org/10.1109/JSTARS.2010.2049342

Zhang, Y., Zhu, Z., Liu, Z., Zeng, Z., Ciais, P., Huang, M., et al. (2016). Seasonal and interannual changes in vegetation activity of tropical forests in Southeast Asia. *Agricultural and Forest Meteorology*, *224*, 1–10. https://doi.org/10.1016/j.agrformet.2016.04.009

Zheng, Z., Wei, Z., Wen, Z., Dong, W., Li, Z., Wen, X., et al. (2017). Inclusion of Solar Elevation Angle in Land Surface Albedo Parameterization Over Bare Soil Surface. *Journal of Advances in Modeling Earth Systems*, *9*(8), 3069–3081. https://doi.org/10.1002/2017MS001109

Appendices

Appendix A – Literature search albedo values

Reference	Modelling / Observation	Replacement vegetation	Publication year	Model/observation method	Δ albedo
(Souza et al., 2013)	In Situ	Soybean	2014	3 metre tower (soybean), 54 metre tower (forest)	0.09
(Eck et al., 1998)	Modelling	Bare Soil	1998	6S (Second Simulation of the Satellite Signal in the Solar Spectrum)	0.088
(Holdaway et al., 2010)	In Situ	Pasture	2010	ABRACOS & LBA eddy covariance towers	0.044
(Voldoire & Royer, 2004)	Modelling	Grass	2004	ARPEGE + ISBA GCM	0.035
(Bastable et al., 1993)	In Situ	Pasture	1993	Automatic weather stations	0.032
(Wei et al., 2001)	Remote Sensing	Grass	2001	AVHRR	0.0505
(Wei et al., 2001)	Modelling	Grass	2001	BATS	0.0775
(Varejao-Silva et al., 1998)	Modelling	Grass	1998	BATS-SDM	0.02

(Varejao-Silva et al., 1998)	Modelling	Grass	1998	BATS-SDM	0.04
(Mei & Wang, 2010)	Modelling	Grass	2009	CAM3-CLM3	0.06
(Devaraju et al., 2015)	Modelling	Grass	2015	CAM5.0 - CLM4	0.075
(Henderson-Sellers et al., 1993)	Modelling	Grass	1993	CCM	0.07
(Dickinson & Kennedy, 1992)	Modelling	Pasture	1992	CCM	0.07
(McGuffie et al., 1995)	Modelling	Grass	1995	CCM1 + BATS GCM	0.07
(H. Zhang et al., 1996)	Modelling	Grass	1996	CCM1 + BATS GCM	0.07
(H. Zhang et al., 2001)	Modelling	Grass	2001	CCM1-Oz + BATS GCM	0.07
(Pitman et al., 1993)	Modelling	Grass	1993	CCM1-Oz + BATS GCM	0.07
(Pitman et al., 1993)	Modelling	Grass	1993	CCM1-Oz + BATS GCM	0.069
(Pitman et al., 1993)	Modelling	Grass	1993	CCM1-Oz + BATS GCM	0.095
(Pitman et al., 1993)	Modelling	Bare Soil	1993	CCM1-Oz + BATS GCM	0.115

(Hahmann & Dickinson, 1997)	Modelling	Grass	1997	CCM2-BATS1e	0.07
(Costa et al., 2007)	Modelling	Soybean	2007	CCM3	0.09
(Costa et al., 2007)	Modelling	Soybean	2007	CCM3	0.08
(Costa et al., 2007)	Modelling	Pasture	2007	CCM3	0.048
(Costa et al., 2007)	Modelling	Pasture	2007	CCM3	0.057
(Snyder et al., 2004)	Modelling	Bare Soil	2004	CCM3-IBIS	0.04
(Sampaio et al., 2007)	Modelling	Soybean	2007	CPTEC-INPE AGCM	0.05
(Sampaio et al., 2007)	Modelling	Pasture	2007	CPTEC-INPE AGCM	0.06
(G. Myhre & Myhre, 2003)	Modelling	Grass	2003	DISTORT (radiative transfer method)	0.06
(Kleidon & Heimann, 1999)	Modelling	Grass	1999	ECHAM-4 GCM	0.06
(Kleidon & Heimann, 1999)	Modelling	Grass	1999	ECHAM-4 GCM	0.08

(Branković et al., 2006)	Modelling	Grass	2006	ECMWF	0.05
(Branković et al., 2006)	Modelling	Grass	2006	ECMWF	0.1
(de Oliveira et al., 2016)	In Situ	Pasture	2016	Fluxnet	0.059
(Manzi & Planton, 1994)	Modelling	Grass	1994	French spectral GCM + ISBA (Interactions between Soil, Biosphere and Atmosphere)	0.05
(Berbet & Costa, 2003)	Modelling	Grass	2003	GENESIS (V2) - IBIS	0.036
(N. Zeng et al., 1996)	Modelling	Forced	1996	Gill GCM	0.05
(Sud et al., 1996)	Modelling	Grass	1996	GLA + SiB GCM	0.05
(Bala et al., 2007)	Modelling	Grass	2007	INCCA	0.04
(Polcher & Laval, 1994)	Modelling	Pasture	1994	LMD + SECHIB A GCM	0.081
(Polcher & Laval, 1994)	Modelling	Pasture	1994	LMD + SECHIB A GCM	0.079
(Manzi & Planton, 1994)	Modelling	Pasture	1994	MCGA (Modelos de Circulação Geral da Atmosfera)	0.07

(Oliveira & Moraes, 2013)	In Situ	Pasture	2013	Microclimatic towers	0.12
(de Oliveira et al., 2016)	Remote Sensing	Pasture	2016	MODIS	0.044
(Loarie et al., 2011)	Remote Sensing	Mixed	2010	MODIS	0.028
(Oliveira & Moraes, 2013)	Remote Sensing	Pasture	2013	MODIS (Terra)	0.04
(Bathiany et al., 2010)	Modelling	Grass	2010	MPI-ESM	0.042
(Dickinson & Henderson-Sellers, 1988)	Modelling	Grass	1988	NCAR CCM1 + BATS GCM	0.07
(Wei et al., 2001)	Modelling	Grass	2001	NCAR LSM	0.0785
(Correia et al., 2008)	Modelling	Pasture	2008	NCEP Eta - SSiB model (National Center for Environmental Protection numerical regional model, coupled with Simplified Simple Biosphere Model)	0.06
(Nobre et al., 1991)	Modelling	Pasture	1991	NMC (National Meteorological Center) Global Spectral Model + SiB GCM	0.07
(Culf et al., 1995)	In Situ	Pasture	1995	Radiometer (Tower)	0.0454

(Gandu et al., 2004)	Modelling	Pasture	2004	RAMS	0.05
(N. Zeng & Neelin, 1999)	Modelling	Forced	1999	RCCM2/BATS	0.07
(Franchito & Rao, 1992)	Modelling	Grass	1992	SDM	0.02
(Franchito & Rao, 1992)	Modelling	Grass	1992	SDM	0.04
(Eck et al., 1998)	Modelling	Bare Soil	1998	SPCTRAL2	0.126
(Eltahir & Humphries, 1998)	In Situ	Pasture	1998	Tower	0.045
(T. W. Giambelluca et al., 2000)	In Situ	Pasture	2000	Tower	0.04
(Thomas W. Giambelluca et al., 1997)	In Situ	Pasture	1997	Tower	0.039
(Lean & Rowntree, 1997)	Modelling	Grass	1997	UKMO GCM	0.05
(Lean & Rowntree, 1997)	Modelling	Pasture	1993	UKMO GCM	0.052
(Mylne & Rowntree, 1992)	Modelling	Grass	1991	UKMO GCM	0.065

(Lean & Warrilow, 1989)	Modelling	Pasture	1989	UKMO GCM	0.052
(Lean & Rowntree, 1997)	Modelling	Pasture	1997	UKMO GCM	0.046
(Salati & Nobre, 1992)	Modelling	Grass	1991	UKMO GCM & COLA GCM - SiB	0.091
(Y. Li, De Noblet-Ducoudré, et al., 2016)	Modelling	Bare Soil	2016	VEGAS (albedo fed by satellite data)	0.26
(Y. Li, De Noblet-Ducoudré, et al., 2016)	Modelling	Bare Soil	2016	VEGAS (albedo fed by satellite data)	0.12

References

Abood, S. A., Lee, J. S. H., Burivalova, Z., Garcia-Ulloa, J., & Koh, L. P. (2015). Relative Contributions of the Logging, Fiber, Oil Palm, and Mining Industries to Forest Loss in Indonesia. *Conservation Letters*, *8*(1), 58–67. https://doi.org/10.1111/conl.12103

Achard, F., Eva, H. D., Stibig, H. J., Mayaux, P., Gallego, J., Richards, T., & Malingreau, J. P. (2002). Determination of deforestation rates of the world's humid tropical forests. *Science*, *297*(5583), 999–1002. https://doi.org/10.1126/science.1070656

Albrecht, B. A. (1989). Aerosols, Cloud Microphysics, and Fractional Cloudiness. *Science*, *245*, 1227–1230. https://doi.org/10.1126/science.245.4923.1227

Alkama, R., & Cescatti, A. (2016a). Biophysical climate impacts of recent changes in global forest cover. *Science*, *351*(6273), 600–604.

Alkama, R., & Cescatti, A. (2016b). Supplementary: Biophysical climate impacts of recent changes in global forest cover. *Science*, *351*(6273), 600–604. https://doi.org/10.1126/science.aac8083

Allan, J. D., Morgan, W. T., Darbyshire, E., Flynn, M. J., Williams, P. I., Oram, D. E., et al. (2014). Airborne observations of IEPOX-derived isoprene SOA in the Amazon during SAMBBA. *Atmospheric Chemistry and Physics*, *14*(20), 11393–11407. https://doi.org/10.5194/acp-14-11393-2014

Allen, M. R., Dube, O. P., Solecki, W., Aragón-Durand, F., Cramer, W., Humphreys, S., et al. (2018).

Framing and Context. In *Global Warming of 1.5°C. An IPCC Special Report on the impacts of global warming of 1.5°C above pre-industrial levels and related global greenhouse gas emission pathways, in the context of strengthening the global response to the threat of climate change,*.

Andre, R. G. B., & Viswanadham, Y. (1983). Radiation balance of soybeans grown in Brazil. *Agricultural Meteorology*, *30*(3), 157–173. https://doi.org/10.1016/0002-1571(83)90049-3

Andrews, T., Betts, R. A., Booth, B. B. B., Jones, C. D., & Jones, G. S. (2017). Effective radiative forcing from historical land use change. *Climate Dynamics*, *48*(11–12), 3489–3505. https://doi.org/10.1007/s00382-016-3280-7

Arjasakusuma, S., Yamaguchi, Y., Hirano, Y., & Zhou, X. (2018). ENSO-and rainfall-sensitive vegetation regions in Indonesia as identified from multi-sensor remote sensing data. *ISPRS International Journal of Geo-Information*, *7*(3). https://doi.org/10.3390/ijgi7030103

Arora, V. K., & Montenegro, A. (2011). Small temperature benefits provided by realistic afforestation efforts. *Nature Geoscience*, *4*(8), 514–518. https://doi.org/10.1038/ngeo1182

As-syakur, A. R., Tanaka, T., Osawa, T., & Mahendra, M. S. (2013). Indonesian rainfall variability observation using TRMM multi-satellite data. *International Journal of Remote Sensing*, *34*(21), 7723–7738. https://doi.org/10.1080/01431161.2013.826837

Austin, K. G., Kasibhatla, P. S., Urban, D. L., Stolle, F., & Vincent, J. (2015). Reconciling oil palm expansion and climate change mitigation in Kalimantan, Indonesia. *PLoS ONE*, *10*(5), 1–17. https://doi.org/10.1371/journal.pone.0127963

Bala, G., Caldeira, K., Wickett, M., Phillips, T. J., Lobell, D. B., Delire, C., & Mirin, a. (2007). Combined climate and carbon-cycle effects of large-scale deforestation. *Proceedings of the National Academy of Sciences of the United States of America*, *104*(16), 6550–5. https://doi.org/10.1073/pnas.0608998104

Bastable, H. G., Shuttleworth, W. J., Dallarosa, R. L. G., Fisch, G., & Nobre, C. A. (1993). Observations of climate, albedo, and surface radiation over cleared and undisturbed amazonian forest. *International Journal of Climatology*, *13*(7), 783–796. https://doi.org/10.1002/joc.3370130706

Bathiany, S., Claussen, M., Brovkin, V., Raddatz, T., & Gayler, V. (2010). Combined biogeophysical and biogeochemical effects of large-scale forest cover changes in the MPI earth system model. *Biogeosciences*, *7*(5), 1383–1399. https://doi.org/10.5194/bg-7-1383-2010

Bazzaz, E. A., & Pickett, S. T. A. (1980). TROPICAL SUCCESSION: A Comparative Review. *Ann Rev. Ecol. Syst.*, *11*(20), 287–310.

Bellouin, N., Quaas, J., Gryspeerdt, E., Kinne, S., Stier, P., Watson-Parris, D., et al. (2019). Bounding global aerosol radiative forcing of climate change. *Reviews of Geophysics*, 1–45. https://doi.org/10.1029/2019rg000660

Berbet, M. L. C., & Costa, M. H. (2003). Climate change after tropical deforestation: Seasonal variability of surface albedo and its effects on precipitation change. *Journal of Climate*, *16*(12), 2099–2104. https://doi.org/10.1175/1520-0442(2003)016<2099:CCATDS>2.0.CO;2

Betts, A. K., Desjardins, R. L., & Worth, D. (2007). Impact of agriculture, forest and cloud feedback on the surface energy budget in BOREAS. *Agricultural and Forest Meteorology*, *142*(2–4), 156–169. https://doi.org/10.1016/j.agrformet.2006.08.020

Betts, R. A. (2000). Offset of the potential carbon sink from boreal forestation by decreases in surface albedo. *Nature*, *408*(6809), 187–190. https://doi.org/10.1038/35041545

Betts, Richard A. (2001). Biogeophysical impacts of land use on present-day climate: Near-surface temperature change and radiative forcing. *Atmospheric Science Letters*, *2*(1–4), 39–51. https://doi.org/10.1006/asle.2001.0023

Blad, B. L., & Baker, D. G. (1971). Reflected Radiation from a Soybean Crop. *Agronomy Journal*, *64*(3), 277–280.

Blois, J. L., Williams, J. W., Fitzpatrick, M. C., Jackson, S. T., & Ferrier, S. (2013). Financial Contraints of Ethnic Entreprenurs. *Proceedings of the National Academy of Sciences*, *110*(23), 9374–9379. https://doi.org/10.5061/dryad.d5f1r.1

Bonan, G. B. (2008a). Forests and climate change: forcings, feedbacks, and the climate benefits of forests. *Science*, *320*, 1444–1449. https://doi.org/10.1126/science.1155121

Bonan, G. B. (2008b). Forests in Flux Forests and Climate of Forests Climate Benefits Change, and the Climate benefit of Forests. *Science*, *320*(5882), 1444–1449.

Bourgeois, C. S., Calanca, P., & Ohmura, A. (2006). A field study of the hemispherical directional reflectance factor and spectral albedo of dry snow. *Journal of Geophysical Research Atmospheres*, *111*(20), 1–13. https://doi.org/10.1029/2006JD007296

Brandon, K. (2015). *Ecosystem Services from Tropical Forests: Review of Current Science*. *CGD Climate and Forest Paper Series #7*. https://doi.org/10.2139/ssrn.2622749

Branković, Č., Molteni, F., & Viterbo, P. (2006). GCM sensitivity experiments with locally modified land surface properties over tropical South America. *Climate Dynamics*, *26*(7–8), 729–749. https://doi.org/10.1007/s00382-006-0112-1

Brito, J., Rizzo, L. V., Morgan, W. T., Coe, H., Johnson, B., Haywood, J., et al. (2014). Ground-based aerosol characterization during the South American Biomass Burning Analysis (SAMBBA) field experiment. *Atmospheric Chemistry and Physics*, *14*(22), 12069–12083. https://doi.org/10.5194/acp-14-12069-2014

Busch, J., Ferretti-gallon, K., Engelmann, J., Wright, M., Kemen, G., Stolle, F., et al. (2018). Reductions in emissions from deforestation from Indonesia's moratorium on new oil palm, timber, and logging concessions, *112*(5), 1–6. https://doi.org/10.7910/DVN/28615

Caiazzo, F., Malina, R., Staples, M. D., Wolfe, P. J., Yim, S. H. L., & Barrett, S. R. H. (2014). Quantifying the climate impacts of albedo changes due to biofuel production: A comparison with biogeochemical effects. *Environmental Research Letters*, *9*(2). https://doi.org/10.1088/1748-9326/9/2/024015

Camredon, M., Aumont, B., Lee-Taylor, J., & Madronich, S. (2007). The SOA/VOC/NOx system: An explicit model of secondary organic aerosol formation. *Atmospheric Chemistry and Physics*, *7*(21), 5599–5610. https://doi.org/10.5194/acp-7-5599-2007

Carswell, F. E., Costa, A. L., Palheta, M., Malhi, Y., Meir, P., Costa, J. D. P. R., et al. (2002). Seasonality in CO2 and H2O flux at an eastern Amazonian rain forest. *Journal of Geophysical Research D: Atmospheres*, *107*(20). https://doi.org/10.1029/2000JD000284

Cescatti, A., Marcolla, B., Santhana Vannan, S. K., Pan, J. Y., Román, M. O., Yang, X., et al. (2012).

Intercomparison of MODIS albedo retrievals and in situ measurements across the global FLUXNET network. *Remote Sensing of Environment*, *121*, 323–334. https://doi.org/10.1016/j.rse.2012.02.019

Chong, K. L., Kanniah, K. D., Pohl, C., & Tan, K. P. (2017). A review of remote sensing applications for oil palm studies. *Geo-Spatial Information Science*, *20*(2), 184–200. https://doi.org/10.1080/10095020.2017.1337317

Claussen, M., Brovkin, V., & Ganopolski, A. (2001). Biophysical versus biogeochemical feedbacks of large-scale land cover change. *Geophysical Research Letters*, *28*(6), 1011–1014. https://doi.org/10.1029/2000GL012471

Coakley, J. A. (2002). Reflectance and Albedo, Surface. In J. A. Curry & J. A. Pyle (Eds.), *Encyclopedia of Atmospheric Sciences* (1st ed., pp. 1914–1923). https://doi.org/10.1016/B0-12-227090-8/00069-5

Correia, F. W. S., Alvalá, R. C. S., & Manzi, A. O. (2008). Modeling the impacts of land cover change in Amazonia: A regional climate model (RCM) simulation study. *Theoretical and Applied Climatology*, *93*(3–4), 225–244. https://doi.org/10.1007/s00704-007-0335-z

Costa, M. H., Yanagi, S. N. M., Souza, P. J. O. P., Ribeiro, A., & Rocha, E. J. P. (2007). Climate change in Amazonia caused by soybean cropland expansion, as compared to caused by pastureland expansion. *Geophysical Research Letters*, *34*(7), 2–5. https://doi.org/10.1029/2007GL029271

Culf, A. D., Fisch, G., & Hodnett, M. G. (1995). The Albedo of Amazonian Forest and Ranch Land. *Journal of Climate*, *8*, 1544–1554.

Curtis, P. G., Slay, C. M., Harris, N. L., Tyukavina, A., & Hansen, M. C. (2018). Classifying drivers of global forest loss. *Science*, *361*(6407), 1108–1111. https://doi.org/10.1126/science.aau3445

Davin, E. L., & de Noblet-Ducoudre, N. (2010). Climatic impact of global-scale Deforestation: Radiative versus nonradiative processes. *Journal of Climate*, *23*(1), 97–112. https://doi.org/10.1175/2009JCLI3102.1

Dawson, J. P., Adams, P. J., & Pandis, S. N. (2007). Sensitivity of ozone to summertime climate in the eastern USA: A modeling case study. *Atmospheric Environment*, *41*(7), 1494–1511. https://doi.org/10.1016/j.atmosenv.2006.10.033

Descals, A., Wich, S., Meijaard, E., Gaveau, D., Peedell, S., & Szantoi, Z. (2020). High-resolution global map of smallholder and industrial closed-canopy oil palm plantations. *Earth System Science Data Discussions*, *Preprint*(August), 1–22. https://doi.org/10.5194/essd-2020-159

Devaraju, N., Bala, G., & Nemani, R. (2015). Modelling the influence of land-use changes on biophysical and biochemical interactions at regional and global scales. *Plant, Cell and Environment*, *38*(9), 1931–1946. https://doi.org/10.1111/pce.12488

Dickinson, R. E., & Henderson-Sellers, A. (1988). Modelling tropical deforestation: A study of GCM land-surface parametrizations. *Quarterly Journal of the Royal Meteorological Society*, *114*(480), 439–462. https://doi.org/10.1256/smsqj.48008

Dickinson, R. E., & Kennedy, P. (1992). Impacts on regional climate of Amazon deforestation. *Geophysical Research Letters*, *19*(19), 1947–1950. https://doi.org/10.1029/92GL01905

Donato, D. C., Kauffman, J. B., Murdiyarso, D., Kurnianto, S., Stidham, M., & Kanninen, M. (2011).

Mangroves among the most carbon-rich forests in the tropics. *Nature Geoscience*, *4*(5), 293–297. https://doi.org/10.1038/ngeo1123

Eck, T. F., Holben, B. N., Slutsker, I., & Setzer, A. (1998). Measurements of irradiance attenuation and estimation of aerosol single scattering albedo for biomass burning aerosols in Amazonia. *Journal of Geophysical Research Atmospheres*, *103*(D24), 31865–31878. https://doi.org/10.1029/98JD00399

Edwards, J. M., & Slingo, A. (1996). Studies with a flexible new radiation code. I: Choosing a configuration for a large-scale model. *Quarterly Journal of the Royal Meteorological Society*, *122*(531), 689–719. https://doi.org/10.1256/smsqj.53106

Eltahir, E. A. B., & Humphries, E. J. (1998). The role of clouds in the surface energy balance over the Amazon forest. *International Journal of Climatology*, *18*(14), 1575–1591. https://doi.org/10.1002/(SICI)1097-0088(19981130)18:14<1575::AID-JOC316>3.0.CO;2-U

Elvidge, C. D., Zhizhin, M., Hsu, F. C., Baugh, K., Khomarudin, M. R., Vetrita, Y., et al. (2015). Long-wave infrared identification of smoldering peat fires in Indonesia with nighttime Landsat data. *Environmental Research Letters*, *10*(6). https://doi.org/10.1088/1748-9326/10/6/065002

Estoque, R. C., Ooba, M., Avitabile, V., Hijioka, Y., DasGupta, R., Togawa, T., & Murayama, Y. (2019). The future of Southeast Asia's forests. *Nature Communications*, *10*(1), 1–12. https://doi.org/10.1038/s41467-019-09646-4

Estoque, R. C., Ooba, M., Avitabile, V., Hijioka, Y., Dasgupta, R., Togawa, T., & Murayama, Y. (2019). The future of Southeast Asia's forests. *Nature Communications*, *10*, 1–12. https://doi.org/10.1038/s41467-019-09646-4

FAO. (2006). *Global Forest Resources Assessment 2005: Progress towards sustainable forest management*.

Fearnside, P. M. (2005). Deforestación en la Amazonía Brasileña: Historia, Tasas y Consecuencias. *Conservation Biology*, *19*(3), 680–688. https://doi.org/10.1111/j.1523-1739.2005.00697.x

Federative Republic of Brazil. (2015). *Brazil Intended Nationally Determined Contribution*. Retrieved from http://www.loc.gov/law/help/guide/nations/brazil.php

Ferrante, L., & Fearnside, P. M. (2019). Brazil's new president and "ruralists" threaten Amazonia's environment, traditional peoples and the global climate. *Environmental Conservation*, 11–13. https://doi.org/10.1017/S0376892919000213

Finegan, B. (1996). Pattern and process in neotropical secondary rain forests: The first 100 years of succession. *Trends in Ecology and Evolution*, *11*(3), 119–124. https://doi.org/10.1016/0169-5347(96)81090-1

Foley, J. A., DeFries, R., Asner, G. P., Barford, C., Bonan, G., Carpenter, S. R., et al. (2005). Global consequences of land use. *Science*, *309*(5734), 570–574. https://doi.org/10.1126/science.1111772

Fontana, D. C., Berlato, M. A., & Bergamaschi, H. (1991). Balanço de radiação da soja em região subtropical do Brasil. *Pesquisa Agropecuária Brasileira*.

Food and Agricultural Organization of the United Nations. (2015). *Global Forest Resources Assessment 2015*. Rome.

Food and Agriculture Organization. (2016). *State of the World's Forests*. *Food and Agriculture Organization of the United Nations* (2012th ed.). Rome: Food and Agriculture Organization.

Food and Agriculture Organsiation of the United Nations. (2015). *Global Forest Resources Assessment 2015*. *Desk Reference*. https://doi.org/10.1002/2014GB005021

Foot, J. S. (1982). Meterological Research Flight Technical Note 13: Thermal Lag of Hercules' Pyranometers.

Forster, P., Ramaswamy, V., Artaxo, P., Berntsen, T., Betts, R., Fahey, D. W., et al. (2007). 2007: Changes in Atmospheric Constituents and in Radiative Forcing. In M. T. and H. L. M. Solomon, S., D. Qin, M. Manning, Z. Chen, M. Marquis, K.B. Averyt (Ed.), *Climate Change 2007: The Physical Science Basis. Contribution of Working Group I to the Fourth Assessment Report of the Intergovernmental Panel on Climate Change*. Cambridge, United Kingdom and New York, NY, USA: Cambridge University Press.

Franchito, S. H., & Rao, V. B. (1992). Climatic change due to land surface alterations. *Climatic Change*, *22*(1), 1–34. https://doi.org/10.1007/BF00143341

Freitas, F. L. M., Sparovek, G., Berndes, G., Persson, U. M., Englund, O., Barretto, A., & Mörtberg, U. (2018). Potential increase of legal deforestation in Brazilian Amazon after Forest Act revision. *Nature Sustainability*, *1*(11), 665–670. https://doi.org/10.1038/s41893-018-0171-4

Fu, T. M., Jacob, D. J., Palmer, P. I., Chance, K., Wang, Y. X., Barletta, B., et al. (2007). Space-based formaldehyde measurements as constrains on volatile organic compound emissions in east and south Asia and implications for ozone. *Journal of Geophysical Research Atmospheres*, *112*(6), 1–15. https://doi.org/10.1029/2006JD007853

Fuchs, H., Hofzumahaus, A., Rohrer, F., Bohn, B., Brauers, T., Dorn, H. P., et al. (2013). Experimental evidence for efficient hydroxyl radical regeneration in isoprene oxidation. *Nature Geoscience*, *6*(12), 1023–1026. https://doi.org/10.1038/ngeo1964

Gandu, A. W., Cohen, J. C. P., & de Souza, J. R. S. (2004). Simulation of deforestation in eastern Amazonia using a high-resolution model. *Theoretical and Applied Climatology*, *78*(1–3), 123–135. https://doi.org/10.1007/s00704-004-0048-5

Gao, F., He, T., Wang, Z., Ghimire, B., Shuai, Y., Masek, J., et al. (2014). Multiscale climatological albedo look-up maps derived from moderate resolution imaging spectroradiometer BRDF/albedo products. *Journal of Applied Remote Sensing*, *8*(1), 083532. https://doi.org/10.1117/1.jrs.8.083532

Giambelluca, T. W., Nullet, M. A., Ziegler, A. D., & Tran, L. (2000). Latent and sensible energy flux over deforested land surfaces in the eastern Amazon and northern Thailand. *Singapore Journal of Tropical Geography*, *21*(2), 107–130. https://doi.org/10.1111/1467-9493.00070

Giambelluca, Thomas W., Hölscher, D., Bastos, T. X., Frazão, R. R., Nullet, M. A., & Ziegler, A. D. (1997). Observations of albedo and radiation balance over postforest land surfaces in the eastern Amazon Basin. *Journal of Climate*, *10*(5), 919–928. https://doi.org/10.1175/1520-0442(1997)010<0919:OOAARB>2.0.CO;2

Gibbs, H. K., Ruesch, A. S., Achard, F., Clayton, M. K., Holmgren, P., Ramankutty, N., & Foley, J. A. (2010). Tropical forests were the primary sources of new agricultural land in the 1980s and 1990s. *Proceedings of the National Academy of Sciences of the United States of America*, *107*(38),

16732–16737. https://doi.org/10.1073/pnas.0910275107

Gibbs, Holly K., Johnston, M., Foley, J. A., Holloway, T., Monfreda, C., Ramankutty, N., & Zaks, D. (2008). Carbon payback times for crop-based biofuel expansion in the tropics: The effects of changing yield and technology. *Environmental Research Letters*, *3*(3). https://doi.org/10.1088/1748-9326/3/3/034001

Godar, J., Gardner, T. A., Tizado, E. J., & Pacheco, P. (2015). Correction: Sustainability science, environmental sciences (Proc Natl Acad Sci USA 111:15591-15596(2014)). *Proceedings of the National Academy of Sciences of the United States of America*, *112*(23), E3089. https://doi.org/10.1073/pnas.1508418112

Goldewijk, K. K. (2001). Estimating global land use change over the past 300 years: The HYDE database. *Global Biogeochemical Cycles*, *15*(2), 417–433. https://doi.org/10.1029/1999GB001232

Goldewijk, K. K., Hall, F. G., Collatz, G. J., Meeson, B. W., Los, S. O., Brown De Colstoun, E., & Landis, D. R. (2007). ISLSCP II Historical Land Cover and Land Use, 1700-1990. *ORNL DAAC*. Oak Ridge,k Tennesee, USA. https://doi.org/10.3334/ORNLDAAC/967

Gruber, N., & Galloway, J. N. (2008). An Earth-system perspective of the global nitrogen cycle. *Nature*, *451*(7176), 293–296. https://doi.org/10.1038/nature06592

Guan, K., Pan, M., Li, H., Wolf, A., Wu, J., Medvigy, D., et al. (2015). Photosynthetic seasonality of global tropical forests constrained by hydroclimate. *Nature Geoscience*, *8*(4), 284–289. https://doi.org/10.1038/ngeo2382

Guenther, A., Nicholas, C., Fall, R., Klinger, L., Mckay, W. A., & Scholes, B. (1995). A global model of natural volatile organic compound emissions s Raja the balance Triangle changes in the atmospheric accumulation rates of greenhouse Triangle Several inventories of natural and Exposure Assessment global scales have been two classes Fores. *J. Geophys. Res.*, *100*(94), 8873–8892.

Gueymard, C. A. (2009). Direct and indirect uncertainties in the prediction of tilted irradiance for solar engineering applications. *Solar Energy*, *83*(3), 432–444. https://doi.org/10.1016/j.solener.2008.11.004

Guyon, P., Graham, B., Beck, J., Boucher, O., Gerasopoulos, E., Mayol-Bracero, O. L., et al. (2003). Physical properties and concentration of aerosol particles over the Amazon tropical forest during background and biomass burning conditions. *Atmospheric Chemistry and Physics*, *3*(4), 951–967. https://doi.org/10.5194/acp-3-951-2003

Haeffelin, M., Kato, S., Smith, A. M., Rutledge, C. K., Charlock, T. P., & Mahan, J. R. (2001). Determination of the thermal offset of the Eppley precision spectral pyranometer. *Applied Optics*, *40*(4), 472. https://doi.org/10.1364/ao.40.000472

Hahmann, A. N., & Dickinson, R. E. (1997). RCCM2-BATS model over tropical South America: Applications to tropical deforestation. *Journal of Climate*, *10*(8), 1944–1964. https://doi.org/10.1175/1520-0442(1997)010<1944:RBMOTS>2.0.CO;2

Hallquist, M., Wenger, J. C., Baltensperger, U., Rudich, Y., Simpson, D., Claeys, M., et al. (2009). The formation, properties and impact of secondary organic aerosol: Current and emerging issues. *Atmospheric Chemistry and Physics*, *9*(14), 5155–5236. https://doi.org/10.5194/acp-9-5155-2009

Hamilton, R. L., Trimmer, M., Bradley, C., & Pinay, G. (2016). Deforestation for oil palm alters the fundamental balance of the soil N cycle. *Soil Biology and Biochemistry*, *95*, 223–232. https://doi.org/10.1016/j.soilbio.2016.01.001

Hansen, J., Sato, M., & Ruedy, R. (1997). Radiative forcing and climate response Abstract . We examine the sensitivity of a climate model to a wide range of radiative including changes of solar forcing introduced times the climate response , specifically the global mean temperature change , is se, *102*, 6831–6864.

Hansen, M. C., Potapov, P. V, Moore, R., Hancher, M., Turubanova, S. a, & Tyukavina, A. (2013). High-Resolution Global Maps of 21st-Century Forest Cover Change. *Science*, *342*(6160), 850–853. https://doi.org/10.1126/science.1244693

He, T., Shao, Q., Cao, W., Huang, L., & Liu, L. (2015). Satellite-observed energy budget change of deforestation in northeastern china and its climate implications. *Remote Sensing*, *7*(9), 11586–11601. https://doi.org/10.3390/rs70911586

Heald, C. L., & Spracklen, D. V. (2015). Land Use Change Impacts on Air Quality and Climate. *Chemical Reviews*, *115*, 4476–4496. https://doi.org/10.1021/cr500446g

Henderson-Sellers, A., Dickinson, R. E., Durbidge, T. B., Kennedy, P. J., McGuffie, K., & Pitman, A. J. (1993). Tropical deforestation: modeling local- to regional-scale climate change. *Journal of Geophysical Research*, *98*(D4), 7289–7315. https://doi.org/10.1029/92JD02830

Henderson-Sellers, A., & Wilson, M. F. (1983). Surface Albedo Data for Climatic Modeling. *Reviews of Geophysics and Space Physics*, *21*(8), 1743–1778.

Hendon, H. H. (2003). Indonesian rainfall variability: Impacts of ENSO and local air-sea interaction. *Journal of Climate*, *16*(11), 1775–1790. https://doi.org/10.1175/1520-0442(2003)016<1775:IRVIOE>2.0.CO;2

Hogrefe, C., Lynn, B., Civerolo, K., Ku, J. Y., Rosenthal, J., Rosenzweig, C., et al. (2004). Simulating changes in regional air pollution over the eastern United States due to changes in global and regional climate and emissions. *Journal of Geophysical Research D: Atmospheres*, *109*(22), 1–13. https://doi.org/10.1029/2004JD004690

Holdaway, R. J., Sparrow, A. D., & Coomes, D. A. (2010). Trends in entropy production during ecosystem development in the Amazon Basin. *Philosophical Transactions of the Royal Society B: Biological Sciences*, *365*(1545), 1437–1447. https://doi.org/10.1098/rstb.2009.0298

Houghton, J. T., Ding, Y., Griggs, D. J., Noguer, M., van der Linden, P. J., Dai, X., et al. (Eds.). (2001). *IPCC, 2001: Climate Change 2001: The Scientific Basis. Contribution of Working Group I to the Third Assessment Report of the Intergovernmental Panel on Climate Change*. Cambridge, United Kingdom and New York, NY, USA: Cambridge University Press.

Hubau, W., Lewis, S. L., Phillips, O. L., Affum-Baffoe, K., Beeckman, H., Cuní-Sanchez, A., et al. (2020). Asynchronous carbon sink saturation in African and Amazonian tropical forests. *Nature*, *579*(7797), 80–87. https://doi.org/10.1038/s41586-020-2035-0

Hurtt, G. C., Chini, L. P., Frolking, S., Betts, R. A., Feddema, J., Fischer, G., et al. (2011). Harmonization of land-use scenarios for the period 1500-2100: 600 years of global gridded annual land-use transitions, wood harvest, and resulting secondary lands. *Climatic Change*, *109*(1), 117–161. https://doi.org/10.1007/s10584-011-0153-2

Jackson, R. B., Randerson, J. T., Canadell, J. G., Anderson, R. G., Avissar, R., Baldocchi, D. D., et al. (2008). Protecting climate with forests. *Environmental Research Letters*, *3*(4). https://doi.org/10.1088/1748-9326/3/4/044006

Jin, Y., Schaaf, C. B., Woodcock, C. E., Gao, F., Li, X., Strahler, A. H., et al. (2003). Consistency of MODIS surface bidirectional reflectance distribution function and albedo retrievals: 1. Validation. *Journal of Geophysical Research D: Atmospheres*, *108*(5), 1–15. https://doi.org/10.1029/2002jd002804

Jin, Y., Randerson, J. T., Goetz, S. J., Beck, P. S. A., Loranty, M. M., & Goulden, M. L. (2012). The influence of burn severity on postfire vegetation recovery and albedo change during early succession in North American boreal forests. *Journal of Geophysical Research: Biogeosciences*, *117*(1), 1–15. https://doi.org/10.1029/2011JG001886

Johnson, B. T., Haywood, J. M., & Hawcroft, M. K. (2019). Are Changes in Atmospheric Circulation Important for Black Carbon Aerosol Impacts on Clouds, Precipitation, and Radiation? *Journal of Geophysical Research: Atmospheres*, *124*(14), 7930–7950. https://doi.org/10.1029/2019JD030568

Karl, T., Guenther, A., Yokelson, R. J., Greenberg, J., Potosnak, M., Blake, D. R., & Artaxo, P. (2007). The tropical forest and fire emissions experiment: Emission, chemistry, and transport of biogenic volatile organic compounds in the lower atmosphere over Amazonia. *Journal of Geophysical Research*, *112*(D18), 1–17. https://doi.org/10.1029/2007jd008539

Kivimäenpää, M., Ghimire, R. P., Sutinen, S., Häikiö, E., Kasurinen, A., Holopainen, T., & Holopainen, J. K. (2016). Increases in volatile organic compound emissions of Scots pine in response to elevated ozone and warming are modified by herbivory and soil nitrogen availability. *European Journal of Forest Research*, *135*(2), 343–360. https://doi.org/10.1007/s10342-016-0939-x

Kleidon, A., & Heimann, M. (1999). Deep-rooted vegetation, Amazonian deforestation, and climate: Results from a modelling study. *Global Ecology and Biogeography*, *8*(5), 397–405. https://doi.org/10.1046/j.1365-2699.1999.00150.x

Knowlton, K., Rosenthal, J. E., Hogrefe, C., Lynn, B., Gaffin, S., Goldberg, R., et al. (2004). Assessing ozone-related health impacts under a changing climate. *Environmental Health Perspectives*, *112*(15), 1557–1563. https://doi.org/10.1289/ehp.7163

Koh, L. P., & Wilcove, D. S. (2008). Is oil palm agriculture really destroying tropical biodiversity? *Conservation Letters*, *1*(2), 60–64. https://doi.org/10.1111/j.1755-263x.2008.00011.x

Kreidenweis, S. M., Petters, M., & Lohmann, U. (2018). 100 Years of Progress in Cloud Physics, Aerosols, and Aerosol Chemistry Research. *Meteorological Monographs*, *59*, 11.1-11.72. https://doi.org/10.1175/amsmonographs-d-18-0024.1

Kvalevåg, M. M., Myhre, G., Bonan, G., & Levis, S. (2010). Anthropogenic land cover changes in a GCM with surface albedo changes based on MODIS data. *International Journal of Climatology*, *30*(13), 2105–2117. https://doi.org/10.1002/joc.2012

Lawrence, D., & Vandecar, K. (2015). Effects of tropical deforestation on climate and agriculture. *Nature Climate Change*, *5*(1), 27–36. https://doi.org/10.1038/nclimate2430

Lean, J., & Rowntree, P. R. (1997). Correction note on "Understanding the sensitivity of a GCM simulation of Amazonian deforestation to the specification of vegetation and soil characteristics."

Journal of Climate, *12*(5 PART 2), 1549–1551. https://doi.org/10.1175/1520-0442(1999)012<1549:cnouts>2.0.co;2

Lean, J., & Warrilow, D. A. (1989). Simulation of the regional climatic impact of Amazon deforestation. *Nature*, *342*(6248), 411–413. https://doi.org/10.1038/342411a0

Lee, X., Goulden, M. L., Hollinger, D. Y., Barr, A., Black, T. A., Bohrer, G., et al. (2011). Observed increase in local cooling effect of deforestation at higher latitudes. *Nature*, *479*(7373), 384–387. https://doi.org/10.1038/nature10588

Lelieveld, J., Butler, T. M., Crowley, J. N., Dillon, T. J., Fischer, H., Ganzeveld, L., et al. (2008). Atmospheric oxidation capacity sustained by a tropical forest. *Nature*, *452*(7188), 737–740. https://doi.org/10.1038/nature06870

Li, L., Dong, J., Tenku, S. N., & Xiao, X. (2015). Mapping oil palm plantations in cameroon using PALSAR 50-m orthorectified mosaic images. *Remote Sensing*, *7*(2), 1206–1224. https://doi.org/10.3390/rs70201206

Li, Y., Zhao, M., Motesharrei, S., Mu, Q., Kalnay, E., & Li, S. (2015). Local cooling and warming effects of forests based on satellite observations. *Nature Communications*, *6*. https://doi.org/10.1038/ncomms7603

Li, Y., Zhao, M., Mildrexler, D. J., Motesharrei, S., Mu, Q., Kalnay, E., et al. (2016). Potential and actual impacts of deforestation and afforestation on land surface temperature. *Journal of Geophysical Research*, *121*(24), 14372–14386. https://doi.org/10.1002/2016JD024969

Li, Y., De Noblet-Ducoudré, N., Davin, E. L., Motesharrei, S., Zeng, N., Li, S., & Kalnay, E. (2016). The role of spatial scale and background climate in the latitudinal temperature response to deforestation. *Earth System Dynamics*, *7*(1), 167–181. https://doi.org/10.5194/esd-7-167-2016

Liang, S. (2000). Narrowband to broadband conversions of land surface albedo I Algorithms. *Remote Sensing of Environment*, *76*, 213–238.

Liu, H., & Randerson, J. T. (2008). Interannual variability of surface energy exchange depends on stand age in a boreal forest fire chronosequence. *Journal of Geophysical Research: Biogeosciences*, *113*(1), 1–13. https://doi.org/10.1029/2007JG000483

Liu, N. F., Liu, Q., Wang, L. Z., Liang, S. L., Wen, J. G., Qu, Y., & Liu, S. H. (2013). A statistics-based temporal filter algorithm to map spatiotemporally continuous shortwave albedo from MODIS data. *Hydrology and Earth System Sciences*, *17*(6), 2121–2129. https://doi.org/10.5194/hess-17-2121-2013

Liu, Y. Y., Van Dijk, A. I. J. M., De Jeu, R. A. M., Canadell, J. G., McCabe, M. F., Evans, J. P., & Wang, G. (2015). Recent reversal in loss of global terrestrial biomass. *Nature Climate Change*, *5*(5), 470–474. https://doi.org/10.1038/nclimate2581

Llusià, J., Peñuelas, J., & Gimeno, B. S. (2002). Seasonal and species-specific response of VOC emissions by Mediterranean woody plant to elevated ozone concentrations. *Atmospheric Environment*, *36*(24), 3931–3938. https://doi.org/10.1016/S1352-2310(02)00321-7

Loarie, S. R., Lobell, D. B., Asner, G. P., & Field, C. B. (2011). Land-Cover and surface water change drive large albedo increases in south america. *Earth Interactions*, *15*(7), 1–16. https://doi.org/10.1175/2010EI342.1

Lohmann, U., & Feichter, J. (2001). Can the direct and semi-direct aerosol effect compete with the indirect effect on a global scale. *Geophysical Research Letters*, *28*(1), 159–161.

Long, C. N., Bucholtz, A., Jonsson, H., Schmid, B., Vogelmann, A., & Wood, J. (2010). A Method of Correcting for Tilt from Horizontal in Downwelling Shortwave Irradiance Measurements on Moving Platforms. *The Open Atmospheric Science Journal*, *4*(1), 78–87. https://doi.org/10.2174/1874282301004010078

Loranty, M. M., Berner, L. T., Goetz, S. J., Jin, Y., & Randerson, J. T. (2014). Vegetation controls on northern high latitude snow-albedo feedback: Observations and CMIP5 model simulations. *Global Change Biology*, *20*(2), 594–606. https://doi.org/10.1111/gcb.12391

MacDicken, K. G. (2015). Global Forest Resources Assessment 2015: What, why and how? *Forest Ecology and Management*, *352*, 3–8. https://doi.org/10.1016/j.foreco.2015.02.006

Manzi, A. O., & Planton, S. (1994). 58-Manzi_ISBA-parametrization-land-surface-in-GCM.pdf. *Journal of Hydrology*, *155*, 353–387.

Marenco, F., Johnson, B., Langridge, J. M., Mulcahy, J., Benedetti, A., Remy, S., et al. (2016). On the vertical distribution of smoke in the Amazonian atmosphere during the dry season. *Atmospheric Chemistry and Physics*, *16*(4), 2155–2174. https://doi.org/10.5194/acp-16-2155-2016

Margono, B. A., Potapov, P. V., Turubanova, S., Stolle, F., & Hansen, M. C. (2014). Primary forest cover loss in indonesia over 2000-2012. *Nature Climate Change*, *4*(8), 730–735. https://doi.org/10.1038/nclimate2277

Marlier, M. E., DeFries, R. S., Kim, P. S., Koplitz, S. N., Jacob, D. J., Mickley, L. J., & Myers, S. S. (2015). Fire emissions and regional air quality impacts from fires in oil palm, timber, and logging concessions in Indonesia. *Environmental Research Letters*, *10*(8). https://doi.org/10.1088/1748-9326/10/8/085005

Martin, S. T., Artaxo, P., MacHado, L. A. T., Manzi, A. O., Souza, R. A. F., Schumacher, C., et al. (2016). Introduction: Observations and Modeling of the Green Ocean Amazon (GoAmazon2014/5). *Atmospheric Chemistry and Physics*, *16*(8), 4785–4797. https://doi.org/10.5194/acp-16-4785-2016

Matsui, T., Beltrán-Przekurat, A., Pielke, R. A., Niyogi, D., & Coughenour, M. B. (2007). Continental-scale multiobservation calibration and assessment of Colorado State University Unified Land Model by application of Moderate Resolution Imaging Spectroradiometer (MODIS) surface albedo. *Journal of Geophysical Research: Biogeosciences*, *112*(2), 1–19. https://doi.org/10.1029/2006JG000229

McGuffie, K., Henderson-Sellers, A., Zhang, H., Durbidge, T. B., & Pitman, A. J. (1995). Global climate sensitivity to tropical deforestation. *Global and Planetary Change*, *10*(1–4), 97–128. https://doi.org/10.1016/0921-8181(94)00022-6

McMorrow, J. (2001). Linear regression modelling for the estimation of oil palm age from Landsat TM. *International Journal of Remote Sensing*, *22*(12), 2243–2264. https://doi.org/10.1080/01431160117188

Mei, R., & Wang, G. (2010). Rain follows logging in the Amazon? Results from CAM3-CLM3. *Climate Dynamics*, *34*(7), 983–996. https://doi.org/10.1007/s00382-009-0592-x

Meijide, A., Röll, A., Fan, Y., Herbst, M., Niu, F., Tiedemann, F., et al. (2017). Controls of water and

energy fluxes in oil palm plantations: Environmental variables and oil palm age. *Agricultural and Forest Meteorology*, *239*, 71–85. https://doi.org/10.1016/j.agrformet.2017.02.034

Meijide, A., Badu, C. S., Moyano, F., Tiralla, N., Gunawan, D., & Knohl, A. (2018). Impact of forest conversion to oil palm and rubber plantations on microclimate and the role of the 2015 ENSO event. *Agricultural and Forest Meteorology*, *252*(January), 208–219. https://doi.org/10.1016/j.agrformet.2018.01.013

Meleux, F., Solmon, F., & Giorgi, F. (2007). Increase in summer European ozone amounts due to climate change. *Atmospheric Environment*, *41*(35), 7577–7587. https://doi.org/10.1016/j.atmosenv.2007.05.048

Miettinen, J., Shi, C., & Liew, S. C. (2011). Deforestation rates in insular Southeast Asia between 2000 and 2010. *Global Change Biology*, *17*(7), 2261–2270. https://doi.org/10.1111/j.1365-2486.2011.02398.x

Miettinen, J., Liew, S. C., & Kwoh, L. K. (2015). Usability of sentinel-1 dual polarization C-band data for plantation detection in Insular Southeast Asia. *ACRS 2015 - 36th Asian Conference on Remote Sensing: Fostering Resilient Growth in Asia, Proceedings*.

Montenegro, A., Eby, M., Mu, Q., Mulligan, M., Weaver, A. J., Wiebe, E. C., & Zhao, M. (2009). The net carbon drawdown of small scale afforestation from satellite observations. *Global and Planetary Change*, *69*(4), 195–204. https://doi.org/10.1016/j.gloplacha.2009.08.005

Moss, R. H., Edmonds, J. A., Hibbard, K. A., Manning, M. R., Rose, S. K., Van Vuuren, D. P., et al. (2010). The next generation of scenarios for climate change research and assessment. *Nature*, *463*(7282), 747–756. https://doi.org/10.1038/nature08823

Moutinho, P., Guerra, R., & Azevedo-Ramos, C. (2016). Achieving zero deforestation in the Brazilian Amazon: What is missing? *Elementa*, *4*, 1–11. https://doi.org/10.12952/journal.elementa.000125

Myers, N. (1997). The world's forests and their ecosystem services. In G. C. Daily (Ed.), *Nature's Services: Societal Dependence On Natural Ecosystems* (pp. 215–236). Washington D.C.: Island Press.

Myhre, G., & Myhre, A. (2003). Uncertainties in Radiative Forcing due to Surface Albedo Changes Caused by Land-Use Changes. *Journal of Climate*, *16*(10), 1511–1524. https://doi.org/10.1175/1520-0442(2003)016<1511:uirfdt>2.0.co;2

Myhre, G., Shindell, D. T., Bréon, F.-M., Collins, W., Fuglestvedt, J., Huang, J., et al. (2013). Anthropogenic and natural radiative forcing. In T. F. Stocker, D. Qin, G.-K. Plattner, M. Tignor, S. K. Allen, J. Boschung, et al. (Eds.), *Climate Change 2013 the Physical Science Basis: Working Group I Contribution to the Fifth Assessment Report of the Intergovernmental Panel on Climate Change* (pp. 659–740). Cambridge, United Kingdom and New York, NY, USA: Cambridge University Press. https://doi.org/10.1017/CBO9781107415324.018

Myhre, Gunnar, Kvalevåg, M. M., & Schaaf, C. B. (2005). Radiative forcing due to anthropogenic vegetation change based on MODIS surface albedo data. *Geophysical Research Letters*, *32*(21), 1–4. https://doi.org/10.1029/2005GL024004

Mylne, M. F., & Rowntree, P. R. (1992). Modelling the effects of albedo change associated with tropical deforestation. *Climatic Change*, *21*(3), 317–343. https://doi.org/10.1007/BF00139730

Naik, V., Voulgarakis, A., Fiore, A. M., Horowitz, L. W., Lamarque, J. F., Lin, M., et al. (2013). Preindustrial to present-day changes in tropospheric hydroxyl radical and methane lifetime from the Atmospheric Chemistry and Climate Model Intercomparison Project (ACCMIP). *Atmospheric Chemistry and Physics*, *13*(10), 5277–5298. https://doi.org/10.5194/acp-13-5277-2013

Nobre, C. A., Sellers, P. J., & Shukla, J. (1991). Amazonian Deforestation and Regional Climate Change. *Journal of Climate*. https://doi.org/10.1175/1520-0442(1991)004<0957:adarcc>2.0.co;2

O'Donnell, D., Tsigaridis, K., & Feichter, J. (2011). Estimating the direct and indirect effects of secondary organic aerosols using ECHAM5-HAM. *Atmospheric Chemistry and Physics*, *11*(16), 8635–8659. https://doi.org/10.5194/acp-11-8635-2011

Oguntoyinbo, J. S. (1970). Reflection coefficient of natural vegetation, crops and urban surfaces in Nigeria. *Quarterly Journal of the Royal Meteorological Society*, *96*(409), 430–441. https://doi.org/10.1002/qj.49709640907

Oleson, K. W., Bonan, G. B., Schaaf, C., Gao, F., Jin, Y., & Strahler, A. (2003). Assessment of global climate model land surface albedo using MODIS data. *Geophysical Research Letters*, *30*(8), 3–6. https://doi.org/10.1029/2002GL016749

Oliveira, G. de, & Moraes, E. C. (2013). Validação do balanço de radiação obtido a partir de dados MODIS/TERRA na Amazônia com medidas de superfície do LBA. *Acta Amazonica*, *43*(3), 353–363. https://doi.org/10.1590/S0044-59672013000300011

de Oliveira, G., Brunsell, N. A., Moraes, E. C., Bertani, G., dos Santos, T. V., Shimabukuro, Y. E., & Aragão, L. E. O. C. (2016). Use of MODIS sensor images combined with reanalysis products to retrieve net radiation in Amazonia. *Sensors (Switzerland)*, *16*(7). https://doi.org/10.3390/s16070956

Pachauri, R. K., Allen, M. R., Barros, V. R., Broome, J., Cramer, W., Christ, R., et al. (2014). *Climate Change 2014 Synthesis Report*.

Pan, Y., Birdsey, R. A., Fang, J., Houghton, R., Kauppi, P. E., Kurz, W. A., et al. (2011). A large and persistent carbon sink in the world's forests. *Science*, *333*(6045), 988–993. https://doi.org/10.1126/science.1201609

Peeters, J., Müller, J. F., Stavrakou, T., & Nguyen, V. S. (2014). Hydroxyl radical recycling in isoprene oxidation driven by hydrogen bonding and hydrogen tunneling: The upgraded LIM1 mechanism. *Journal of Physical Chemistry A*, *118*(38), 8625–8643. https://doi.org/10.1021/jp5033146

Pendleton, L., Donato, D. C., Murray, B. C., Crooks, S., Jenkins, W. A., Sifleet, S., et al. (2012). Estimating Global "Blue Carbon" Emissions from Conversion and Degradation of Vegetated Coastal Ecosystems. *PLoS ONE*, *7*(9). https://doi.org/10.1371/journal.pone.0043542

Peng, S. S., Piao, S., Zeng, Z., Ciais, P., Zhou, L., Li, L. Z. X., et al. (2014). Afforestation in China cools local land surface temperature. *Proceedings of the National Academy of Sciences of the United States of America*, *111*(8), 2915–2919. https://doi.org/10.1073/pnas.1315126111

Peñuelas, J., Llusià, J., & Gimeno, B. S. (1999). Effects of ozone concentrations on biogenic volatile organic compounds emission in the Mediterranean region. *Environmental Pollution*, *105*(1), 17–23. https://doi.org/10.1016/S0269-7491(98)00214-0

Pitman, A. J., Durbidge, T. B., Henderson-Sellers, A., & McGuffie, K. (1993). Assessing climate model sensitivity to prescribed deforested landscapes. *International Journal of Climatology*, *13*(8), 879–898. https://doi.org/10.1002/joc.3370130806

Polcher, J., & Laval, K. (1994). A statistical study of the regional impact of deforestation on climate in the LMD GCM. *Climate Dynamics*, *10*(4–5), 205–219. https://doi.org/10.1007/BF00208988

Pongratz, J., Reick, C. H., Raddatz, T., & Claussen, M. (2010). Biogeophysical versus biogeochemical climate response to historical anthropogenic land cover change. *Geophysical Research Letters*, *37*(8), 1–5. https://doi.org/10.1029/2010GL043010

Pongratz, J., Reick, C. H., Raddatz, T., Caldeira, K., & Claussen, M. (2011). Past land use decisions have increased mitigation potential of reforestation. *Geophysical Research Letters*, *38*(15), 1–5. https://doi.org/10.1029/2011GL047848

Potter, L. (2015). *Managing oil palm landscapes: A seven-country survey of the modern palm oil industry in Southeast Asia, Latin America and West Africa*. *Managing oil palm landscapes: A seven-country survey of the modern palm oil industry in Southeast Asia, Latin America and West Africa*. https://doi.org/10.17528/cifor/005612

Le Quéré, C., Raupach, M. R., Canadell, J. G., Marland, G., Bopp, L., Ciais, P., et al. (2009). Trends in the sources and sinks of carbon dioxide. *Nature Geoscience*, *2*(12), 831–836. https://doi.org/10.1038/ngeo689

Querino, A. C. S., Beneditti, C. A., Machado, N. G., Silva, M. J. G. da, Querino, J. K. A. da S., Neto, L. A. dos S., & Biudes, M. S. (2016). Spatiotemporal NDVI, LAI, albedo, and surface temperature dynamics in the southwest of the Brazilian Amazon forest. *Journal of Applied Remote Sensing*, *10*(2), 036012. https://doi.org/10.1117/1.JRS.10

Ramaswamy, V., Boucher, O., Haigh, J., Hauglustaine, D., Haywood, J., Myhre, G., et al. (2001). Radiative forcing of climate change. In *Climate Change 2001: The Scientific Basis, Contribution of Working Group I to the Third Assessment Report of the Intergovernmental Panel on Climate Change* (pp. 349–416). Cambridge: Cambridge University Press. https://doi.org/10.1023/A:1026752230256

Rap, A., Scott, C. E., Spracklen, D. V., Bellouin, N., Forster, P. M., Carslaw, K. S., et al. (2013). Natural aerosol direct and indirect radiative effects. *Geophysical Research Letters*, *40*(12), 3297–3301. https://doi.org/10.1002/grl.50441

Razali, S. M., Marin, A., Nuruddin, A. A., Shafri, H. Z. M., & Hamid, H. A. (2014). Capability of integrated MODIS imagery and ALOS for oil palm, rubber and forest areas mapping in tropical forest regions. *Sensors (Switzerland)*, *14*(5), 8259–8282. https://doi.org/10.3390/s140508259

Rechid, D., Hagemann, S., & Jacob, D. (2009). Sensitivity of climate models to seasonal variability of snow-free land surface albedo. *Theoretical and Applied Climatology*, *95*(1–2), 197–221. https://doi.org/10.1007/s00704-007-0371-8

Reddington, C. L., Butt, E. W., Ridley, D. A., Artaxo, P., Morgan, W. T., Coe, H., & Spracklen, D. V. (2015). Air quality and human health improvements from reductions in deforestation-related fire in Brazil. *Nature Geoscience*, *8*(10), 768–771. https://doi.org/10.1038/ngeo2535

Reick, C. H., Raddatz, T., Pongratz, J., & Claussen, M. (2010). Contribution of anthropogenic land cover change emissions to pre-industrial atmospheric CO2. *Tellus, Series B: Chemical and Physical Meteorology*, *62*(5), 329–336. https://doi.org/10.1111/j.1600-0889.2010.00479.x

Rein, G., Cohen, S., & Simeoni, A. (2009). Carbon emissions from smouldering peat in shallow and strong fronts. *Proceedings of the Combustion Institute*, *32 II*, 2489–2496.

https://doi.org/10.1016/j.proci.2008.07.008

Riahi, K., Grübler, A., & Nakicenovic, N. (2007). Scenarios of long-term socio-economic and environmental development under climate stabilization. *Technological Forecasting and Social Change*, *74*(7), 887–935. https://doi.org/10.1016/j.techfore.2006.05.026

Richards, D. R., & Friess, D. A. (2016). Rates and drivers of mangrove deforestation in Southeast Asia, 2000-2012. *Proceedings of the National Academy of Sciences of the United States of America*, *113*(2), 344–349. https://doi.org/10.1073/pnas.1510272113

Rinnan, R., Rinnan, Å., Holopainen, T., Holopainen, J. K., & Pasanen, P. (2005). Emission of non-methane volatile organic compounds (VOCs) from boreal peatland microcosms - Effects of ozone exposure. *Atmospheric Environment*, *39*(5), 921–930. https://doi.org/10.1016/j.atmosenv.2004.09.076

Rogers, B. M., Randerson, J. T., & Bonan, G. B. (2013). High-latitude cooling associated with landscape changes from North American boreal forest fires. *Biogeosciences*, *10*(2), 699–718. https://doi.org/10.5194/bg-10-699-2013

Rogers, Brendan M., Soja, A. J., Goulden, M. L., & Randerson, J. T. (2015). Influence of tree species on continental differences in boreal fires and climate feedbacks. *Nature Geoscience*, *8*(3), 228–234. https://doi.org/10.1038/ngeo2352

Román, M. O., Schaaf, C. B., Woodcock, C. E., Strahler, A. H., Yang, X., Braswell, R. H., et al. (2009). The MODIS (Collection V005) BRDF/albedo product: Assessment of spatial representativeness over forested landscapes. *Remote Sensing of Environment*, *113*(11), 2476–2498. https://doi.org/10.1016/j.rse.2009.07.009

Rossow, W. B., & Schiffer, R. A. (1999). Advances in Understanding Clouds from ISCCP. *Bulletin of the American Meteorological Society*, *80*(11), 2261–2287. https://doi.org/10.1175/1520-0477(1999)080<2261:AIUCFI>2.0.CO;2

Rotenberg, E., & Yakir, D. (2011). Distinct patterns of changes in surface energy budget associated with forestation in the semiarid region. *Global Change Biology*, *17*(4), 1536–1548. https://doi.org/10.1111/j.1365-2486.2010.02320.x

Rudel, T. K., Defries, R., Asner, G. P., & Laurance, W. F. (2009). Changing drivers of deforestation and new opportunities for conservation. *Conservation Biology*, *23*(6), 1396–1405. https://doi.org/10.1111/j.1523-1739.2009.01332.x

Sabajo, C. R., Le Maire, G., June, T., Meijide, A., Roupsard, O., & Knohl, A. (2017). Expansion of oil palm and other cash crops causes an increase of the land surface temperature in the Jambi province in Indonesia. *Biogeosciences*, *14*(20), 4619–4635. https://doi.org/10.5194/bg-14-4619-2017

Sakai, R. K., Fitzjarrald, D. R., Moraes, O. L. L., Staebler, R. M., Acevedo, O. C., Czikowsky, M. J., et al. (2004). Land-use change effects on local energy, water, and carbon balances in an Amazonian agricultural field. *Global Change Biology*, *10*(5), 895–907. https://doi.org/10.1111/j.1529-8817.2003.00773.x

Salati, E., & Nobre, C. A. (1992). Possible climatic impacts of tropical deforestation. *Tropical Forests and Climate*, 177–196. https://doi.org/10.1007/978-94-017-3608-4_18

Saldarriaga, J. G., & Luxmoore, R. J. (1991). Solar energy conversion efficiencies during succession of a tropical rain forest in Amazonia. *Journal of Tropical Ecology*, *7*(2), 233–242.

https://doi.org/10.1017/S0266467400005393

Sampaio, G., Nobre, C., Costa, M. H., Satyamurty, P., Soares-Filho, B. S., & Cardoso, M. (2007). Regional climate change over eastern Amazonia caused by pasture and soybean cropland expansion. *Geophysical Research Letters*, *34*(17), 1–7. https://doi.org/10.1029/2007GL030612

Schaaf, C. B., Gao, F., Strahler, A. H., Lucht, W., Li, X., Tsang, T., et al. (2002). First operational BRDF, albedo nadir reflectance products from MODIS. *Remote Sensing of Environment*, *83*, 135–148.

Scott, C. E., Monks, S. A., Spracklen, D. V., Arnold, S. R., Forster, P. M., Rap, A., et al. (2017). Impact on short-lived climate forcers (SLCFs) from a realistic land-use change scenario via changes in biogenic emissions. *Faraday Discussions*, *200*, 101–120. https://doi.org/10.1039/c7fd00028f

Scott, C. E., Monks, S. A., Spracklen, D. V., Arnold, S. R., Forster, P. M., Rap, A., et al. (2018). Impact on short-lived climate forcers increases projected warming due to deforestation. *Nature Communications*, *9*(1), 1–9. https://doi.org/10.1038/s41467-017-02412-4

Sena, E. T., Artaxo, P., & Correia, A. L. (2013). Spatial variability of the direct radiative forcing of biomass burning aerosols and the effects of land use change in Amazonia. *Atmospheric Chemistry and Physics*, *13*(3), 1261–1275. https://doi.org/10.5194/acp-13-1261-2013

Shafri, H. Z. M., Hamdan, N., & Saripan, M. I. (2011). Semi-automatic detection and counting of oil palm trees from high spatial resolution airborne imagery. *International Journal of Remote Sensing*, *32*(8), 2095–2115. https://doi.org/10.1080/01431161003662928

Siikamäki, J., Sanchirico, J. N., & Jardine, S. L. (2012). Global economic potential for reducing carbon dioxide emissions from mangrove loss. *Proceedings of the National Academy of Sciences of the United States of America*, *109*(36), 14369–14374. https://doi.org/10.1073/pnas.1200519109

Silva Junior, C. H. L., Pessôa, A. C. M., Carvalho, N. S., Reis, J. B. C., Anderson, L. O., & Aragão, L. E. O. C. (2020). The Brazilian Amazon deforestation rate in 2020 is the greatest of the decade. *Nature Ecology and Evolution*, 0–1. https://doi.org/10.1038/s41559-020-01368-x

Situ, S., Guenther, A., Wang, X., Jiang, X., Turnipseed, A., Wu, Z., et al. (2013). Impacts of seasonal and regional variability in biogenic VOC emissions on surface ozone in the Pearl river delta region, China. *Atmospheric Chemistry and Physics*, *13*(23), 11803–11817. https://doi.org/10.5194/acp-13-11803-2013

Snyder, P. K., Delire, C., & Foley, J. A. (2004). Evaluating the influence of different vegetation biomes on the global climate. *Climate Dynamics*, *23*(3–4), 279–302. https://doi.org/10.1007/s00382-004-0430-0

Sodhi, N. S., Koh, L. P., Brook, B. W., & Ng, P. K. L. (2004). Southeast Asian biodiversity: An impending disaster. *Trends in Ecology and Evolution*, *19*(12), 654–660. https://doi.org/10.1016/j.tree.2004.09.006

Sodhi, N. S., Posa, M. R. C., Lee, T. M., Bickford, D., Koh, L. P., & Brook, B. W. (2010). The state and conservation of Southeast Asian biodiversity. *Biodiversity and Conservation*, *19*(2), 317–328. https://doi.org/10.1007/s10531-009-9607-5

Souza, P. J. de O. P. de, Rocha, E. J. P. da, & Ribeiro, A. (2013). Impacts of soybean expansion on radiation balance in eastern Amazon. *Acta Amazonica*, *43*(2), 169–178. https://doi.org/10.1590/S0044-59672013000200006

Spracklen, D. V., Bonn, B., & Carslaw, K. S. (2008). Boreal forests, aerosols and the impacts on clouds and climate. *Philosophical Transactions of the Royal Society A: Mathematical, Physical and Engineering Sciences*, *366*(1885), 4613–4626. https://doi.org/10.1098/rsta.2008.0201

Stabile, M. C. C., Guimarães, A. L., Silva, D. S., Ribeiro, V., Macedo, M. N., Coe, M. T., et al. (2020). Solving Brazil's land use puzzle: Increasing production and slowing Amazon deforestation. *Land Use Policy*, *91*(May 2019), 104362. https://doi.org/10.1016/j.landusepol.2019.104362

Stedman, J. R. (2004). The predicted number of air pollution related deaths in the UK during the August 2003 heatwave. *Atmospheric Environment*, *38*(8), 1087–1090. https://doi.org/10.1016/j.atmosenv.2003.11.011

Stevenson, D. S., Young, P. J., Naik, V., Lamarque, J. F., Shindell, D. T., Voulgarakis, A., et al. (2013). Tropospheric ozone changes, radiative forcing and attribution to emissions in the Atmospheric Chemistry and Climate Model Intercomparison Project (ACCMIP). *Atmospheric Chemistry and Physics*, *13*(6), 3063–3085. https://doi.org/10.5194/acp-13-3063-2013

Stjern, C. W., Samset, B. H., Myhre, G., Forster, P. M., Hodnebrog, Ø., Andrews, T., et al. (2017). Rapid Adjustments Cause Weak Surface Temperature Response to Increased Black Carbon Concentrations. *Journal of Geophysical Research: Atmospheres*, *122*(21), 11,462-11,481. https://doi.org/10.1002/2017JD027326

Stocker, T. F., Qin, D., Plattner, G.-K., Tignor, M., Allen, S. K., Boschung, J., et al. (Eds.). (2013). *IPCC, 2013: Climate Change 2013: The Physical Science Basis. Contribution of Working Group I to the Fifth Assessment Report of the Intergovernmental Panel on Climate Change*. Cambridge, United Kingdom and New York, NY, USA: Cambridge University Press. https://doi.org/10.1017/CBO9781107415324.Summary

Strahler, A. H., Wanner, W., Schaaf, C. B., Li, X., Hu, B., Muller, J. P., et al. (1996). MODIS BRDF/albedo product: Algorithm theoretical basis document version 4.0. *NASA EOS MODIS Technical Document, Greenbelt, MD, USA*, (November). Retrieved from papers3://publication/uuid/14BC3FA6-52A4-4B63-92E9-A7F3581D5C7B

Strong, J., Whyatt, J. D., Metcalfe, S. E., Derwent, R. G., & Hewitt, C. N. (2013). Investigating the impacts of anthropogenic and biogenic VOC emissions and elevated temperatures during the 2003 ozone episode in the UK. *Atmospheric Environment*, *74*(August 2003), 393–401. https://doi.org/10.1016/j.atmosenv.2013.04.006

Sud, Y. C., Lau, W. K.-M., Walker, G. K., Kim, J.-H., Liston, G. E., & Sellers, P. J. (1996). Biogeophysical Consequences of a Tropical Deforestation Scenario: A GCM Simulation Study. *Journal of Climate*. https://doi.org/10.1175/1520-0442(1996)009<3225:bcoatd>2.0.co;2

Swann, A. L. S., Fung, I. Y., & Chiang, J. C. H. (2012). Mid-latitude afforestation shifts general circulation and tropical precipitation. *Proceedings of the National Academy of Sciences of the United States of America*, *109*(3), 712–716. https://doi.org/10.1073/pnas.1116706108

Taraborrelli, D., Lawrence, M. G., Crowley, J. N., Dillon, T. J., Gromov, S., Groß, C. B. M., et al. (2012). Hydroxyl radical buffered by isoprene oxidation over tropical forests. *Nature Geoscience*, *5*(3), 190–193. https://doi.org/10.1038/ngeo1405

Thornton, P. E., Lamarque, J. F., Rosenbloom, N. A., & Mahowald, N. M. (2007). Influence of carbon-nitrogen cycle coupling on land model response to CO2 fertilization and climate variability. *Global Biogeochemical Cycles*, *21*(4). https://doi.org/10.1029/2006GB002868

Tian, Y., Dickinson, R. E., Zhou, L., Myneni, R. B., Friedl, M., Schaaf, C. B., et al. (2004). Land boundary conditions from MODIS data and consequences for the albedo of a climate model. *Geophysical Research Letters*, *31*(5), n/a-n/a. https://doi.org/10.1029/2003gl019104

Tosca, M. G., Randerson, J. T., Zender, C. S., Nelson, D. L., Diner, D. J., & Logan, J. A. (2011). Dynamics of fire plumes and smoke clouds associated with peat and deforestation fires in Indonesia. *Journal of Geophysical Research Atmospheres*, *116*(8), 1–14. https://doi.org/10.1029/2010JD015148

Trenberth, K. E., Fasullo, J. T., & Kiehl, J. (2009). Earth's global energy budget. *Bulletin of the American Meteorological Society*, *90*(3), 311–323. https://doi.org/10.1175/2008BAMS2634.1

Turnock, S. T., Butt, E. W., Richardson, T. B., Mann, G. W., Reddington, C. L., Forster, P. M., et al. (2016). The impact of European legislative and technology measures to reduce air pollutants on air quality, human health and climate. *Environmental Research Letters*, *11*(2), 0. https://doi.org/10.1088/1748-9326/11/2/024010

Twomey, S. (1977). The Influence of Pollution on the Shortwave Albedo of Clouds. *Journal of the Atmospheric Sciences*. https://doi.org/10.1175/1520-0469(1977)034<1149:tiopot>2.0.co;2

Uryu, Y., Mott, C., Foead, N., Yulianto, K., Budiman, A., Setiabudi, et al. (2008). Deforestation, Forest Degredation, Biodiversity Loss and CO2 Emissions in Riau, Sumatra, Indonesia. *WWF Indonesia Technical Report*.

Varejao-Silva, M. A., Franchito, S. H., & Rao, V. B. (1998). A Coupled Biosphere-Atmosphere Climate Model Suitable for Studies of Climatic Change Due to Land Surface Alterations. *Journal of Climate*, *11*(7), 1749–1767. https://doi.org/10.1175/1520-0442(1998)011<1749:ACBACM>2.0.CO;2

Voldoire, A., & Royer, J. F. (2004). Tropical deforestation and climate variability. *Climate Dynamics*, *22*(8), 857–874. https://doi.org/10.1007/s00382-004-0423-z

van Vuuren, D. P., Edmonds, J., Kainuma, M., Riahi, K., Thomson, A., Hibbard, K., et al. (2011). The representative concentration pathways: An overview. *Climatic Change*, *109*(1), 5–31. https://doi.org/10.1007/s10584-011-0148-z

Wang, A., & Price, D. T. (2007). Estimating global distribution of boreal, temperate, and tropical tree plant functional types using clustering techniques. *Journal of Geophysical Research: Biogeosciences*, *112*(1), 1–15. https://doi.org/10.1029/2006JG000252

Wang, R., Balkanski, Y., Boucher, O., Ciais, P., Schuster, G. L., Chevallier, F., et al. (2016). Estimation of global black carbon direct radiative forcing and its uncertainty constrained by observations. *Journal of Geophysical Research*, *121*(10), 5948–5971. https://doi.org/10.1002/2015JD024326

Wang, Zhuo, Zeng, X., Barlage, M., Dickinson, R. E., Gao, F., & Schaaf, C. B. (2004). Using MODIS BRDF and albedo data to evaluate global model land surface albedo. *Journal of Hydrometeorology*, *5*(1), 3–14. https://doi.org/10.1175/1525-7541(2004)005<0003:UMBAAD>2.0.CO;2

Wang, Zhuosen, Schaaf, C. B., Strahler, A. H., Chopping, M. J., Román, M. O., Shuai, Y., et al. (2014). Evaluation of MODIS albedo product (MCD43A) over grassland, agriculture and forest surface types during dormant and snow-covered periods. *Remote Sensing of Environment*, *140*, 60–77. https://doi.org/10.1016/j.rse.2013.08.025

Wei, X., Hahmann, A. N., Dickinson, R. E., Yang, Z. L., Zeng, X., Schaudt, K. J., et al. (2001). Comparison of albedos computed by land surface models and evaluation against remotely sensed data.

Journal of Geophysical Research Atmospheres, *106*(D18), 20687–20702. https://doi.org/10.1029/2001JD900218

Van Der Werf, G. R., Morton, D. C., Defries, R. S., Olivier, J. G. J., Kasibhatla, P. S., Jackson, R. B., et al. (2009). CO2 emissions from forest loss. *Nature Geoscience*, *2*(November), 9–11.

Van Der Werf, G. R., Randerson, J. T., Giglio, L., Collatz, G. J., Mu, M., Kasibhatla, P. S., et al. (2010). Global fire emissions and the contribution of deforestation, savanna, forest, agricultural, and peat fires (1997-2009). *Atmospheric Chemistry and Physics*, *10*(23), 11707–11735. https://doi.org/10.5194/acp-10-11707-2010

Wicke, B., Sikkema, R., Dornburg, V., & Faaij, A. (2011). Exploring land use changes and the role of palm oil production in Indonesia and Malaysia. *Land Use Policy*, *28*(1), 193–206. https://doi.org/10.1016/j.landusepol.2010.06.001

Wickham, J., Barnes, C. A., Nash, M. S., & Wade, T. G. (2015). Combining NLCD and MODIS to create a land cover-albedo database for the continental United States. *Remote Sensing of Environment*, *170*, 143–152. https://doi.org/10.1016/j.rse.2015.09.012

Wickham, J. D., Wade, T. G., & Riitters, K. H. (2013). Empirical analysis of the influence of forest extent on annual and seasonal surface temperatures for the continental United States. *Global Ecology and Biogeography*, *22*(5), 620–629. https://doi.org/10.1111/geb.12013

Wilcove, D. S., Giam, X., Edwards, D. P., Fisher, B., & Koh, L. P. (2013). Navjot's nightmare revisited: Logging, agriculture, and biodiversity in Southeast Asia. *Trends in Ecology and Evolution*, *28*(9), 531–540. https://doi.org/10.1016/j.tree.2013.04.005

Williams, M. (2000). Dark ages and dark areas: Global deforestation in the deep past. *Journal of Historical Geography*, *26*(1), 28–46. https://doi.org/10.1006/jhge.1999.0189

Wright, I. R., Nobre, C. A., Tomasella, J., Rocha, H. R. da, Roberts, J. M., Vertamatti, E., et al. (1996). Towards a GCM surface parameterisation for Amazonia. *Amazonian Deforestation and Climate*, (September 2015).

Yang, Y., Smith, S. J., Wang, H., Mills, C. M., & Rasch, P. J. (2019). Variability, timescales, and nonlinearity in climate responses to black carbon emissions. *Atmospheric Chemistry and Physics*, *19*(4), 2405–2420. https://doi.org/10.5194/acp-19-2405-2019

Young, P. J., Arneth, A., Schurgers, G., Zeng, G., & Pyle, J. a. (2009). The CO2 inhibition of isoprene significantly affects future ozone projection. *Atmos. Chem. Phys.*, *9*, 2793–2803. https://doi.org/10.5194/acp-9-2793-2009

Young, P. J., Archibald, a. T., Bowman, K. W., Lamarque, J.-F., Naik, V., Stevenson, D. S., et al. (2013). Pre-industrial to end 21st century projections of tropospheric ozone from the Atmospheric Chemistry and Climate Model Intercomparison Project (ACCMIP). *Atmospheric Chemistry and Physics*, *13*(4), 2063–2090. https://doi.org/10.5194/acp-13-2063-2013

Zanon, M., Davis, B. A. S., Marquer, L., Brewer, S., & Kaplan, J. O. (2018). European forest cover during the past 12,000 years: A palynological reconstruction based on modern analogs and remote sensing. *Frontiers in Plant Science*, *9*(March), 1–25. https://doi.org/10.3389/fpls.2018.00253

Zarin, D. J., Harris, N. L., Baccini, A., Aksenov, D., Hansen, M. C., Azevedo-Ramos, C., et al. (2016). Can carbon emissions from tropical deforestation drop by 50% in 5 years? *Global Change Biology*, *22*(4), 1336–1347. https://doi.org/10.1111/gcb.13153

Zeng, G., Pyle, J. a., & Young, P. J. (2007). Impact of climate change on tropospheric ozone and its global budgets. *Atmospheric Chemistry and Physics Discussions*, *7*(4), 11141–11189. https://doi.org/10.5194/acpd-7-11141-2007

Zeng, N., & Neelin, J. D. (1999). A land-atmosphere interaction theory for the tropical deforestation problem. *Journal of Climate*, *12*(2–3), 857–872. https://doi.org/10.1175/1520-0442(1999)012<0857:alaitf>2.0.co;2

Zeng, N., Dickinson, R. E., & Zeng, X. (1996). Climatic Impact of Amazon Deforestation - A Mechanistic Model Study. *Journal of Climate*, *9*, 859–883.

Zhang, H., Henderson-Sellers, A., & McGuffie, K. (1996). Impacts of tropical deforestation. Part I: Process analysis of local climatic change. *Journal of Climate*. https://doi.org/10.1175/1520-0442(1996)009<1497:IOTDPI>2.0.CO;2

Zhang, H., Henderson-Sellers, A., & Mcguffie, K. (2001). The compounding effects of tropical deforestation and greenhouse warming on climate. *Climatic Change*, *49*(3), 309–338. https://doi.org/10.1023/A:1010662425950

Zhang, X., Gui, S., Li, L., Zhang, X., Gui, S., Liang, S., & Wang, K. (2010). Analysis of Global Land Surface Shortwave Broadband Albedo From Multiple Data Sources. *IEEE Journal of Selected Topics in Applied Earth Observations and Remote Sensing*, *3*(3), 296–305. https://doi.org/10.1109/JSTARS.2010.2049342

Zhang, Y., Zhu, Z., Liu, Z., Zeng, Z., Ciais, P., Huang, M., et al. (2016). Seasonal and interannual changes in vegetation activity of tropical forests in Southeast Asia. *Agricultural and Forest Meteorology*, *224*, 1–10. https://doi.org/10.1016/j.agrformet.2016.04.009

Zheng, Z., Wei, Z., Wen, Z., Dong, W., Li, Z., Wen, X., et al. (2017). Inclusion of Solar Elevation Angle in Land Surface Albedo Parameterization Over Bare Soil Surface. *Journal of Advances in Modeling Earth Systems*, *9*(8), 3069–3081. https://doi.org/10.1002/2017MS001109

Appendix B – Monthly plots of surface albedo response to fractional forest cover and loss in the Amazon

The following twenty-four plots show the response of surface albedo to fractional forest cover for each 0.01° domain in the Amazon for each month in chronological order (January to December). The first twelve correspond to the 2000 – 2003 period, the second to 2013 – 2015.

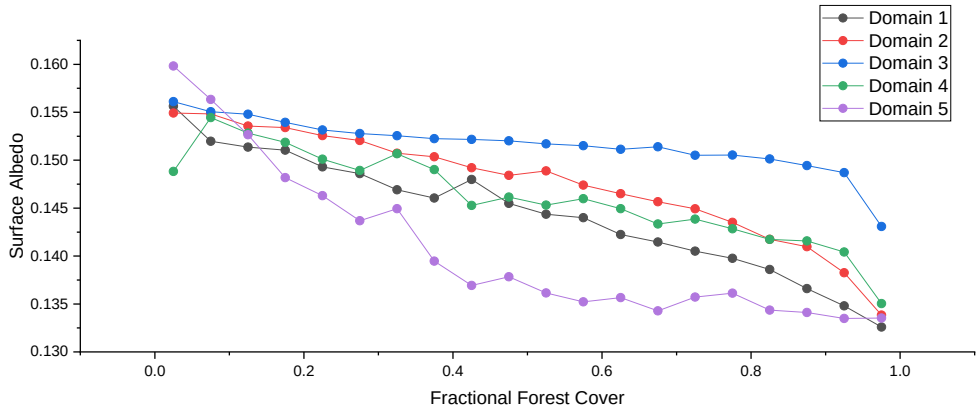

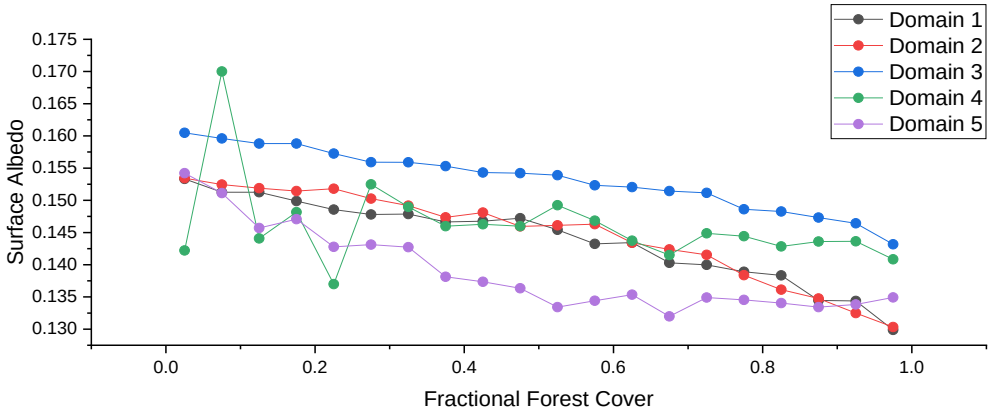

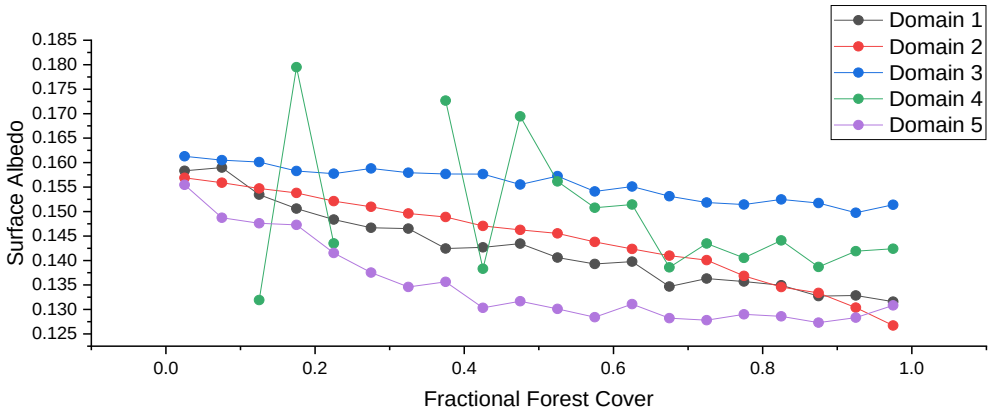

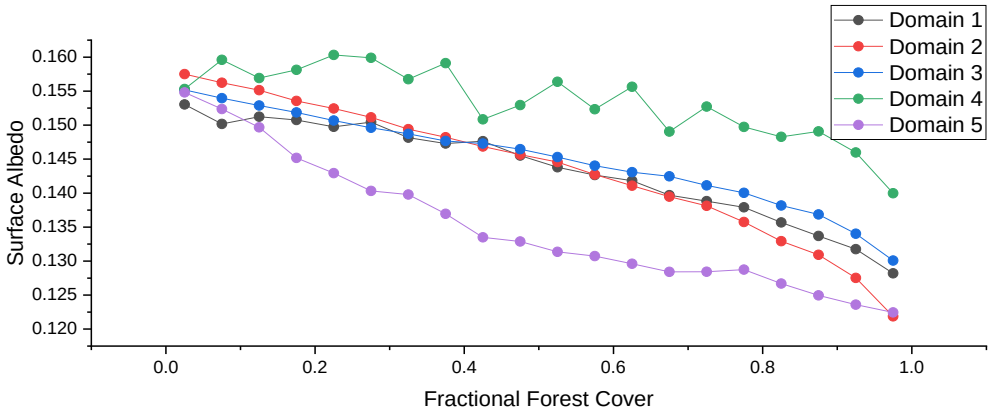
Domain 1
Domain 2
Domain 3
Domain 4
Domain 5
Surface Albedo
0.160
0.155
0.150
0.145
0.140
0.135
0.130
0.125
0.120
0.0
0.2
0.4
0.6
0.8
1.0
Fractional Forest Cover

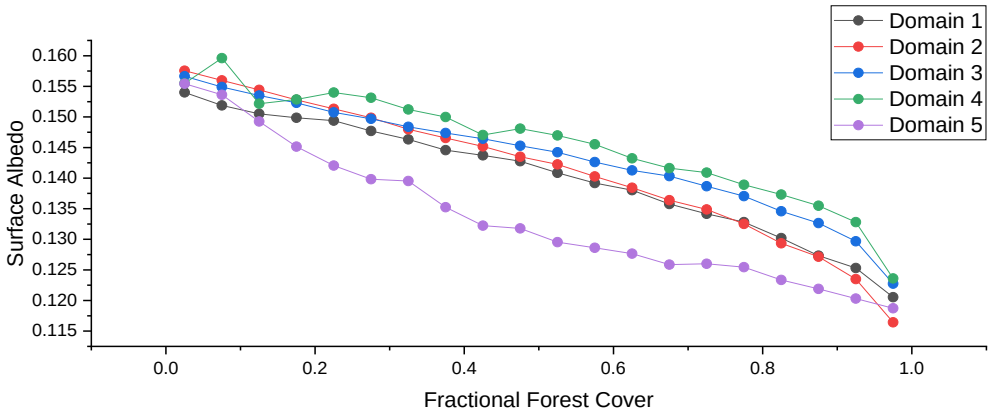
Domain 1
Domain 2
Domain 3
Domain 4
Domain 5
Surface Albedo
0.160
0.155
0.150
0.145
0.140
0.135
0.130
0.125
0.120
0.115
0.0
0.2
0.4
0.6
0.8
1.0
Fractional Forest Cover

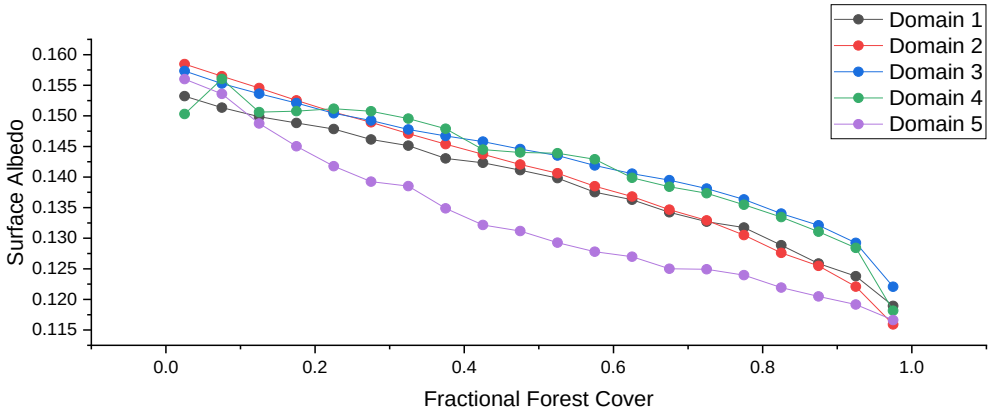
Domain 1
Domain 2
Domain 3
Domain 4
Domain 5
Surface Albedo
0.160
0.155
0.150
0.145
0.140
0.135
0.130
0.125
0.120
0.115
0.0
0.2
0.4
0.6
0.8
1.0
Fractional Forest Cover

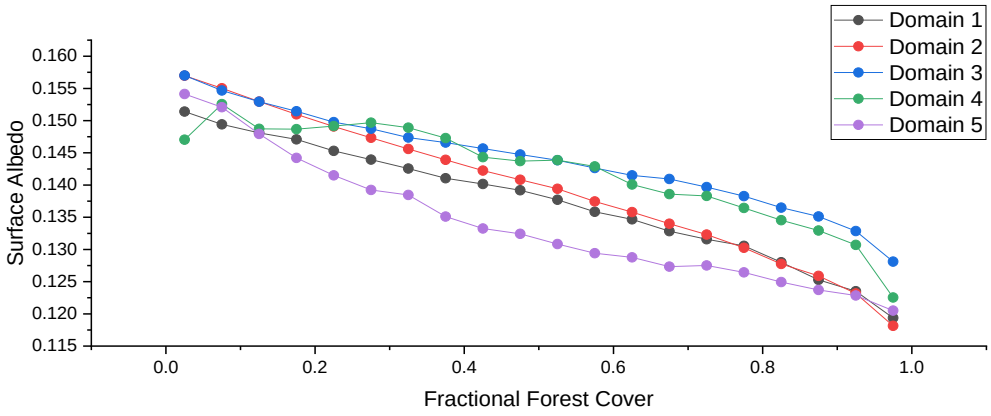
Domain 1
Domain 2
Domain 3
Domain 4
Domain 5
Surface Albedo
0.160
0.155
0.150
0.145
0.140
0.135
0.130
0.125
0.120
0.115
0.0
0.2
0.4
0.6
0.8
1.0
Fractional Forest Cover

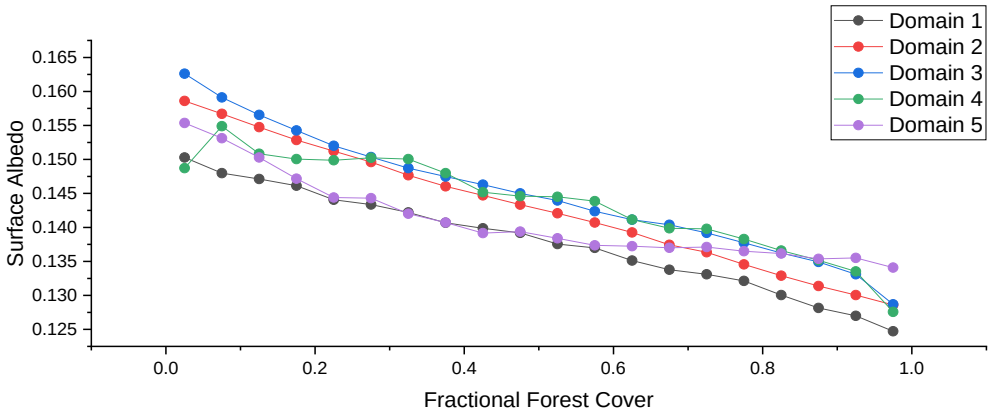
Domain 1
Domain 2
Domain 3
Domain 4
Domain 5
Surface Albedo
0.165
0.160
0.155
0.150
0.145
0.140
0.135
0.130
0.125
0.0
0.2
0.4
0.6
0.8
1.0
Fractional Forest Cover

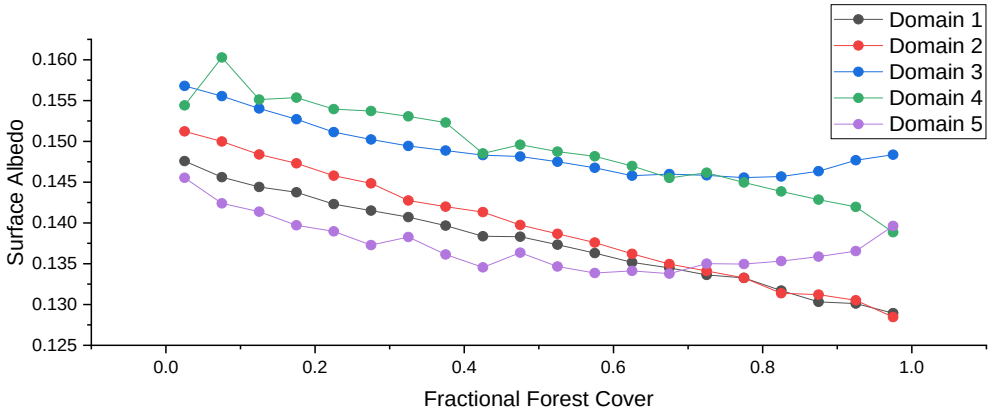
Domain 1
Domain 2
Domain 3
Domain 4
Domain 5
Surface Albedo
0.160
0.155
0.150
0.145
0.140
0.135
0.130
0.125
0.0
0.2
0.4
0.6
0.8
1.0
Fractional Forest Cover

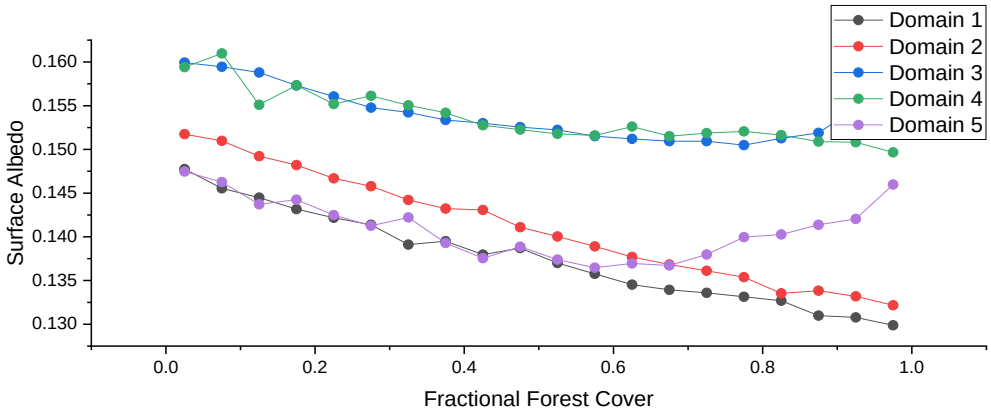
Domain 1
Domain 2
Domain 3
Domain 4
Domain 5
Surface Albedo
0.160
0.155
0.150
0.145
0.140
0.135
0.130
0.0
0.2
0.4
0.6
0.8
1.0
Fractional Forest Cover

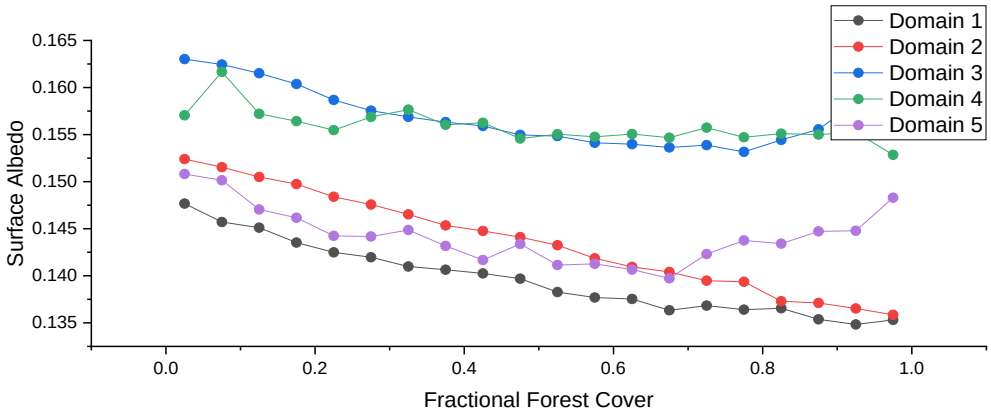
Domain 1
Domain 2
Domain 3
Domain 4
Domain 5
Surface Albedo
0.165
0.160
0.155
0.150
0.145
0.140
0.135
0.0
0.2
0.4
0.6
0.8
1.0
Fractional Forest Cover

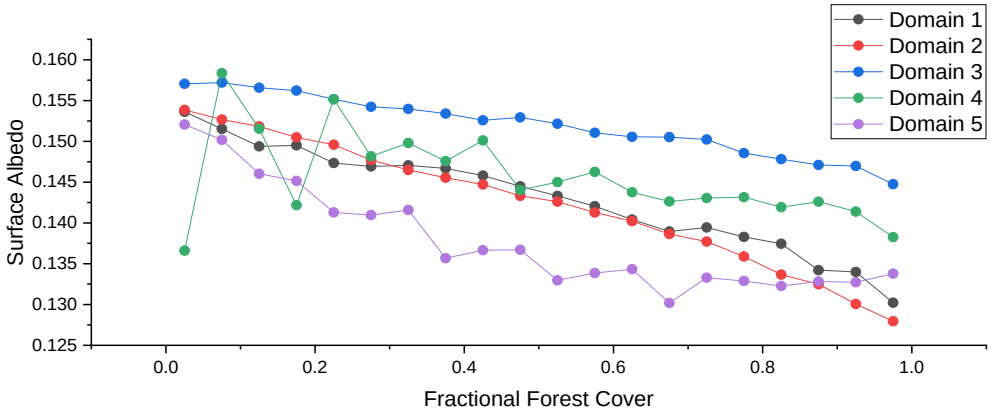
Domain 1
Domain 2
Domain 3
Domain 4
Domain 5
Surface Albedo
0.160
0.155
0.150
0.145
0.140
0.135
0.130
0.125
0.0
0.2
0.4
0.6
0.8
1.0
Fractional Forest Cover

2013 – 2015:

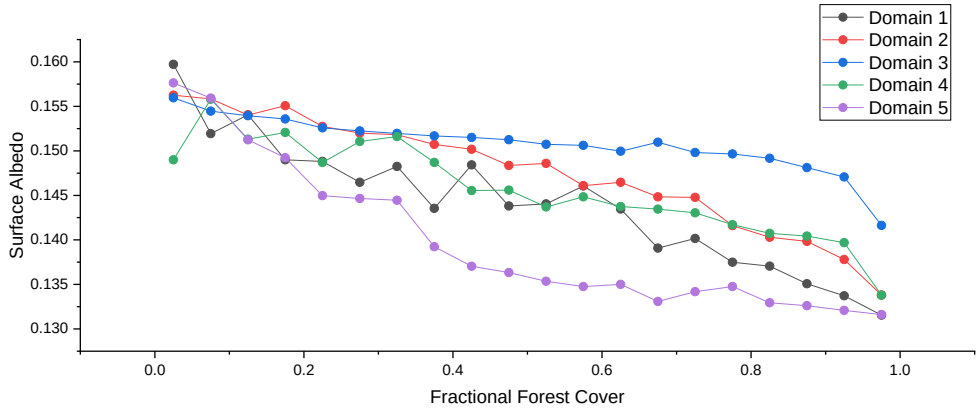
Domain 1
Domain 2
Domain 3
Domain 4
Domain 5
Surface Albedo
0.160
0.155
0.150
0.145
0.140
0.135
0.130
0.0
0.2
0.4
0.6
0.8
1.0
Fractional Forest Cover

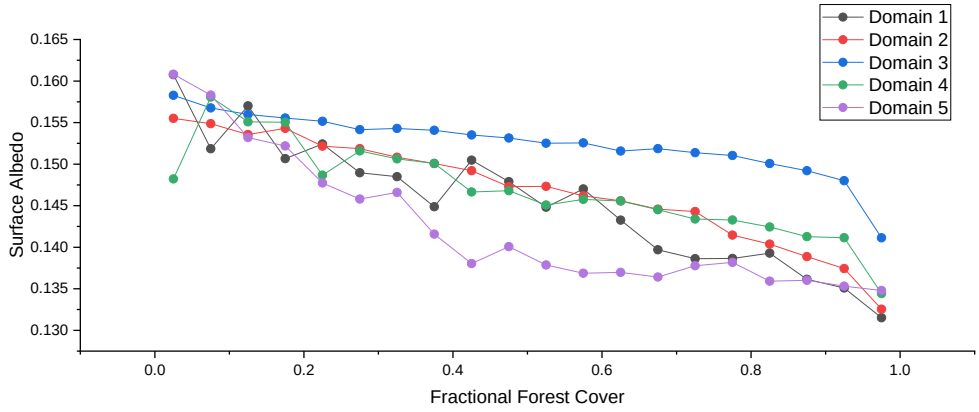
Domain 1
Domain 2
Domain 3
Domain 4
Domain 5
Surface Albedo
0.165
0.160
0.155
0.150
0.145
0.140
0.135
0.130
0.0
0.2
0.4
0.6
0.8
1.0
Fractional Forest Cover

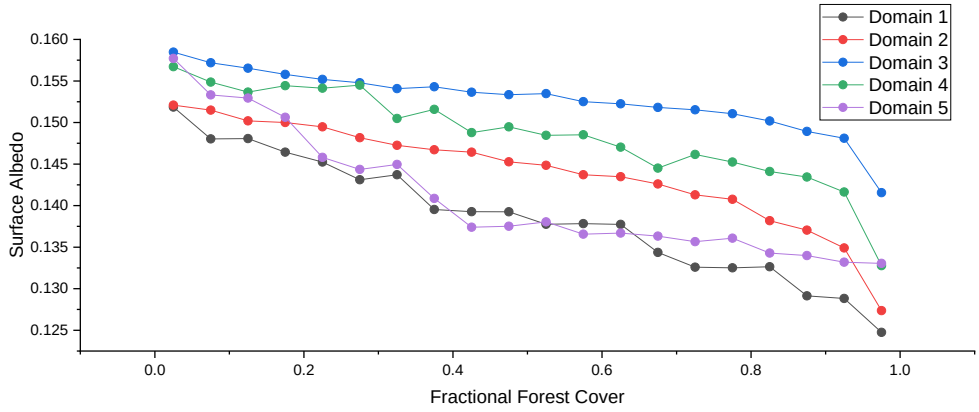
Domain 1
Domain 2
Domain 3
Domain 4
Domain 5
Surface Albedo
0.160
0.155
0.150
0.145
0.140
0.135
0.130
0.125
0.0
0.2
0.4
0.6
0.8
1.0
Fractional Forest Cover

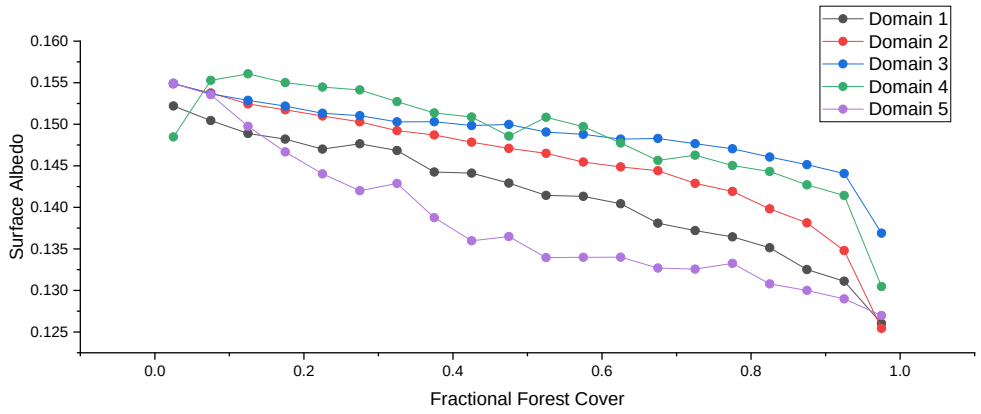
Domain 1
Domain 2
Domain 3
Domain 4
Domain 5
Surface Albedo
0.160
0.155
0.150
0.145
0.140
0.135
0.130
0.125
0.0
0.2
0.4
0.6
0.8
1.0
Fractional Forest Cover

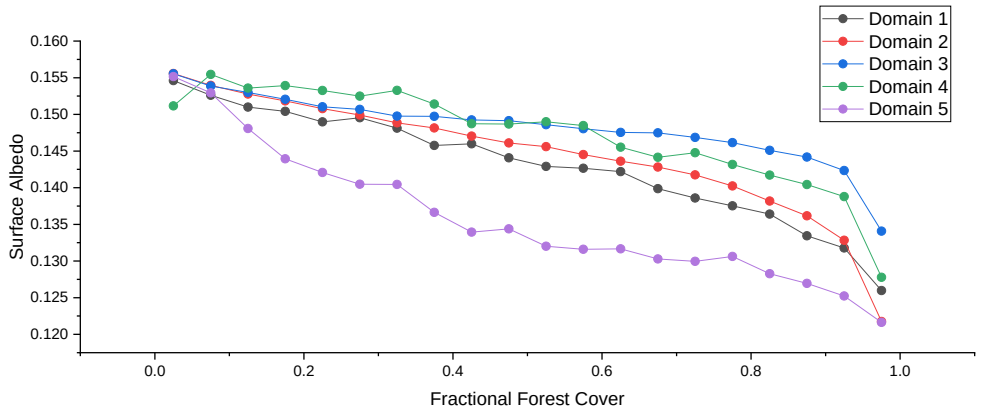
Domain 1
Domain 2
Domain 3
Domain 4
Domain 5
Surface Albedo
0.160
0.155
0.150
0.145
0.140
0.135
0.130
0.125
0.120
0.0
0.2
0.4
0.6
0.8
1.0
Fractional Forest Cover

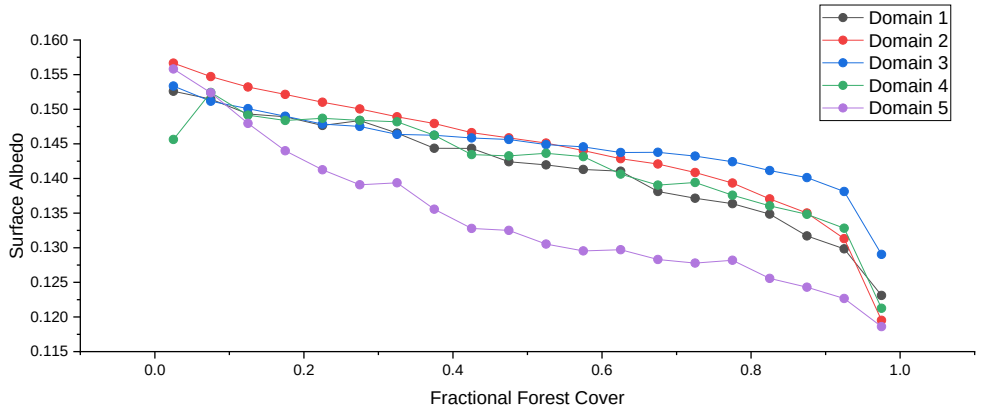
Domain 1
Domain 2
Domain 3
Domain 4
Domain 5
Surface Albedo
0.160
0.155
0.150
0.145
0.140
0.135
0.130
0.125
0.120
0.115
0.0
0.2
0.4
0.6
0.8
1.0
Fractional Forest Cover

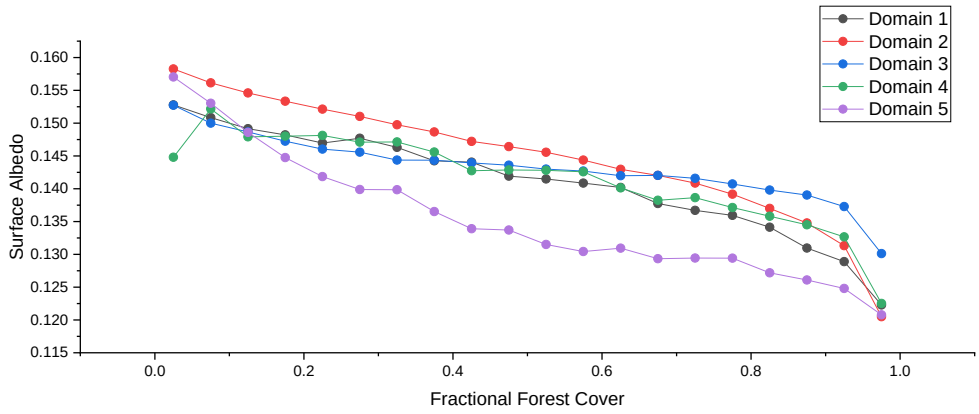
Domain 1
Domain 2
Domain 3
Domain 4
Domain 5
Surface Albedo
0.160
0.155
0.150
0.145
0.140
0.135
0.130
0.125
0.120
0.115
0.0
0.2
0.4
0.6
0.8
1.0
Fractional Forest Cover

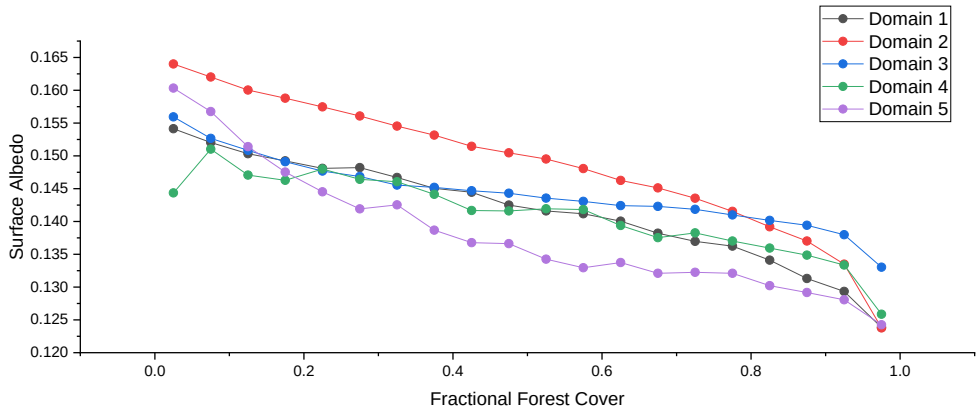
Domain 1
Domain 2
Domain 3
Domain 4
Domain 5
Surface Albedo
0.165
0.160
0.155
0.150
0.145
0.140
0.135
0.130
0.125
0.120
0.0
0.2
0.4
0.6
0.8
1.0
Fractional Forest Cover

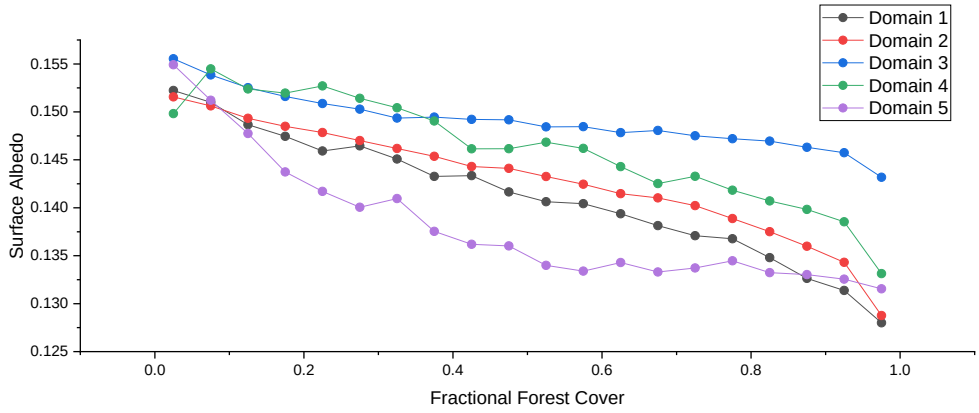
Domain 1
Domain 2
Domain 3
Domain 4
Domain 5
Surface Albedo
0.155
0.150
0.145
0.140
0.135
0.130
0.125
0.0
0.2
0.4
0.6
0.8
1.0
Fractional Forest Cover

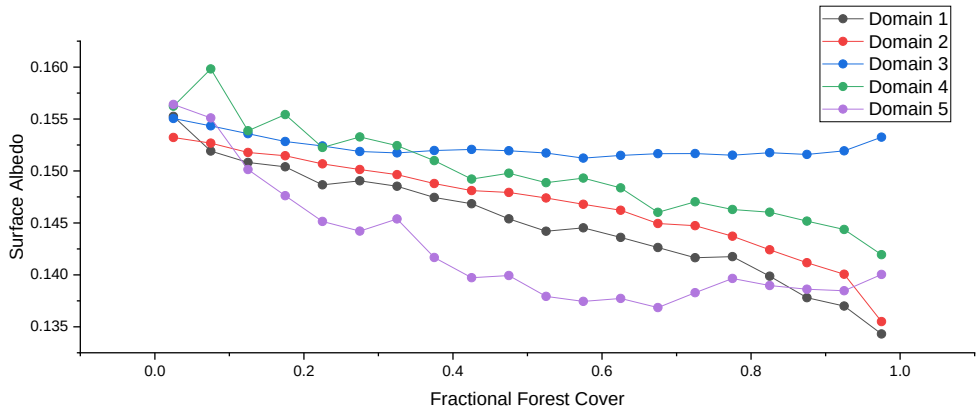
Domain 1
Domain 2
Domain 3
Domain 4
Domain 5
Surface Albedo
0.160
0.155
0.150
0.145
0.140
0.135
0.0
0.2
0.4
0.6
0.8
1.0
Fractional Forest Cover

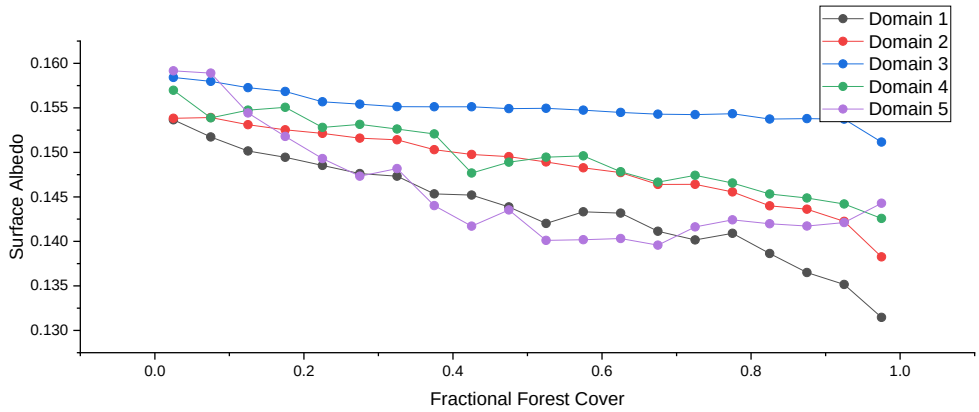
Domain 1
Domain 2
Domain 3
Domain 4
Domain 5
Surface Albedo
0.160
0.155
0.150
0.145
0.140
0.135
0.130
0.0
0.2
0.4
0.6
0.8
1.0
Fractional Forest Cover

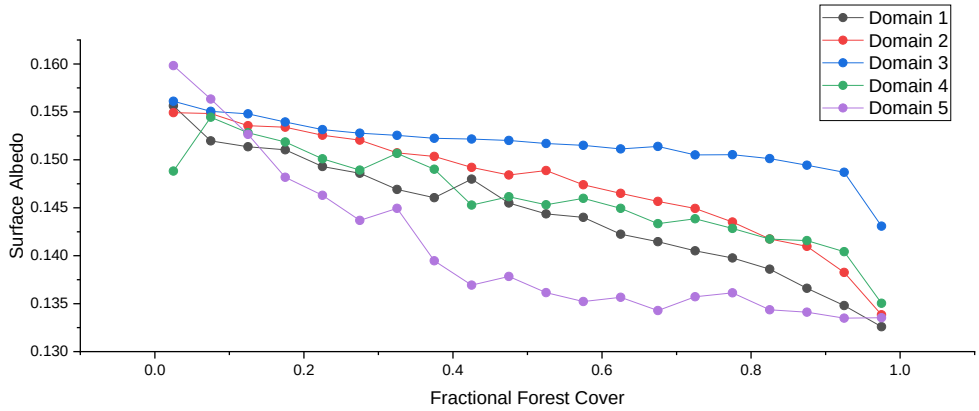
Domain 1
Domain 2
Domain 3
Domain 4
Domain 5
Surface Albedo
0.160
0.155
0.150
0.145
0.140
0.135
0.130
0.0
0.2
0.4
0.6
0.8
1.0
Fractional Forest Cover

The following twelve plots show the response of surface albedo to fractional forest loss between 2000 – 2015 for each 0.01° domain in the Amazon for each month in chronological order (January to December).

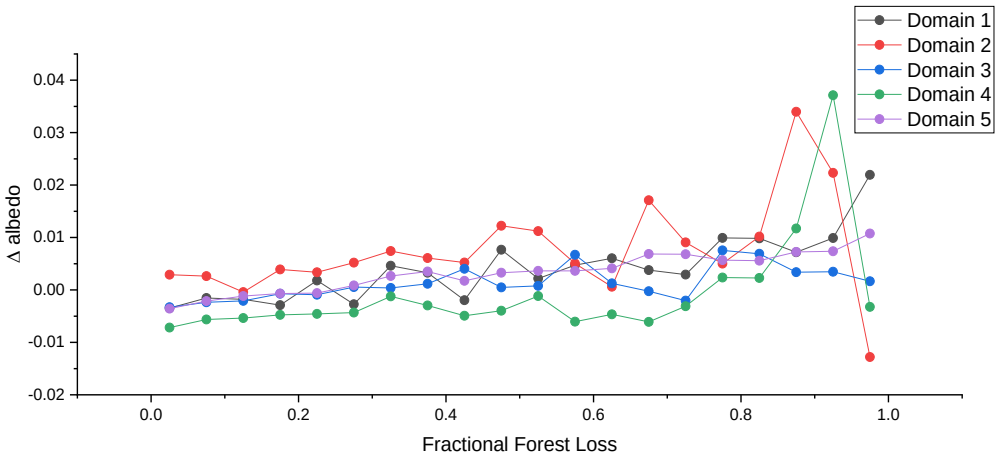

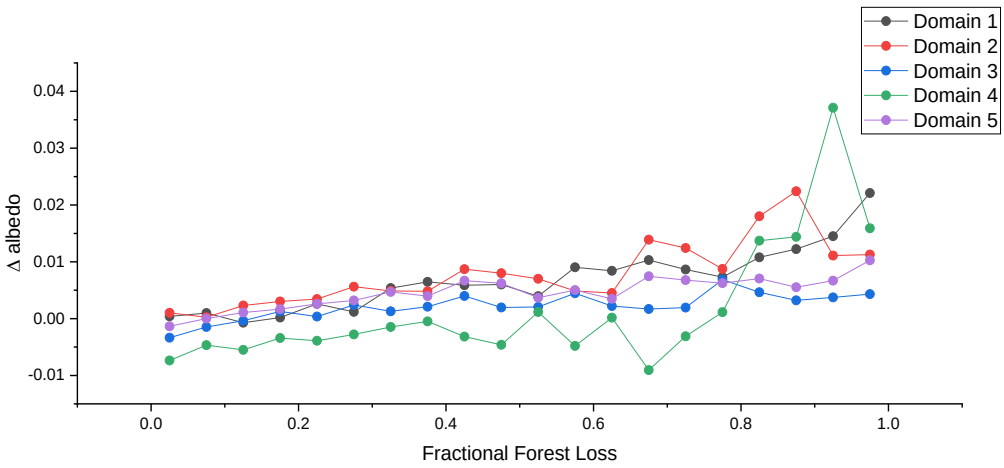

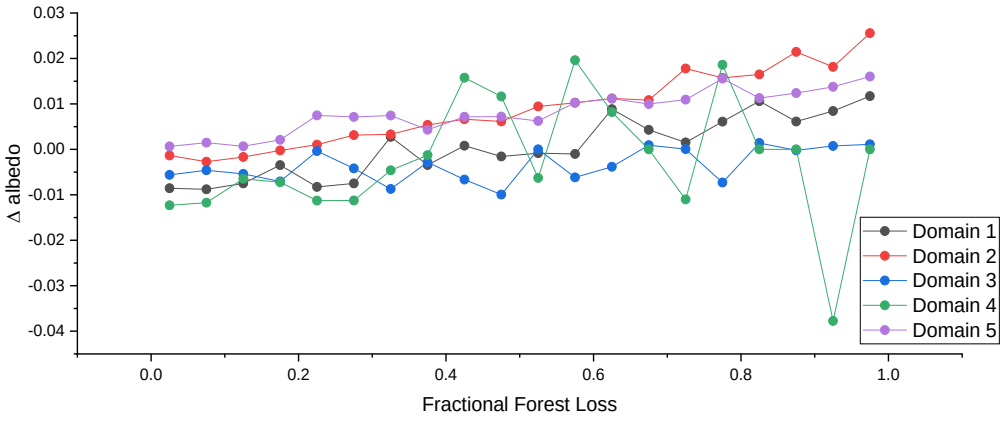

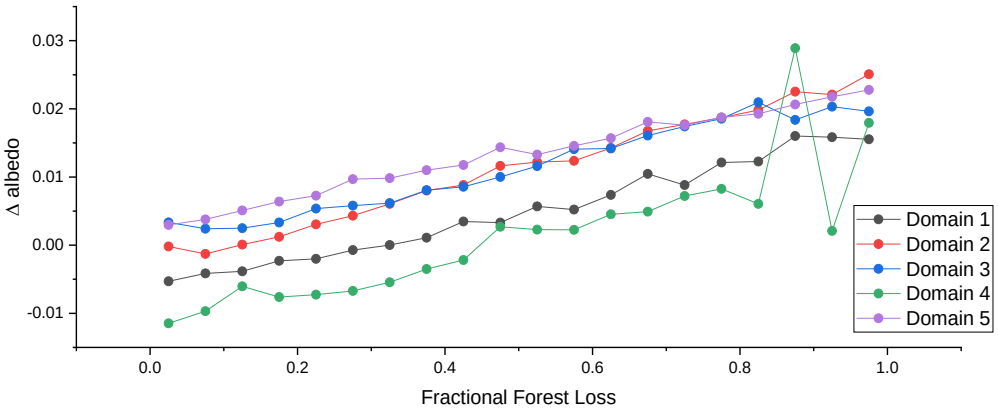
0.03
0.02
0.01
0.00
-0.01
Δ albedo
0.0
0.2
0.4
0.6
0.8
1.0
Fractional Forest Loss
Domain 1
Domain 2
Domain 3
Domain 4
Domain 5

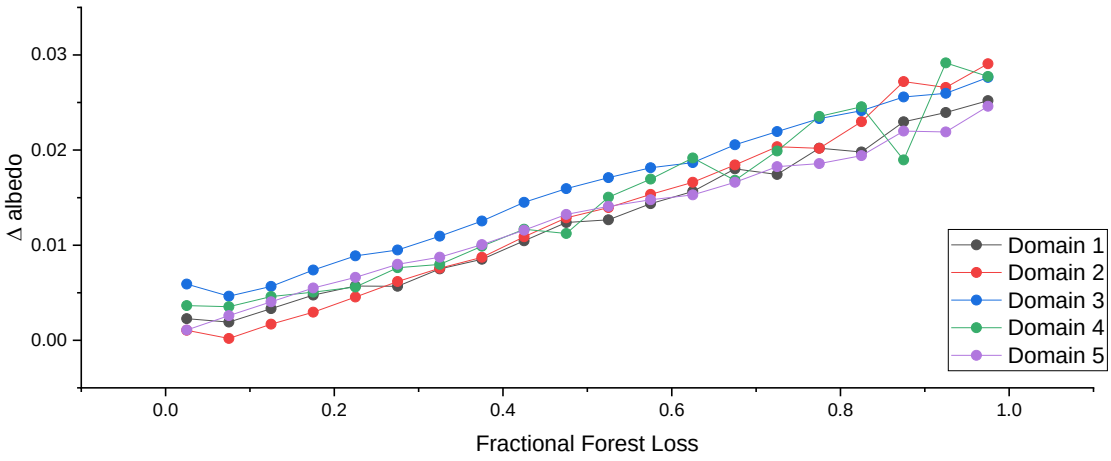
0.03
0.02
0.01
0.00
Δ albedo
0.0
0.2
0.4
0.6
0.8
1.0
Fractional Forest Loss
Domain 1
Domain 2
Domain 3
Domain 4
Domain 5

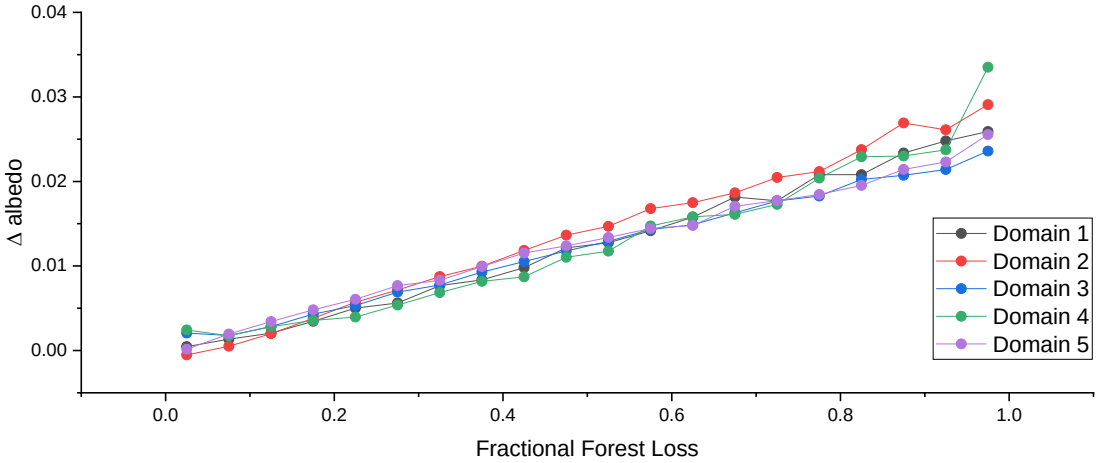
0.04
0.03
0.02
0.01
0.00
Δ albedo
0.0
0.2
0.4
0.6
0.8
1.0
Fractional Forest Loss
Domain 1
Domain 2
Domain 3
Domain 4
Domain 5

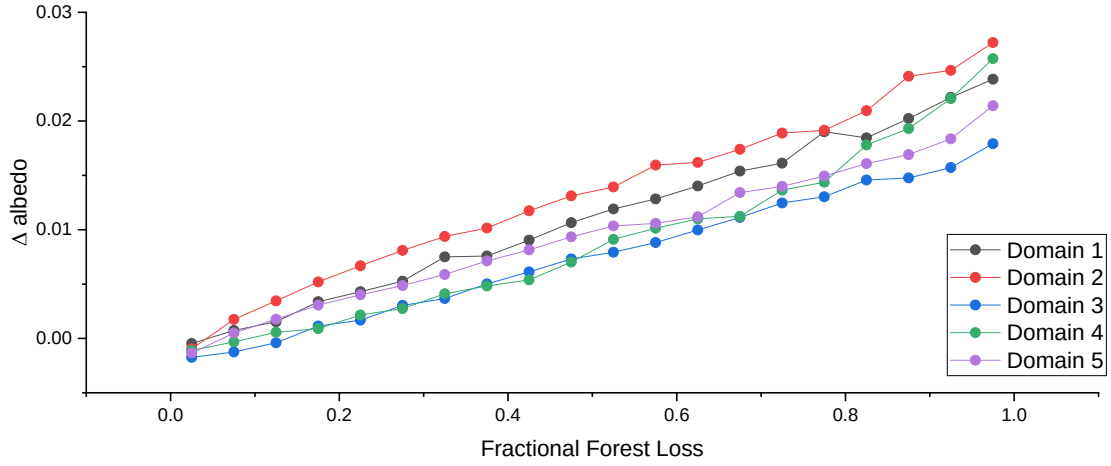
0.03
0.02
0.01
0.00
Δ albedo
0.0
0.2
0.4
0.6
0.8
1.0
Fractional Forest Loss
Domain 1
Domain 2
Domain 3
Domain 4
Domain 5

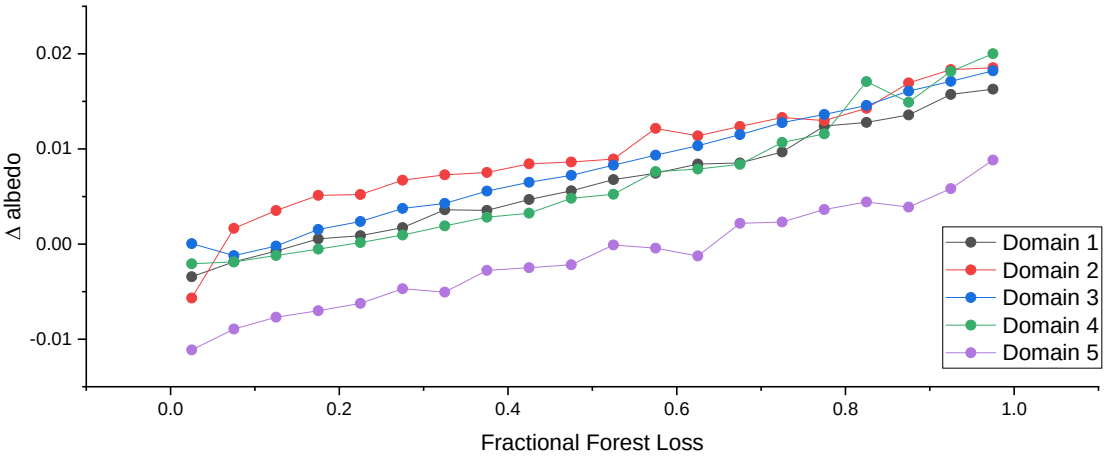
0.02
0.01
0.00
-0.01
Δ albedo
0.0
0.2
0.4
0.6
0.8
1.0
Fractional Forest Loss
Domain 1
Domain 2
Domain 3
Domain 4
Domain 5

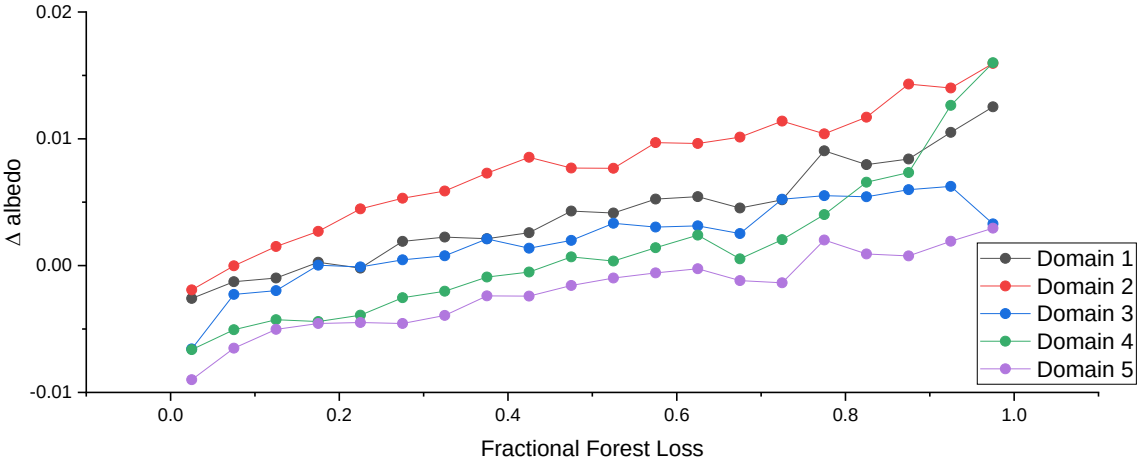
0.02
0.01
0.00
-0.01
Δ albedo
0.0
0.2
0.4
0.6
0.8
1.0
Fractional Forest Loss
Domain 1
Domain 2
Domain 3
Domain 4
Domain 5

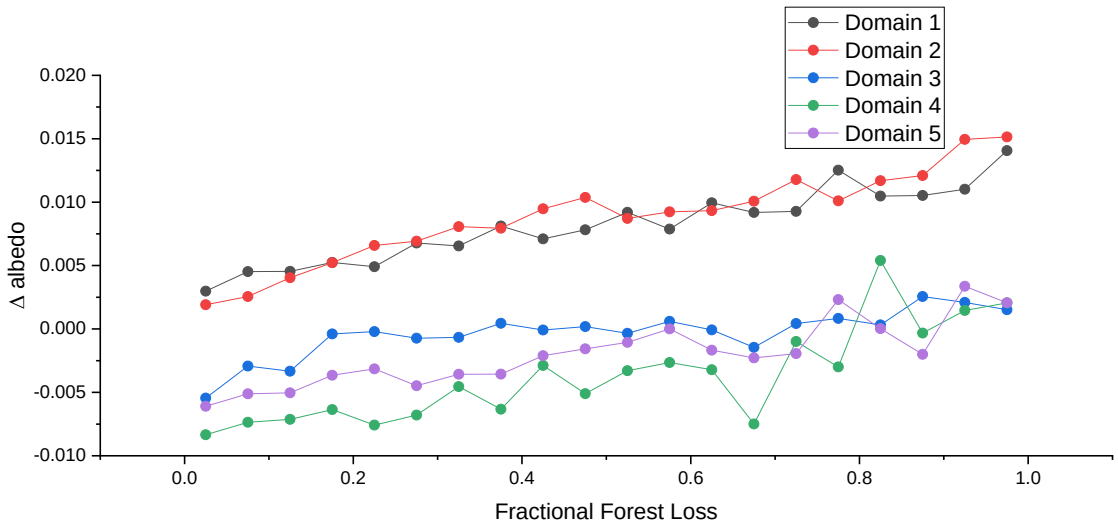
Domain 1
Domain 2
Domain 3
Domain 4
Domain 5
Δ albedo
0.020
0.015
0.010
0.005
0.000
-0.005
-0.010
0.0
0.2
0.4
0.6
0.8
1.0
Fractional Forest Loss

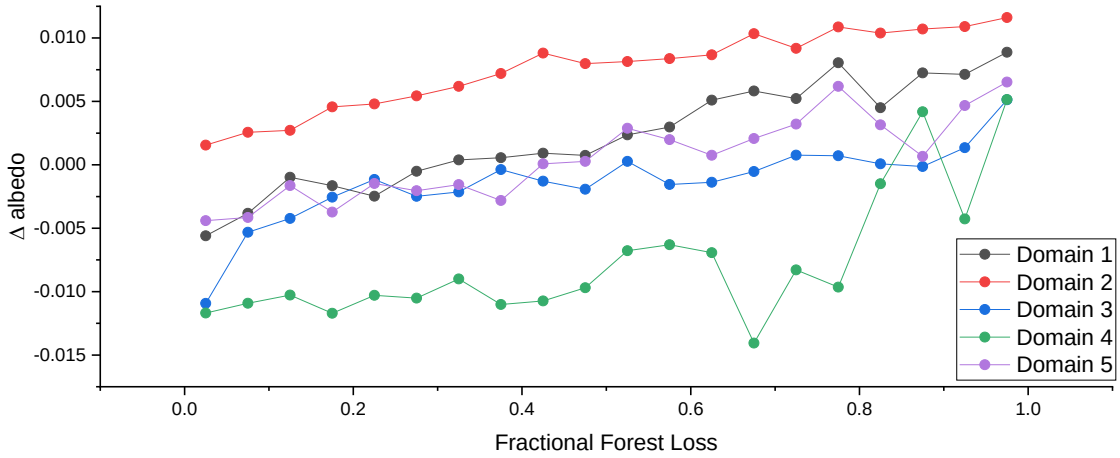
Δ albedo
0.010
0.005
0.000
-0.005
-0.010
-0.015
Domain 1
Domain 2
Domain 3
Domain 4
Domain 5
0.0
0.2
0.4
0.6
0.8
1.0
Fractional Forest Loss

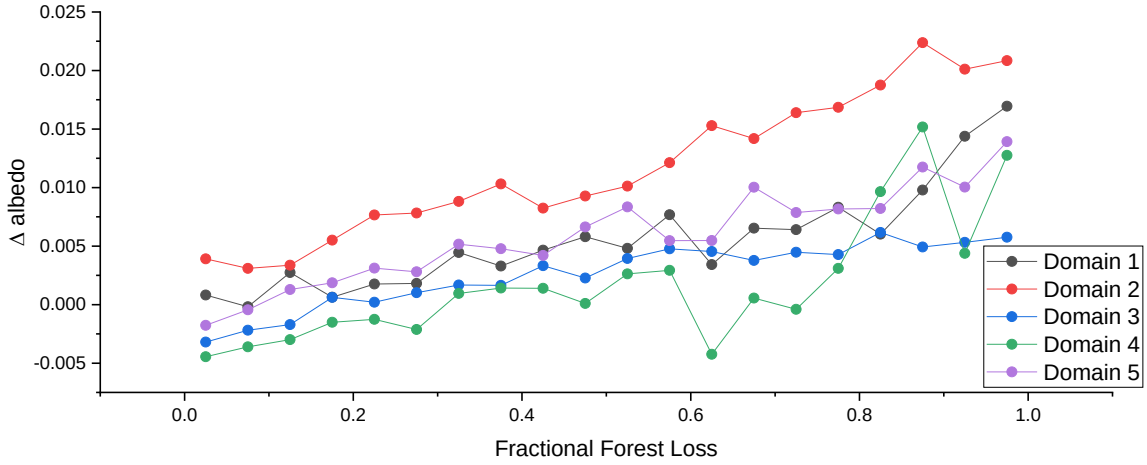
Δ albedo
0.025
0.020
0.015
0.010
0.005
0.000
-0.005
Domain 1
Domain 2
Domain 3
Domain 4
Domain 5
0.0
0.2
0.4
0.6
0.8
1.0
Fractional Forest Loss